ROBUST ADAPTIVE SAMPLED-DATA CONTROL DESIGN FOR MIMO SYSTEMS: APPLICATIONS IN CYBER-PHYSICAL SECURITY

BY

HAMIDREZA JAFARNEJADSANI

DISSERTATION

Submitted in partial fulfillment of the requirements
for the degree of Doctor of Philosophy in Mechanical Engineering
in the Graduate College of the
University of Illinois at Urbana-Champaign, 2018

Urbana, Illinois

Doctoral Committee:

Professor Naira Hovakimyan, Chair
Professor Lui Sha
Professor Petros G. Voulgaris
Professor Srinivasa M. Salapaka

ABSTRACT

This dissertation extends the $\mathcal{L}_1$ adaptive control theory to sampled-data (SD) framework. Multi-input multi-output non-square (underactuated) systems are considered with different sampling rates for inputs and outputs. The sampled-data framework allows to address non-minimum phase systems, subject to less restrictive assumptions as compared to continuous-time framework. It is shown that the closed-loop system can recover the response of a continuous-time reference system as the sampling time of the SD controller tends to zero. In this thesis, the $\mathcal{L}_1$ sampled-data adaptive controller is integrated with the Simplex fault-tolerant architecture for resilient control of cyber-physical systems (CPSs). Detection and mitigation of zero-dynamics attacks are addressed and validated in flight tests of a quadrotor in Intelligent Robotics Laboratory of UIUC. The experiments show that the multirate L1 controller can effectively detect stealthy zero-dynamics attacks and recover the stability of the perturbed system, where the single-rate conventional $\mathcal{L}_1$ adaptive controller fails.

From the perspective of applications, the dissertation considers navigation and control of autonomous vehicles and proposes a two-loop framework, in which the high-level reference commands are limited by a saturation function, while the low-level controller tracks the reference by compensating for disturbances and uncertainties. A class of nested, uncertain, multi-input multi-output (MIMO) systems subject to reference command saturation, possibly with non-minimum phase zeros, is considered. Robust stability and performance of the overall closed-loop system with command saturation and multirate $\mathcal{L}_1$ adaptive controller are analyzed.

Finally, a systematic analysis and synthesis method is proposed for the optimal design of filters in the $\mathcal{L}_1$ adaptive output-feedback structure, where the lowpass filter is the key to the trade-off between the performance and robustness of the closed-loop system. An optimization problem is formulated using the constraint on the input time-delay margin and a cost-function based on mixed $\mathcal{L}_1/\mathcal{H}_2$-norm performance measure. The optimization problem can be efficiently solved using linear/quadratic programming.

We note that the framework of this dissertation and the multi-loop problem formulation of navigation and control of autonomous systems provide suitable synthesis and analysis tools for autonomous cyber-physical systems (CPSs), including self-driving cars, unmanned aerial vehicles (UAVs), and industrial/medical robots, to name just a few. The SD design facilitates the implementation of control laws on digital computers in CPSs, where the input/output signals are available at discrete time instances with different sampling rates.

To my family and my wife Wei with endless love and respect

ACKNOWLEDGMENTS

I am very thankful to my doctoral advisor Prof. Naira Hovakimyan for her guidance and support throughout my Ph.D. studies. Her supervision taught me the importance of cutting-edge research with roots in mathematical rigor and impact on real-life engineering applications. I would like to express my gratitude to the committee members Prof. Petros Voulgaris, Prof. Lui Sha, and Prof. Srinivasa Salapaka for their helpful comments. Many meetings and discussions with Prof. Voulgaris and Prof. Sha provided me with deep insight and knowledge in the areas crucial to my research.

I want to thank our research group members. I had the opportunity to collaborate with Hanmin Lee, Donglei Sun, Hyung Jin Yoon, and Neng Wan. I benefited from fruitful discussions with them on various research topics, which provided significant help in developing the ideas for this dissertation. My labmates have been great friends who supported me through my Ph.D. studies at the University of Illinois at Urbana-Champaign.

Last but not least, I sincerely appreciate the support, unconditional love, and devotion of my parents and sister. I acknowledge the hardship they endured from being far away from me. Special thanks go to my dear wife, whose presence beside me and her endless love and support made it possible to complete this work.

TABLE OF CONTENTS

CHAPTER 1

Introduction

The last two decades have witnessed significant progress in the development of autonomous systems, including industrial/medical robots, unmanned aerial vehicles (UAVs), and self-driving cars, to name just a few. The control structure in these complex systems is often nested with multiple levels such as mission management, guidance/steering/navigation, and low-level controllers. These control loops are subject to contingencies and uncertainties due to dynamic environments where they operate, making it challenging to achieve trustable autonomy. Also, the resilience of these control systems against cyber and physical failures/attacks has recently become a grave concern. In conventional designs, a human operator is a last-ditch defense for safe and secure control of autonomous systems under unforeseen situations such as failures and attacks. For instance, an Airbus 320 passenger plane (US Airways flight 1549) lost both engines minutes after take-off from the New York City's LaGuardia airport due to the aircraft striking a flock of birds in 2009 [1]. The pilot, Captain Sullenberger, safely landed the plane in the nearby Hudson River. This example highlights the challenges of resilient and secure control designs to achieve the goal of replacing human operators with fully autonomous equipment.

Autonomous systems are important examples of cyber-physical systems (CPSs), where physical components and processes are tightly coupled with computational elements via sensors, actuators, and communication links. These CPSs often rely on control algorithms that run on digital computers for their operations, safety monitoring, performance, etc. Traditionally, there have been two separate approaches to assure the safety of controlled CPSs, which have been developed independently of each other. First, a significant amount of work in the field of control theory has been dedicated to developing robust, adaptive, and fault-tolerant control algorithms. The second approach utilities software assurance technologies to safeguard the real-time operation of CPSs. In most cases, these methods suffer from inaccurate models, unrealistic assumptions, and overlooked vulnerabilities due to the lack of comprehensive analysis. For example, many control design techniques cannot deal with software failures. On the other hand, software assurance methods require an accurate model of the physical process and correct measurement of the system states, which may not be available due to uncertainties in physical plants or sensor/actuator failures. In the following, an overview of the control designs for resilient CPSs is presented.

1.1. Overview of Control Designs for Resilient Cyber-Physical Systems

In autonomous CPSs, uncertainties and failures originate from both cyber and physical domains. Malicious attacks can fail computational elements. In the last several years, many cyber attack incidents have been reported against control systems of CPSs [2]. Consequently, numerous studies have been dedicated to provide security guarantees for resilient CPSs and reveal vulner-

abilities of critical infrastructures against such attacks. For example, cyber infiltration in the supervisory control and data acquisition (SCADA) systems in power grids have been investigated in [3–6], to name a few. In [7], the firmware in the engine control module is maliciously hacked, while the car is running. Studies in [8–10] show that communication channels, global positioning system (GPS), and on-board autopilot in UAVs are vulnerable to attacks. In 2011, the Predator and Reaper fleets of the U.S. military were infected by a computer virus [11]. Stuxnet worm is another notable example of cyber attacks against CPSs [12]. The aviation industry has also faced similar challenges. For instance, it was revealed that one could use the entertainment system in early Boeing 787 to take over the control of the aircraft [13].

Due to the complexity of software in modern systems, the verification for possible faults or cyber attack infiltrations becomes hard or even impossible. Simplex architecture is recognized as a useful approach for protection of CPSs against various software failures [14–18]. The main element of Simplex is the realization of a secure computing base. Simplex software architecture runs two separate control environments that provide different levels of functionalities and protection: *(i) high performance control (HPC) environment* runs software components during the normal operation of the system, which includes advanced controls and supplementary software, such as networking applications that are more susceptible to malicious attacks; *(ii) high assurance control (HAC) environment* runs a minimal set of software components that are critically required to control the physical system even when the normal environment is wholly taken over by an adversary and does not function. A *security and safety monitoring module* in the HAC environment monitors the physical state of the system and also implements a set of security monitors to detect potential security violations. This architecture is achieved by leveraging modern multicore processors and virtualization technology [18].

For detection and mitigation of malicious activities, Simplex relies on true system models, stored profiles, and accurate measurements, which are not always available in real-world systems. Physical components in CPSs are often subject to different uncertainties, such as change of parameters, physical damage, exogenous disturbances, measurement errors, such as noise and delay, etc. Also, deliberate physical attacks against CPSs, including sensor/actuator attacks and disruption of communication links, are quite conceivable. Coordinated cyber and physical attacks (CCPAs) are on the top alert list of Homeland Security Agency [19]. Simplex does not address either the problem of robust design for HAC or possible false negative/positive alarms that often arise in anomaly detection. In the field of cybersecurity and software verification, CPSs with uncertain physical plants have not been investigated rigorously. Traditionally, the control community has dealt with uncertain systems by developing robust, adaptive, and fault-tolerant control techniques. Robust control approaches have been developed for systems with uncertainties [20–22]. Adaptive control schemes can deal with large variation of system parameters [23–25]. Also, fault detection and isolation (FDI) methods have been developed for monitoring safety-critical systems and addressing the control problems under physical faults [26, 27]. For example, a fault detection filter is used in [28]

for detecting aircraft sensor and actuator fails. The multiple model adaptive estimation (MMAE) method has been applied to many FDI problems, including the aircraft flight control [29, 30] and inertial navigation systems subject to interference/jamming and spoofing [31]. In [32], an FDI technique using a fuzzy-tuned interacting multiple-model (IMM) filter for flight control systems is proposed. Following the residual detection, decision making tools such as cumulative sum algorithm [33], sequential probability ratio test [34], generalized likelihood ratio test [35], and local approach [36] are used. Finally, FDI is followed by the controller reconfiguration methods such as multiple-model techniques [37, 38] and adaptive control schemes [39, 40].

In addition to software failures and uncertainties in physical plants, as described above, inadequate models for analysis of CPSs present other challenges yet to be addressed. In autonomous CPSs, controllers are implemented on computers equipped with the sample and hold mechanisms for sending/receiving a physical system's input/output data. The sampled-data (SD) nature of controller implementation generates additional vulnerability to stealthy attacks due to the sampling zeros (so-called zero-dynamics attack) [41, 42], which remains unreported in CPS modeling and analysis. If a closed-loop system possesses an unstable zero, an (ultimately) unbounded actuator (or sensor) attack may not be observed by the monitoring data, *i.e.*, the sampled outputs and the command signals. From a control theory perspective, stealthy zero-dynamics attacks are hard to detect and mitigate [42], rendering them as a benchmark problem to tackle for CPS security. Therefore, a sampled-data framework for development and implementation of control algorithms becomes necessary to capture the real underlying structure of CPSs and defend against cyber and physical attacks.

1.2. $\mathcal{L}_1$ Adaptive Sampled-Data Control Design

Towards the goal of bridging the gap between control theory and software assurance techniques, L1Simplex in [43] develops a unified framework that integrates the robust control design with Simplex fault-tolerant architecture [15, 44]. This approach is based on co-design and analysis of co-stability in cyber and physical components of the system to ensure the security of the overall system [43,45]. In L1Simplex approach, $\mathcal{L}_1$ adaptive control is used as the high assurance controller. $\mathcal{L}_1$ adaptive control is known as a robust technique, with quantifiable performance bounds and robustness margins [46–48]. The controller compensates for uncertainties and disturbances within the bandwidth of a lowpass filter. The performance of $\mathcal{L}_1$ adaptive control has been verified on manned and unmanned aerial vehicles [49–53], as well as several high-fidelity simulation models [54–58]. This thesis extends $\mathcal{L}_1$ adaptive control theory to the SD framework for improved safety and security of the control implementation in Simplex architecture. Such an approach allows analyzing continuous-time physical processes that interact with digital controllers through sensors/actuators and communication links, [59]. As mentioned, the analysis of control systems in the SD framework has significant cyber-physical security implications. For example, stealthy zero-dynamics attacks can be implemented in the cyberspace as an additive disturbance to destabilize a feedback system.

To deal with this problem, a multirate SD scheme can be applied, since it allows the attack to be detected by ensuring that there are no relevant unstable zeros in the lifted system. As shown in [42], unbounded zero-dynamics attacks can be detected if the control system is designed using the dual-rate SD scheme.

Sampled-data control systems are extensively analyzed in the literature [60–64]. The SD control designs are mainly based on the controller emulation methods, where an SD controller is developed in two stages: first, a continuous-time controller which satisfies certain performance/robustness requirements is designed; next, a discrete-time controller is obtained for digital implementation using an approximation technique [65–67]. The main issue in this approach is the selection of the sampling period that guarantees the stability of SD system with the emulated controller. In practice, the sampling period cannot be chosen arbitrarily small due to hardware limitations, such as the limits in the central processing unit (CPU) and communication links. On the other hand, a larger sampling period reduces the performance and robustness of digital controllers. The conditions under which the SD controllers recover the properties of the underlying continuous-time design are investigated in [65, 68]. The problem of SD output-feedback control is addressed by introducing high-gain observers to estimate the unmeasured states [69–71]. SD output-feedback control of systems with uncertainties and disturbances has been addressed in [66,67,72,73] for a class of single-input single-output (SISO) nonlinear systems under a lower-triangular linear growth condition. Multirate sampling has been studied extensively in the context of SD control, and relevant analysis and synthesis results have been reported in [74–76], to mention only a few.

We extend the results in the SD literature by considering a class of uncertain multi-input multi-output (MIMO) systems with unknown nonlinearities subject to the locally Lipschitz continuity assumption. In the $\mathcal{L}_1$ adaptive SD control design, we maintain the key benefits of a continuous-time $\mathcal{L}_1$ adaptive controller, [46–48, 77]. Conditions are derived, under which the SD closed-loop system uniformly recovers the underlying continuous-time reference system as the sampling time tends to zero. The related preliminary results can be found in [78–80]. Recently, $\mathcal{L}_1$ adaptive control has been developed in [81, 82] for under-actuated MIMO systems, where the number of outputs is greater than or equal to the number of inputs, with minimum-phase transmission zeros. This thesis extends $\mathcal{L}_1$ adaptive SD controllers to under-actuated systems with non-minimum phase zeros. Also, compared to a continuous-time approach, the proposed SD scheme provides a richer and more agile architecture for control of CPSs with discrete-continuous hybrid dynamics. We notice that a few adaptive SD schemes that study SISO non-minimum phase systems are given in [83–86].

In addition, we extend the results to a multi-level control architecture, where a high-level controller provides reference commands to a low-level controller. This multi-loop structure is used for navigation and control of autonomous CPSs in aerospace, robotics, and many other applications [87–90]. The primary objective of multi-level control architectures is the decoupling between the outer loop and the inner loop for reliable implementation and to satisfy input/state constraints

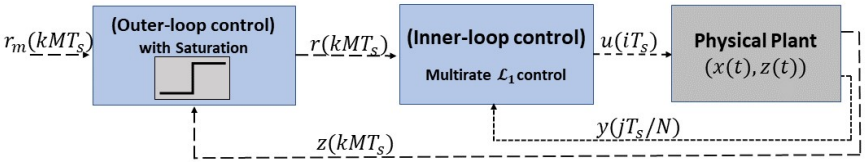

Figure 1.1: Structure of the proposed multil-level multirate SD controller for navigation and control of autonomous CPSs.

[91, 92]. In such systems, it is desirable to limit the commands by saturation functions [91]. Nested saturation for navigation and control of UAVs has been studied in [93–95]. In [96], it is shown that a chain of multiple integrators can be globally stabilized using nested saturation functions. In this thesis, the navigation and control problem for autonomous CPSs is formulated utilizing the multirate SD scheme. The control structure consists of a high-level (outer-loop) control for reference command generation and a low-level (inner-loop) adaptive control for reference tracking, as shown in Figure 1.1. The high-level controller is limited by saturation bounds to maintain the closed-loop system within an operational safety envelope. The low-level controller is a multirate $\mathcal{L}_1$ adaptive controller for tracking the generated reference command by compensating for uncertainties and disturbances.

The low-level controller compensates for disturbances within the bandwidth of a lowpass filter, similar to other $\mathcal{L}_1$ adaptive controllers. We extend the results by considering the output-feedback control problem for a class of nested, uncertain, MIMO systems subject to reference command saturation, with possibly non-minimum phase zeros. The unknown nonlinearities are assumed to be locally Lipschitz continuous. The multi-rate SD design addresses the digital implementation of the control law on computers, where the inputs and measurements are available at discrete time instances with different sampling rates. Also, the multi-level structure of the problem formulation allows for the design of the feedback loops for the high-level/low-level subsystems with their respective control objectives, while the stability and robustness of the overall nested system subject to command saturation are taken into account. Figure 1.2 illustrates an application of integrating the Simplex architecture with the proposed multi-level multirate approach for safe and secure navigation and control of an autonomous air vehicle in the presence of possible failures/attacks.

1.3. Main Contributions and Thesis Organization

In this thesis, a sampled-data approach is developed for resilient and secure control of autonomous CPSs using the $\mathcal{L}_1$ adaptive output-feedback control structure. The main contributions are: (i) an adaptive SD control is developed for a class of nested, uncertain, MIMO systems subject to reference command saturation, possibly with non-minimum phase zeros; (ii) the SD control design facilitates the direct implementation of control laws on digital computers in CPSs, where the input/output signals are available at discrete time instances with different sampling rates; (iii) stealthy zero-dynamics attacks become detectable by considering a multi-rate SD scheme for control

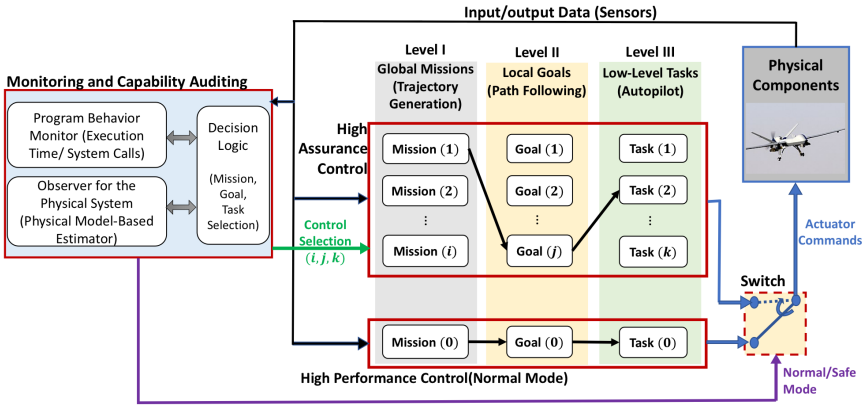

Figure 1.2: Simplex structure can be integrated with the proposed multi-level multirate approach for navigation and control of autonomous CPSs.

design in secure CPSs; (iv) a navigation and control problem for autonomous CPSs is formulated and solved using a multi-level multirate SD control structure; (v) a systematic analysis and synthesis method is proposed for optimal design of filters in the $\mathcal{L}_1$ adaptive controllers.

In Chapter 2, we introduce a few preliminary definitions and mathematical notations.

Chapter 3 develops an SD controller for a class of uncertain MIMO systems using the $\mathcal{L}_1$ adaptive control architecture. Sufficient conditions for robust stability of the closed-loop system with SD controller are obtained, where the input/output signals are held constant over a sampling period. It is shown that the hybrid closed-loop system can recover the performance of a continuous-time reference system as the sampling time tends to zero. Simulation examples are provided to validate the theoretical findings.

In Chapter 4, the results on SD control design are extended by considering the output-feedback problem for a class of nested, uncertain, MIMO systems subject to reference command saturation, with possibly non-minimum phase zeros. While the controller design with uniform rate is considered in Chapter 3, a multi-rate SD approach is proposed in Chapter 4. The multirate scheme allows the zero-dynamics attacks to be detected. We formulate a navigation and control problem for autonomous systems using a multi-level control structure, in which the high-level reference commands are limited by a saturation function, while the low-level controller tracks the reference by compensating for disturbances and uncertainties. Simulation scenarios for a fixed-wing drone under failures/attacks are provided to validate the theoretical findings.

Chapter 5 aims to extend the $\mathcal{L}_1$ adaptive SD control to under-actuated systems with non-minimum-phase zeros. The multirate $\mathcal{L}_1$ adaptive control design of Chapter 4 is limited to square MIMO systems with the same number of inputs and outputs. The controller is integrated with the Simplex architecture for detection and mitigation of actuator attacks. The experimental results from the flight test of a small quadrotor are provided. The experiments show that the multirate $\mathcal{L}_1$ controller can effectively detect a zero-dynamics actuator attack and recover the stability of the

perturbed quadrotor.

In Chapter 6, a systematic analysis and synthesis method is proposed for optimal design of filters in $\mathcal{L}_1$ adaptive feedback structure, where the low-pass filter is the key to the trade-off between performance and robustness of the closed-loop system. An optimization problem is formulated using a constraint on the input time-delay margin and a cost-function based on mixed $\mathcal{L}_1/\mathcal{H}_2$-norm performance measure. The problem can be efficiently solved using a linear/quadratic programming optimization method. In this chapter, an $\mathcal{L}_1$ controller with optimized filter is used for precision trajectory tracking control of a Crazyflie quadrotor in an experimental setup. The controller demonstrates robustness to input delay, noise, disturbances, and uncertainties in the modeling of the quadrotor.

Finally, Chapter 7 presents the concluding remarks and the future research directions.

CHAPTER 2

Preliminaries

In this chapter, we introduce a few preliminary definitions and mathematical notations.

Throughout this thesis, the notation $\|.\|_p$ represents the vector or matrix p-norms with $1 \leq p \leq \infty$. For a vector $v \in \mathbb{R}^q$, the notation $\mathrm{sat}\{v\}$ represents the saturation function, defined by

$$\mathrm{sat}\{v\} = \begin{bmatrix} \mathrm{sgn}\{v_1\} \min\{|v_1|, 1\} \\ \vdots \\ \mathrm{sgn}\{v_q\} \min\{|v_q|, 1\} \end{bmatrix}, \tag{2.1}$$

where $\mathrm{sgn}\{\cdot\}$ is the standard sign function, and v_i's are the elements of the vector v.

Definition 2.1 ($\mathcal{L}_p^n$ space [97, 98])**.** *The $\mathcal{L}_p^n$ space is defined as the set of measurable functions, such that*

$$\mathcal{L}_p^n = \{f : \mathbb{R} \to \mathbb{R}^n; \|f\|_{\mathcal{L}_p} < \infty\},$$

where $\|\cdot\|_{\mathcal{L}_p}$ is given by

$$\|f\|_{\mathcal{L}_p} = \left(\int_{\mathbb{R}} \|f\|_p^p dt \right)^{1/p}, \quad 1 \leq p \leq \infty,$$
$$\|f\|_{\mathcal{L}_\infty} = \sup_{\mathbb{R}} \|f(t)\|_\infty .$$

The notation $\|x_\tau\|_{\mathcal{L}_p}$ represents the $\mathcal{L}_p$ norm of the truncated signal $x_\tau(t)$ for a signal $x(t) \in \mathbb{R}^n$, such that

$$x_\tau(t) = x(t), \quad \forall t \leq \tau,$$
$$x_\tau(t) = 0, \quad \text{otherwise.}$$

Consider a continuous-time LTI system P_c with the minimal realization ($A_\mathrm{c} \in \mathbb{R}^{n\times n}$, $B_\mathrm{c} \in \mathbb{R}^{n\times p}$, $C_\mathrm{c} \in \mathbb{R}^{q\times n}$, $D_\mathrm{c} \in \mathbb{R}^{q\times p}$) and the corresponding discrete-time LTI system $P_\mathrm{d} = \mathcal{S}P_\mathrm{c}\mathcal{H}$, which is defined with the standard zero-order hold and sample devices $\mathcal{H}$ and $\mathcal{S}$, respectively. The relationship between P_c and P_d follows from the following definition.

Definition 2.2 (Step-invariant discrete-time equivalent system)**.** *Given an LTI system P_c, the step-invariant discrete-time equivalent system P_d is given by the following state-space matrices:*

$$A_\mathrm{d} = e^{A_\mathrm{c}T_\mathrm{s}}, \quad B_\mathrm{d} = \int_0^{T_\mathrm{s}} e^{A_\mathrm{c}\tau} B_\mathrm{c} d\tau, \quad C_\mathrm{d} = C_\mathrm{c}, \quad D_\mathrm{d} = D_\mathrm{c}, \tag{2.2}$$

where $T_\mathrm{s} > 0$ is a sampling period.

Definition 2.3 (Pathological sampling [41]). *Consider the continuous-time system P_{c} and its step-invariant equivalent system P_{d}. The sampling frequency $\omega_{\mathrm{s}} = \frac{2\pi}{T_{\mathrm{s}}}$ is pathological, if the matrix A_{c} has at least two eigenvalues λ and λ', such that for some $k \in \mathbb{Z}\backslash\{0\}$ the following relationship holds:*

$$\lambda = \lambda' + jk\omega_{\mathrm{s}}. \tag{2.3}$$

The $\mathcal{L}_1$ norm of the continuous-time LTI system P_{c} can be computed as follows:

$$\|P_{\mathrm{c}}\|_{\mathcal{L}_1} = \max_{1\leq i\leq q} \int_0^\infty \left(\sum_{j=1}^{p} \left| c_i e^{A_{\mathrm{c}} t} b_j(\tau) \right| \right) d\tau + \|D_{\mathrm{c}}\|_\infty,$$

where $c_i \in \mathbb{R}^{1\times n}$ is i^{th} row of C_{c}, and $b_j \in \mathbb{R}^{n\times 1}$ is the j^{th} column of B_{c}.

Definition 2.4 (Relative degree). *A MIMO system with the state-space realization $(A,\, B,\, C)$ has relative degree $r > 1$, if*

$$\begin{aligned} CA^i B &= 0, \quad i \in \{0,\, ...,\, r-2\}, \\ CA^{r-1}B &\neq 0. \end{aligned}$$

Definition 2.5 (Transmission zero). *Consider a MIMO system with the minimum realization $(A,\, B,\, C,\, D)$, where $(A,\, B)$ is controllable and $(A,\, C)$ is observable. The system has a finite transmission zero at $z_0 \in \mathbb{C}$, if the Rosenbrock matrix*

$$\begin{bmatrix} s\mathbb{I} - A & -B \\ C & D \end{bmatrix}$$

loses rank at $s = z_0$.

Definition 2.6 (Zero-dynamics actuator attack [42]). *Assume the system P_{d} with the state-space matrices in (2.2) has an unstable transmission zero at $z_0 \in \mathbb{C}$. Then, an unbounded actuator attack signal of the form $d[k] = \epsilon {z_0}^k$, which can be implemented as an additive input disturbance and remain undetected for small enough ϵ at the sampled output while causing the states of the system expand exponentially, is referred to as zero-dynamics actuator attack.*

Definition 2.7 ([99]). *Let $a > 0$ be a positive constant.*

(a) A function $\alpha : [0, a) \to [0, \infty)$ is called a class $\mathcal{K}$ function, if $\alpha(0) = 0$ and $\alpha(\cdot)$ is strictly increasing.

(b) A function $\beta : [0, \infty) \times [0, a) \to [0, \infty)$ is called a class $\mathcal{KL}$ function, if for each $t \in [0, \infty)$, $\beta(t, r)$ is in class $\mathcal{K}$ with respect to r, for each $r \in [0, a)$, $\beta(t, r)$ is decreasing with respect to t, and for each $r \in [0, a)$, $\beta(t, r) \to 0$ as $t \to \infty$.

Definition 2.8 ($\mathcal{L}_p$ stability [98,99])**.** *Consider the following input-output map $\mathcal{H}: \mathcal{L}_p^m \to \mathcal{L}_p^n$ with $y = \mathcal{H}u$, where $u(t) \in \mathcal{L}_p^m$ and $y(t) \in \mathcal{L}_p^n$; the map $\mathcal{H}$ is not necessarily linear. The map $\mathcal{H}$ is called $\mathcal{L}_p$-stable, if there exist a class $\mathcal{K}$ function α, defined on $[0, \infty)$, and a nonnegative constant b such that*

$$\|(\mathcal{H}u)_\tau\|_{\mathcal{L}_p} \leq \alpha(\|u_\tau\|_{\mathcal{L}_p}) + b, \quad \forall u \in \mathcal{L}_p^m, \quad \forall \tau \in [0, \infty).$$

Remark 2.1. *The $\mathcal{L}_\infty$ stability is often referred to as Bounded-Input Bounded-Output (BIBO) stability.*

Consider the system

$$\dot{x} = f(x, u, t, \theta), \quad x(t_0) = x_0, \quad t \geq t_0, \tag{2.4}$$

where $x_0 \in \mathbb{R}^n$ is an initial condition, and $\theta \in \Theta$ with $\Theta \subseteq \mathbb{R}^l$ being a set of constant parameters. In addition, suppose that for each $\theta \in \Theta$, $f_\theta(x, u, t)$ is locally Lipschitz continuous in (x, u), and piecewise continuous in t, where $f_\theta(x, u, t) = f(x, u, t, \theta)$.

Definition 2.9. *(Semi-globally Practically Input to State Stability (SPISS) [100]) The system given in* (2.4) *is said to be semi-globally practically input to state stable, if for each $d > 0$, $\delta_{\mathrm{x}} > 0$, and $\delta_{\mathrm{r}} > 0$ satisfying $\delta_{\mathrm{x}} > d$, there exist $\theta^\star(d, \delta_{\mathrm{x}}, \delta_{\mathrm{r}}) \in \Theta$, a class $\mathcal{K}$ function γ, and a class $\mathcal{KL}$ function β such that for all $x_0 \in \mathcal{D}_0$ and $t_0 \geq 0$*

$$\|x(t; t_0, x_0, \theta^\star)\| \leq \beta(\|x_0\|, t - t_0) + \gamma(\sup_{t_0 \leq \tau \leq t} \|u(\tau)\|) + d, \quad \|u\|_{\mathcal{L}_\infty} < \delta_{\mathrm{r}}, \quad \forall t \geq t_0, \tag{2.5}$$

where $\mathcal{D}_0 = \{x \in \mathbb{R}^n : \|x\| < \delta_{\mathrm{x}}\}$.

Definition 2.10 (L1Simplex Architecture [43])**.** *As shown in Figure 2.1, the L1Simplex architecture includes the RHAC, the HPC, the safety monitoring system, and the decision logic:*

- *Robust High-Assurance Controller (RHAC): The RHAC is a simple and verified controller that ensures safe and stable operation of the system, but provides limited levels of performance and reduced functionalities; the RHAC is designed based on the $\mathcal{L}_1$ adaptive controller;*
- *High-Performance Controller (HPC): The HPC is a complex controller providing high levels of performance and advanced functionalities and is active during the normal operation of the system; it, however, may not be (fully) verified and may experience software faults;*
- *Safety Monitor: This verified monitor provides estimates of the uncertainties inside the system with fast adaptation, which takes the form of the state predictor in the $\mathcal{L}_1$ adaptive control architecture;*
- *Decision Logic: This logic, which needs to be verified, is responsible for switching from the complex HPC to the verified RHAC in the event of failures.*

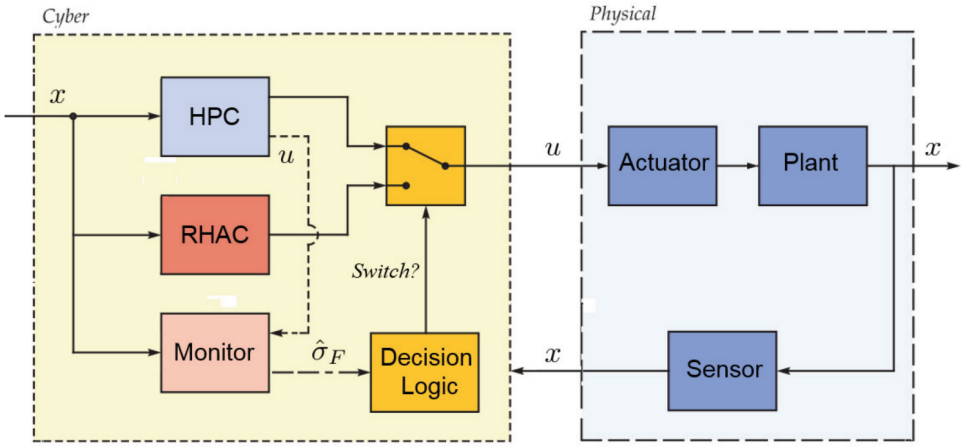

Figure 2.1: L1Simplex architecture [43, 101].

CHAPTER 3

Sampled-Data Output-Feedback Control Design for a Class of Uncertain Systems

This chapter develops a sampled-data (SD) output-feedback control approach for nonlinear uncertain MIMO systems, using the $\mathcal{L}_1$ adaptive control structure. The $\mathcal{L}_1$ adaptive control theory is extended to the SD framework while maintaining the key benefits of a continuous-time $\mathcal{L}_1$ controller implementation. Compared to continuous-time design, the proposed SD approach provides a more accurate model for cyber-physical systems (CPSs), with hybrid discrete/continuous nature. Conditions are derived, under which the SD controller uniformly recovers the performance of the underlying continuous-time control design. The unknown nonlinearities are assumed to be locally Lipschitz. Also, the system under consideration can have non-minimum phase dynamics. The controller compensates for disturbances within the bandwidth of a lowpass filter, and similar to other $\mathcal{L}_1$ controllers, achieves uniform transient and steady-state performance. In this chapter, using the method of controller emulation, a discrete-time $\mathcal{L}_1$ adaptive controller is derived from a continuous-time reference system. Uniform bounds between the response of the closed-loop SD system and the reference system are derived, which can be made arbitrarily small as the sampling time tends to zero.

3.1. Problem Formulation

Consider the following MIMO system

$$\begin{aligned} &\dot{x}(t) = A_{\rm p}x(t) + B_{\rm p}\left(u(t) + f(t, x(t))\right), \quad x(0) = x_0, \\ &y(t) = C_{\rm p}x(t), \end{aligned} \tag{3.1}$$

where $x(t) \in \mathbb{R}^n$ is the state vector, $u(t) \in \mathbb{R}^q$ is the input signal, and $y(t) \in \mathbb{R}^q$ is the system output vector. Also, $\{A_{\rm p} \in \mathbb{R}^{n\times n}, B_{\rm p} \in \mathbb{R}^{n\times q}, C_{\rm p} \in \mathbb{R}^{q\times n}\}$ is a known observable-controllable triple. The unknown initial condition $x_0 \in \mathbb{R}^n$ is assumed to be inside an arbitrarily large set, so that $\|x_0\|_\infty \leq \rho_0 < \infty$ for some known $\rho_0 > 0$. Let $f\left(t, x\right) \in \mathbb{R}^q$ represent the time-varying uncertainties, physical failures, and disturbances subject to the following assumption.

Assumption 3.1. *There exist K_δ for arbitrary $\delta > 0$, and constant $L_0 > 0$ such that*

$$\begin{aligned} \|f(t, x_2) - f(t, x_1)\|_\infty &\leq K_\delta \|x_2 - x_1\|_\infty, \\ \|f(t, 0)\|_\infty &\leq L_0 \end{aligned}$$

hold for all $\|x_i\|_\infty \leq \delta,\ i \in \{1,\, 2\}$, uniformly in $t \geq 0$.

The control input, which is implemented via a zero-order hold mechanism with the time period

of $T_{\rm s} > 0$, is given by

$$u(t) = u_{\rm d}[i], \quad t \in [iT_{\rm s}, (i+1)T_{\rm s}), \quad i \in \mathbb{Z}_{\geq 0}, \tag{3.2}$$

where $u_{\rm d}[i]$ is a discrete-time control input signal. The output $y(t)$ is sampled with the sampling time of $T_{\rm s}$, such that the discrete-time output measurement $y_{\rm d}[i]$ is given by

$$y_{\rm d}[i] = y(iT_{\rm s}). \tag{3.3}$$

Assumption 3.2. *The desired dynamics are defined by*

$$M(s) \triangleq C_{\rm m}(s\mathbb{I}_{n_{\rm m}} - A_{\rm m})^{-1} B_{\rm m}, \tag{3.4}$$

where the triple $\{A_{\rm m} \in \mathbb{R}^{n_{\rm m}\times n_{\rm m}}, B_{\rm m} \in \mathbb{R}^{n_{\rm m}\times q}, C_{\rm m} \in \mathbb{R}^{q\times n_{\rm m}}\}$ *represents a minimal state-space realization. The desired system* $M(s)$ *should satisfy one of the following conditions:*

- *the triple* $(A_{\rm m}, B_{\rm m}, C_{\rm m})$ *is selected such that* $C_{\rm m}B_{\rm m}$ *is nonsingular,* $A_{\rm m}$ *is Hurwitz, and* $M(s)$ *does not have a non-minimum-phase transmission zero,*
- *or, if the system defined by* $(A_{\rm p}, B_{\rm p}, C_{\rm p})$ *does not have a non-minimum-phase transmission zero, one can select*

  $$A_{\rm m} = A_{\rm p} - B_{\rm p}F, \quad B_{\rm m} = B_{\rm p}, \quad C_{\rm m} = C_{\rm p}, \tag{3.5}$$

  where $F \in \mathbb{R}^{q\times n}$ *is selected such that* $A_{\rm p} - B_{\rm p}F$ *is Hurwitz. In this case* $C_{\rm m}B_{\rm m}$ *can be rank deficient.*

The desired response $y_{\rm m}(t)$ *is given by the Laplace transform* $y_{\rm m}(s) = M(s)K_{\rm g}r(s)$*, where*

$$K_{\rm g} \triangleq -\left(C_{\rm m}A_{\rm m}^{-1}B_{\rm m}\right)^{-1},$$

and $r(s)$ *is the Laplace transform of* $r(t)$*, given by*

$$r(t) = r_{\rm d}[i], \quad t \in [iT_{\rm s}, (i+1)T_{\rm s}), \quad i \in \mathbb{Z}_{\geq 0}, \tag{3.6}$$

where $r_{\rm d}[i]$ *is a given discrete-time reference command. The command signal is assumed to be bounded, such that* $\|r_{\rm d}[i]\|_\infty \leq M_{\rm r}$*,* $i \in \mathbb{Z}_{\geq 0}$*, where* $M_{\rm r}$ *is a known positive constant.*

In the following, a sampled-data $\mathcal{L}_1$ adaptive controller is formulated to compensate for uncertainties and disturbances, such that the output $y(t)$ of the system in (3.1) tracks the desired response $y_{\rm m}(t)$.

3.2. Proposed Sampled-Data Output-Feedback Controller

In this section, the proposed adaptive SD controller is presented. The conditions for selection of the control parameters and the detailed analysis of the closed-loop system are provided in Section 3.3. Elements of the output-feedback $\mathcal{L}_1$ adaptive SD controller are given next.

Let $T_{\rm s} > 0$ be the sampling time of the digital controller. Consider a strictly proper stable transfer function $C(s)$ such that $C(0) = \mathbb{I}_q$. In the $\mathcal{L}_1$ adaptive control structure, $C(s)$ represents the low-pass filter at the control input [47]. Also, define $O(s) \triangleq C(s)M^{-1}(s)C_{\rm m}(s\mathbb{I}_{n_{\rm m}} - A_{\rm m})^{-1}$, and let $\{A_{\rm o} \in \mathbb{R}^{v\times v}, B_{\rm o} \in \mathbb{R}^{v\times q}, C_{\rm o} \in \mathbb{R}^{q\times v}\}$ be a minimal state-space realization, such that

$$C_{\rm o}(s\mathbb{I}_v - A_{\rm o})^{-1}B_{\rm o} = O(s). \tag{3.7}$$

The control law is given by

$$\begin{aligned} x_{\rm u}[i+1] &= e^{A_{\rm o}T_{\rm s}}x_{\rm u}[i] + A_{\rm o}^{-1}\left(e^{A_{\rm o}T_{\rm s}} - \mathbb{I}_v\right)B_{\rm o}e^{-A_{\rm m}T_{\rm s}}\hat{\sigma}_{\rm d}[i], \quad x_{\rm u}[0] = 0, \quad i \in \mathbb{Z}_{\geq 0}, \\ u_{\rm d}[i] &= K_{\rm g}r_{\rm d}[i] - C_{\rm o}x_{\rm u}[i], \end{aligned} \tag{3.8}$$

where $\hat{\sigma}_{\rm d}[\cdot] \in \mathbb{R}^n$ is given by the adaptation law in (3.13), and $r_{\rm d}[\cdot]$ is a given discrete-time reference command.

The construction of $\hat{\sigma}_{\rm d}[\cdot]$ is based on an output predictor that follows. The output predictor is given by

$$\begin{aligned} \hat{x}_{\rm d}[i+1] =& e^{A_{\rm m}T_{\rm s}}\hat{x}_{\rm d}[i] + A_{\rm m}^{-1}(e^{A_{\rm m}T_{\rm s}} - \mathbb{I}_{n_{\rm m}})\left(B_{\rm m}u_{\rm d}[i] + \hat{\sigma}_{\rm d}[i]\right), \quad \hat{x}_{\rm d}[0] = C_{\rm m}^{\dagger}y_0, \\ \hat{y}_{\rm d}[i] =& C_{\rm m}\hat{x}_{\rm d}[i], \end{aligned} \tag{3.9}$$

where $u_{\rm d}(t)$ is provided by (3.8).

Given that $A_{\rm m} \in \mathbb{R}^{n_{\rm m}\times n_{\rm m}}$ is Hurwitz, there exists a positive definite matrix $P \in \mathbb{R}^{n_{\rm m}\times n_{\rm m}}$ solving $A_{\rm m}^{\top}P + PA_{\rm m} = -Q$ for a given positive definite matrix $Q \in \mathbb{R}^{n_{\rm m}\times n_{\rm m}}$. Define

$$\Lambda \triangleq \begin{bmatrix} C_{\rm m} \\ D\sqrt{P} \end{bmatrix}, \tag{3.10}$$

where $\sqrt{P}$ satisfies $P = \sqrt{P}^{\top}\sqrt{P}$, and $D \in \mathbb{R}^{(n_{\rm m}-q)\times n_{\rm m}}$ is a matrix that is in the null space of $C_{\rm m}\left(\sqrt{P}\right)^{-1}$, *i.e.*

$$D\left(C_{\rm m}\left(\sqrt{P}\right)^{-1}\right)^{\top} = 0\,. \tag{3.11}$$

Further, let $\Phi\left(\cdot\right)$ be the $n_{\rm m} \times n_{\rm m}$ matrix

$$\Phi\left(T_{\rm s}\right) \triangleq \int_0^{T_{\rm s}} e^{\Lambda A_{\rm m}\Lambda^{-1}(T_{\rm s}-\tau)}\Lambda d\tau. \tag{3.12}$$

Finally, the adaptation law is given by

$$\hat{\sigma}_{\mathrm{d}}[i] = -\Phi^{-1}\left(T_{\mathrm{s}}\right) e^{\Lambda A_{\mathrm{m}} \Lambda^{-1} T_{\mathrm{s}}} \mathbf{1}_{n_{\mathrm{m}} q} \tilde{y}_{\mathrm{d}}[i], \tag{3.13}$$

where $\tilde{y}_{\mathrm{d}}[i] = \hat{y}_{\mathrm{d}}[i] - y_{\mathrm{d}}[i]$, and $\mathbf{1}_{n_{\mathrm{m}} q}$ is given by

$$\mathbf{1}_{n_{\mathrm{m}} q} \triangleq \begin{bmatrix} \mathbb{I}_q \\ 0_{(n_{\mathrm{m}}-q)\times q} \end{bmatrix} \in \mathbb{R}^{n_{\mathrm{m}} \times q}. \tag{3.14}$$

3.3. Analysis of the Closed-Loop Sampled-Data System

This section provides the analysis of stability and performance of the closed-loop SD system with the proposed controller. Also, the conditions for selection of the control parameters T_{s} and $C(s)$ are provided. First, we define a few variables of interest and design constraints. Let

$$\begin{aligned}
P(s) &\triangleq C_{\mathrm{p}}(s\mathbb{I}_n - A_{\mathrm{p}} + B_{\mathrm{p}}F)^{-1}B_{\mathrm{p}}, \\
H_0(s) &\triangleq (s\mathbb{I}_n - A_{\mathrm{p}} + B_{\mathrm{p}}F)^{-1}B_{\mathrm{p}}, \\
H_1(s) &\triangleq \left(\mathbb{I}_q + \left(M^{-1}(s)P(s) - \mathbb{I}_q\right)C(s)\right)^{-1}, \\
H_2(s) &\triangleq H_0(s) - H_0(s)C(s)H_1(s)\left(M^{-1}(s)P(s) - \mathbb{I}_q\right), \\
H_3(s) &\triangleq H_1(s)M^{-1}(s)P(s), \\
H_4(s) &\triangleq H_1(s)\left(M^{-1}(s)P(s) - \mathbb{I}_q\right), \\
H_5(s) &\triangleq H_0(s)C(s)H_1(s)M^{-1}(s), \\
G(s) &\triangleq H_0(s) - H_5(s)P(s),
\end{aligned} \tag{3.15}$$

where $F \in \mathbb{R}^{q\times n}$ is selected such that $A_{\mathrm{p}} - B_{\mathrm{p}}F$ is Hurwitz, as mentioned in Assumption 3.2. Let $y_0 \triangleq C_{\mathrm{p}}x_0$ be the known initial output. We define an auxiliary system with the same input-output mapping as the system (3.1), using the state-space matrices (A_{m}, B_{m}, C_{m}) of the desired dynamics. The uncertainties are lumped into a variable denoted by $\sigma(t)$ in the auxiliary system. The control input $u(t)$ compensates for the matched uncertainty $\sigma(t)$ to recover the desired output tracking response (introduced in Assumption 3.2). Let the auxiliary system be

$$\begin{aligned}
\dot{x}_{\mathrm{a}}(t) &= A_{\mathrm{m}}x_{\mathrm{a}}(t) + B_{\mathrm{m}}\left(u(t) + \sigma(t)\right), \quad x_{\mathrm{a}}(0) = C_{\mathrm{m}}^{\dagger}y_0, \\
y(t) &= C_{\mathrm{m}}x_{\mathrm{a}}(t),
\end{aligned} \tag{3.16}$$

where $x_{\mathrm{a}}(t) \in \mathbb{R}^{n_{\mathrm{m}}}$ is the state vector, the Laplace transform of $\sigma(t)$ is given by

$$\sigma(s) = M^{-1}(s)\left(\left(P(s) - M(s)\right)u(s) + P(s)w(s) + H_{\mathrm{in}}(s)x_0\right),$$

with

$$H_{\text{in}}(s) \triangleq C_{\text{p}}(s\mathbb{I}_n - A_{\text{p}} + B_{\text{p}}F)^{-1} - C_{\text{m}}\left(s\mathbb{I}_{n_{\text{m}}} - A_{\text{m}}\right)^{-1} C_{\text{m}}^{\dagger} C_{\text{p}},$$

and $w(s)$ is the Laplace transform of $w(t)$, given by

$$w(t) \triangleq Fx(t) + f\left(t, x(t)\right). \tag{3.17}$$

Since the full state measurement is not available, $Fx(t)$ is unknown. Therefore, $Fx(t)$ is added to the uncertainty term $f(t,\, x(t))$, and the addition of the two unknown signals is denoted by $w(t)$.

Remark 3.1. *Given that $M(s)$ does not have an unstable transmission zero, $M^{-1}(s)P(s)$ is proper and stable. In addition, Assumption 3.2 implies that $sM^{-1}(s)H_{\text{in}}(s)$ is proper and stable. Therefore, $\sigma(t)$, defined in* (3.16)*, is a casual signal.*

Further, for every $\delta > 0$, let

$$L_\delta \triangleq \frac{\bar{\gamma}_1 + \delta}{\delta}\left(K_{(\bar{\gamma}_1+\delta)} + \|F\|_\infty\right), \tag{3.18}$$

where K_δ is introduced in Assumption 3.1, and $\bar{\gamma}_1$ is an arbitrarily small positive constant. It can be shown that the following bound on $w(t)$ holds

$$\|w_t\|_{\mathcal{L}_\infty} \leq L_\delta \|x_t\|_{\mathcal{L}_\infty} + L_0. \tag{3.19}$$

The design of the controller proceeds by considering a strictly proper stable transfer function $C(s)$ such that $C(0) = \mathbb{I}_q$. The selection of $C(s)$ must ensure that

$$H_1(s) \quad \text{is stable}, \tag{3.20}$$

where $H_1(s)$ is defined in (3.15), and

$$C(s)M^{-1}(s) \quad \text{is proper}. \tag{3.21}$$

Also, for a given ρ_0, there should exist $\rho_{\text{r}} > \rho_0$ such that the following $\mathcal{L}_1$-norm condition holds

$$\|G(s)\|_{\mathcal{L}_1} < \frac{\rho_{\text{r}} - \rho_1 - \rho_2}{L_{\rho_{\text{r}}}\rho_{\text{r}} + L_0}, \tag{3.22}$$

where

$$\rho_1 \triangleq \left\| s(s\mathbb{I}_n - A_{\text{p}} + B_{\text{p}}F)^{-1} - sH_5(s)H_{\text{in}}(s) \right\|_{\mathcal{L}_1} \rho_0, \quad \rho_2 \triangleq \|H_2(s)K_{\text{g}}\|_{\mathcal{L}_1} M_{\text{r}}. \tag{3.23}$$

Remark 3.2. *If the system with state-space matrices $(A_{\text{p}},\, B_{\text{p}},\, C_{\text{p}})$ does not have a non-minimum-phase transmission zero, one can select the desired system as $M(s) = P(s)$ (as stated in Assumption*

3.2), where $P(s)$ is introduced in (3.15)*. Then, we have $H_1(s) = \mathbb{I}_q$. Also, $G(s)$ can be rewritten as*

$$G(s) = H_0(s)\left(\mathbb{I}_q - C(s)\right). \tag{3.24}$$

Therefore, a filter $C(s)$ with sufficiently high bandwidth and high relative degree, such that $C^{-1}(s)M(s)$ is proper, always satisfies the conditions in (3.20)-(3.22)*. In the case $(A_{\rm p},\, B_{\rm p},\, C_{\rm p})$ defines a non-minimum phase system, the selection of $C(s)$ and $M(s)$ that would verify* (3.20)-(3.22) *is not trivial, as reported in [102].*

Remark 3.3. *The bandwidth of the filter $C(s)$ provides a trade-off between performance in terms of disturbance compensation and robustness in terms of input-delay margin. A mixed-norm optimization of the filter for $\mathcal{L}_1$ adaptive control structure can be found in [103]. More results on filter design are provided in [100, 104–107].*

Let $P_1 \in \mathbb{R}^{q\times q}$ and $P_2 \in \mathbb{R}^{(n_{\rm m}-q)\times(n_{\rm m}-q)}$ be positive definite matrices:

$$P_1 \triangleq \left(C_{\rm m}\sqrt{P}^{-1}\sqrt{P}^{-\top}C_{\rm m}^{\top}\right)^{-1}, \quad P_2 \triangleq (DD^{\top})^{-1}. \tag{3.25}$$

Define

$$\left[\begin{array}{cc} \eta_1^{\top}(t) & \eta_2^{\top}(t) \end{array}\right] \triangleq \mathbf{1}_{n_{\rm m}q}^{\top} e^{\Lambda A_{\rm m}\Lambda^{-1}t}, \tag{3.26}$$

where $\eta_1(t) \in \mathbb{R}^{q\times q}$ and $\eta_2(t) \in \mathbb{R}^{(n_{\rm m}-q)\times q}$, and

$$\kappa(T_{\rm s}) \triangleq \int_0^{T_{\rm s}} \left\| \mathbf{1}_{n_{\rm m}q}^{\top} e^{\Lambda A_{\rm m}\Lambda^{-1}(T_{\rm s}-\tau)}\Lambda B_{\rm m}\right\|_2 d\tau. \tag{3.27}$$

Define the function

$$\Gamma\left(T_{\rm s}\right) \triangleq \alpha_1(T_{\rm s})\left\|(s\mathbb{I}_v - A_{\rm o})^{-1}B_{\rm o}\right\|_{\mathcal{L}_1} + \alpha_2(T_{\rm s}), \tag{3.28}$$

where

$$\alpha_1(T_{\rm s}) \triangleq \max_{t\in[0,\,T_{\rm s}]} \left\|C_{\rm o}\left(e^{A_{\rm o}t} - \mathbb{I}_v\right)\right\|_{\infty}, \quad \alpha_2(T_{\rm s}) \triangleq \max_{t\in[0,\,T_{\rm s}]} \int_0^t \left\|C_{\rm o}e^{A_{\rm o}(t-\tau)}B_{\rm o}\right\|_{\infty} d\tau.$$

Let

$$
\begin{aligned}
\Upsilon(T_{\rm s}) =&\left\|e^{-A_{\rm m}T_{\rm s}}\Phi^{-1}\left(T_{\rm s}\right)e^{\Lambda A_{\rm m}\Lambda^{-1}T_{\rm s}}\mathbf{1}_{n_{\rm m}q}\right\|_{\infty},\\
\Psi\left(T_{\rm s}\right) =&\left\|H_5(s)C_{\rm m}(s\mathbb{I}_{n_{\rm m}}-A_m)^{-1}\left(e^{A_{\rm m}T_{\rm s}}-\mathbb{I}_{n_{\rm m}}\right)\right\|_{\mathcal{L}_1},\\
\Omega_1(T_{\rm s}) =&\left(\left\|H_2(s)C(s)M^{-1}(s)\right\|_{\mathcal{L}_1}+\|H_2(s)\|_{\mathcal{L}_1}\left(\Gamma\left(T_{\rm s}\right)+\Psi\left(T_{\rm s}\right)\right)\Upsilon\left(T_{\rm s}\right)\right)\left(1-\|G(s)\|_{\mathcal{L}_1}L_{\rho_{\rm r}}\right)^{-1},\\
\Theta(T_{\rm s}) =&\|H_3(s)\|_{\mathcal{L}_1}L_{\rho_{\rm r}}\Omega_1(T_{\rm s})+\left\|H_4(s)C(s)M^{-1}(s)\right\|_{\mathcal{L}_1}+\|H_4(s)\|_{\mathcal{L}_1}\left(\Gamma\left(T_{\rm s}\right)+\Psi\left(T_{\rm s}\right)\right)\Upsilon\left(T_{\rm s}\right),\\
\rho_{\Delta} =&\|H_3(s)\|_{\mathcal{L}_1}\left(L_{\rho_{\rm r}}\rho_{\rm r}+L_0\right)+\|H_4(s)K_{\rm g}\|_{\mathcal{L}_1}M_{\rm r}+\left\|sH_1(s)M^{-1}(s)H_{\rm in}(s)\right\|_{\mathcal{L}_1}\rho_0,\\
\Omega_2(T_{\rm s}) =&\left\|C(s)M^{-1}(s)\right\|_{\mathcal{L}_1}+\|C(s)\|_{\mathcal{L}_1}L_{\rho_{\rm r}}\Omega_1(T_{\rm s})+\left(\Gamma\left(T_{\rm s}\right)+\Psi\left(T_{\rm s}\right)\right)\Upsilon\left(T_{\rm s}\right),\\
\rho_{\rm ur} =&\|C(s)H_3(s)\|_{\mathcal{L}_1}\left(L_{\rho_{\rm r}}\rho_{\rm r}+L_0\right)+\left\|sC(s)H_1(s)M^{-1}(s)H_{\rm in}(s)\right\|_{\mathcal{L}_1}\rho_0+\|(\mathbb{I}_q-C(s)H_4(s))K_{\rm g}\|_{\mathcal{L}_1}M_{\rm r},
\end{aligned}
\tag{3.29}
$$

where $H_i(\cdot)$'s are defined in (3.15). Next, we introduce the functions

$$
\beta_1(T_{\rm s})\triangleq\max_{t\in[0,\,T_{\rm s}]}\|\eta_1(t)\|_2\,,\quad \beta_2(T_{\rm s})\triangleq\max_{t\in[0,\,T_{\rm s}]}\|\eta_2(t)\|_2\,,
\tag{3.30}
$$

where $\eta_1(t)$ and $\eta_2(t)$ are given in (3.26). Also

$$
\beta_3(T_{\rm s})\triangleq\max_{t\in[0,\,T_{\rm s}]}\eta_3(t,T_{\rm s}),\quad \beta_4(T_{\rm s})\triangleq\max_{t\in[0,\,T_{\rm s}]}\eta_4(t),
\tag{3.31}
$$

where

$$
\begin{aligned}
\eta_3(t,T_{\rm s})&\triangleq\int_0^t\left\|\mathbf{1}_{n_{\rm m}q}^{\top}e^{\Lambda A_{\rm m}\Lambda^{-1}(t-\tau)}\Lambda\Phi^{-1}\left(T_{\rm s}\right)e^{\Lambda A_{\rm m}\Lambda^{-1}T_{\rm s}}\mathbf{1}_{n_{\rm m}q}\right\|_2 d\tau,\\
\eta_4(t)&\triangleq\int_0^t\left\|\mathbf{1}_{n_{\rm m}q}^{\top}e^{\Lambda A_{\rm m}\Lambda^{-1}(t-\tau)}\Lambda B_{\rm m}\right\|_2 d\tau.
\end{aligned}
\tag{3.32}
$$

For $\bar{\gamma}_0>0$, let

$$
\begin{aligned}
\Delta_1(\bar{\gamma}_0)\triangleq&\rho_{\Delta}+\Theta(T_{\rm s})\bar{\gamma}_0,\\
\Delta_2(\bar{\gamma}_0)\triangleq&\lambda_{\max}\left(\Lambda^{-\top}P\Lambda^{-1}\right)\left(\frac{2\sqrt{q}\Delta_1(\bar{\gamma}_0)\left\|\Lambda^{-\top}PB_{\rm m}\right\|_2}{\lambda_{\min}\left(\Lambda^{-\top}Q\Lambda^{-1}\right)}\right)^2,
\end{aligned}
\tag{3.33}
$$

where, ρ_{Δ} and $\Theta(\cdot)$ are defined in (3.29). Also, let

$$
\varsigma(\bar{\gamma}_0,T_{\rm s})\triangleq\left\|\eta_2\left(T_{\rm s}\right)\right\|_2\sqrt{\frac{\Delta_2(\bar{\gamma}_0)}{\lambda_{\max}(P_2)}}+\sqrt{q}\kappa(T_{\rm s})\Delta_1(\bar{\gamma}_0),
\tag{3.34}
$$

where $\eta_2(\cdot)$ is defined in (3.26) and $\kappa(\cdot)$ is given in (3.27).

Finally, define

$$
\gamma_0(\bar{\gamma}_0,T_{\rm s})\triangleq\beta_1(T_{\rm s})\varsigma(\bar{\gamma}_0,T_{\rm s})+\beta_2(T_{\rm s})\sqrt{\frac{\Delta_2(\bar{\gamma}_0)}{\lambda_{\max}(P_2)}}+\beta_3(T_{\rm s})\varsigma(\bar{\gamma}_0,T_{\rm s})+\sqrt{q}\beta_4(T_{\rm s})\Delta_1(\bar{\gamma}_0).
\tag{3.35}
$$

Lemma 3.1. *For all $\bar{\gamma}_0 > 0$, the following relationships hold:*

$$\lim_{T_\mathrm{s}\to 0} \gamma_0(\bar{\gamma}_0, T_\mathrm{s}) = 0, \tag{3.36}$$

where $\gamma_0(\cdot,\cdot)$ is given in (3.35).

Proof. It is similar to the proof of Lemma 3.3.1 in [47] and hence omitted here. ■

Lemma 3.2. *There exist $T_\mathrm{s} > 0$ and arbitrarily small positive constant $\bar{\gamma}_0$, such that*

$$\gamma_0(\bar{\gamma}_0, T_\mathrm{s}) < \bar{\gamma}_0, \quad \Omega_1(T_\mathrm{s})\bar{\gamma}_0 < \bar{\gamma}_1, \tag{3.37}$$

where $\bar{\gamma}_1$ is introduced in (3.18) *and $\gamma_0(\cdot,\cdot)$ is defined in* (3.35)*, while $\Omega_1(\cdot)$ is given in* (3.29).

Proof. It is straightforward to verify that $\Omega_1(T_\mathrm{s})$ is a bounded function as T_s tends to zero. In addition, Lemma 3.1 shows that $\gamma_0(\bar{\gamma}_0, T_\mathrm{s})$ approaches arbitrarily closely to zero for all $\bar{\gamma}_0$ with sufficiently small T_s. Therefore, there always exist constants T_s and $\bar{\gamma}_0$ that satisfy the inequalities in (3.37).

Lemma 3.3. *For arbitrary $\xi = \begin{bmatrix} y \\ z \end{bmatrix} \in \mathbb{R}^{n_\mathrm{m}}$, where $y \in \mathbb{R}^q$ and $z \in \mathbb{R}^{(n_\mathrm{m}-q)}$, there exist positive definite $P_1 \in \mathbb{R}^{q\times q}$ and $P_2 \in \mathbb{R}^{(n_\mathrm{m}-q)\times(n_\mathrm{m}-q)}$, such that*

$$\xi^\top \left(\Lambda^{-1}\right)^\top P \Lambda^{-1} \xi = y^\top P_1 y + z^\top P_2 z, \tag{3.38}$$

where Λ is given in (3.10)*, and P_1 and P_2 are defined in* (3.25).

Proof. The proof of Lemma 3.3 is given in [47].

Consider the following closed-loop reference system

$$\begin{aligned} \dot{x}_\mathrm{ref}(t) &= A_\mathrm{p} x_\mathrm{ref}(t) + B_\mathrm{p}\left(u_\mathrm{ref}(t) + f\left(t, x_\mathrm{ref}(t)\right)\right), \quad x_\mathrm{ref}(0) = x_0 \\ u_\mathrm{ref}(s) &= K_\mathrm{g} r(s) - C(s)\sigma_\mathrm{ref}(s), \\ y_\mathrm{ref}(t) &= C_\mathrm{p} x_\mathrm{ref}(t), \end{aligned} \tag{3.39}$$

where

$$\begin{aligned} \sigma_\mathrm{ref}(s) =& \left[\left(P(s) - M(s)\right)C(s) + M(s)\right]^{-1}\left(P(s) - M(s)\right)K_\mathrm{g} r(s) \\ &+ \left[\left(P(s) - M(s)\right)C(s) + M(s)\right]^{-1}\left(P(s) w_\mathrm{ref}(s) + H_\mathrm{in}(s) x_0\right), \end{aligned} \tag{3.40}$$

and $w_\mathrm{ref}(s)$ is the Laplace transform of $w_\mathrm{ref}(t)$ given by

$$w_\mathrm{ref}(t) = F x_\mathrm{ref}(t) + f\left(t, x_\mathrm{ref}(t)\right). \tag{3.41}$$

The reference system can be rewritten as

$$y_{\rm ref}(s) = M(s)K_{\rm g}r(s) + M(s)\left(\mathbb{I}_q - C(s)\right)\sigma_{\rm ref}(s) + C_{\rm m}\left(s\mathbb{I}_q - A_{\rm m}\right)^{-1}C_{\rm m}^{\dagger}y_0. \tag{3.42}$$

From (3.42), we notice that the unknown uncertainty $\sigma_{\rm ref}(t)$, given by the Laplace transform in (3.40), is mitigated within the bandwidth of $C(s)$, and the desired response (in Assumption 3.2) is recovered. The reference system in (3.39) defines the *achievable performance* by the closed-loop sampled-data system given in (3.1), (3.8)-(3.13), as the sampling time $T_{\rm s}$ of the digital controller tends to zero. In the following, it is first proven that $\sigma_{\rm ref}(t)$ is bounded, and the reference system in (3.39) is stable. Then, we establish uniform bounds between the closed-loop system defined by (3.1), (3.8)-(3.13), and the reference system.

Lemma 3.4. *For the closed-loop reference system in* (3.39)*, subject to the conditions in* (3.20)-(3.22)*, if* $\|x_0\|_\infty \leq \rho_0$*, then*

$$\|x_{\rm ref}\|_{\mathcal{L}_\infty} < \rho_{\rm r}, \tag{3.43}$$

$$\|u_{\rm ref}\|_{\mathcal{L}_\infty} < \rho_{\rm ur}, \tag{3.44}$$

where $\rho_{\rm r}$ *is introduced in* (3.22)*, and* $\rho_{\rm ur}$ *is given in* (3.29)*.*

Proof. It follows from (3.39) and the definitions of $H_0(s)$, $H_5(s)$, $P(s)$ and $G(s)$ in (3.15) that

$$x_{\rm ref}(s) = \left[H_0(s) - H_5(s)\left(P(s) - M(s)\right)\right]K_{\rm g}r(s) + G(s)w_{\rm ref}(s) - H_5(s)H_{\rm in}(s)x_0 + \left(s\mathbb{I}_n - A_{\rm p} + B_{\rm p}F\right)^{-1}x_0. \tag{3.45}$$

Then for $\tau > 0$ the following upper bound can be established

$$\begin{aligned}\|x_{{\rm ref}\tau}\|_{\mathcal{L}_\infty} \leq & \|G(s)\|_{\mathcal{L}_1}\|w_{{\rm ref}\tau}\|_{\mathcal{L}_\infty} + \|H_2(s)K_{\rm g}\|_{\mathcal{L}_1}\|r\|_{\mathcal{L}_\infty} \\ & + \left\|s(s\mathbb{I}_n - A_{\rm p} + B_{\rm p}F)^{-1} - sH_5(s)H_{\rm in}(s)\right\|_{\mathcal{L}_1}\left\|\frac{1}{s}x_0\right\|_{\mathcal{L}_\infty}.\end{aligned} \tag{3.46}$$

We have $\|x_{\rm ref}(0)\|_\infty = \|x_0\|_\infty < \rho_{\rm r}$. In addition, $x_{\rm ref}(t)$ is continuous. Therefore, if the bound in (3.43) is not true, there exists a time $\tau_1 > 0$ such that

$$\|x_{\rm ref}(t)\|_\infty < \rho_{\rm r}, \quad \forall t \in [0,\, \tau_1), \quad \|x_{\rm ref}(\tau_1)\|_\infty = \rho_{\rm r},$$

which implies that $\left\|x_{{\rm ref}\tau_1}\right\|_{\mathcal{L}_\infty} = \rho_{\rm r}$. Then it follows from Assumption 3.1 and the redefinition in (3.18) that

$$\left\|w_{{\rm ref}\tau_1}\right\|_{\mathcal{L}_\infty} \leq L_{\rho_{\rm r}}\left\|x_{{\rm ref}\tau_1}\right\|_{\mathcal{L}_\infty} + L_0. \tag{3.47}$$

The bound in (3.47), together with the upper bound in (3.46), lead to

$$\left\|x_{{\rm ref}\tau_1}\right\|_{\mathcal{L}_\infty} \leq \frac{\|G(s)\|_{\mathcal{L}_1}L_0 + \rho_1 + \rho_2}{1 - \|G(s)\|_{\mathcal{L}_1}L_{\rho_{\rm r}}}.$$

The condition in (3.22) can be solved for ρ_{r} to obtain the bound

$$\rho_{\mathrm{r}} > \tfrac{\|G(s)\|_{\mathcal{L}_1} L_0 + \rho_1 + \rho_2}{1 - \|G(s)\|_{\mathcal{L}_1} L_{\rho_{\mathrm{r}}}},$$

which leads to $\left\|x_{\mathrm{ref}\tau_1}\right\|_{\mathcal{L}_\infty} < \rho_{\mathrm{r}}$. This contradicts $\left\|x_{\mathrm{ref}\tau_1}\right\|_{\mathcal{L}_\infty} = \rho_{\mathrm{r}}$, thus proving the bound in (3.43). This further implies that the upper bound in (3.47) holds for all $\tau_1 > 0$ with strict inequality, which in turn implies that

$$\|w_{\mathrm{ref}}\|_{\mathcal{L}_\infty} < L_{\rho_{\mathrm{r}}} \rho_{\mathrm{r}} + L_0. \tag{3.48}$$

The bound on $u_{\mathrm{ref}}(t)$ follows from (3.39), (3.40), and (3.48), which proves (3.44). ■

Remark 3.4. *We can rewrite* $\sigma_{\mathrm{ref}}(s)$ *in* (3.40) *as*

$$\sigma_{\mathrm{ref}}(s) = H_1(s)\left(M^{-1}(s)P(s) - \mathbb{I}_q\right) K_{\mathrm{g}} r(s) + H_1(s)\left(M^{-1}(s)P(s)w_{\mathrm{ref}}(s) + M^{-1}(s)H_{\mathrm{in}}(s)x_0\right).$$

Then Remark 3.1 implies that $\sigma_{\mathrm{ref}}(s)$ *is casual. In addition, the stability of* $H_1(s)$ *in* (3.20) *together with the results of Lemma 3.4 imply that* $\sigma_{\mathrm{ref}}(s)$ *is bounded:*

$$\|\sigma_{\mathrm{ref}}\|_{\mathcal{L}_\infty} \leq \rho_\Delta, \tag{3.49}$$

where ρ_Δ *is defined in* (3.29)*.*

In the proposed SD control structure, discrete-time output predictor dynamics are introduced in (3.9), where the unknown uncertainty $\sigma(t)$ (formulated in (3.16)) is replaced with an adaptation variable $\hat{\sigma}_{\mathrm{d}}[i]$. We consider a continuous-time equivalent state-space model of the predictor dynamics in (3.9), given by

$$\begin{aligned} \dot{\hat{x}}(t) &= A_{\mathrm{m}}\hat{x}(t) + B_{\mathrm{m}}u(t) + \hat{\sigma}(t), \quad \hat{x}(0) = C_{\mathrm{m}}^{\dagger}x_0, \\ \hat{y}(t) &= C_{\mathrm{m}}\hat{x}(t), \end{aligned} \tag{3.50}$$

where

$$\hat{\sigma}(t) = \hat{\sigma}_{\mathrm{d}}[i], \quad t \in [iT_{\mathrm{s}},\ (i+1)T_{\mathrm{s}}), \quad i \in \mathbb{Z}_{\geq 0}, \tag{3.51}$$

and $u(t)$ is given in (3.2) and (3.8). Since $\hat{\sigma}(t)$ and $u(t)$ in (3.50) are held constant over sampling intervals, we notice that (3.9) is a step-invariant discrete-time approximation of (3.50), such that

$$\hat{y}\left(iT_{\mathrm{s}}\right) = \hat{y}_{\mathrm{d}}[i]. \tag{3.52}$$

Let $\tilde{x}(t) = \hat{x}(t) - x_{\mathrm{a}}(t)$, where $x_{\mathrm{a}}(t)$ is defined in (3.16). Then the prediction error dynamics between (3.16) and (3.50) are given by

$$\begin{aligned} \dot{\tilde{x}}(t) &= A_{\mathrm{m}}\tilde{x}(t) + \hat{\sigma}(t) - B_{\mathrm{m}}\sigma(t), \quad \tilde{x}(0) = 0_{n_{\mathrm{m}}\times 1}, \\ \tilde{y}(t) &= C_{\mathrm{m}}\tilde{x}(t), \end{aligned} \tag{3.53}$$

where $\hat{\sigma}(t)$ is defined in (3.51).

Lemma 3.5. *Consider the closed-loop system defined by* (3.1), (3.8)-(3.13), *and the closed-loop reference system in* (3.39). *The following upper bound holds*

$$\|(x_{\mathrm{ref}} - x)_t\|_{\mathcal{L}_\infty} \leq \Omega_1(T_{\mathrm{s}})\|\tilde{y}_t\|_{\mathcal{L}_\infty},$$

where $\Omega_1(\cdot)$ *is given in* (3.29), *and* $\tilde{y}(t)$ *is the prediction error defined in* (3.53).

Proof. Let

$$u_{\mathrm{C}}(s) = K_{\mathrm{g}} r(s) - C(s)M^{-1}(s)C_{\mathrm{m}}(s\mathbb{I}_{n_{\mathrm{m}}} - A_{\mathrm{m}})^{-1}\hat{\sigma}(s), \tag{3.54}$$

$$u_{\mathrm{M}}(s) = K_{\mathrm{g}} r(s) - C(s)M^{-1}(s)C_{\mathrm{m}}(s\mathbb{I}_{n_{\mathrm{m}}} - A_{\mathrm{m}})^{-1}e^{-A_{\mathrm{m}}T_{\mathrm{s}}}\hat{\sigma}(s). \tag{3.55}$$

It follows from (3.53) that

$$\tilde{y}(s) = -M(s)\sigma(s) + C_{\mathrm{m}}(s\mathbb{I}_{n_{\mathrm{m}}} - A_{\mathrm{m}})^{-1}\hat{\sigma}(s). \tag{3.56}$$

Letting $e(t) \triangleq x_{\mathrm{ref}}(t) - x(t)$ and denoting by $d_{\mathrm{e}}(s)$ the Laplace transform of

$$d_{\mathrm{e}}(t) \triangleq w_{\mathrm{ref}}(t) - w(t), \tag{3.57}$$

from (3.1), (3.17), (3.8), (3.39), (3.54), (3.55), and (3.56) it follows that

$$\begin{aligned} e(s) =& H_0(s)C(s)M^{-1}(s)\tilde{y}(s) + H_0(s)d_{\mathrm{e}}(s) + H_0(s)\left(u_{\mathrm{C}}(s) - u_{\mathrm{M}}(s)\right) + H_0(s)\left(u_{\mathrm{M}}(s) - u(s)\right) \\ & - H_0(s)C(s)\left(\sigma_{\mathrm{ref}}(s) - \sigma(s)\right), \end{aligned} \tag{3.58}$$

where $H_0(s)$ is defined in (3.15). Further

$$\begin{aligned} & H_0(s)C(s)\left(\sigma_{\mathrm{ref}}(s) - \sigma(s)\right) = H_5(s)P(s)d_{\mathrm{e}}(s) - H_5(s)\left(P(s) - M(s)\right)\left(u_{\mathrm{C}}(s) - u_{\mathrm{M}}(s)\right) \\ & -H_5(s)\left(P(s) - M(s)\right)\left(u_{\mathrm{M}}(s) - u(s)\right) + H_5(s)\left(P(s) - M(s)\right)C(s)M^{-1}(s)\tilde{y}(s). \end{aligned} \tag{3.59}$$

From (3.58) and (3.59) one can obtain

$$\begin{aligned} e(s) =& \left(H_0(s) - H_5(s)\left(P(s) - M(s)\right)\right)C(s)M^{-1}(s)\tilde{y}(s) + \left(H_0(s) - H_5(s)\left(P(s) - M(s)\right)\right)\left(u_{\mathrm{C}}(s) - u_{\mathrm{M}}(s)\right) \\ & + \left(H_0(s) - H_5(s)\left(P(s) - M(s)\right)\right)\left(u_{\mathrm{M}}(s) - u(s)\right) + \left(H_0(s) - H_5(s)P(s)\right)d_{\mathrm{e}}(s). \end{aligned} \tag{3.60}$$

Then the upper bound is given by

$$\begin{aligned} & \|e_t\|_{\mathcal{L}_\infty} \leq \\ & \left\|\left(H_0(s) - H_5(s)\left(P(s) - M(s)\right)\right)C(s)M^{-1}(s)\right\|_{\mathcal{L}_1}\|\tilde{y}_t\|_{\mathcal{L}_\infty} + \|\left(H_0(s) - H_5(s)\left(P(s) - M(s)\right)\right)\|_{\mathcal{L}_1}\left\|\left(u_{\mathrm{C}} - u_{\mathrm{M}}\right)_t\right\|_{\mathcal{L}_\infty} \\ & + \|\left(H_0(s) - H_5(s)\left(P(s) - M(s)\right)\right)\|_{\mathcal{L}_1}\left\|\left(u_{\mathrm{M}} - u\right)_t\right\|_{\mathcal{L}_\infty} + \|G(s)\|_{\mathcal{L}_1}L_{\rho_{\mathrm{r}}}\|e_t\|_{\mathcal{L}_\infty}. \end{aligned} \tag{3.61}$$

From (3.52) we have

$$\tilde{y}\left(iT_{\mathrm{s}}\right) = \tilde{y}_{\mathrm{d}}[i], \quad i \in \mathbb{Z}_{\geq 0}. \tag{3.62}$$

From (3.13), (3.51) and (3.62) the following relation follows

$$\left\|e^{-A_{\mathrm{m}}T_{\mathrm{s}}}\hat{\sigma}_t\right\|_{\mathcal{L}_\infty} \leq \Upsilon\left(T_{\mathrm{s}}\right)\left\|\tilde{y}_t\right\|_{\mathcal{L}_\infty}, \tag{3.63}$$

where $\Upsilon(\cdot)$ is defined in (3.29). Notice that $u_{\mathrm{d}}[i]$ given in (3.8) is a step-invariant discrete-time approximation of $u_{\mathrm{M}}(s)$, given in (3.55). Therefore, the discretization error bound between (3.2) and (3.55) is given by

$$\left\|(u_{\mathrm{M}}-u)_t\right\|_{\mathcal{L}_\infty} \leq \Gamma\left(T_{\mathrm{s}}\right)\Upsilon\left(T_{\mathrm{s}}\right)\left\|\tilde{y}_t\right\|_{\mathcal{L}_\infty}, \tag{3.64}$$

where $\Gamma(\cdot)$ is introduced in (3.28). Moreover, from (3.54), (3.55) and (3.63) one can obtain

$$\left\|(u_{\mathrm{C}}-u_{\mathrm{M}})_t\right\|_{\mathcal{L}_\infty} \leq \Psi\left(T_{\mathrm{s}}\right)\Upsilon\left(T_{\mathrm{s}}\right)\left\|\tilde{y}_t\right\|_{\mathcal{L}_\infty}, \tag{3.65}$$

where $\Psi(\cdot)$ is defined in (3.29). From (3.61), (3.64) and (3.65) the following upper bound follows

$$\left\|e_t\right\|_{\mathcal{L}_\infty} \leq \Omega_1(T_{\mathrm{s}})\left\|\tilde{y}_t\right\|_{\mathcal{L}_\infty}. \tag{3.66}$$

This concludes the proof. ■

Theorem 3.1. *Consider the system in* (3.1) *and the controller in* (3.8)-(3.13)*, subject to the conditions in* (3.20)-(3.22)*. Assume that* T_{s} *is selected sufficiently small such that the inequalities in* (3.37) *hold. If* $\|x_0\|_\infty \leq \rho_0$*, then*

$$\left\|\tilde{y}\right\|_{\mathcal{L}_\infty} < \bar{\gamma}_0, \tag{3.67}$$

$$\left\|x_{\mathrm{ref}}-x\right\|_{\mathcal{L}_\infty} < \Omega_1(T_{\mathrm{s}})\bar{\gamma}_0, \quad \left\|u_{\mathrm{ref}}-u\right\|_{\mathcal{L}_\infty} < \Omega_2(T_{\mathrm{s}})\bar{\gamma}_0, \tag{3.68}$$

where $\tilde{y}(t)$ *is the prediction error defined in* (3.53)*, and* $\bar{\gamma}_0 > 0$ *is a given arbitrarily small constant that satisfies* (3.37)*. Also,* $\Omega_1(T_{\mathrm{s}})$ *and* $\Omega_2(T_{\mathrm{s}})$ *are defined in* (3.29)*.*

Proof. Let $\bar{\gamma}_0$ be a constant that satisfies (3.37). First, we prove the bound in (3.67) by a contradiction argument. Since $\tilde{y}(0)=0$, and $\tilde{y}(t)$ is continuous, then assuming the opposite implies that there exists τ_1 such that

$$\begin{aligned} \left\|\tilde{y}(t)\right\|_\infty &< \bar{\gamma}_0, \quad \forall\, 0 \leq t < \tau_1, \\ \left\|\tilde{y}(\tau_1)\right\|_\infty &= \bar{\gamma}_0, \end{aligned} \tag{3.69}$$

which leads to

$$\left\|\tilde{y}_{\tau_1}\right\|_{\mathcal{L}_\infty} = \bar{\gamma}_0. \tag{3.70}$$

Let $e(t) \triangleq x_{\mathrm{ref}}(t)-x(t)$. The sampling time T_{s} is selected such that the inequalities in (3.37) hold. Then the bound in (3.37), Lemma 3.5 and the upper bound in (3.43) can be used to derive the

following bound

$$\|x_{\tau_1}\|_{\mathcal{L}_\infty} \leq \left\|x_{\mathrm{ref}_{\tau_1}}\right\|_{\mathcal{L}_\infty} + \|e_{\tau_1}\|_{\mathcal{L}_\infty} < \rho_r + \bar{\gamma}_1, \tag{3.71}$$

which implies

$$\|w_{\tau_1}\|_{\mathcal{L}_\infty} \leq L_{\rho_\mathrm{r}}\rho_\mathrm{r} + L_0. \tag{3.72}$$

Then one can obtain from (3.40) that

$$\left\|\sigma_{\mathrm{ref}_{\tau_1}}\right\|_{\mathcal{L}_\infty} \leq \rho_\Delta, \tag{3.73}$$

where ρ_Δ is defined in (3.29). Also, we have

$$\sigma_{\mathrm{ref}}(s) - \sigma(s) = H_3(s)d_\mathrm{e}(s) - H_4(s)\left(u_\mathrm{M}(s) - u(s)\right) - H_4(s)\left(u_\mathrm{C}(s) - u_\mathrm{M}(s)\right) + H_4(s)C(s)M^{-1}(s)\tilde{y}(s), \tag{3.74}$$

which along with (3.73) implies

$$\|\sigma_{\tau_1}\|_{\mathcal{L}_\infty} \leq \Delta_1(\bar{\gamma}_0), \tag{3.75}$$

where $\Delta(\cdot)$ is defined in (3.33).

Now, consider the state transformation

$$\tilde{\xi} = \Lambda\tilde{x}, \tag{3.76}$$

where Λ is defined in (3.10), and $\tilde{x}(t) = \hat{x}(t) - x_\mathrm{a}(t)$. From (3.53) and (3.76) it follows

$$\begin{aligned} \dot{\tilde{\xi}}(t) &= \Lambda A_\mathrm{m}\Lambda^{-1}\tilde{\xi}(t) + \Lambda\hat{\sigma}(t) - \Lambda B_\mathrm{m}\sigma(t), \quad \tilde{\xi}(0) = 0_{n_\mathrm{m}\times 1} \\ \tilde{y}(t) &= \mathbf{1}_{n_\mathrm{m}q}\tilde{\xi}(t). \end{aligned} \tag{3.77}$$

From (3.77) we have

$$\tilde{\xi}\left(iT_\mathrm{s}+t\right) = e^{\Lambda A_\mathrm{m}\Lambda^{-1}t}\tilde{\xi}\left(iT_\mathrm{s}\right) + \int_0^t e^{\Lambda A_\mathrm{m}\Lambda^{-1}(t-\tau)}\Lambda\left(\hat{\sigma}\left(iT_\mathrm{s}\right) - B_\mathrm{m}\sigma\left(iT_\mathrm{s}+\tau\right)\right)d\tau. \tag{3.78}$$

Since

$$\tilde{\xi}\left(iT_\mathrm{s}+t\right) = \begin{bmatrix} \tilde{y}(iT_\mathrm{s}+t) \\ 0_{(n_\mathrm{m}-q)\times 1} \end{bmatrix} + \begin{bmatrix} 0_{q\times 1} \\ \tilde{z}(iT_\mathrm{s}+t) \end{bmatrix},$$

where $\tilde{z}(t) = \left[\tilde{\xi}_{q+1}(t),\, ...,\, \tilde{\xi}_{n_\mathrm{m}}(t)\right]^\top$, $\tilde{\xi}(iT_\mathrm{s}+t)$ can be decomposed as

$$\tilde{\xi}\left(iT_\mathrm{s}+t\right) = \chi\left(iT_\mathrm{s}+t\right) + \zeta\left(iT_\mathrm{s}+t\right), \tag{3.79}$$

such that

$$\chi\left(iT_{\mathrm{s}}+t\right)=e^{\Lambda A_{\mathrm{m}}\Lambda^{-1}t}\left[\begin{array}{c}\tilde{y}\left(iT_{\mathrm{s}}\right)0_{(n_{\mathrm{m}}-q)\times 1}\end{array}\right]+\int_{0}^{t}e^{\Lambda A_{\mathrm{m}}\Lambda^{-1}(t-\tau)}\Lambda\hat{\sigma}\left(jT_{\mathrm{s}}\right)d\tau, \tag{3.80}$$

$$\zeta\left(iT_{\mathrm{s}}+t\right)=e^{\Lambda A_{\mathrm{m}}\Lambda^{-1}t}\left[\begin{array}{c}0_{q\times 1}\\ \tilde{z}(iT_{\mathrm{s}})\end{array}\right]-\int_{0}^{t}e^{\Lambda A_{\mathrm{m}}\Lambda^{-1}(t-\tau)}\Lambda B_{\mathrm{m}}\sigma\left(iT_{\mathrm{s}}+\tau\right)d\tau. \tag{3.81}$$

Now we prove that

$$\begin{array}{c}\left\|\tilde{y}\left(iT_{\mathrm{s}}\right)\right\|_{2}\leq\varsigma(\bar{\gamma}_{0},T_{\mathrm{s}}),\\ \tilde{z}^{\top}\left(iT_{\mathrm{s}}\right)P_{2}\tilde{z}\left(iT_{\mathrm{s}}\right)\leq\Delta_{2}(\bar{\gamma}_{0}),\quad\forall iT_{\mathrm{s}}\leq\tau_{1},\end{array} \tag{3.82}$$

where $\Delta(\cdot)$ and $\varsigma(\cdot,\,\cdot)$ are defined in (3.33) and (3.34), respectively. It is straightforward to show that $\|\tilde{y}(0)\|_{2}\leq\varsigma(\bar{\gamma}_{0},T_{\mathrm{s}})$, $\tilde{z}^{\top}(0)P_{2}\tilde{z}(0)\leq\Delta_{2}(\bar{\gamma}_{0})$. Next, for arbitrary $k\in\mathbb{Z}_{\geq 0}$, such that $(k+1)T_{\mathrm{s}}\leq\tau_{1}$, we prove that if

$$\left\|\tilde{y}\left(kT_{\mathrm{s}}\right)\right\|_{2}\leq\varsigma(\bar{\gamma}_{0},T_{\mathrm{s}}), \tag{3.83}$$

$$\tilde{z}^{\top}\left(kT_{\mathrm{s}}\right)P_{2}\tilde{z}\left(kT_{\mathrm{s}}\right)\leq\Delta_{2}(\bar{\gamma}_{0}), \tag{3.84}$$

then the inequalities in (3.83)-(3.84) hold for $k+1$ as well, which would imply that the bounds in (3.83)-(3.84) hold for all $k\in\mathbb{Z}_{\geq 0}$, such that $kT_{\mathrm{s}}\leq\tau_{1}$. To this end, suppose that (3.83) and (3.84) hold for $k\in\mathbb{Z}_{\geq 0}$, and in addition that $(k+1)T_{\mathrm{s}}\leq\tau_{1}$. Then it follows from (3.79) that

$$\tilde{\xi}\left((k+1)T_{\mathrm{s}}\right)=\chi\left((k+1)T_{\mathrm{s}}\right)+\zeta\left((k+1)T_{\mathrm{s}}\right), \tag{3.85}$$

where

$$\chi\left((k+1)T_{\mathrm{s}}\right)=e^{\Lambda A_{\mathrm{m}}\Lambda^{-1}T_{\mathrm{s}}}\left[\begin{array}{c}\tilde{y}(kT_{\mathrm{s}})\\ 0_{(n_{\mathrm{m}}-q)\times 1}\end{array}\right]+\int_{0}^{T_{\mathrm{s}}}e^{\Lambda A_{\mathrm{m}}\Lambda^{-1}(T_{\mathrm{s}}-\tau)}\Lambda\hat{\sigma}\left(kT_{\mathrm{s}}\right)d\tau, \tag{3.86}$$

$$\zeta\left((k+1)T_{\mathrm{s}}\right)=e^{\Lambda A_{\mathrm{m}}\Lambda^{-1}T_{\mathrm{s}}}\left[\begin{array}{c}0_{q\times 1}\\ \tilde{z}(kT_{\mathrm{s}})\end{array}\right]-\int_{0}^{T_{\mathrm{s}}}e^{\Lambda A_{\mathrm{m}}\Lambda^{-1}(T_{\mathrm{s}}-\tau)}\Lambda B_{\mathrm{m}}\sigma\left(kT_{\mathrm{s}}+\tau\right)d\tau. \tag{3.87}$$

Using (3.62) and substituting the adaptive law from (3.13) and (3.51) for $\hat{\sigma}\left(kT_{\mathrm{s}}\right)$ in (3.86), we have

$$\chi\left((k+1)T_{\mathrm{s}}\right)=0. \tag{3.88}$$

From (3.87) it follows that $\zeta(t)$ is the solution of the system:

$$\dot{\zeta}(t)=\Lambda A_{\mathrm{m}}\Lambda^{-1}\zeta(t)-\Lambda B_{\mathrm{m}}\sigma(t),\quad\zeta\left(kT_{\mathrm{s}}\right)=\left[\begin{array}{c}0_{(n_{\mathrm{m}}-q)\times 1}\\ \tilde{z}(kT_{\mathrm{s}})\end{array}\right],\quad t\in\left[kT_{\mathrm{s}},\;(k+1)T_{\mathrm{s}}\right). \tag{3.89}$$

Let

$$V(t)=\zeta^{\top}(t)\Lambda^{-\top}P\Lambda^{-1}\zeta(t),\quad\forall t\in\left[kT_{\mathrm{s}},\,(k+1)T_{\mathrm{s}}\right).$$

Since Λ is nonsingular and P is positive definite, $\Lambda^{-\top}P\Lambda^{-1}$ is positive definite and, hence, $V(t)$ is a positive-definite function. Using Lemma 3.3 and Equation (3.89), it follows that

$$V\left(\zeta\left(kT_{\mathrm{s}}\right)\right) = \tilde{z}^{\top}\left(kT_{\mathrm{s}}\right)\Lambda^{-\top}P\Lambda^{-1}\tilde{z}\left(kT_{\mathrm{s}}\right),$$

which, along with the upper bound in (3.84), yields

$$V\left(\zeta\left(kT_{\mathrm{s}}\right)\right) \leq \Delta_2(\bar{\gamma}_0). \tag{3.90}$$

From (3.89) it follows that for all $t \in [kT_{\mathrm{s}},\, (k+1)T_{\mathrm{s}})$ we have

$$\begin{aligned}\dot{V}(t) &= \zeta^{\top}(t)\Lambda^{-\top}P\Lambda^{-1}\Lambda A_{\mathrm{m}}\Lambda^{-1}\zeta(t) + \zeta^{\top}(t)\Lambda^{-\top}A_{\mathrm{m}}^{\top}\Lambda^{\top}\Lambda^{-\top}P^{\top}\Lambda^{-1}\zeta(t) - 2\zeta^{\top}(t)\Lambda^{-\top}P\Lambda^{-1}\Lambda B_{\mathrm{m}}\sigma(t)\\ &= -\zeta^{\top}(t)\Lambda^{-\top}Q\Lambda^{-1}\zeta(t) - 2\zeta^{\top}(t)\Lambda^{-\top}P\Lambda^{-1}\Lambda B_{\mathrm{m}}\sigma(t).\end{aligned}$$

Using the upper bound from (3.75), for all $t \in [kT_{\mathrm{s}},\, (k+1)T_{\mathrm{s}})$ one can derive

$$\dot{V}(t) \leq -\lambda_{\min}\left(\Lambda^{-\top}Q\Lambda^{-1}\right)\|\zeta(t)\|_2^2 + 2\,\|\zeta(t)\|_2\left\|\Lambda^{-\top}PB_{\mathrm{m}}\right\|_2\sqrt{q}\Delta_1(\bar{\gamma}_0). \tag{3.91}$$

Notice that if

$$V(t) > \Delta_2(\bar{\gamma}_0), \quad \forall t \in [kT_{\mathrm{s}},\, (k+1)T_{\mathrm{s}}), \tag{3.92}$$

the following holds

$$\|\zeta(t)\|_2 > \sqrt{\frac{\Delta_2(\bar{\gamma}_0)}{\lambda_{\max}\left(\Lambda^{-\top}P\Lambda^{-1}\right)}} = \frac{2\sqrt{q}\Delta_1(\bar{\gamma}_0)\left\|\Lambda^{-\top}PB_{\mathrm{m}}\right\|_2}{\lambda_{\min}\left(\Lambda^{-\top}Q\Lambda^{-1}\right)}.$$

Moreover, the upper bound in (3.91) yields

$$\dot{V}(t) < 0. \tag{3.93}$$

From (3.90), (3.92) and (3.93), it follows that

$$V(t) \leq \Delta_2(\bar{\gamma}_0), \quad \forall t \in [kT_{\mathrm{s}},\, (k+1)T_{\mathrm{s}}),$$

and therefore

$$\zeta^{\top}((k+1)T_{\mathrm{s}})\Lambda^{-\top}P\Lambda^{-1}\zeta\left((k+1)T_{\mathrm{s}}\right) \leq \Delta_2(\bar{\gamma}_0). \tag{3.94}$$

Then, (3.85), (3.88) and the upper bound in (3.94) lead to the following inequality

$$\tilde{\xi}^{\top}((k+1)T_{\mathrm{s}})\Lambda^{-\top}P\Lambda^{-1}\tilde{\xi}\left((k+1)T_{\mathrm{s}}\right) \leq \Delta_2(\bar{\gamma}_0).$$

Using the result of Lemma 3.3, one can drive

$$\tilde{z}^{\top}((k+1)T_{\mathrm{s}})P_2\tilde{z}\left((k+1)T_{\mathrm{s}}\right) \leq \tilde{\xi}^{\top}((k+1)T_{\mathrm{s}})\Lambda^{-\top}P\Lambda^{-1}\tilde{\xi}\left((k+1)T_{\mathrm{s}}\right) \leq \Delta_2(\bar{\gamma}_0),$$

which implies that the upper bound in (3.84) holds for $k+1$.

Next, from (3.77), (3.85) and (3.88) it follows

$$\tilde{y}\left((k+1)T_{\mathrm{s}}\right) = \mathbf{1}_{n_{\mathrm{m}}q}^{\top}\zeta\left((k+1)T_{\mathrm{s}}\right),$$

and the definition of $\zeta\left((k+1)T_{\mathrm{s}}\right)$ in (3.87) leads to the following expression

$$\tilde{y}\left((k+1)T_{\mathrm{s}}\right) = \mathbf{1}_{n_{\mathrm{m}}q}^{\top} e^{\Lambda A_{\mathrm{m}}\Lambda^{-1}T_{\mathrm{s}}} \begin{bmatrix} 0_{q\times 1} \\ \tilde{z}(kT_{\mathrm{s}}) \end{bmatrix} - \mathbf{1}_{n_{\mathrm{m}}q}^{\top} \int_0^{T_{\mathrm{s}}} e^{\Lambda A_{\mathrm{m}}\Lambda^{-1}(T_{\mathrm{s}}-\tau)}\Lambda B_{\mathrm{m}}\sigma\left(kT_{\mathrm{s}}+\tau\right)d\tau.$$

The upper bounds in (3.75) and (3.84) yield the following upper bound

$$\left\|\tilde{y}\left((k+1)T_{\mathrm{s}}\right)\right\|_2 \leq \left\|\eta_2(T_{\mathrm{s}})\right\|_2 \left\|\tilde{z}(kT_{\mathrm{s}})\right\|_2 + \int_0^{T_{\mathrm{s}}} \left\|\mathbf{1}_{n_{\mathrm{m}}q}^{\top} e^{\Lambda A_{\mathrm{m}}\Lambda^{-1}(T_{\mathrm{s}}-\tau)}\Lambda B_{\mathrm{m}}\right\|_2 \left\|\sigma\left(kT_{\mathrm{s}}+\tau\right)\right\|_2 d\tau \leq \varsigma(\bar{\gamma}_0, T_{\mathrm{s}}),$$

where $\eta_2(\cdot)$, $\kappa(\cdot)$ and $\varsigma(\cdot,\,\cdot)$ are defined in (3.26), (3.27) and (3.34), respectively. This confirms the upper bound in (3.83) for $k+1$. Hence, Equation (3.82) holds for all $iT_{\mathrm{s}} \leq \tau_1$.

For all $iT_{\mathrm{s}}+t \leq \tau_1$ and $t \in [0,\, T_{\mathrm{s}}]$, using the expression from (3.78), we obtain

$$\tilde{y}\left(iT_{\mathrm{s}}+t\right) = \mathbf{1}_{n_{\mathrm{m}}q}^{\top} e^{\Lambda A_{\mathrm{m}}\Lambda^{-1}t}\tilde{\xi}\left(iT_{\mathrm{s}}\right) + \mathbf{1}_{n_{\mathrm{m}}q}^{\top} \int_0^t e^{\Lambda A_{\mathrm{m}}\Lambda^{-1}(t-\tau)}\Lambda\hat{\sigma}\left(iT_{\mathrm{s}}\right)d\tau - \mathbf{1}_{n_{\mathrm{m}}q}^{\top} \int_0^t e^{\Lambda A_{\mathrm{m}}\Lambda^{-1}(t-\tau)}\Lambda B_{\mathrm{m}}\sigma\left(iT_{\mathrm{s}}+\tau\right)d\tau.$$

The upper bound in (3.75) and the expressions of $\eta_1(\cdot)$, $\eta_2(\cdot)$, $\eta_3(\cdot,\,\cdot)$ and $\eta_4(\cdot,\,\cdot)$, given in (3.26) and (3.32), lead to

$$\left\|\tilde{y}\left(iT_{\mathrm{s}}+t\right)\right\|_2 \leq \left\|\eta_1(t)\right\|_2 \left\|\tilde{y}\left(iT_{\mathrm{s}}\right)\right\|_2 + \left\|\eta_2(t)\right\|_2 \left\|\tilde{z}\left(iT_{\mathrm{s}}\right)\right\|_2 + \eta_3\left(t, T_{\mathrm{s}}\right)\left\|\tilde{y}\left(iT_{\mathrm{s}}\right)\right\|_2 + \eta_4\left(t\right)\sqrt{q}\Delta_1(\bar{\gamma}_0).$$

Consider (3.82) and $\beta_1(\cdot)$, $\beta_2(\cdot)$, $\beta_3(\cdot)$, $\beta_4(\cdot)$ defined in (3.30)-(3.31). For arbitrary nonnegative integer i subject to $iT_{\mathrm{s}}+t \leq \tau_1$ and for all $t \in [0,\, T_{\mathrm{s}}]$, we have

$$\left\|\tilde{y}\left(iT_{\mathrm{s}}+t\right)\right\|_2 \leq \beta_1\left(T_{\mathrm{s}}\right)\varsigma(\bar{\gamma}_0, T_{\mathrm{s}}) + \beta_2\left(T_{\mathrm{s}}\right)\sqrt{\frac{\Delta_2(\bar{\gamma}_0)}{\lambda_{\max}\left(P_2\right)}} + \beta_3\left(T_{\mathrm{s}}\right)\varsigma(\bar{\gamma}_0, T_{\mathrm{s}}) + \sqrt{q}\beta_4\left(T_{\mathrm{s}}\right)\Delta_1(\bar{\gamma}_0).$$

Since the right-hand side coincides with the definition of $\gamma_0(\bar{\gamma}_0, T_{\mathrm{s}})$ in (3.35), we have the bound

$$\left\|\tilde{y}\left(t\right)\right\|_2 \leq \gamma_0(\bar{\gamma}_0, T_{\mathrm{s}}), \quad \forall t \in [0,\, \tau_1],$$

which, along with the design constraint on T_{s} introduced in (3.37), yields

$$\left\|\tilde{y}_{\tau_1}\right\|_{\mathcal{L}_\infty} < \bar{\gamma}_0.$$

This clearly contradicts the statement in (3.70). Therefore, $\left\|\tilde{y}\right\|_{\mathcal{L}_\infty} < \bar{\gamma}_0$, which proves (3.67).

Further, it follows from Lemma 3.5 that

$$\|e_t\|_{\mathcal{L}_\infty} < \Omega_1(T_\mathrm{s})\bar{\gamma}_0,$$

which holds uniformly for all $t \geq 0$ and therefore leads to the first upper bound in (3.68).

To prove the second bound in (3.68), from (3.1), (3.8), (3.39), (3.54), (3.55) and (3.56), it follows that

$$u_\mathrm{ref}(s) - u(s) = C(s)M^{-1}(s)\tilde{y}(s) - C(s)d_\mathrm{e}(s) + (u_\mathrm{C}(s) - u_\mathrm{M}(s)) + (u_\mathrm{M}(s) - u(s))\,, \tag{3.95}$$

where $d_\mathrm{e}(s)$ is the Laplace transform of $d_\mathrm{e}(t)$ defined in (3.57). Also, u_C and u_M are defined in (3.54) and (3.55). Then, it leads to

$$\|u_\mathrm{ref}(s) - u(s)\|_{\mathcal{L}_\infty} \leq \left\|C(s)M^{-1}(s)\right\|_{\mathcal{L}_1}\|\tilde{y}\|_{\mathcal{L}_\infty} + \|u_\mathrm{C}(s) - u_\mathrm{M}(s)\|_{\mathcal{L}_\infty} + \|u_\mathrm{M}(s) - u(s)\|_{\mathcal{L}_\infty} + \|C(s)\|_{\mathcal{L}_1}L_{\rho_\mathrm{r}}\|e\|_{\mathcal{L}_\infty}. \tag{3.96}$$

Combining (3.64), (3.65), (3.67), (3.68) and (3.96) leads to

$$\|u_\mathrm{ref}(s) - u(s)\|_{\mathcal{L}_\infty} < \Omega_2(T_\mathrm{s})\bar{\gamma}_0. \tag{3.97}$$

This concludes the proof. ■

Remark 3.5. *Lemmas 3.1 and 3.2 indicate that an arbitrarily small bound $\bar{\gamma}_0$ on the prediction error can be achieved as T_s goes to zero. In addition, it can be shown that $\Omega_1(T_\mathrm{s})$ and $\Omega_2(T_\mathrm{s})$ are bounded as T_s tends to zero. Therefore, the uniform bounds in* (3.68) *can be made arbitrarily small. This implies that the closed-loop sampled-data system recovers the performance of the continuous-time reference system in* (3.39)*, as the sampling time goes to zero.*

Corollary 3.1. *The system in* (3.1) *with the controller in* (3.8)-(3.13)*, subject to the conditions in* (3.20)-(3.22) *and* (3.37)*, is semi-globally practically input to state stable (SPISS) according to [100, 108], if the system defined by the triple* (A_p, B_p, C_p) *does not have a non-minimum-phase transmission zero.*

Proof. By combining the results of Theorem 3.1 and Lemma 3.4, one can immediately conclude that the closed-loop system is locally stable. To show the semi-global practical input-to-state stability of the closed-loop system in the case of minimum-phase (A_p, B_p, C_p), we first show that the reference system in (3.39) is SPISS.

From (3.45) we have

$$x_\mathrm{ref}(s) = H_2(s)K_\mathrm{g}r(s) + G(s)w_\mathrm{ref}(s) + \left((s\mathbb{I}_n - A_\mathrm{p} + B_\mathrm{p}F)^{-1} - H_5(s)H_\mathrm{in}(s)\right)x_0., \tag{3.98}$$

We notice that $G(s)$, $H_2(s)$, $H_5(s)$ and $H_{in}(s)$ are stable transfer functions if $H_1(s)$ is stable (the condition in (3.20) is met). As indicated in Remark 3.2, we have $H_1(s) = \mathbb{I}_q$ for $M(s) = P(s)$.

Therefore, $H_1(s)$ is obviously stable. In addition, the term due to the initial condition x_0 in (3.98) decays to zero exponentially, and it can be bounded by a class $\mathcal{KL}$ function $\beta(\|x_0\|, t)$. Moreover, we know from Assumption 3.2 that $\|r\|_{\mathcal{L}_\infty} \leq M_{\rm r}$. Therefore, there exists a class $\mathcal{K}$ function $\gamma(\sup_{0\leq\tau\leq t}\|r\|)$ to bound the term $H_2(s)K_{\rm g}r(s)$ in (3.98).

The left hand side of the condition in (3.22), given by $\|G(s)\|_{\mathcal{L}_1}$, can be made arbitrarily small by increasing the bandwidth of $C(s)$, as stated in Remark 3.2. Then there always exists a $\rho_{\rm r}$ that satisfies (3.22). Using Lemma 3.4, we have

$$\|x_{\rm ref}\|_{\mathcal{L}_\infty} < \rho_{\rm r},$$

and from (3.47) one can obtain the bound in (3.48) on $w_{\rm ref}$. Therefore, the term $G(s)w_{\rm ref}(s)$ in (3.98) can be bounded by the arbitrarily given $d > 0$. Hence, the reference system in (3.39) is SPISS.

Finally, the results of Theorem 3.1 and Remark 3.5 imply that the difference between the closed-loop system and the reference system in (3.39) is semi-globally attractive with arbitrarily small bounds, which together with semi-global stability of the reference system in (3.39) prove the closed-loop SPISS. This concludes the proof. ■

3.4. Simulation Examples: Aircraft Flight Control

Two flight control examples are provided to validate the theoretical claims, and to verify the effectiveness of the proposed SD controller. The first example is the simulation of the lateral dynamics of F-16 aircraft with two inputs and two outputs. In the second example, a controller for the F-16 flight-path angle tracking is developed, where the dynamics from the control input (elevator deflection) to the flight-path angle is non-minimum-phase and unstable.

3.4.1. *Aircraft lateral dynamics*

A model for the lateral dynamics of F-16 aircraft at the airspeed of $V = 502$ ft/s and the angle of attack $\alpha = 2.11^{\rm o}$, found in [109], is given by

$$A_{\rm p} = \begin{bmatrix} -0.3320 & 0.064 & 0.0364 & -0.9917 \\ 0 & 0 & 1 & 0.0393 \\ -30.6490 & 0 & -3.6784 & 0.6646 \\ 8.5395 & 0 & -0.0254 & -0.4764 \end{bmatrix}, \quad B_{\rm p} = \begin{bmatrix} 0 & 0 \\ 0 & 0 \\ -0.7331 & 0.1315 \\ -0.0319 & -0.0620 \end{bmatrix}, \quad C_{\rm p} = \begin{bmatrix} 1 & 0 & 0 & 0 \\ 0 & 1 & 0 & 0 \end{bmatrix}.$$

The state vector of the lateral dynamics model is $x(t) = [\beta(t),\, \phi(t),\, p_{\rm s}(t),\, r_{\rm s}(t)]^\top$, where the variables β, ϕ, $p_{\rm s}$ and $r_{\rm s}$ represent the angle of sideslip, the roll angle, the stability axis roll and yaw rates, respectively. The system dynamics are stable, however the eigenvalues are slow. The objective is to design a control input $u_{\rm d}[i] = [\delta_{\rm a}[i],\, \delta_{\rm r}[i]]^\top$, where $\delta_{\rm a}$ and $\delta_{\rm r}$ are the aileron and the rudder deflections, such that the output vector $y(t) = [\beta(t),\, \phi(t)]^\top$ tracks the reference command

$r(t)$, given by (3.6), where $r_{\rm d}[i]$ is

$$r_{\rm d}[i] = \begin{bmatrix} 0.2\left(-\frac{0.5}{1+e^{iT_{\rm s}-8}} + \frac{1}{1+e^{iT_{\rm s}-30}} - 0.5\right) \\ 0.2\left(-\frac{0.5}{1+e^{iT_{\rm s}-8}} + \frac{1}{1+e^{iT_{\rm s}-30}} - 0.2\right) \end{bmatrix}, \quad i \in \mathbb{Z}_{\geq 0}, \tag{3.99}$$

and $T_{\rm s}$ is the sampling time. The desired tracking dynamics $M(s)$ are given by the state-space matrices

$$A_{\rm m} = \begin{bmatrix} -4.0538 & -4.5045 & -0.8386 & -2.0633 \\ 1.2602 & 1.1254 & -2.0913 & 1.0746 \\ 2.7591 & 4.2500 & -1.4731 & 1.3436 \\ 3.1833 & -1.6250 & 6.5772 & -3.3832 \end{bmatrix}, \quad B_{\rm m} = \begin{bmatrix} -0.0021 & 0.1053 \\ -0.0402 & 0.0347 \\ 0.1562 & -0.0134 \\ -0.1722 & -0.0174 \end{bmatrix},$$
$$C_{\rm m} = \begin{bmatrix} 0.0234 & 0.0894 & 0.0908 & 0.0597 \\ -0.2073 & 0.6566 & -0.2254 & -0.1419 \end{bmatrix}.$$

In this simulation, input uncertainties of the form

$$\begin{aligned} f_{\delta_{\rm a}}(t, x(t)) =& 0.01\left(|\beta(t)| + |\phi(t)| + p_{\rm s}(t)\cos(4t)\right) + 0.02 r_{\rm s}(t)\sin(t) + 0.25\cos(0.8t), \\ f_{\delta_{\rm r}}(t, x(t)) =& 0.01\left(|p_{\rm s}(t)| + |r_{\rm s}(t)| + \phi(t)\cos(0.7t)\right) + 0.02 r_{\rm s}(t)\sin(4t) + 0.25\sin(1.1t) \end{aligned}$$

are considered. The non-zero initial condition is $x_0 = [0 \text{ rad}, 0.06 \text{ rad}, 0.02 \text{ rad/s}, -0.02 \text{ rad/s}]^\top$, leading to $y_0 = [0 \text{ rad}, 0.06 \text{ rad}]^\top$. Next, we select the design parameters for the sampled-data $\mathcal{L}_1$ controller. Let $\rho_0 = M_{\rm r} = 0.25$, $K_\delta = 0.05$, $\bar{\gamma}_0 = 0.1$, $\bar{\gamma}_1 = 9 \times 10^3$, and $F = 0_{2\times 4}$. With $\rho_{\rm r} = 6.7 \times 10^3$, the uncertainty bounds $L_{\rho_{\rm r}} = 0.1172$ and $L_0 = 0.25$ (which satisfy (3.18)), and the filter

$$C(s) = \begin{bmatrix} \frac{10}{s+10} & 0 \\ 0 & \frac{40}{s+40} \end{bmatrix},$$

the stability conditions in (3.20) and (3.22) are met. For the selected parameters we can calculate $\rho_1 = 20.549$ and $\rho_2 = 9.633$. Then the right hand side of (3.22) is equal to 8.492, which is larger than $\|G(s)\|_{\mathcal{L}_1} = 0.256$, and thus the inequality in (3.22) is verified. Finally, by selecting the sampling time $T_{\rm s} = 10^{-7}$ sec, we have $\gamma_0(\bar{\gamma}_0, T_{\rm s}) = 0.0956$ and $\Omega_1(T_{\rm s}) = 8.996 \times 10^4$. Therefore, we can verify that the inequalities in (3.37) hold. The response of the closed-loop SD system is shown in Figures 3.1-3.2. The output tracks the desired response in the presence of disturbances, as illustrated in Figure 3.1. The control input is shown in Figure 3.2. Figures 3.3-3.4 show the response of the closed-loop SD system for the step reference commands $r(t) = [0.05 \text{ rad}, 0.2 \text{ rad}]^\top$, $r(t) = [0.075 \text{ rad}, 0.3 \text{ rad}]^\top$, and $r(t) = [0.1 \text{ rad}, 0.4 \text{ rad}]^\top$ in the presence of uncertainties and time delay of 0.01 sec at the control input. In this simulation, the sampling time of the SD controller is $T_{\rm s} = 0.01$ sec. We notice that the controller leads to scaled control inputs and outputs for scaled reference commands.

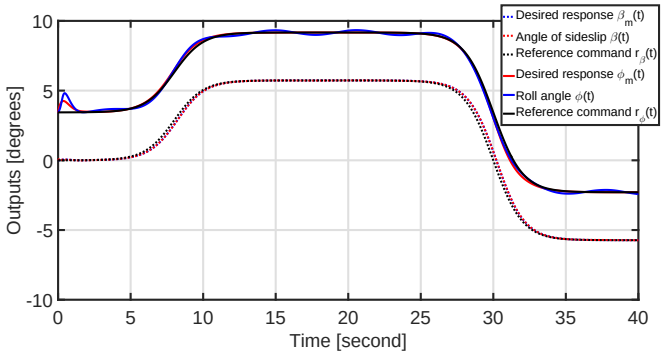

Figure 3.1: The outputs, the reference commands, and the desired responses. The outputs of the closed-loop lateral dynamics, $\beta(t)$ and $\phi(t)$, track the desired responses $\beta_{\rm m}(t)$ and $\phi_{\rm m}(t)$ for the given reference command in (3.99).

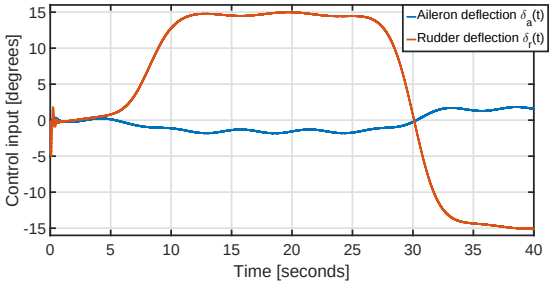

Figure 3.2: The control inputs $\delta_{\rm a}(t)$ and $\delta_{\rm r}(t)$.

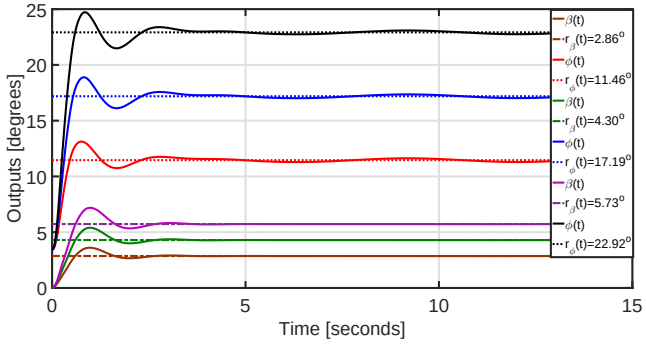

Figure 3.3: Scaled responses of the closed-loop lateral dynamics to scaled reference inputs.

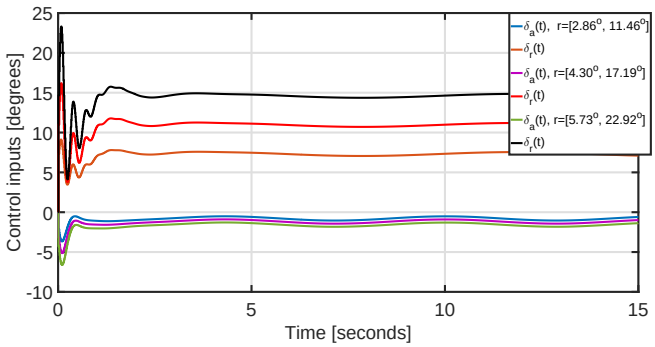

Figure 3.4: Scaled control inputs.

3.4.2. *Aircraft flight-path angle*

We consider the problem of flight-path angle, γ, tracking, using the elevator deflection, $\delta_{\rm e}$, for a longitudinal model of an F-16 aircraft. The state-space model, from [110], with $\gamma(t)$ as the output and $\delta_{\rm e}(t)$ as the input, is non-minimum-phase and unstable, and is given by the matrices

$$A_{\rm p} = \begin{bmatrix} -11.707 & 0 & -75.666 \\ 0 & 11.141 & -79.908 \\ 0.723 & 0.907 & -1.844 \end{bmatrix}, \quad B_{\rm p} = \begin{bmatrix} 0 \\ 0 \\ 0.117 \end{bmatrix}, \quad C_{\rm p} = \begin{bmatrix} 0 & 0 & 1 \end{bmatrix},$$

for Mach=0.7 and altitude of $h = 10,000$ ft. This system has an unstable pole at $s = 1.051$, and a non-minimum-phase zero at $s = 11.141$. The state vector is $x(t) = [x_1(t),\, x_2(t),\, x_3(t)]^\top$, and the output is $\gamma(t) = x_3(t)$. We choose the desired dynamics $M(s)$ and the filter $C(s)$ as

$$M(s) = -\frac{469.6\ s^2 + 1.384 \times 10^4\ s + 9.76 \times 10^4}{2174\ s^3 + 7868\ s^2 + 4348\ s + 579.8}, \quad C(s) = \frac{17^4}{(s+17)^4}.$$

This choice of $M(s)$ and $C(s)$ satisfy the condition (3.20). The sampling time of the SD controller is $T_{\rm s} = 0.01$ sec. The initial condition of the simulation is $x_0 = [0.001,\, 0,\, -0.001]^\top$, and the nonlinear input disturbance is given by

$$f(t, x(t)) = 0.001 x_1(t) x_2(t) \cos(5t) + 0.001 \sin(x_1(t) x_2(t)) + 0.003 x_2(t) x_3(t) \sin(3t).$$

In addition, a delay of 0.03 sec is considered at the control input. A white noise with the power spectral density of 10^{-10} and the sample time of 0.01 sec is considered at the measured output. The simulation results in Figures 3.5-3.6 indicate that the digital controller is robust to measurement noise, input delay and nonlinear disturbances. The closed-loop system with the SD controller is stable and tracks the desired flight-path angle in the presence of uncertainties, as illustrated in Figure 3.5. The control input is shown in Figure 3.6. While many output feedback approaches based on high-gain observer amplify the noise at the control input, the filter in the SD $\mathcal{L}_1$ controller

limits the noise amplification at the input channel.

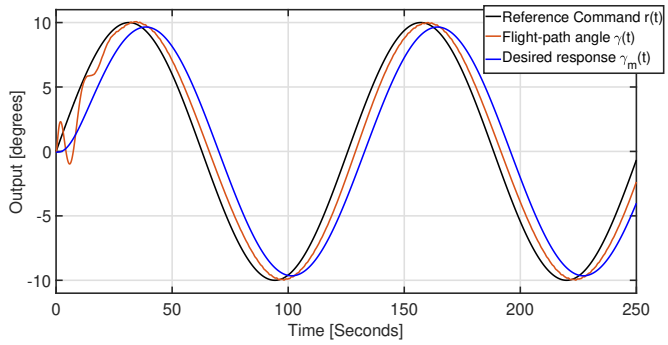

Figure 3.5: The output, the reference command and the desired response. The flight-path angle, $\gamma(t)$, tracks the desired $\gamma_{\mathrm{m}}(t)$ for a sinusoidal reference command.

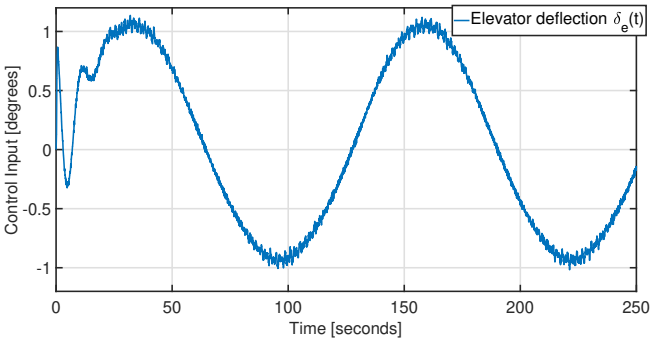

Figure 3.6: The control input $\delta_{\mathrm{e}}(t)$.

CHAPTER 4

Multi-Rate Sampled-Data Output-Feedback Control Design For a Class of Uncertain Autonomous Systems

This chapter extends the results of Chapter 3 on sampled-data (SD) control design, by considering the output-feedback SD control problem for a class nested uncertain MIMO systems subject to reference command saturation, with possibly non-minimum phase zeros. Examples of such systems include industrial/medical robots, unmanned aerial vehicles (UAVs), self-driving cars, and many other autonomous systems. While the controller design with uniform rate is considered in Chapter 3, the multi-rate SD design of this chapter addresses the digital implementation of the control law on computers, where the control inputs and the measurements are available at discrete time instances with different sampling rates. Also, the multirate scheme allows the zero-dynamics attacks to be detected by ensuring that there are no relevant unstable zeros in the lifted system. As shown in [42], unbounded zero-dynamics attacks can be detected if the control system is designed in the dual rate sampled-data framework.

In this chapter, the navigation and control problem for autonomous systems is formulated using the multirate SD control approach. The control structure consists of a high-level (outer-loop) control for reference command generation and a low-level (inner-loop) adaptive control for reference tracking, as shown in Figure 1.1. The high-level controller is limited by saturation bounds to maintain the closed-loop system within an operational safety envelope. The low-level controller is a multirate $\mathcal{L}_1$ adaptive controller for tracking the generated reference command by compensating for uncertainties and disturbances. Conditions are derived, under which the SD controller uniformly recovers the performance of the underlying continuous-time reference system as the sampling time tends to zero. The related preliminary results by authors can be found in [79, 80]. The multi-level structure of the problem formulation allows for the design of the feedback loops for the high-level/low-level subsystems with their respective control objectives, while the stability and robustness of the overall nested system subject to command saturation are taken into account.

The effectiveness of the proposed approach is evaluated using the simulation study of a fixed-wing UAV in the presence of uncertainties, zero-dynamics attack, and mechanical failure. In this example, the multi-level SD control strategy is leveraged for navigation and control of the UAV model, where the theoretical conditions for the control design are verified. A high-fidelity simulation environment of an Unmanned Aerial Vehicle (UAV) is used to verify the effectiveness and the benefits of the proposed control framework. A multi-level altitude tracking controller is designed for the linearized UAV longitudinal dynamics and then validated in the high-fidelity UAV simulation environment. Scenarios with and without saturation of reference command are considered. In the end, a zero-dynamics attack on altitude measurement is simulated to show the benefits of the multi-rate framework in detecting stealthy attacks.

4.1. Problem Formulation

As depicted in Figure 1.1, consider the following multi-level model for an autonomous system subject to uncertainties, disturbances, physical faults, and attack signals, comprised of a low-level (inner-loop) subsystem

$$\begin{aligned} \dot{x}(t) &= A_{\mathrm{x}}x(t) + B_{\mathrm{x}}\left(u(t) + f(t,\, x(t)) + d(t)\right), \quad x(0) = x_0, \\ y(t) &= C_{\mathrm{x}}x(t), \end{aligned} \tag{4.1}$$

and a high-level (outer-loop) subsystem

$$\dot{z}(t) = A_{\mathrm{z}}z(t) + B_{\mathrm{z}}y(t) + g(t,\, x(t)), \quad z(0) = z_0, \tag{4.2}$$

where $x(t) \in \mathbb{R}^n$ and $z(t) \in \mathbb{R}^p$ are the state vectors, $u(t) \in \mathbb{R}^q$ is the input signal, and $y(t) \in \mathbb{R}^q$ is the system output vector. Also, $\{A_{\mathrm{x}} \in \mathbb{R}^{n\times n}, B_{\mathrm{x}} \in \mathbb{R}^{n\times q}, C_{\mathrm{x}} \in \mathbb{R}^{q\times n}\}$ is an observable-controllable triple and $\{A_{\mathrm{z}} \in \mathbb{R}^{p\times p}, B_{\mathrm{z}} \in \mathbb{R}^{p\times q}\}$ is a controllable pair. The unknown initial condition $x_0 \in \mathbb{R}^n$ is assumed to be inside an arbitrarily large set, so that $\|x_0\|_\infty \leq \rho_0 < \infty$ for some known $\rho_0 > 0$, and $z_0 \in \mathbb{R}^p$ is a known initial condition. Let $d(t) \in \mathbb{R}^q$ be an exogenous additive disturbance on the control input, which can represent a CPS attack (ex. stealthy zero-dynamics attack signal) or failure. Also, let $f\left(t, x(t)\right) \in \mathbb{R}^q$ and $g\left(t, x(t)\right) \in \mathbb{R}^p$ represent the time-varying uncertainties and disturbances, subject to the following assumption.

Assumption 4.1. *Given arbitrary $\delta > 0$, there exist $K_\delta > 0$, $G_\delta > 0$ and constants $L_0 > 0$, $L_1 > 0$, such that*

$$\|f(t, x_2) - f(t, x_1)\|_\infty \leq K_\delta \|x_2 - x_1\|_\infty, \quad \|f(t, 0)\|_\infty \leq L_0, \quad \|d(t)\|_\infty \leq L_1, \quad \|g\left(t, x_1\right)\|_\infty \leq G_\delta,$$

hold for all $\|x_i\|_\infty \leq \delta,\ i \in \{1,\, 2\}$, uniformly in $t \geq 0$.

Using a multirate SD control approach, the control input and the measurements are available at discrete time instances with different sampling periods. The control input, which is implemented via a zero-order hold mechanism with time period of $T_{\mathrm{s}} > 0$, is given by

$$u(t) = u_{\mathrm{d}}[i], \quad t \in \left[iT_{\mathrm{s}}, (i+1)T_{\mathrm{s}}\right), \quad i \in \mathbb{Z}_{\geq 0}, \tag{4.3}$$

where $u_{\mathrm{d}}[i]$ is a discrete-time control input signal. The output of the low-level subsystem $y(t)$ is sampled $N \in \mathbb{N}$ times faster with the sampling time of $\frac{T_{\mathrm{s}}}{N}$, such that the discrete-time output signal $y_{\mathrm{d}}[j]$ is given by

$$y_{\mathrm{d}}[j] = y\left(j\frac{T_{\mathrm{s}}}{N}\right), \quad t \in \left[j\frac{T_{\mathrm{s}}}{N}, (j+1)\frac{T_{\mathrm{s}}}{N}\right), \quad j \in \mathbb{Z}_{\geq 0}, \tag{4.4}$$

and the high-level subsystem state $z(t)$ is sampled $M \in \mathbb{N}$ times slower with the period of MT_{s},

such that

$$z_{\mathrm{d}}[k] = z\left(kMT_{\mathrm{s}}\right), \quad t \in [kMT_{\mathrm{s}}, (k+1)MT_{\mathrm{s}}), \quad k \in \mathbb{Z}_{\geq 0}. \tag{4.5}$$

Assumption 4.2. *The desired dynamics for the low-level subsystem in* (4.1) *is defined by*

$$M(s) = C_{\mathrm{m}}\left(s\mathbb{I}_{n_{\mathrm{m}}} - A_{\mathrm{m}}\right)^{-1} B_{\mathrm{m}}, \tag{4.6}$$

where the triple $\{A_{\mathrm{m}} \in \mathbb{R}^{n_{\mathrm{m}} \times n_{\mathrm{m}}}, B_{\mathrm{m}} \in \mathbb{R}^{n_{\mathrm{m}} \times q}, C_{\mathrm{m}} \in \mathbb{R}^{q \times n_{\mathrm{m}}}\}$ *is a minimal state-space realization of* $M(s)$*, with* A_{m} *being Hurwitz, and* $(C_{\mathrm{m}}B_{\mathrm{m}})$ *is nonsingular. Also,* $M(s)$ *does not have any unstable transmission zeros.*

The desired response $y_{\mathrm{m}}(t)$ *is given by the Laplace transform* $y_{\mathrm{m}}(s) = M(s)K_{\mathrm{g}}r(s)$*, where*

$$K_{\mathrm{g}} \triangleq -\left(C_{\mathrm{m}}A_{\mathrm{m}}^{-1}B_{\mathrm{m}}\right)^{-1},$$

and $r(s)$ *is the Laplace transform of* $r(t)$ *given by*

$$r(t) = r_{\mathrm{d}}[k], \quad t \in [kMT_{\mathrm{s}}, (k+1)MT_{\mathrm{s}}), \quad k \in \mathbb{Z}_{\geq 0}, \tag{4.7}$$

where $r_{\mathrm{d}}[k]$ *is a discrete-time reference command.*

Assumption 4.3. *The reference command is constrained to a convex polytope as a safe operation region, defined by the set*

$$\mathcal{R} = \{r \in \mathbb{R}^q | \, \|Wr\|_\infty \leq 1\}, \tag{4.8}$$

where $W = \mathrm{diag}\{\mathrm{r}_{\mathrm{max}_1}^{-1}, ..., \mathrm{r}_{\mathrm{max}_{\mathrm{q}}}^{-1}\}$*, and the positive constants* r_{max_i}*'s are the saturation bounds on control inputs. Then the weighted reference command is bounded by*

$$\|Wr_{\mathrm{d}}[k]\|_\infty \leq 1, \quad k \in \mathbb{Z}_{\geq 0}.$$

Remark 4.1. *For large uncertainties outside normal conditions, the low-level control inputs can saturate or drive the system to unsafe states. By restricting the reference commands (generated by high-level control) to a safe operational envelope, as defined in Assumption 4.3, the safety of the autonomous system can be improved.*

Assumption 4.4. *The desired system for the high-level subsystem in* (4.2) *is defined by*

$$\dot{z}_{\mathrm{m}}(t) = A_{\mathrm{z}}z_{\mathrm{m}}(t) + B_{\mathrm{z}}r_{\mathrm{m}}(t), \quad z_{\mathrm{m}}(0) = z_0, \tag{4.9}$$

where $z_{\mathrm{m}}(t) \in \mathbb{R}^p$ *is the desired state for the high-level subsystem, and*

$$r_{\mathrm{m}}(t) = r_{\mathrm{m_d}}[k], \quad t \in [kMT_{\mathrm{s}}, (k+1)MT_{\mathrm{s}}), \quad k \in \mathbb{Z}_{\geq 0}, \tag{4.10}$$

is the precalculated reference command for the desired system. It is assumed that

$$\|Wr_{\mathrm{m_d}}[k]\|_\infty \leq \alpha, \quad k \in \mathbb{Z}_{\geq 0}, \tag{4.11}$$

where $\alpha \in (0,\, 1)$ *is a given constant, and* W *is defined in* (4.8)*. In addition, we assume that* $r_{\mathrm{m_d}}[0] = 0$*, and*

$$\frac{1}{MT_{\mathrm{s}}} \|r_{\mathrm{m_d}}[k+1] - r_{\mathrm{m_d}}[k]\|_\infty \leq \delta_{\mathrm{r_m}}, \quad k \in \mathbb{Z}_{\geq 0}, \tag{4.12}$$

where $\delta_{\mathrm{r_m}} > 0$ *is the bound on the rate of change of the reference command.*

In the following, a multi-level multirate adaptive controller is formulated to:

- compensate for physical failures, uncertainties, and disturbances, such that the low-level system in (4.1) is stable, and the output $y(t)$ closely tracks the desired response $y_{\mathrm{m}}(t)$;
- maintain the reference command $r(t)$ within the safe operation envelope $\mathcal{R}$ defined in (4.8);
- bound the error between the states of the high-level subsystem, $z(t)$, and the desired trajectory $z_{\mathrm{m}}(t)$ given in (4.9);
- detect sensor/actuator attacks (including stealthy zero-dynamics attacks), and recover stability of the perturbed system.

4.2. Proposed Multi-Level Multirate Controller

In this section, the proposed multi-level multirate controller is presented. The conditions for selection of the control parameters and the detailed analysis of the closed-loop system are provided in Section 4.3. First, the elements of the multirate output-feedback $\mathcal{L}_1$ adaptive controller that generates the input $u(t)$ to the low-level subsystem in (4.1) are given.

Let $T_{\mathrm{s}} > 0$ be the sampling time of the control input. Consider a strictly proper stable transfer function $C(s)$, such that $C(0) = \mathbb{I}_q$. In the $\mathcal{L}_1$ adaptive control structure, $C(s)$ represents the low-pass filter at the control input [47]. Also, define $O(s) \triangleq C(s)M^{-1}(s)C_{\mathrm{m}}(s\mathbb{I}_{n_{\mathrm{m}}} - A_{\mathrm{m}})^{-1}$, and let $\{A_{\mathrm{o}} \in \mathbb{R}^{v\times v},\, B_{\mathrm{o}} \in \mathbb{R}^{v\times q},\, C_{\mathrm{o}} \in \mathbb{R}^{q\times v}\}$ be a minimal state-space realization such that

$$C_{\mathrm{o}}(s\mathbb{I}_v - A_{\mathrm{o}})^{-1}B_{\mathrm{o}} = O(s). \tag{4.13}$$

The control laws are given by

$$\begin{aligned} x_{\mathrm{u}}[j+1] &= e^{A_{\mathrm{o}}\frac{T_{\mathrm{s}}}{N}} x_{\mathrm{u}}[j] + A_{\mathrm{o}}^{-1}\left(e^{A_{\mathrm{o}}\frac{T_{\mathrm{s}}}{N}} - \mathbb{I}_v\right) B_{\mathrm{o}} e^{-A_{\mathrm{m}}\frac{T_{\mathrm{s}}}{N}} \hat{\sigma}_{\mathrm{d}}[j], \quad x_{\mathrm{u}}[0] = 0, \quad j \in \mathbb{Z}_{\geq 0}, \\ u_{\mathrm{N_d}}[j] &= -C_{\mathrm{o}} x_{\mathrm{u}}[j], \\ u_{\mathrm{N}}(t) &= u_{\mathrm{N_d}}[j], \quad t \in \left[j\frac{T_{\mathrm{s}}}{N}, (j+1)\frac{T_{\mathrm{s}}}{N}\right), \\ u_{\mathrm{d}}[i] &= u_{\mathrm{N}}(iT_{\mathrm{s}}) + K_{\mathrm{g}} r(iT_{\mathrm{s}}), \quad i \in \mathbb{Z}_{\geq 0}, \end{aligned} \tag{4.14}$$

where $\hat{\sigma}_{\mathrm{d}}[\cdot] \in \mathbb{R}^n$ is provided by the adaptation law in (4.20). Also, the reference command $r(\cdot) \in \mathbb{R}^q$ is given by (4.7) and the high-level controller in (4.22).

The update of $\hat{\sigma}_{\mathrm{d}}[\cdot]$ is based on an output predictor, given by

$$\begin{aligned} \hat{x}_{\mathrm{d}}[j+1] =& e^{A_{\mathrm{m}}\frac{T_{\mathrm{s}}}{N}} \hat{x}_{\mathrm{d}}[j] + A_{\mathrm{m}}^{-1}(e^{A_{\mathrm{m}}\frac{T_{\mathrm{s}}}{N}} - \mathbb{I}_{n_{\mathrm{m}}})\left(B_{\mathrm{m}} u_{\mathrm{P}}[j] + \hat{\sigma}_{\mathrm{d}}[j]\right), \quad \hat{x}_{\mathrm{d}}[0] = C_{\mathrm{m}}^{\dagger} y_0, \quad j \in \mathbb{Z}_{\geq 0}, \\ \hat{y}_{\mathrm{d}}[j] =& C_{\mathrm{m}} \hat{x}_{\mathrm{d}}[j]. \end{aligned} \tag{4.15}$$

The predictor control input $u_{\mathrm{P}}[j]$ is defined by

$$u_{\mathrm{P}}[j] = u\left(j\frac{T_{\mathrm{s}}}{N}\right), \quad j \in \mathbb{Z}_{\geq 0}, \tag{4.16}$$

where $u(t)$ is defined by (4.3) and (4.14).

Given that $A_{\mathrm{m}} \in \mathbb{R}^{n_{\mathrm{m}} \times n_{\mathrm{m}}}$ is Hurwitz, for a given positive definite matrix $Q \in \mathbb{R}^{n_{\mathrm{m}} \times n_{\mathrm{m}}}$ there exists a positive definite matrix $P \in \mathbb{R}^{n_{\mathrm{m}} \times n_{\mathrm{m}}}$ solving $A_{\mathrm{m}}^{\top} P + P A_{\mathrm{m}} = -Q$. Define

$$\Lambda \triangleq \begin{bmatrix} C_{\mathrm{m}} \\ D\sqrt{P} \end{bmatrix}, \tag{4.17}$$

where $\sqrt{P}$ satisfies $P = \sqrt{P}^{\top}\sqrt{P}$, and $D \in \mathbb{R}^{(n_{\mathrm{m}}-q) \times n_{\mathrm{m}}}$ is a matrix that is in the null space of $C_{\mathrm{m}}\left(\sqrt{P}\right)^{-1}$, *i.e.*

$$D\left(C_{\mathrm{m}}\left(\sqrt{P}\right)^{-1}\right)^{\top} = 0\,. \tag{4.18}$$

Further, let $\Phi(\cdot)$ be the $n_{\mathrm{m}} \times n_{\mathrm{m}}$ matrix

$$\Phi(T_{\mathrm{s}}) \triangleq \int_0^{\frac{T_{\mathrm{s}}}{N}} e^{\Lambda A_{\mathrm{m}} \Lambda^{-1}\left(\frac{T_{\mathrm{s}}}{N} - \tau\right)} \Lambda d\tau. \tag{4.19}$$

The adaptation law is governed by the following equation

$$\hat{\sigma}_{\mathrm{d}}[j] = -\Phi^{-1}(T_{\mathrm{s}})\, e^{\Lambda A_{\mathrm{m}} \Lambda^{-1}\frac{T_{\mathrm{s}}}{N}} \mathbf{1}_{n_{\mathrm{m}} q} \tilde{y}_{\mathrm{d}}[j], \quad j \in \mathbb{Z}_{\geq 0}, \tag{4.20}$$

where $\tilde{y}_{\mathrm{d}}[j] = \hat{y}_{\mathrm{d}}[j] - y_{\mathrm{d}}[j]$, and $\mathbf{1}_{n_{\mathrm{m}}q} \in \mathbb{R}^{n_{\mathrm{m}} \times q}$ is given by

$$\mathbf{1}_{n_{\mathrm{m}}q} \triangleq \begin{bmatrix} \mathbb{I}_q \\ 0_{(n_{\mathrm{m}}-q)\times q} \end{bmatrix}. \tag{4.21}$$

Finally, the reference command $r_d[k]$, which is generated by the high-level control law, is given by

$$r_{\mathrm{d}}[k] = r_{\mathrm{m_d}}[k] + (1-\alpha)W^{-1}\mathrm{sat}\left\{\frac{1}{1-\alpha}WF_{\mathrm{z}}\left(z_{\mathrm{m_d}}[k] - z_{\mathrm{d}}[k]\right)\right\}, \quad k \in \mathbb{Z}_{\geq 0}, \tag{4.22}$$

where $r_{\mathrm{m_d}}[k]$ is the desired reference command introduced in Assumption 4.4, and $F_{\mathrm{z}} \in \mathbb{R}^{q\times p}$ is the state-feedback gain, while α is introduced in Assumption 4.4. Also, $z_{\mathrm{d}}[k]$ is the measured high-level state given by (4.2) and (4.5). Using (4.9), the desired high-level state $z_{\mathrm{m_d}}[k]$ is obtained by

$$\begin{aligned} &z_{\mathrm{m_d}}[0] = z_0, \\ &z_{\mathrm{m_d}}[k] = e^{A_{\mathrm{z}}(kMT_{\mathrm{s}})}z_0 + \sum_{l=0}^{k-1}\left(\int_0^{MT_{\mathrm{s}}} e^{A_{\mathrm{z}}((k-l)MT_{\mathrm{s}}-\tau)}B_{\mathrm{z}}d\tau\right) r_{\mathrm{m_d}}[l], \quad k \in \mathbb{Z}_{>0}. \end{aligned} \tag{4.23}$$

Notice that the saturation function in (4.22) ensures that the reference command always remains within the safety envelope $\mathcal{R}$ defined in (4.8).

4.3. Analysis of the Closed-Loop Multilevel Multirate System

This section provides the analysis of stability and performance of the closed-loop SD system with the proposed controller. Also, the conditions for selection of the control parameters T_s, $C(s)$, and F_{z} are provided. The analysis is summarized in Theorems 4.1 and 4.2 at the end of this section. Towards this goal, we need to define a few variables of interest and design constraints. Let

$$\begin{aligned} P(s) &\triangleq C_{\mathrm{x}}(s\mathbb{I}_n - A_{\mathrm{x}} + B_{\mathrm{x}}F_{\mathrm{x}})^{-1}B_{\mathrm{x}}, \\ H_0(s) &\triangleq (s\mathbb{I}_n - A_{\mathrm{x}} + B_{\mathrm{x}}F_{\mathrm{x}})^{-1}B_{\mathrm{x}}, \\ H_1(s) &\triangleq \left(\mathbb{I}_q + \left(M^{-1}(s)P(s) - \mathbb{I}_q\right)C(s)\right)^{-1}, \\ H_2(s) &\triangleq H_0(s) - H_0(s)C(s)H_1(s)\left(M^{-1}(s)P(s) - \mathbb{I}_q\right), \\ H_3(s) &\triangleq H_1(s)M^{-1}(s)P(s), \\ H_4(s) &\triangleq H_1(s)\left(M^{-1}(s)P(s) - \mathbb{I}_q\right), \\ H_5(s) &\triangleq H_0(s)C(s)H_1(s)M^{-1}(s), \\ G(s) &\triangleq H_0(s) - H_5(s)P(s), \end{aligned} \tag{4.24}$$

where $F_{\mathrm{x}} \in \mathbb{R}^{q\times n}$ is selected such that $A_{\mathrm{x}} - B_{\mathrm{x}}F_{\mathrm{x}}$ is Hurwitz. Let $y_0 \triangleq C_{\mathrm{x}}x_0$ be the known initial output. Define the auxiliary system

$$\begin{aligned} \dot{x}_{\mathrm{a}}(t) &= A_{\mathrm{m}}x_{\mathrm{a}}(t) + B_{\mathrm{m}}\left(u(t)+\sigma(t)\right), \quad x_{\mathrm{a}}(0) = C_{\mathrm{m}}^{\dagger}y_0, \\ y(t) &= C_{\mathrm{m}}x_{\mathrm{a}}(t), \end{aligned} \tag{4.25}$$

with the same input-to-output $u(t) -> y(t)$ mapping as the system in (4.1), where $x_{\mathrm{a}}(t) \in \mathbb{R}^{\mathrm{n_m}}$ is the state vector, and the Laplace transform of $\sigma(t)$ is given by

$$\sigma(s) = M^{-1}(s)\left(\left(P(s)-M(s)\right)u(s) + P(s)w(s) + H_{\mathrm{in}}(s)x_0\right),$$

with

$$H_{\mathrm{in}}(s) \triangleq C_{\mathrm{x}}(s\mathbb{I}_n - A_{\mathrm{x}} + B_{\mathrm{x}}F_{\mathrm{x}})^{-1} - C_{\mathrm{m}}\left(s\mathbb{I}_{n_{\mathrm{m}}} - A_{\mathrm{m}}\right)^{-1}C_{\mathrm{m}}^{\dagger}C_{\mathrm{x}},$$

and $w(s)$ is the Laplace transform of $w(t)$ given by

$$w(t) \triangleq F_{\mathrm{x}}x(t) + f\left(t, x(t)\right) + d(t). \tag{4.26}$$

Remark 4.2. *Assumption 4.2 implies that $\frac{1}{s}M^{-1}(s)$ is a proper transfer function. Given that $M(s)$ does not have an unstable transmission zero, $M^{-1}(s)P(s)$ is proper and stable, and $M^{-1}(s)H_{\mathrm{in}}(s)$ is strictly proper and stable ($H_{\mathrm{in}}(s)$ has total relative degree of two or higher). Therefore, $\sigma(t)$, defined in* (4.25)*, is a casual signal.*

Further, for every $\delta > 0$, let

$$L_\delta \triangleq \frac{\bar{\gamma}_1 + \delta}{\delta}\left(K_{(\bar{\gamma}_1+\delta)} + \|F_{\mathrm{x}}\|_\infty\right), \tag{4.27}$$

where K_δ is introduced in Assumption 4.1, and $\bar{\gamma}_1$ is an arbitrarily small positive constant. It can be shown that the following bound on $w(t)$ holds

$$\|w_t\|_{\mathcal{L}_\infty} \leq L_\delta \|x_t\|_{\mathcal{L}_\infty} + L_2, \tag{4.28}$$

where $L_2 \triangleq L_0 + L_1$. Also, define

$$M_{\mathrm{r}} \triangleq \max\{r_{\max_1}, \ldots, r_{\max_{\mathrm{q}}}\}, \tag{4.29}$$

where $r_{\max_i}$'s are introduced in (4.8). The design of the controller proceeds by finding a low-pass filter $C(s)$ such that $C(0) = \mathbb{I}_q$. The selection of $C(s)$ must ensure that

$$H_1(s) \quad \text{is stable}, \tag{4.30}$$

where $H_1(s)$ is defined in (4.24), and for a given ρ_0, there exists $\rho_{\mathrm{r}} > \rho_0$, such that the following

$\mathcal{L}_1$-norm condition holds:

$$\|G(s)\|_{\mathcal{L}_1} < \frac{\rho_{\mathrm{r}} - \rho_1 - \rho_2}{L_{\rho_{\mathrm{r}}}\rho_{\mathrm{r}} + L_2}, \tag{4.31}$$

where

$$\rho_1 \triangleq \left\| s(s\mathbb{I}_n - A_{\mathrm{x}} + B_{\mathrm{x}}F_{\mathrm{x}})^{-1} - sH_5(s)H_{\mathrm{in}}(s) \right\|_{\mathcal{L}_1} \rho_0, \quad \rho_2 \triangleq \|H_2(s)K_{\mathrm{g}}\|_{\mathcal{L}_1} M_{\mathrm{r}}. \tag{4.32}$$

Remark 4.3. *Selection of the filter $C(s)$ provides a trade-off between performance in terms of disturbance compensation and robustness in terms of input-delay margin. A mixed-norm optimization of the filter for $\mathcal{L}_1$ adaptive control structure can be found in [103].*

Let $P_1 \in \mathbb{R}^{q\times q}$ and $P_2 \in \mathbb{R}^{(n_{\mathrm{m}}-q)\times(n_{\mathrm{m}}-q)}$ be positive definite matrices given by

$$P_1 \triangleq \left(C_{\mathrm{m}}\sqrt{P}^{-1}\sqrt{P}^{-\top}C_{\mathrm{m}}^{\top}\right)^{-1}, \quad P_2 \triangleq (DD^{\top})^{-1}. \tag{4.33}$$

Define

$$\begin{bmatrix} \eta_1^{\top}(t) & \eta_2^{\top}(t) \end{bmatrix} \triangleq \mathbf{1}_{n_{\mathrm{m}}q}^{\top} e^{\Lambda A_{\mathrm{m}}\Lambda^{-1}t}, \tag{4.34}$$

where $\eta_1(t) \in \mathbb{R}^{q\times q}$ and $\eta_2(t) \in \mathbb{R}^{(n_{\mathrm{m}}-q)\times q}$, and

$$\kappa(T_{\mathrm{s}}) \triangleq \int_0^{\frac{T_{\mathrm{s}}}{N}} \left\| \mathbf{1}_{n_{\mathrm{m}}q}^{\top} e^{\Lambda A_{\mathrm{m}}\Lambda^{-1}(\frac{T_{\mathrm{s}}}{N}-\tau)}\Lambda B_{\mathrm{m}} \right\|_2 d\tau. \tag{4.35}$$

Define the function

$$\Gamma\left(T_{\mathrm{s}}\right) \triangleq \alpha_1(T_{\mathrm{s}}) \left\| (s\mathbb{I}_v - A_{\mathrm{o}})^{-1}B_{\mathrm{o}} \right\|_{\mathcal{L}_1} + \alpha_2(T_{\mathrm{s}}), \tag{4.36}$$

where the system matrices $(A_{\mathrm{o}}, B_{\mathrm{o}}, C_{\mathrm{o}})$ satisfy (4.13), and

$$\alpha_1(T_{\mathrm{s}}) \triangleq \max_{t\in[0,\,\frac{T_{\mathrm{s}}}{N}]} \left\| C_{\mathrm{o}}\left(e^{A_{\mathrm{o}}t} - \mathbb{I}_v\right) \right\|_{\infty}, \quad \alpha_2(T_{\mathrm{s}}) \triangleq \max_{t\in[0,\,\frac{T_{\mathrm{s}}}{N}]} \int_0^t \left\| C_{\mathrm{o}}e^{A_{\mathrm{o}}(t-\tau)}B_{\mathrm{o}} \right\|_{\infty} d\tau.$$

Let

$$
\begin{aligned}
\Upsilon(T_{\rm s}) =&\left\| e^{-A_{\rm m}\frac{T_{\rm s}}{N}}\Phi^{-1}\left(T_{\rm s}\right)e^{\Lambda A_{\rm m}\Lambda^{-1}\frac{T_{\rm s}}{N}}\mathbf{1}_{n_{\rm m}q}\right\|_{\infty},\\
\Psi\left(T_{\rm s}\right) =&\left\| H_5(s)C_{\rm m}(s\mathbb{I}_{n_{\rm m}}-A_{\rm m})^{-1}\left(e^{A_m\frac{T_{\rm s}}{N}}-\mathbb{I}_{n_{\rm m}}\right)\right\|_{\mathcal{L}_1},\\
\Omega_1(T_{\rm s}) =&\left(1-\|G(s)\|_{\mathcal{L}_1}L_{\rho_{\rm r}}\right)^{-1}\left(\left\|H_2(s)C(s)M^{-1}(s)\right\|_{\mathcal{L}_1}+\|H_2(s)\|_{\mathcal{L}_1}\left(N\Gamma\left(T_{\rm s}\right)+\Psi\left(T_{\rm s}\right)\right)\Upsilon\left(T_{\rm s}\right)\right),\\
\Theta(T_{\rm s}) =&\|H_3(s)\|_{\mathcal{L}_1}L_{\rho_{\rm r}}\Omega_1(T_{\rm s})+\left\|H_4(s)C(s)M^{-1}(s)\right\|_{\mathcal{L}_1}+\|H_4(s)\|_{\mathcal{L}_1}\left(N\Gamma\left(T_{\rm s}\right)+\Psi\left(T_{\rm s}\right)\right)\Upsilon\left(T_{\rm s}\right),\\
\rho_\Delta =&\|H_3(s)\|_{\mathcal{L}_1}\left(L_{\rho_{\rm r}}\rho_{\rm r}+L_2\right)+\|H_4(s)K_{\rm g}\|_{\mathcal{L}_1}M_{\rm r}+\left\|sH_1(s)M^{-1}(s)H_{\rm in}(s)\right\|_{\mathcal{L}_1}\rho_0,\\
\Omega_2(T_{\rm s}) \triangleq&\left\|C(s)M^{-1}(s)\right\|_{\mathcal{L}_1}+\|C(s)\|_{\mathcal{L}_1}L_{\rho_{\rm r}}\Omega_1(T_{\rm s})+\left(N\Gamma\left(T_{\rm s}\right)+\Psi\left(T_{\rm s}\right)\right)\Upsilon\left(T_{\rm s}\right),\\
\rho_{\rm ur} \triangleq&\|C(s)H_3(s)\|_{\mathcal{L}_1}\left(L_{\rho_{\rm r}}\rho_{\rm r}+L_2\right)+\left\|sC(s)H_1(s)M^{-1}(s)H_{\rm in}(s)\right\|_{\mathcal{L}_1}\rho_0+\left\|\left(\mathbb{I}_q-C(s)H_4(s)\right)K_{\rm g}\right\|_{\mathcal{L}_1}M_{\rm r},
\end{aligned}
\tag{4.37}
$$

where $H_i(\cdot)$'s are defined in (4.24). Next, we introduce the functions

$$
\beta_1(T_{\rm s})\triangleq\max_{t\in\left[0,\ \frac{T_{\rm s}}{N}\right]}\|\eta_1(t)\|_2,\quad \beta_2(T_{\rm s})\triangleq\max_{t\in\left[0,\ \frac{T_{\rm s}}{N}\right]}\|\eta_2(t)\|_2,
\tag{4.38}
$$

where $\eta_1(t)$ and $\eta_2(t)$ are given in (4.34). Also

$$
\beta_3(T_{\rm s})\triangleq\max_{t\in\left[0,\ \frac{T_{\rm s}}{N}\right]}\eta_3(t,T_{\rm s}),\quad \beta_4(T_{\rm s})\triangleq\max_{t\in\left[0,\ \frac{T_{\rm s}}{N}\right]}\eta_4(t),
\tag{4.39}
$$

where

$$
\eta_3(t,T_{\rm s})\triangleq\int_0^t\left\|\mathbf{1}_{n_{\rm m}q}^\top e^{\Lambda A_{\rm m}\Lambda^{-1}(t-\tau)}\Lambda\Phi^{-1}\left(T_{\rm s}\right)e^{\Lambda A_{\rm m}\Lambda^{-1}\frac{T_{\rm s}}{N}}\mathbf{1}_{n_{\rm m}q}\right\|_2 d\tau,\quad \eta_4(t)\triangleq\int_0^t\left\|\mathbf{1}_{n_{\rm m}q}^\top e^{\Lambda A_{\rm m}\Lambda^{-1}(t-\tau)}\Lambda B_{\rm m}\right\|_2 d\tau.
\tag{4.40}
$$

For $\bar\gamma_0>0$, let

$$
\Delta_1(\bar\gamma_0)\triangleq\rho_\Delta+\Theta(T_{\rm s})\bar\gamma_0,\quad \Delta_2(\bar\gamma_0)\triangleq\lambda_{\max}\left(\Lambda^{-\top}P\Lambda^{-1}\right)\left(\frac{2\sqrt{q}\Delta_1(\bar\gamma_0)\left\|\Lambda^{-\top}PB_{\rm m}\right\|_2}{\lambda_{\min}\left(\Lambda^{-\top}Q\Lambda^{-1}\right)}\right)^2,
\tag{4.41}
$$

where ρ_Δ and $\Theta(\cdot)$ are defined in (4.37). Also, let

$$
\varsigma(\bar\gamma_0,T_{\rm s})\triangleq\left\|\eta_2\left(\frac{T_{\rm s}}{N}\right)\right\|_2\sqrt{\frac{\Delta_2(\bar\gamma_0)}{\lambda_{\max}(P_2)}}+\sqrt{q}\kappa(T_{\rm s})\Delta_1(\bar\gamma_0),
\tag{4.42}
$$

where $\eta_2(\cdot)$ is defined in (4.34), and $\kappa(\cdot)$ is given in (4.35). Let

$$
\gamma_0(\bar\gamma_0,T_{\rm s})\triangleq\beta_1(T_{\rm s})\varsigma(\bar\gamma_0,T_{\rm s})+\beta_2(T_{\rm s})\sqrt{\frac{\Delta_2(\bar\gamma_0)}{\lambda_{\max}(P_2)}}+\beta_3(T_{\rm s})\varsigma(\bar\gamma_0,T_{\rm s})+\sqrt{q}\beta_4(T_{\rm s})\Delta_1(\bar\gamma_0).
\tag{4.43}
$$

Let μ be a positive constant, and $T_{s_{\max}}>0$ be a given upper bound on the sampling time $T_{\rm s}$.

For $F_{\rm z} \in \mathbb{R}^{q\times p}$, define

$$\begin{aligned}
\Delta_{\rm s}(\mu,\, F_{\rm z}) \triangleq & \frac{\|B_{\rm z}\|_\infty}{\mu} M_{\rm r} \|WF_{\rm z}\|_\infty \nu_1, \\
\Delta_{\mathcal{F}}(\mu,\, F_{\rm z}) \triangleq & \|B_{\rm z}\|_\infty \|M(s)(\mathbb{I}_q - C(s))\|_{\mathcal{L}_1} \rho_\Delta + \|B_{\rm z}\|_\infty \|C_{\rm x}\|_\infty \bar{\gamma}_1 + \|B_{\rm z}\|_\infty \left\| \frac{\mu}{s+\mu}\mathbb{I}_q - M(s)K_{\rm g} \right\|_{\mathcal{L}_1} M_{\rm r} \\
& + \|B_{\rm z}\|_\infty \left\| sC_{\rm m}\left(s\mathbb{I}_q - A_{\rm m}\right)^{-1} C_{\rm m}^\dagger C_{\rm m} \right\|_{\mathcal{L}_1} \rho_0 + \frac{\|B_{\rm z}\|_\infty}{\mu}\left(\delta_{\rm r_m} + M_{\rm r}\|WF_{\rm z}\|_\infty G_{\rho_r+\bar{\gamma}_1}\nu_2\right) \\
& + \frac{M_{\rm r}}{\mu}\|B_{\rm z}\|_\infty^2 \|WF_{\rm z}\|_\infty \left(\alpha M_{\rm r} + \|C_{\rm x}\|_\infty (\rho_{\rm r} + \bar{\gamma}_1)\right)\nu_2 + G_{\rho_{\rm r}+\bar{\gamma}_1} + \bar{\gamma}_{\rm r},
\end{aligned} \tag{4.44}$$

where $\bar{\gamma}_{\rm r}$ is an arbitrarily small positive constant, and

$$\nu_1 \triangleq \sup_{t\in(0,\, MT_{s\max}]} \frac{1}{t}\left\|e^{A_{\rm z}t} - \mathbb{I}_p\right\|_\infty, \quad \nu_2 \triangleq \sup_{t\in(0,\, MT_{s\max}]} \frac{1}{t}\int_0^t \left\|e^{A_{\rm z}(t-\tau)}\right\|_\infty d\tau. \tag{4.45}$$

Following a notation similar to [111], let $\mathcal{D}$ be the set of $q\times q$ diagonal matrices, whose diagonal elements are either 1 or 0. There are 2^q elements in $\mathcal{D}$, and we denote its elements as $D_i,\ i \in \{1,\, ...,\, 2^q\}$. Denote $D_i^- = \mathbb{I}_q - D_i$. It is easy to see that $D_i^- \in \mathcal{D}$. Let the positive definite matrix $S \in \mathbb{R}^{p\times p}$ be given. Next, the high-level controller design proceeds by considering $F_{\rm z},\, H_{\rm z} \in \mathbb{R}^{q\times p}$, a positive definite $R \in \mathbb{R}^{p\times p}$, and a constant $\mu > 0$, such that

$$\left(A_{\rm z} - B_{\rm z}(D_iF_{\rm z} + D_i^-H_{\rm z})\right)^\top R + R\left(A_{\rm z} - B_{\rm z}(D_iF_{\rm z} + D_i^-H_{\rm z})\right) + S \prec 0_{p\times p}, \quad \forall i \in \{1,\, ...,\, 2^q\}, \tag{4.46}$$

and

$$\|WH_{\rm z}\|_\infty \le (1-\alpha)\rho_{\rm z}^{-1}, \tag{4.47}$$

where α is introduced in Assumption 4.4, and

$$\rho_{\rm z} = \left(1 - \frac{2\sqrt{p}\,\|R\|_2\,\Delta_{\rm s}(\mu,\, F_{\rm z})}{\lambda_{\min}(S)}\right)^{-1} \frac{2\sqrt{p}\,\|R\|_2\,\Delta_{\mathcal{F}}(\mu,\, F_{\rm z})}{\lambda_{\min}(S)}, \tag{4.48}$$

with $\Delta_{\rm s}(\mu,\, F_{\rm z})$ and $\Delta_{\mathcal{F}}(\mu,\, F_{\rm z})$ defined in (4.44).

Finally, define

$$\begin{aligned}
\gamma_{\rm z}(\bar{\gamma}_0,\, T_{\rm s}) \triangleq & \alpha_3(T_{\rm s})\rho_{\rm z} + \alpha_4(T_{\rm s})\left(\|B_{\rm z}\|_\infty\left(\alpha M_{\rm r} + \|C_{\rm x}\|_\infty(\rho_{\rm r} + \Omega_1(T_{\rm s})\bar{\gamma}_0)\right) + G_{\rho_{\rm r}+\bar{\gamma}_1}\right), \\
\gamma_{\rm r}(\bar{\gamma}_0,\, T_{\rm s}) \triangleq & \|B_{\rm z}\|_\infty M_{\rm r}\left(2(1-e^{-\mu MT_{\rm s}}) + \|WF_{\rm z}\|_\infty \gamma_{\rm z}(\bar{\gamma}_0,\, T_{\rm s})\right),
\end{aligned} \tag{4.49}$$

where

$$\alpha_3(T_{\rm s}) \triangleq \max_{t\in[0,\,MT_{\rm s}]} \left\|e^{A_{\rm z}t} - \mathbb{I}_p\right\|_\infty, \quad \alpha_4(T_{\rm s}) \triangleq \max_{t\in[0,\,MT_{\rm s}]} \int_0^t \left\|e^{A_{\rm z}(t-\tau)}\right\|_\infty d\tau. \tag{4.50}$$

Lemma 4.1. *For all $\bar{\gamma}_0 > 0$, the following relationships hold:*

$$\lim_{T_{\rm s}\to 0} \gamma_0(\bar{\gamma}_0, T_{\rm s}) = 0, \quad \lim_{T_{\rm s}\to 0} \gamma_{\rm r}(\bar{\gamma}_0, T_{\rm s}) = 0, \tag{4.51}$$

where $\gamma_0(\cdot,\,\cdot)$ and $\gamma_{\rm z}(\cdot,\,\cdot)$ are given in (4.43) *and* (4.49) *respectively.*

Proof. The proof is similar to the proof of Lemma 3.3.1 in [47] and hence is omitted here. ■

Lemma 4.2. *There exist $T_{\rm s} > 0$ and an arbitrarily small positive constant $\bar{\gamma}_0$, such that*

$$\gamma_0(\bar{\gamma}_0,\, T_{\rm s}) < \bar{\gamma}_0, \quad \Omega_1(T_{\rm s})\bar{\gamma}_0 < \bar{\gamma}_1, \quad \gamma_{\rm r}(\bar{\gamma}_0,\, T_{\rm s}) < \bar{\gamma}_{\rm r}, \tag{4.52}$$

where $\bar{\gamma}_1$ and $\bar{\gamma}_{\rm r}$ are introduced in (4.27) *and* (4.44). *Also, $\Omega_1(\cdot)$, $\gamma_0(\cdot,\,\cdot)$, and $\gamma_{\rm r}(\cdot,\,\cdot)$ are defined in* (4.37), (4.43), *and* (4.49), *respectively.*

Proof. It is straightforward to verify that $\Omega_1(T_{\rm s})$ is a bounded function as $T_{\rm s}$ tends to zero. In addition, Lemma 4.1 shows that $\gamma_0(\bar{\gamma}_0, T_{\rm s})$ and $\gamma_{\rm z}(\bar{\gamma}_0, T_{\rm s})$ both approach arbitrarily close to zero for all $\bar{\gamma}_0$ with sufficiently small $T_{\rm s}$. Therefore, there always exist constants $T_{\rm s}$ and $\bar{\gamma}_0$ that satisfy the inequalities in (4.52). ■

The sampling time $T_{\rm s}$ of the digital controller is selected such that $T_{\rm s} \le T_{s_{\max}}$, and the inequalities in (4.52) hold.

Lemma 4.3. *For arbitrary $\xi = \begin{bmatrix} y_1 \\ y_2 \end{bmatrix} \in \mathbb{R}^{n_{\rm m}}$, where $y_1 \in \mathbb{R}^q$ and $y_2 \in \mathbb{R}^{(n_{\rm m}-q)}$, there exist positive definite $P_1 \in \mathbb{R}^{q\times q}$ and $P_2 \in \mathbb{R}^{(n_{\rm m}-q)\times(n_{\rm m}-q)}$ such that*

$$\xi^\top \left(\Lambda^{-1}\right)^\top P \Lambda^{-1} \xi = y_1^\top P_1 y_1 + y_2^\top P_2 y_2, \tag{4.53}$$

where Λ is given in (4.17). *Also, P_1 and P_2 are defined in* (4.33).

Proof. The proof of Lemma 4.3 can be found in [47]. ■

Consider the following closed-loop reference system

$$\begin{aligned} \dot{x}_{\rm ref}(t) &= A_{\rm x} x_{\rm ref}(t) + B_{\rm x}\left(u_{\rm ref}(t) + f\left(t, x_{\rm ref}(t)\right) + d(t)\right), \quad x_{\rm ref}(0) = x_0 \\ u_{\rm ref}(s) &= K_{\rm g} r(s) - C(s)\sigma_{\rm ref}(s), \\ y_{\rm ref}(t) &= C_{\rm x} x_{\rm ref}(t), \end{aligned} \tag{4.54}$$

where

$$\begin{aligned}\sigma_{\rm ref}(s) =&[(P(s)-M(s))\,C(s)+M(s)]^{-1}\,(P(s)-M(s))\,K_{\rm g}r(s)\\ &+[(P(s)-M(s))\,C(s)+M(s)]^{-1}\,(P(s)w_{\rm ref}(s)+H_{\rm in}(s)x_0)\,,\end{aligned}\tag{4.55}$$

and $w_{\rm ref}(s)$ is the Laplace transform of $w_{\rm ref}(t)$ given by

$$w_{\rm ref}(t)=F_{\rm x}x_{\rm ref}(t)+f\,(t,x_{\rm ref}(t))+d(t).\tag{4.56}$$

The reference system can be rewritten as

$$y_{\rm ref}(s) =M(s)K_{\rm g}r(s)+M(s)\,(\mathbb{I}_q-C(s))\,\sigma_{\rm ref}(s)+C_{\rm m}\,(s\mathbb{I}_{n_{\rm m}}-A_{\rm m})^{-1}\,C_{\rm m}^{\dagger}y_0.\tag{4.57}$$

From (4.57) we notice that the unknown uncertainty $\sigma_{\rm ref}(t)$, given by the Laplace transform in (4.55), is mitigated within the bandwidth of $C(s)$, and the desired response (in Assumption 4.2) is recovered. The reference system in (4.54) defines the *achievable performance* by the closed-loop multirate system given in (4.1), (4.14)-(4.20), as the sampling time $T_{\rm s}$ of the digital controller tends to zero. In the following, we first prove that $\sigma_{\rm ref}(t)$ is bounded, and the reference system in (4.54) is stable. Then we establish uniform bounds between the closed-loop system defined by (4.1), (4.14)-(4.20) and the reference system.

Lemma 4.4. *For the closed-loop reference system in* (4.54)*, subject to the* $\mathcal{L}_1$*-norm condition* (4.31)*, if* $\|x_0\|_\infty\le\rho_0$*, then*

$$\|x_{\rm ref}\|_{\mathcal{L}_\infty}<\rho_{\rm r},\tag{4.58}$$

$$\|u_{\rm ref}\|_{\mathcal{L}_\infty}<\rho_{\rm ur},\tag{4.59}$$

where $\rho_{\rm r}$ *and* $\rho_{\rm ur}$ *are given in* (4.37)*.*

Proof. It follows from (4.54) and the definition of $H_0(s)$, $H_5(s)$, $P(s)$ and $G(s)$ in (4.24) that

$$x_{\rm ref}(s)=[H_0(s)-H_5(s)\,(P(s)-M(s))]\,K_{\rm g}r(s)-G(s)w_{\rm ref}(s)-H_5(s)H_{\rm in}(s)x_o+(s\mathbb{I}_n-A_{\rm x}+B_{\rm x}F_{\rm x})^{-1}x_0.$$

Then the following upper bound can be established for $\tau>0$

$$\|x_{{\rm ref}\,\tau}\|_{\mathcal{L}_\infty}\le\|G(s)\|_{\mathcal{L}_1}\|w_{{\rm ref}\,\tau}\|_{\mathcal{L}_\infty}+\|H_2(s)K_{\rm g}\|_{\mathcal{L}_1}\|r\|_{\mathcal{L}_\infty}+\left\|s(s\mathbb{I}_n-A_{\rm x}+B_{\rm x}F_{\rm x})^{-1}-sH_5(s)H_{\rm in}(s)\right\|_{\mathcal{L}_1}\left\|\frac{1}{s}x_0\right\|_{\mathcal{L}_\infty}.\tag{4.60}$$

We have $\|x_{\rm ref}(0)\|_\infty=\|x_0\|_\infty<\rho_{\rm r}$. In addition, $x_{\rm ref}(t)$ is continuous. Therefore, if the bound in (4.58) is not true, there exists a time $\tau_1>0$, such that

$$\|x_{\rm ref}(t)\|_\infty<\rho_{\rm r},\quad\forall t\in[0,\,\tau_1),\quad\|x_{\rm ref}(\tau_1)\|_\infty=\rho_{\rm r},$$

which implies that $\left\|x_{{\rm ref}\,\tau_1}\right\|_{\mathcal{L}_\infty}=\rho_{\rm r}$. Then it follows from Assumption 4.1 and the redefinition in

(4.27) that

$$\left\|w_{\mathrm{ref}\,\tau_1}\right\|_{\mathcal{L}_\infty} \leq L_{\rho_\mathrm{r}} \left\|x_{\mathrm{ref}\,\tau_1}\right\|_{\mathcal{L}_\infty} + L_2. \tag{4.61}$$

The bound in (4.61), together with the upper bound in (4.60), lead to

$$\left\|x_{\mathrm{ref}\,\tau_1}\right\|_{\mathcal{L}_\infty} \leq \tfrac{\|G(s)\|_{\mathcal{L}_1} L_2 + \rho_1 + \rho_2}{1 - \|G(s)\|_{\mathcal{L}_1} L_{\rho_\mathrm{r}}}.$$

The condition in (4.31) can be solved for ρ_r to obtain the bound

$$\rho_\mathrm{r} > \tfrac{\|G(s)\|_{\mathcal{L}_1} L_2 + \rho_1 + \rho_2}{1 - \|G(s)\|_{\mathcal{L}_1} L_{\rho_\mathrm{r}}},$$

which leads to $\left\|x_{\mathrm{ref}\,\tau_1}\right\|_{\mathcal{L}_\infty} < \rho_\mathrm{r}$. This contradicts $\left\|x_{\mathrm{ref}\,\tau_1}\right\|_{\mathcal{L}_\infty} = \rho_r$, thus proving the bound in (4.58). This further implies that the upper bound in (4.61) holds for all $\tau_1 > 0$ with strict inequality, which in turn implies that

$$\|w_{\mathrm{ref}}\|_{\mathcal{L}_\infty} < L_{\rho_\mathrm{r}} \rho_\mathrm{r} + L_2. \tag{4.62}$$

The bound on $u_{\mathrm{ref}}(t)$ follows from (4.54), (4.55) and (4.62), which proves (4.59). ■

Remark 4.4. *Lemma 4.4 implies that $\sigma_{\mathrm{ref}}(t)$, with its Laplace transform defined in* (4.55)*, is bounded*

$$\|\sigma_{\mathrm{ref}}\|_{\mathcal{L}_\infty} \leq \rho_\Delta, \tag{4.63}$$

where ρ_Δ is defined in (4.37)*.*

We consider an equivalent state-space model of the predictor dynamics in (4.15) given by

$$\begin{aligned} \dot{\hat{x}}(t) &= A_\mathrm{m}\hat{x}(t) + B_\mathrm{m}u(t) + \hat{\sigma}(t), \quad \hat{x}(0) = C_\mathrm{m}^\dagger y_0 \\ \hat{y}(t) &= C_\mathrm{m}\hat{x}(t), \end{aligned} \tag{4.64}$$

where

$$\hat{\sigma}(t) = \hat{\sigma}_\mathrm{d}[j], \quad t \in \left[j\frac{T_\mathrm{s}}{N},\ (j+1)\frac{T_\mathrm{s}}{N} \right), \quad j \in \mathbb{Z}_{\geq 0}, \tag{4.65}$$

and $u(t)$ is given by (4.3) and (4.14). Since $\hat{\sigma}(t)$ and $u(t)$ are piecewise constants in (4.64), from (4.15) we have

$$\hat{y}\left(j\frac{T_\mathrm{s}}{N}\right) = \hat{y}_\mathrm{d}[j], \quad j \in \mathbb{Z}_{\geq 0}. \tag{4.66}$$

Let $\tilde{x}(t) = \hat{x}(t) - x_\mathrm{a}(t)$, where $x_\mathrm{a}(t)$ is defined in (4.25). Then the prediction error dynamics between (4.25) and (4.64) are given by

$$\begin{aligned} \dot{\tilde{x}}(t) &= A_\mathrm{m}\tilde{x}(t) + \hat{\sigma}(t) - B_\mathrm{m}\sigma(t), \quad \tilde{x}(0) = 0_{n_\mathrm{m}\times 1}, \\ \tilde{y}(t) &= C_\mathrm{m}\tilde{x}(t), \end{aligned} \tag{4.67}$$

where $\hat{\sigma}(t)$ is defined in (4.65).

Lemma 4.5. *Consider the closed-loop system defined by* (4.1), (4.14)-(4.20), *and the closed-loop reference system in* (4.54). *The following upper bound holds*

$$\|(x_{\rm ref}-x)_t\|_{\mathcal{L}_\infty}\leq \Omega_1(T_{\rm s})\|\tilde{y}_t\|_{\mathcal{L}_\infty},$$

where $\Omega_1(\cdot)$ *is given in* (4.37), *and* $\tilde{y}(t)$ *is the prediction error defined in* (4.67).

Proof. Let

$$u_{\rm C}(s)=K_{\rm g}r(s)-C(s)M^{-1}(s)C_{\rm m}(s\mathbb{I}_{n_{\rm m}}-A_{\rm m})^{-1}\hat{\sigma}(s), \tag{4.68}$$

$$u_{\rm M}(s)=K_{\rm g}r(s)-C(s)M^{-1}(s)C_{\rm m}(s\mathbb{I}_{n_{\rm m}}-A_{\rm m})^{-1}e^{-A_{\rm m}\frac{T_{\rm s}}{N}}\hat{\sigma}(s). \tag{4.69}$$

It follows from (4.67) that

$$\tilde{y}(s)=-M(s)\sigma(s)+C_{\rm m}(s\mathbb{I}_{n_{\rm m}}-A_{\rm m})^{-1}\hat{\sigma}(s). \tag{4.70}$$

Letting $e(t)\triangleq x_{\rm ref}(t)-x(t)$ and denoting by $d_{\rm e}(s)$ the Laplace transform of

$$d_{\rm e}(t)\triangleq w_{\rm ref}(t)-w(t), \tag{4.71}$$

it follows from (4.1), (4.26), (4.14), (4.54), (4.68), (4.69) and (4.70)

$$\begin{aligned}e(s)=&H_0(s)C(s)M^{-1}(s)\tilde{y}(s)+H_0(s)d_{\rm e}(s)+H_0(s)\left(u_{\rm C}(s)-u_{\rm M}(s)\right)+H_0(s)\left(u_{\rm M}(s)-u(s)\right)\\&-H_0(s)C(s)\left(\sigma_{\rm ref}(s)-\sigma(s)\right),\end{aligned} \tag{4.72}$$

where $H_0(s)$ is defined in (4.24). Further

$$\begin{aligned}H_0(s)C(s)\left(\sigma_{\rm ref}(s)-\sigma(s)\right)=&H_5(s)P(s)d_{\rm e}(s)-H_5(s)\left(P(s)-M(s)\right)\left(u_{\rm C}(s)-u_{\rm M}(s)\right)\\&-H_5(s)\left(P(s)-M(s)\right)\left(u_{\rm M}(s)-u(s)\right)+H_5(s)\left(P(s)-M(s)\right)C(s)M^{-1}(s)\tilde{y}(s).\end{aligned} \tag{4.73}$$

From (4.72) and (4.73) one can obtain

$$\begin{aligned}e(s)=&\left(H_0(s)-H_5(s)\left(P(s)-M(s)\right)\right)C(s)M^{-1}(s)\tilde{y}(s)+\left(H_0(s)-H_5(s)\left(P(s)-M(s)\right)\right)\left(u_{\rm C}(s)-u_{\rm M}(s)\right)\\&+\left(H_0(s)-H_5(s)\left(P(s)-M(s)\right)\right)\left(u_{\rm M}(s)-u(s)\right)+\left(H_0(s)-H_5(s)P(s)\right)d_{\rm e}(s).\end{aligned} \tag{4.74}$$

Then the upper bound is given by

$$\begin{aligned}\|e_t\|_{\mathcal{L}_\infty}\leq&\left\|\left(H_0(s)-H_5(s)\left(P(s)-M(s)\right)\right)C(s)M^{-1}(s)\right\|_{\mathcal{L}_1}\|\tilde{y}_t\|_{\mathcal{L}_\infty}+\|\left(H_0(s)-H_5(s)\left(P(s)-M(s)\right)\right)\|_{\mathcal{L}_1}\left\|\left(u_{\rm C}-u_{\rm M}\right)_t\right\|_{\mathcal{L}_\infty}\\&+\|\left(H_0(s)-H_5(s)\left(P(s)-M(s)\right)\right)\|_{\mathcal{L}_1}\left\|\left(u_{\rm M}-u\right)_t\right\|_{\mathcal{L}_\infty}+\|G(s)\|_{\mathcal{L}_1}L_{\rho_{\rm r}}\|e_t\|_{\mathcal{L}_\infty}.\end{aligned} \tag{4.75}$$

From (4.66) we have

$$\tilde{y}\left(j\frac{T_{\rm s}}{N}\right)=\tilde{y}_{\rm d}[j],\quad j\in\mathbb{Z}_{\geq 0}. \tag{4.76}$$

From (4.20), (4.65) and (4.76) the following relation can be derived

$$\left\|e^{-A_{\rm m}\frac{T_{\rm s}}{N}}\hat{\sigma}_t\right\|_{\mathcal{L}_\infty}\leq\Upsilon\left(T_{\rm s}\right)\left\|\tilde{y}_t\right\|_{\mathcal{L}_\infty}, \tag{4.77}$$

where $\Upsilon(\cdot)$ is defined in (4.37). Notice that $u_{\rm d}[i]$ in (4.14) is a step-invariant discrete-time approximation of $u_{\rm M}(s)$, given in (4.69). Therefore, the discretization error bound between (4.3) and (4.69) is given by

$$\left\|(u_{\rm M}-u)_t\right\|_{\mathcal{L}_\infty}\leq N\Gamma\left(T_{\rm s}\right)\Upsilon\left(T_{\rm s}\right)\left\|\tilde{y}_t\right\|_{\mathcal{L}_\infty}, \tag{4.78}$$

where $\Gamma(\cdot)$ is introduced in (4.36). Moreover, from (4.68), (4.69) and (4.77) one can obtain

$$\left\|(u_{\rm C}-u_{\rm M})_t\right\|_{\mathcal{L}_\infty}\leq\Psi\left(T_{\rm s}\right)\Upsilon\left(T_{\rm s}\right)\left\|\tilde{y}_t\right\|_{\mathcal{L}_\infty}, \tag{4.79}$$

where $\Psi(\cdot)$ is defined in (4.37). From (4.75), (4.78) and (4.79) the following upper bound can be deduced

$$\left\|e_t\right\|_{\mathcal{L}_\infty}\leq\Omega_1(T_{\rm s})\left\|\tilde{y}_t\right\|_{\mathcal{L}_\infty}. \tag{4.80}$$

This concludes the proof. ■

Theorem 4.1. *Consider the system in* (4.1) *and the controller in* (4.14)-(4.20)*, subject to conditions in* (4.30) *and* (4.31)*. Assume that* $T_{\rm s}\leq T_{s_{\max}}$ *is selected sufficiently small, such that the inequalities in* (4.52) *hold. If* $\left\|x_0\right\|_\infty\leq\rho_0$*, then*

$$\left\|\tilde{y}\right\|_{\mathcal{L}_\infty}<\bar{\gamma}_0, \tag{4.81}$$

$$\left\|x_{\rm ref}-x\right\|_{\mathcal{L}_\infty}<\Omega_1(T_{\rm s})\bar{\gamma}_0,\quad \left\|u_{\rm ref}-u\right\|_{\mathcal{L}_\infty}<\Omega_2(T_{\rm s})\bar{\gamma}_0, \tag{4.82}$$

where $\tilde{y}(t)$ *is the prediction error, defined in* (4.67)*, and* $\bar{\gamma}_0>0$ *is a given arbitrarily small constant. Also,* $\Omega_1(T_{\rm s})$ *and* $\Omega_2(T_{\rm s})$ *are defined in* (4.37) *respectively.*

Proof. Let $\bar{\gamma}_0$ be a constant satisfying (4.52). First, we prove the bound in (4.81) by a contradiction argument. Since $\tilde{y}(0)=0$, and $\tilde{y}(t)$ is continuous, then assuming the opposite implies that there exists τ_1, such that

$$\begin{aligned}\left\|\tilde{y}(t)\right\|_\infty&<\bar{\gamma}_0,\quad \forall\, 0\leq t<\tau_1,\\ \left\|\tilde{y}(\tau_1)\right\|_\infty&=\bar{\gamma}_0,\end{aligned} \tag{4.83}$$

which leads to

$$\left\|\tilde{y}_{\tau_1}\right\|_{\mathcal{L}_\infty}=\bar{\gamma}_0. \tag{4.84}$$

Let $e(t) \triangleq x_{\rm ref}(t) - x(t)$. The sampling time $T_{\rm s}$ is selected such that the inequities in (4.52) hold. Then the bound in (4.52), Lemma 4.5 and the upper bound in (4.58) can be used to derive the following bound

$$\|x_{\tau_1}\|_{\mathcal{L}_\infty} \leq \left\|x_{{\rm ref}_{\tau_1}}\right\|_{\mathcal{L}_\infty} + \|e_{\tau_1}\|_{\mathcal{L}_\infty} < \rho_{\rm r} + \bar{\gamma}_1, \tag{4.85}$$

which implies

$$\|w_{\tau_1}\|_{\mathcal{L}_\infty} \leq L_{\rho_{\rm r}}\rho_{\rm r} + L_2. \tag{4.86}$$

One can obtain from (4.55)

$$\left\|\sigma_{{\rm ref}_{\tau_1}}\right\|_{\mathcal{L}_\infty} \leq \rho_\Delta, \tag{4.87}$$

where ρ_Δ is defined in (4.37). Also, we have

$$\sigma_{\rm ref}(s) - \sigma(s) = H_3(s)d_{\rm e}(s) - H_4(s)\left(u_{\rm M}(s) - u(s)\right) - H_4(s)\left(u_{\rm C}(s) - u_{\rm M}(s)\right) + H_4(s)C(s)M^{-1}(s)\tilde{y}(s), \tag{4.88}$$

which along with (4.87) implies

$$\|\sigma_{\tau_1}\|_{\mathcal{L}_\infty} \leq \Delta_1(\bar{\gamma}_0), \tag{4.89}$$

where $\Delta(\cdot)$ is defined in (4.41).

Now consider the state transformation

$$\tilde{\xi} = \Lambda\tilde{x}, \tag{4.90}$$

where Λ is defined in (4.17), and $\tilde{x}(t) = \hat{x}(t) - x_{\rm a}(t)$. From (4.67) and (4.90) it follows

$$\begin{aligned} &\dot{\tilde{\xi}}(t) = \Lambda A_{\rm m}\Lambda^{-1}\tilde{\xi}(t) + \Lambda\hat{\sigma}(t) - \Lambda B_{\rm m}\sigma(t), \quad \tilde{\xi}(0) = 0_{n_{\rm m}\times 1} \\ &\tilde{y}(t) = \mathbf{1}_{n_{\rm m}q}\tilde{\xi}(t). \end{aligned} \tag{4.91}$$

From (4.91) we have

$$\tilde{\xi}\left(j\frac{T_{\rm s}}{N} + t\right) = e^{\Lambda A_m\Lambda^{-1}t}\tilde{\xi}\left(j\frac{T_{\rm s}}{N}\right) + \int_0^t e^{\Lambda A_m\Lambda^{-1}(t-\tau)}\Lambda\left(\hat{\sigma}\left(j\frac{T_{\rm s}}{N}\right) - B_{\rm m}\sigma\left(j\frac{T_{\rm s}}{N} + \tau\right)\right)d\tau. \tag{4.92}$$

Since

$$\tilde{\xi}\left(j\frac{T_{\rm s}}{N} + t\right) = \left[\begin{array}{c} \tilde{y}(j\frac{T_{\rm s}}{N} + t) \\ 0_{(n_m-q)\times 1} \end{array}\right] + \left[\begin{array}{c} 0_{q\times 1} \\ \tilde{z}(j\frac{T_{\rm s}}{N} + t) \end{array}\right],$$

where $\tilde{z}(t) = \left[\tilde{\xi}_{q+1}(t), ..., \tilde{\xi}_{n_{\rm m}}(t)\right]^\top$, $\tilde{\xi}(j\frac{T_{\rm s}}{N} + t)$ can be decomposed as

$$\tilde{\xi}\left(j\frac{T_{\rm s}}{N} + t\right) = \chi\left(j\frac{T_{\rm s}}{N} + t\right) + \zeta\left(j\frac{T_{\rm s}}{N} + t\right), \tag{4.93}$$

such that

$$\chi\left(j\frac{T_{\rm s}}{N}+t\right)=e^{\Lambda A_{\rm m}\Lambda^{-1}t}\left[\begin{array}{c}\tilde{y}\left(j\frac{T_{\rm s}}{N}\right)\\ 0_{(n_{\rm m}-q)\times 1}\end{array}\right]+\int_0^t e^{\Lambda A_{\rm m}\Lambda^{-1}(t-\tau)}\Lambda\hat{\sigma}\left(j\frac{T_{\rm s}}{N}\right)d\tau, \tag{4.94}$$

$$\zeta\left(j\frac{T_{\rm s}}{N}+t\right)=e^{\Lambda A_{\rm m}\Lambda^{-1}t}\left[\begin{array}{c}0_{q\times 1}\\ \tilde{z}(j\frac{T_{\rm s}}{N})\end{array}\right]-\int_0^t e^{\Lambda A_{\rm m}\Lambda^{-1}(t-\tau)}\Lambda B_{\rm m}\sigma\left(j\frac{T_{\rm s}}{N}+\tau\right)d\tau. \tag{4.95}$$

Next we prove that

$$\left\|\tilde{y}\left(j\frac{T_{\rm s}}{N}\right)\right\|_2\leq\varsigma(\bar{\gamma}_0,T_{\rm s}),\quad \tilde{z}^\top\left(j\frac{T_{\rm s}}{N}\right)P_2\tilde{z}\left(j\frac{T_{\rm s}}{N}\right)\leq\Delta_2(\bar{\gamma}_0),\quad \forall j\frac{T_{\rm s}}{N}\leq\tau_1, \tag{4.96}$$

where $\Delta(\cdot)$ and $\varsigma(\cdot,\cdot)$ are defined in (4.41) and (4.42) respectively. It is straightforward to show that $\|\tilde{y}(0)\|_2\leq\varsigma(\bar{\gamma}_0,T_{\rm s})$, $\tilde{z}^\top(0)P_2\tilde{z}(0)\leq\Delta_2(\bar{\gamma}_0)$. Next, for arbitrary $k\in\mathbb{Z}_{\geq 0}$, such that $(k+1)\frac{T_{\rm s}}{N}\leq\tau_1$, we prove that if

$$\left\|\tilde{y}\left(k\frac{T_{\rm s}}{N}\right)\right\|_2\leq\varsigma(\bar{\gamma}_0,T_{\rm s}), \tag{4.97}$$

$$\tilde{z}^\top\left(k\frac{T_{\rm s}}{N}\right)P_2\tilde{z}\left(k\frac{T_{\rm s}}{N}\right)\leq\Delta_2(\bar{\gamma}_0), \tag{4.98}$$

then the inequalities in (4.97)-(4.98) hold for $k+1$ as well, which would imply that the bounds in (4.97)-(4.98) hold for all $k\in\mathbb{Z}_{\geq 0}$, such that $k\frac{T_{\rm s}}{N}\leq\tau_1$. To this end, suppose that (4.97) and (4.98) hold for $k\in\mathbb{Z}_{\geq 0}$, and in addition that $(k+1)\frac{T_{\rm s}}{N}\leq\tau_1$. Then it follows from (4.93) that

$$\tilde{\xi}\left((k+1)\frac{T_{\rm s}}{N}\right)=\chi\left((k+1)\frac{T_{\rm s}}{N}\right)+\zeta\left((k+1)\frac{T_{\rm s}}{N}\right), \tag{4.99}$$

where

$$\chi\left((k+1)\frac{T_{\rm s}}{N}\right)=e^{\Lambda A_{\rm m}\Lambda^{-1}\frac{T_{\rm s}}{N}}\left[\begin{array}{c}\tilde{y}(k\frac{T_{\rm s}}{N})\\ 0_{(n_{\rm m}-q)\times 1}\end{array}\right]+\int_0^{\frac{T_{\rm s}}{N}} e^{\Lambda A_{\rm m}\Lambda^{-1}(\frac{T_{\rm s}}{N}-\tau)}\Lambda\hat{\sigma}\left(k\frac{T_{\rm s}}{N}\right)d\tau, \tag{4.100}$$

$$\zeta\left((k+1)\frac{T_{\rm s}}{N}\right)=e^{\Lambda A_{\rm m}\Lambda^{-1}\frac{T_{\rm s}}{N}}\left[\begin{array}{c}0_{q\times 1}\\ \tilde{z}(k\frac{T_{\rm s}}{N})\end{array}\right]-\int_0^{\frac{T_{\rm s}}{N}} e^{\Lambda A_{\rm m}\Lambda^{-1}(\frac{T_{\rm s}}{N}-\tau)}\Lambda B_{\rm m}\sigma\left(k\frac{T_{\rm s}}{N}+\tau\right)d\tau. \tag{4.101}$$

Using (4.76) and substituting the adaptive law from (4.20) and (4.65) for $\hat{\sigma}\left(k\frac{T_{\rm s}}{N}\right)$ in (4.100), we have

$$\chi\left((k+1)\frac{T_{\rm s}}{N}\right)=0. \tag{4.102}$$

From (4.95), it follows that $\zeta(t)$ is the solution of the system:

$$\begin{aligned}\dot{\zeta}(t)&=\Lambda A_{\rm m}\Lambda^{-1}\zeta(t)-\Lambda B_{\rm m}\sigma(t),\\ \zeta\left(k\frac{T_{\rm s}}{N}\right)&=\left[\begin{array}{c}0_{(n_{\rm m}-q)\times 1}\\ \tilde{z}(k\frac{T_{\rm s}}{N})\end{array}\right],\quad t\in\left[k\frac{T_{\rm s}}{N},\ (k+1)\frac{T_{\rm s}}{N}\right).\end{aligned} \tag{4.103}$$

Let

$$V(t) = \zeta^\top(t)\Lambda^{-\top}P\Lambda^{-1}\zeta(t), \quad \forall t \in \left[k\frac{T_\mathrm{s}}{N}, (k+1)\frac{T_\mathrm{s}}{N}\right).$$

Since Λ is nonsingular, and P is positive definite, $\Lambda^{-\top}P\Lambda^{-1}$ is positive definite, and, hence, $V(t)$ is a positive-definite function. Using Lemma 4.3 and Equation (4.103), we can derive

$$V\left(\zeta\left(k\frac{T_\mathrm{s}}{N}\right)\right) = \tilde{z}^\top\left(k\frac{T_\mathrm{s}}{N}\right)\Lambda^{-\top}P\Lambda^{-1}\tilde{z}\left(k\frac{T_\mathrm{s}}{N}\right),$$

which, along with the upper bound in (4.98), yields

$$V\left(\zeta\left(k\frac{T_\mathrm{s}}{N}\right)\right) \leq \Delta_2(\bar{\gamma}_0). \tag{4.104}$$

From (4.103) it follows that for all $t \in \left[k\frac{T_\mathrm{s}}{N}, (k+1)\frac{T_\mathrm{s}}{N}\right)$

$$\begin{aligned}\dot{V}(t) =& \zeta^\top(t)\Lambda^{-\top}P\Lambda^{-1}\Lambda A_\mathrm{m}\Lambda^{-1}\zeta(t) + \zeta^\top(t)\Lambda^{-\top}A_\mathrm{m}^\top\Lambda^\top\Lambda^{-\top}P^\top\Lambda^{-1}\zeta(t) - 2\zeta^\top(t)\Lambda^{-\top}P\Lambda^{-1}\Lambda B_\mathrm{m}\sigma(t)\\ =& -\zeta^\top(t)\Lambda^{-\top}Q\Lambda^{-1}\zeta(t) - 2\zeta^\top(t)\Lambda^{-\top}P\Lambda^{-1}\Lambda B_\mathrm{m}\sigma(t).\end{aligned}$$

Using the upper bound from (4.89), for all $t \in \left[k\frac{T_\mathrm{s}}{N}, (k+1)\frac{T_\mathrm{s}}{N}\right)$, one can derive

$$\dot{V}(t) \leq -\lambda_{\min}\left(\Lambda^{-\top}Q\Lambda^{-1}\right)\|\zeta(t)\|_2^2 + 2\|\zeta(t)\|_2\left\|\Lambda^{-\top}PB_m\right\|_2\sqrt{q}\Delta_1(\bar{\gamma}_0). \tag{4.105}$$

Notice that if

$$V(t) > \Delta_2(\bar{\gamma}_0), \quad \forall t \in \left[k\frac{T_\mathrm{s}}{N}, (k+1)\frac{T_\mathrm{s}}{N}\right), \tag{4.106}$$

the following holds

$$\|\zeta(t)\|_2 > \sqrt{\frac{\Delta_2(\bar{\gamma}_0)}{\lambda_{\max}\left(\Lambda^{-\top}P\Lambda^{-1}\right)}} = \frac{2\sqrt{q}\Delta_1(\bar{\gamma}_0)\left\|\Lambda^{-\top}PB_\mathrm{m}\right\|_2}{\lambda_{\min}\left(\Lambda^{-\top}Q\Lambda^{-1}\right)}.$$

Moreover, the upper bound in (4.105) yields

$$\dot{V}(t) < 0. \tag{4.107}$$

From (4.104), (4.106) and (4.107), it follows

$$V(t) \leq \Delta_2(\bar{\gamma}_0), \quad \forall t \in \left[k\frac{T_\mathrm{s}}{N}, (k+1)\frac{T_\mathrm{s}}{N}\right),$$

and therefore

$$\zeta^\top\left((k+1)\frac{T_\mathrm{s}}{N}\right)\Lambda^{-\top}P\Lambda^{-1}\zeta\left((k+1)\frac{T_\mathrm{s}}{N}\right) \leq \Delta_2(\bar{\gamma}_0). \tag{4.108}$$

Then (4.99), (4.102) and the upper bound in (4.108) lead to the following inequality

$$\tilde{\xi}^\top\left((k+1)\frac{T_\mathrm{s}}{N}\right)\Lambda^{-\top}P\Lambda^{-1}\tilde{\xi}\left((k+1)\frac{T_\mathrm{s}}{N}\right)\leq\Delta_2(\bar{\gamma}_0).$$

Using the result of Lemma 4.3, one can derive

$$\tilde{z}^\top\left((k+1)\tfrac{T_\mathrm{s}}{N}\right)P_2\tilde{z}\left((k+1)\tfrac{T_\mathrm{s}}{N}\right)\leq\tilde{\xi}^\top\left((k+1)\tfrac{T_\mathrm{s}}{N}\right)\Lambda^{-\top}P\Lambda^{-1}\tilde{\xi}\left((k+1)\tfrac{T_\mathrm{s}}{N}\right)\leq\Delta_2(\bar{\gamma}_0),$$

which implies that the upper bound in (4.98) holds for $k+1$.

Next, from (4.91), (4.99) and (4.102) it follows

$$\tilde{y}\left((k+1)\frac{T_\mathrm{s}}{N}\right)=\mathbf{1}_{n_\mathrm{m}q}^\top\zeta\left((k+1)\frac{T_\mathrm{s}}{N}\right),$$

and the definition of $\zeta\left((k+1)\frac{T_\mathrm{s}}{N}\right)$ in (4.101) leads to the following expression

$$\tilde{y}\left((k+1)\frac{T_\mathrm{s}}{N}\right)=\mathbf{1}_{n_\mathrm{m}q}^\top e^{\Lambda A_\mathrm{m}\Lambda^{-1}\frac{T_\mathrm{s}}{N}}\begin{bmatrix}0_{q\times1}\\ \tilde{z}(k\frac{T_\mathrm{s}}{N})\end{bmatrix}-\mathbf{1}_{n_\mathrm{m}q}^\top\int_0^{\frac{T_\mathrm{s}}{N}}e^{\Lambda A_\mathrm{m}\Lambda^{-1}(\frac{T_\mathrm{s}}{N}-\tau)}\Lambda B_\mathrm{m}\sigma\left(k\frac{T_\mathrm{s}}{N}+\tau\right)d\tau.$$

The upper bounds in (4.89) and (4.98) yield the following upper bound

$$\left\|\tilde{y}\left((k+1)\tfrac{T_\mathrm{s}}{N}\right)\right\|_2\leq\left\|\eta_2(\tfrac{T_\mathrm{s}}{N})\right\|_2\left\|\tilde{z}(k\tfrac{T_\mathrm{s}}{N})\right\|_2+\int_0^{\frac{T_\mathrm{s}}{N}}\left\|\mathbf{1}_{n_\mathrm{m}q}^\top e^{\Lambda A_\mathrm{m}\Lambda^{-1}(\frac{T_\mathrm{s}}{N}-\tau)}\Lambda B_\mathrm{m}\right\|_2\left\|\sigma\left(k\tfrac{T_\mathrm{s}}{N}+\tau\right)\right\|_2d\tau\leq\varsigma(\bar{\gamma}_0,T_\mathrm{s}),$$

where $\eta_2(\cdot)$, $\kappa(\cdot)$ and $\varsigma(\cdot,\,\cdot)$ are defined in (4.34), (4.35) and (4.42) respectively. This confirms the upper bound in (4.97) for $k+1$. Hence, Equation (4.96) holds for all $j\frac{T_\mathrm{s}}{N}\leq\tau_1$.

For all $j\frac{T_\mathrm{s}}{N}+t\leq\tau_1$ and $t\in\left[0,\,\frac{T_\mathrm{s}}{N}\right]$, using the expression from (4.92), we obtain

$$\begin{aligned}\tilde{y}\left(j\frac{T_\mathrm{s}}{N}+t\right)=&\mathbf{1}_{n_\mathrm{m}q}^\top e^{\Lambda A_\mathrm{m}\Lambda^{-1}t}\tilde{\xi}\left(j\frac{T_\mathrm{s}}{N}\right)+\mathbf{1}_{n_\mathrm{m}q}^\top\int_0^t e^{\Lambda A_\mathrm{m}\Lambda^{-1}(t-\tau)}\Lambda\hat{\sigma}\left(j\frac{T_\mathrm{s}}{N}\right)d\tau\\&-\mathbf{1}_{n_\mathrm{m}q}^\top\int_0^t e^{\Lambda A_\mathrm{m}\Lambda^{-1}(t-\tau)}\Lambda B_\mathrm{m}\sigma\left(j\frac{T_\mathrm{s}}{N}+\tau\right)d\tau.\end{aligned}$$

The upper bound in (4.89) and the expressions of $\eta_1(\cdot)$, $\eta_2(\cdot)$, $\eta_3(\cdot,\,\cdot)$ and $\eta_4(\cdot,\,\cdot)$, given in (4.34) and (4.40), lead to

$$\left\|\tilde{y}\left(j\frac{T_\mathrm{s}}{N}+t\right)\right\|_2\leq\left\|\eta_1(t)\right\|_2\left\|\tilde{y}\left(j\frac{T_\mathrm{s}}{N}\right)\right\|_2+\left\|\eta_2(t)\right\|_2\left\|\tilde{z}\left(j\frac{T_\mathrm{s}}{N}\right)\right\|_2+\eta_3\left(t,T_\mathrm{s}\right)\left\|\tilde{y}\left(j\frac{T_\mathrm{s}}{N}\right)\right\|_2+\eta_4\left(t\right)\sqrt{q}\Delta_1(\bar{\gamma}_0).$$

Consider (4.96) and $\beta_1(\cdot)$, $\beta_2(\cdot)$, $\beta_3(\cdot)$, $\beta_4(\cdot)$ defined in (4.38)-(4.39). For arbitrary nonnegative integer j, subject to $j\frac{T_\mathrm{s}}{N}+t\leq\tau_1$, and for all $t\in\left[0,\,\frac{T_\mathrm{s}}{N}\right]$, we have

$$\left\|\tilde{y}\left(j\frac{T_\mathrm{s}}{N}+t\right)\right\|_2\leq\beta_1\left(T_\mathrm{s}\right)\varsigma(\bar{\gamma}_0,T_\mathrm{s})+\beta_2\left(T_\mathrm{s}\right)\sqrt{\frac{\Delta_2(\bar{\gamma}_0)}{\lambda_{\max}\left(P_2\right)}}+\beta_3\left(T_\mathrm{s}\right)\varsigma(\bar{\gamma}_0,T_\mathrm{s})+\sqrt{q}\beta_4\left(T_\mathrm{s}\right)\Delta_1(\bar{\gamma}_0).$$

Since the right-hand side coincides with the definition of $\gamma_0(\bar{\gamma}_0, T_\mathrm{s})$ in (4.43), we have the bound

$$\|\tilde{y}\,(t)\|_2 \leq \gamma_0(T_\mathrm{s},\, \bar{\epsilon}),\ \ \forall t \in [0,\, \tau_1],$$

which, along with the design constraint on T_s introduced in (4.52), yields

$$\|\tilde{y}_{\tau_1}\|_{\mathcal{L}_\infty} < \bar{\gamma}_0.$$

This clearly contradicts the statement in (4.84). Therefore, $\|\tilde{y}\|_{\mathcal{L}_\infty} < \bar{\gamma}_0$, which proves (4.81). Further, it follows from Lemma 4.5 that

$$\|e_t\|_{\mathcal{L}_\infty} < \Omega_1(T_\mathrm{s})\bar{\gamma}_0,$$

which holds uniformly for all $t \geq 0$ and therefore leads to the first upper bound in (4.82).

To prove the second bound in (4.82), we notice that it follows from (4.1), (4.14), (4.54), (4.68), (4.69) and (4.70) that

$$u_\mathrm{ref}(s) - u(s) = C(s)M^{-1}(s)\tilde{y}(s) - C(s)d_\mathrm{e}(s) + (u_\mathrm{C}(s) - u_\mathrm{M}(s)) + (u_\mathrm{M}(s) - u(s))\,, \tag{4.109}$$

where $d_\mathrm{e}(s)$ is the Laplace transform of $d_\mathrm{e}(t)$ defined in (4.71). Also, u_C and u_M are defined in (4.68) and (4.69). We have

$$\|u_\mathrm{ref}(s) - u(s)\|_{\mathcal{L}_\infty} \leq \left\|C(s)M^{-1}(s)\right\|_{\mathcal{L}_1}\|\tilde{y}\|_{\mathcal{L}_\infty} + \|u_\mathrm{C}(s) - u_\mathrm{M}(s)\|_{\mathcal{L}_\infty} + \|u_\mathrm{M}(s) - u(s)\|_{\mathcal{L}_\infty} + \|C(s)\|_{\mathcal{L}_1}L_{\rho_\mathrm{r}}\|e\|_{\mathcal{L}_\infty}. \tag{4.110}$$

Combining (4.78), (4.79), (4.81), (4.82) and (4.110) leads to

$$\|u_\mathrm{ref}(s) - u(s)\|_{\mathcal{L}_\infty} < \Omega_2(T_\mathrm{s})\bar{\gamma}_0. \tag{4.111}$$

This concludes the proof. ■

Remark 4.5. *Lemmas 4.1 and 4.2 indicate that an arbitrarily small bound on the prediction error $\bar{\gamma}_0$ can be achieved as T_s goes to zero. We can show also that $\Omega_1(T_\mathrm{s})$ and $\Omega_2(T_\mathrm{s})$ are bounded, as T_s tends to zero. Therefore the bounds in* (4.82) *can be made arbitrarily small. This implies that the closed-loop sampled-data system recovers the performance of the continuous-time reference system in* (4.54)*, as the sampling time goes to zero.*

Lemma 4.6. *Let $u, v \in \mathbb{R}^q$ with $u = [u_1,\, ...,\, u_q]^\top$ and $v = [v_1,\, ...,\, v_q]^\top$. Suppose that $|v_j| \leq 1$ for all $j \in [1,\, ...,\, q]$. Then $\mathrm{sat}\{u\} \in \mathrm{co}\{D_i u + D_i^- v : i \in [1,\, ...,\, 2^q]\}$, where $\mathrm{co}\{\cdot\}$ denotes the convex hull.*

Proof. See [112] for the proof.

Theorem 4.2. *Consider the high-level subsystem in* (4.2)*, the desired system in* (4.9) *and the reference command law in* (4.22)*. Let the positive definite matrix $S \in \mathbb{R}^{p\times p}$ be given. Then if there*

exist $F_{\rm z}$, $H_{\rm z} \in \mathbb{R}^{q\times p}$ *and a positive definite* $R \in \mathbb{R}^{p\times p}$, *such that the conditions in* (4.46) *and* (4.47) *hold, then the error* $e_{\rm z}(t) = z_{\rm m}(t) - z(t)$ *is uniformly bounded*

$$\|e_{\rm z}\|_{\mathcal{L}_\infty} < \rho_{\rm z}, \tag{4.112}$$

where $\rho_{\rm z}$ *is given in* (4.48).

Proof. Using (4.2) and (4.9), the error $e_{\rm z}(t)$ is governed by

$$\dot{e}_{\rm z}(t) = A_{\rm z}e_{\rm z}(t) + B_{\rm z}\left(r_{\rm m}(t) - y(t)\right) - g(x(t),t),\, e_{\rm z}(0) = 0. \tag{4.113}$$

Then we can rewrite (4.113) as

$$\begin{aligned}\dot{e}_{\rm z}(t) =& A_{\rm z}e_{\rm z}(t) - (1-\alpha)B_{\rm z}W^{-1}{\rm sat}\{\frac{1}{1-\alpha}WF_{\rm z}e_{\rm z}(t)\} + B_{\rm z}\left(y_{\rm ref}(t) - y(t)\right) + B_{\rm z}\left(r_{\rm F}(t) - y_{\rm ref}(t)\right)\\ &+ B_{\rm z}\left(r_{\rm m}(t) - r(t) + (1-\alpha)W^{-1}{\rm sat}\{\frac{1}{1-\alpha}WF_{\rm z}e_{\rm z}(t)\}\right) - g(x(t),t) + B_{\rm z}\left(r(t) - r_{\rm F}(t)\right).\end{aligned} \tag{4.114}$$

where the Laplace transform of $r_{\rm F}(t)$ is given by

$$r_{\rm F}(s) = \frac{\mu}{s+\mu}r(s). \tag{4.115}$$

Let

$$\begin{aligned}\mathcal{F}(t) =& B_{\rm z}\left(y_{\rm ref}(t) - y(t)\right) + B_{\rm z}\left(r_{\rm m}(t) - r(t)\right) - g(x(t),t) + (1-\alpha)B_{\rm z}W^{-1}{\rm sat}\{\frac{1}{1-\alpha}WF_{\rm z}e_{\rm z}(t)\}\\ &+ B_{\rm z}\left(r(t) - r_{\rm F}(t)\right) + B_{\rm z}\left(r_{\rm F}(t) - y_{\rm ref}(t)\right).\end{aligned} \tag{4.116}$$

Then the equation in (4.114) can be rewritten as

$$\dot{e}_{\rm z}(t) = A_{\rm z}e_{\rm z}(t) - (1-\alpha)B_{\rm z}W^{-1}{\rm sat}\{\frac{1}{1-\alpha}WF_{\rm z}e_{\rm z}(t)\} + \mathcal{F}(t). \tag{4.117}$$

Select $V_{\rm z}(t) = e_{\rm z}^\top(t)Re_{\rm z}(t)$ as the Lyapunov function for the closed-loop error dynamics in (4.117). Then the derivative of $V_{\rm z}$ can be obtained as

$$\dot{V}_{\rm z}(t) = 2e_{\rm z}^\top(t)R\left(A_{\rm z}e_{\rm z}(t) + \mathcal{F}(t)\right) - 2e_{\rm z}^\top(t)RB_{\rm z}(1-\alpha)W^{-1}{\rm sat}\{\frac{1}{1-\alpha}WF_{\rm z}e_{\rm z}(t)\}. \tag{4.118}$$

We have $\|e_{\rm z}(0)\|_\infty = 0 < \rho_{\rm z}$. In addition, $e_{\rm z}(t)$ is continuous. Therefore, if the bound in (4.58) is not true, there exists a time $\tau_1 > 0$ such that

$$\|e_{\rm z}(t)\|_\infty < \rho_{\rm z}, \quad \forall t \in [0,\, \tau_1), \quad \|e_{\rm z}(\tau_1)\|_\infty = \rho_{\rm z},$$

which implies that $\|e_{\mathrm{z}\tau_1}\|_{\mathcal{L}_\infty} = \rho_{\mathrm{z}}$. Then, by Lemma 4.6 and the condition in (4.47), we have for $\forall t \in [0,\, \tau_1]$ that

$$\dot{V}_{\mathrm{z}}(t) \leq \max_{i\in\{1,\ldots,2^q\}} \{2e_{\mathrm{z}}^{\top}(t)R\left(A_{\mathrm{z}}e_{\mathrm{z}}(t) - B_{\mathrm{z}}\left(D_iF_{\mathrm{z}} + D_i^{-}H_{\mathrm{z}}\right)e_{\mathrm{z}}(t) + \mathcal{F}(t)\right)\}. \tag{4.119}$$

Furthermore, from the condition in (4.46) we obtain

$$\dot{V}_{\mathrm{z}}(t) \leq -e_{\mathrm{z}}^{\top}(t)Se_{\mathrm{z}}(t) + 2e_{\mathrm{z}}^{\top}(t)R\mathcal{F}(t). \tag{4.120}$$

Using the upper bound from (4.120), for $t \in [0,\, \tau_1]$ one can derive

$$\dot{V}_{\mathrm{z}}(t) \leq -\lambda_{\min}(S)\,\|e_{\mathrm{z}}(t)\|_2^2 + 2\sqrt{p}\,\|e_{\mathrm{z}}(t)\|_2\,\|R\|_2\,\|\mathcal{F}_{\tau_1}\|_{\mathcal{L}_\infty}. \tag{4.121}$$

Notice that if

$$V_{\mathrm{z}}(t) > \lambda_{\max}(R)\left(\frac{2\sqrt{p}\,\|R\|_2\,\|\mathcal{F}_{\tau_1}\|_{\mathcal{L}_\infty}}{\lambda_{\min}(S)}\right)^2, \tag{4.122}$$

the following holds

$$\|e_{\mathrm{z}}(t)\|_2 > \frac{2\sqrt{p}\,\|R\|_2\,\|\mathcal{F}_{\tau_1}\|_{\mathcal{L}_\infty}}{\lambda_{\min}(S)}. \tag{4.123}$$

Moreover, the upper bound in (4.121) yields

$$\dot{V}_{\mathrm{z}}(t) < 0. \tag{4.124}$$

From (4.122)-(4.124) it follows

$$V_{\mathrm{z}}(t) \leq \lambda_{\max}(R)\left(\frac{2\sqrt{p}\,\|R\|_2\,\|\mathcal{F}_{\tau_1}\|_{\mathcal{L}_\infty}}{\lambda_{\min}(S)}\right)^2, \tag{4.125}$$

and therefore

$$\left\|e_{\mathrm{z}_{\tau_1}}\right\|_{\mathcal{L}_\infty} \leq \frac{2\sqrt{p}\,\|R\|_2\,\|\mathcal{F}_{\tau_1}\|_{\mathcal{L}_\infty}}{\lambda_{\min}(S)}. \tag{4.126}$$

In the following, we obtain the bound on $\mathcal{F}(t)$ for $t \in [0,\, \tau_1]$. Using the result of Theorem 4.1, it follows that $\|x\|_{\mathcal{L}_\infty} < \rho_{\mathrm{r}} + \bar{\gamma}_1$. Then Assumption 4.1 implies that

$$\|g(x(t),t)\|_{\mathcal{L}_\infty} \leq G_{\rho_{\mathrm{r}}+\bar{\gamma}_1}. \tag{4.127}$$

Moreover, from Theorem 4.1 one can obtain

$$\|y - y_{\mathrm{ref}}\|_{\mathcal{L}_\infty} < \|C_{\mathrm{x}}\|_\infty\,\Omega_1(T_{\mathrm{s}})\bar{\gamma}_0. \tag{4.128}$$

Also, from (4.57) and (4.115) we have

$$r_{\rm F}(s) - y_{\rm ref}(s) = \left(\frac{\mu}{s+\mu}\mathbb{I}_q - M(s)K_{\rm g}\right) r(s) - C_{\rm m}\left(s\mathbb{I}_q - A_{\rm m}\right)^{-1} C_{\rm m}^{\dagger} y_0 - M(s)\left(\mathbb{I}_q - C(s)\right)\sigma_{\rm ref}(s). \tag{4.129}$$

It follows

$$\|r_{\rm F} - y_{\rm ref}\|_{\mathcal{L}_\infty} \leq \left\|\tfrac{\mu}{s+\mu}\mathbb{I}_q - M(s)K_{\rm g}\right\|_{\mathcal{L}_1} M_{\rm r} + \left\|sC_{\rm m}\left(s\mathbb{I}_q - A_{\rm m}\right)^{-1} C_{\rm m}^{\dagger} C_{\rm m}\right\|_{\mathcal{L}_\infty} \rho_0 + \left\|M(s)\left(\mathbb{I}_q - C(s)\right)\right\|_{\mathcal{L}_1} \rho_\Delta. \tag{4.130}$$

For all $t \in [kMT_{\rm s}, (k+1)MT_{\rm s}) \cap [0,\, \tau_1]$, $\quad k \in \mathbb{Z}_{\geq 0}$, we obtain form (4.22) that

$$\begin{aligned}\left\|r_{\rm m}(t) - r(t) + (1-\alpha)W^{-1}{\rm sat}\{\frac{1}{1-\alpha}WFe_{\rm z}(t)\}\right\|_\infty &\leq \left\|(1-\alpha)W^{-1}\left({\rm sat}\{\frac{WF_{\rm z}}{1-\alpha}e_{\rm z}(t)\} - {\rm sat}\{\frac{WF_{\rm z}}{1-\alpha}e_{\rm z}(kMT_{\rm s})\}\right)\right\|_\infty \\ &\leq M_{\rm r}\left\|WF_{\rm z}\left(e_{\rm z}(t) - e_{\rm z}(kMT_{\rm s})\right)\right\|_\infty \\ &\leq M_{\rm r}\left\|WF_{\rm z}\right\|_\infty \left\|\left(e_{\rm z}(t) - e_{\rm z}(kMT_{\rm s})\right)\right\|_\infty .\end{aligned} \tag{4.131}$$

From (4.113) one can obtain

$$e_{\rm z}(t) = e^{A_{\rm z}(t-kMT_{\rm s})}e_{\rm z}(kMT_{\rm s}) + \int_{kMT_{\rm s}}^{t} e^{A_{\rm z}(t-\tau)}\left(B_{\rm z}\left(r_{\rm m}(\tau) - y(\tau)\right) - g(x(\tau),\tau)\right)d\tau. \tag{4.132}$$

Using Theorem 4.1, Lemma 4.4 and the bounds defined in (4.50), from (4.127) and (4.132) it follows

$$\left\|e_{\rm z}(t) - e_{\rm z}(kMT_{\rm s}))\right\|_\infty \leq \gamma_{\rm z}(\bar{\gamma}_0,\, T_{\rm s}), \tag{4.133}$$

where $\gamma_{\rm z}(\cdot,\,\cdot)$ is defined in (4.49).

Let

$$r_{\rm F_d}[k] = r_{\rm F}(kMT_{\rm s}),\ t \in [kMT_{\rm s}, (k+1)MT_{\rm s}),\quad k \in \mathbb{Z}_{\geq 0}. \tag{4.134}$$

Then from (4.115) and (4.134) we have

$$r_{\rm F_d}[k] = \sum_{l=0}^{k} e^{-\mu l MT_{\rm s}}(1 - e^{-\mu MT_{\rm s}})r_{\rm d}[k-l]. \tag{4.135}$$

Using summation by part, it follows from (4.135) that

$$r_{\rm F_d}[k] = r_{\rm d}[k] + \sum_{l=0}^{k} e^{-\mu(l+1)MT_{\rm s}}(r_{\rm d}[k+1-l] - r_{\rm d}[k-l]). \tag{4.136}$$

Then one can obtain

$$\left\|r_{\rm F_d}[k] - r_{\rm d}[k]\right\|_\infty \leq \sum_{l=0}^{k} e^{-\mu(l+1)MT_{\rm s}}\left\|r_{\rm d}[k+1-l] - r_{\rm d}[k-l]\right\|_\infty . \tag{4.137}$$

From (4.4), (4.22), (4.131), (4.133), and for any $k \in \mathbb{Z}_{\geq 0}$, we have

$$\|r_{\mathrm{d}}[k+1] - r_{\mathrm{d}}[k]\|_{\infty} \leq M_{\mathrm{r}} \|WF_{\mathrm{z}}\|_{\infty} \gamma_{\mathrm{z}}(\bar{\gamma}_0,\, T_{\mathrm{s}}) + MT_{\mathrm{s}}\delta_{\mathrm{r_m}}. \tag{4.138}$$

From (4.137) and (4.138) it follows

$$\|r_{\mathrm{F_d}}[k] - r_{\mathrm{d}}[k]\|_{\infty} \leq \tfrac{e^{-\mu MT_{\mathrm{s}}}}{1-e^{-\mu MT_{\mathrm{s}}}}(M_{\mathrm{r}} \|WF_{\mathrm{z}}\|_{\infty} \gamma_{\mathrm{z}}(\bar{\gamma}_0,\, T_{\mathrm{s}}) + MT_{\mathrm{s}}\delta_{\mathrm{r_m}}). \tag{4.139}$$

Taking the discretization error into account, we have

$$\|r_{\mathrm{F}} - r\|_{\mathcal{L}_\infty} \leq \tfrac{e^{-\mu MT_{\mathrm{s}}}}{1-e^{-\mu MT_{\mathrm{s}}}}(M_{\mathrm{r}} \|WF_{\mathrm{z}}\|_{\infty} \gamma_{\mathrm{z}}(\bar{\gamma}_0,\, T_{\mathrm{s}}) + MT_{\mathrm{s}}\delta_{\mathrm{r_m}}) + 2(1 - e^{-\mu MT_{\mathrm{s}}})M_{\mathrm{r}}. \tag{4.140}$$

Then from (4.127)-(4.140) it follows

$$\begin{aligned}\|\mathcal{F}\|_{\mathcal{L}_\infty} \leq{}& \|B_{\mathrm{z}}\|_{\infty} \|M(s)(\mathbb{I}_q - C(s))\|_{\mathcal{L}_1} \rho_{\Delta} + \|B_{\mathrm{z}}\|_{\infty} \|C_{\mathrm{x}}\|_{\infty} \Omega_1(T_{\mathrm{s}})\bar{\gamma}_0 + \gamma_{\mathrm{r}}(\bar{\gamma}_0,\, T_{\mathrm{s}}) + G_{\rho_{\mathrm{r}}+\bar{\gamma}_1} \\ &+ \|B_{\mathrm{z}}\|_{\infty} \left\| \frac{\mu}{s+\mu}\mathbb{I}_q - M(s)K_{\mathrm{g}} \right\|_{\mathcal{L}_1} M_{\mathrm{r}} + \|B_{\mathrm{z}}\|_{\infty} \left\| sC_{\mathrm{m}} \left(s\mathbb{I}_q - A_{\mathrm{m}}\right)^{-1} C_{\mathrm{m}}^{\dagger} C_{\mathrm{m}} \right\|_{\mathcal{L}_1} \rho_0 \\ &+ \frac{1}{\mu} \|B_{\mathrm{z}}\|_{\infty} \left(\frac{1}{MT_{\mathrm{s}}} M_{\mathrm{r}} \|WF_{\mathrm{z}}\|_{\infty} \gamma_{\mathrm{z}}(\bar{\gamma}_0,\, T_{\mathrm{s}}) + \delta_{\mathrm{r_m}}\right).\end{aligned} \tag{4.141}$$

Since $T_{\mathrm{s}} \leq T_{s_{\max}}$ is selected such that the inequalities in (4.52) hold, we have $\gamma_{\mathrm{r}}(\bar{\gamma}_0,\, T_{\mathrm{s}}) < \bar{\gamma}_{\mathrm{r}}$. Therefore

$$\|\mathcal{F}_{\tau_1}\|_{\mathcal{L}_\infty} < \left(1 - \frac{2\sqrt{p}\,\|R\|_2\, \Delta_{\mathrm{s}}(\mu,\, F_{\mathrm{z}})}{\lambda_{\min}(S)}\right)^{-1} \Delta_{\mathcal{F}}(\mu,\, F_{\mathrm{z}}), \tag{4.142}$$

where $\Delta_{\mathrm{s}}(\mu,\, F_{\mathrm{z}})$ and $\Delta_{\mathcal{F}}(\mu,\, F_{\mathrm{z}})$ are defined in (4.44). From (4.126) and (4.142) it follows

$$\left\|e_{\mathrm{z}_{\tau_1}}\right\|_{\mathcal{L}_\infty} < \rho_{\mathrm{z}}, \tag{4.143}$$

which contradicts with $\|e_{\mathrm{z}_{\tau_1}}\|_{\mathcal{L}_\infty} = \rho_{\mathrm{z}}$. Hence, the inequality in (4.112) is true. ■

4.4. Simulation Example: Navigation and Control of an Autonomous UAV

A high-fidelity simulation environment of an Unmanned Aerial Vehicle (UAV) is used to verify the effectiveness and the benefits of the proposed control framework. To substantiate the existence of a feasible controller that satisfies the theoretical conditions, a multi-level altitude tracking controller is designed for linearized UAV longitudinal dynamics. We then validate the multi-level SD control framework in a high-fidelity UAV simulator. Scenarios with and without saturation of reference command are considered. In the end, a zero-dynamics attack on altitude measurement is simulated to show the advantages of the multi-rate framework in detecting stealthy attacks.

4.4.1. *Linearized Longitudinal Dynamics*

A multi-level SD controller is designed for linearized UAV longitudinal dynamics that satisfies (4.31), (4.46), (4.47) and (4.52). Consider the following trim condition within the desired flight operating envelope of an *Ultra Stick*^{TM} *25e* model UAV [113]: inertial frame position of $[0, 0, -100]$ m, body frame velocities of $[17, 0, 0.369]$ m/s, Euler orientation (roll, pitch, and yaw) of $[0, 0.0217, 1.5708]$ rad, surface of elevator at -0.091 rad, aileron and rudder at zero position, throttle at 55.9%, and engine speed at 827 rad/s. Define the state vector $x = (u, w, q, \theta)^\top \in \mathbb{R}$, where u, w, q, and θ respectively denote the changes of forward velocity, vertical velocity, pitch rate, and pitch angle deviated from the trim condition. With the high-fidelity UAV simulation software developed by the University of Minnesota [113], the following linearized UAV longitudinal dynamics is considered for the inner-loop dynamics:

$$\dot{x}(t) = A_{\mathrm{x}} x(t) + B_{\mathrm{x}} \delta_e(t), \quad y(t) = \theta(t), \tag{4.144}$$

where

$$\begin{aligned}
A_{\mathrm{x}} &= \begin{pmatrix} -0.5961 & 0.8011 & -0.871 & -9.791 \\ -0.7454 & -7.581 & 15.72 & -0.5272 \\ 1.042 & -7.427 & -15.85 & 0 \\ 0 & 0 & 1 & 0 \end{pmatrix}, \\
B_{\mathrm{x}} &= \begin{pmatrix} 0.4681 & -2.711 & -134.1 & 0 \end{pmatrix}^\top, \\
C_{\mathrm{x}} &= \begin{pmatrix} 0 & 0 & 0 & 1 \end{pmatrix}
\end{aligned}$$

with δ_{e} being the control input, indicating the deviation of the elevator surface from the trim condition, and the pitch angle θ chosen as the output for feedback. The outer-loop dynamics from the pitch angle θ to the UAV altitude h takes the form of (4.145) after linearization:

$$\dot{h}(t) = 17 \cdot \theta(t). \tag{4.145}$$

Subject to the dynamical models given in (4.144) and (4.145), a multi-level SD controller is designed with the following design parameters: $\rho_0 = 0.01$, $\rho_{\mathrm{r}} = 8.1$, $\alpha = 0.1$, $\bar{\gamma}_1 = 0.015$, $\delta = 0.01$, $\bar{\gamma}_{\mathrm{z}} = 0.01$, $\mu = 9.4$, $M = 1$, $\bar{\gamma}_0 = 6.5 \times 10^{-11}$, $G_{\rho_{\mathrm{r}}+\bar{\gamma}_1} = 0.01$, $H_{\mathrm{z}} = 1.177 \times 10^{-3}$, $K_{(\bar{\gamma}_1+\delta)} = 0.01$, $L_0 = 0.01$, $L_1 = 0.01$, $M_{\mathrm{r}} = 0.4363$, $N = 5$, $Q = I_2$, $R = 1$, $S = 0.04$, $T_{\mathrm{s}} = 10^{-15}$ and $T_{s_{\max}} = 0.01$. For the outer-loop controller, given by (4.22), we choose the feedback gain $F_{\mathrm{z}} = 0.008$ and the weight $W = 1/M_{\mathrm{r}}$. The inner-loop multi-rate $\mathcal{L}_1$ adaptive controller is designed with the desired model

$$M(s) = \frac{-1.339 \times 10^{-3} s - 133.9}{s^2 + 134.5 s + 1193}, \tag{4.146}$$

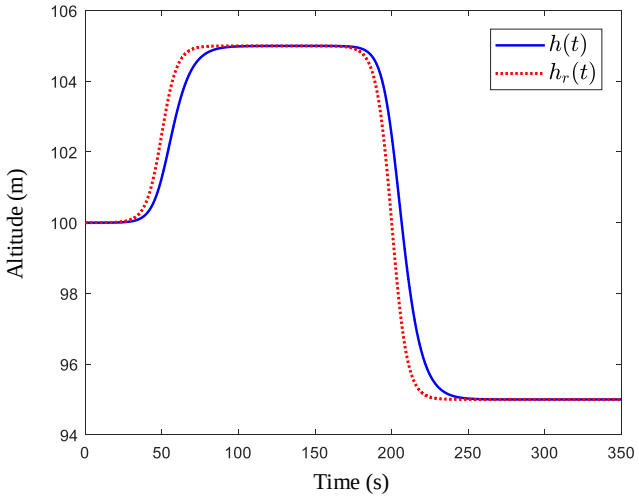

Figure 4.1: The UAV tracks the desired altitude.

and the low-pass filter

$$C(s) = \frac{15000}{s + 15000}. \tag{4.147}$$

With the preceding parameters, conditions (4.31), (4.46), (4.47) and (4.52) are fulfilled with $\|G(s)\|_{\mathcal{L}_1} = 1.819 \times 10^{-2} < (\rho_{\rm r} - \rho_1 - \rho_2)/(L_{\rho_{\rm r}}\rho_{\rm r} + L_2) = 1.826 \times 10^{-2}$ in (4.31), $\|WH_{\rm z}\|_\infty = 2.698{\times}10^{-3} < (1{-}\alpha)\rho_{\rm z}^{-1} = 2.702{\times}10^{-3}$ in (4.47), and $\gamma_0(\bar{\gamma}_0, T_{\rm s}) = 6.369{\times}10^{-11} < \bar{\gamma}_0 = 6.5{\times}10^{-11}$, $\Omega_1(T_{\rm s})\bar{\gamma}_0 = 1.468{\times}10^{-2} < \bar{\gamma}_1 = 1.5{\times}10^{-2}$ and $\gamma_{\rm r}(\bar{\gamma}_0, T_{\rm s}) = 1.589{\times}10^{-13} < \bar{\gamma}_{\rm r} = 1.0{\times}10^{-2}$ in (4.52). The simulations below illustrate the conservativeness of the design parameters, which follows from the sufficient conditions.

With the multi-level SD controller, the UAV tracks the following reference altitude (height) signal:

$$h_{\rm r}(t) = 10 \cdot \left(\frac{-0.5}{1 + e^{t/5-10}} + \frac{1}{1 + e^{t/5-40}} - 0.5 \right) + 100. \tag{4.148}$$

The reference altitude signal $h_{\rm r}(t)$ and the UAV altitude $h(t)$ are given in Figure 4.1. Due to the conservativeness of the design parameters, certain amount of tracking error exists in Figure 4.1, which can be efficiently reduced by increasing the proportional gain $F_{\rm z}$ in the outer-loop controller. Figure 4.2 shows the commanded pitch angle $h_{\rm r}(t)$, generated by the outer-loop controller, UAV pitch angle $\theta(t)$ and the deviation of the elevator surface $\delta_{\rm e}(t)$. From the results one can see that the reference signal $r(t)$ is within the bound $M_{\rm r} = 0.4363$ rad $\approx 25^\circ$; the UAV pitch angle $\theta(t)$ tracks the reference pitch angle $r(t)$ precisely with the multi-rate $\mathcal{L}_1$ inner-loop controller, and the deviation of the elevator is also within the saturation bound.

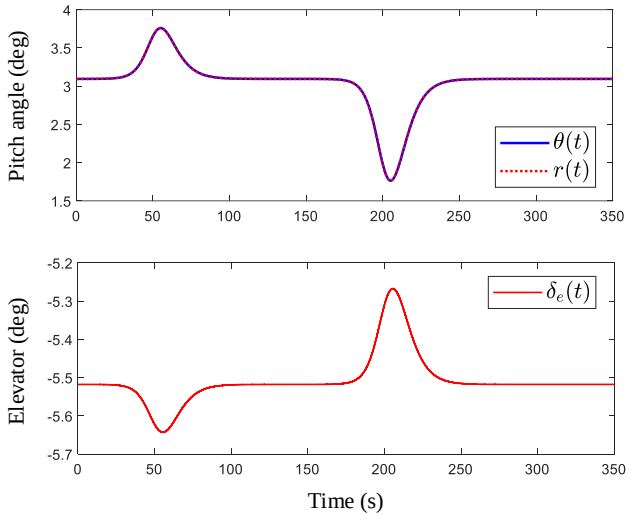

Figure 4.2: Pitch angle $\theta(t)$ and elevator deviation δ_e.

4.4.2. *Nonlinear Model with Motor Failures*

We now test this multi-level SD control framework in a high-fidelity UAV simulation environment [113]. Assume that the lateral dynamics are stabilized by some existing controller along the roll and yaw channels, and consider a scenario when the propulsion level of the UAV decreases by 80% for two minutes (as a large unplanned uncertainty), while the UAV still tries to track a commanded altitude signal at $h_{\rm r}(t) = 100$. The saturation limits of UAV elevator are $\pm 25^\circ$. Some design parameters are adjusted to adapt to the high-fidelity UAV dynamics and environmental factors. The desired dynamics are selected as

$$M(s) = \frac{-0.2067s - 20.67}{s^2 + 2.9s + 3.793}, \tag{4.149}$$

with the low-pass filter

$$C(s) = \frac{4}{s+4}. \tag{4.150}$$

The sampling period is $T_{\rm s} = 0.02$, and all the other parameters are unaltered. We compare a multi-level controller with reference pitch angle $r_{\rm w}(t)$, constrained by saturation bounds within $[-8^\circ, 8^\circ]$, and a multi-level controller with unconstrained reference signal $r_{\rm w/o}(t)$. This constraint does not limit the maneuverability of the UAV, since the safety constraint is on the generated command signal, not on the actuators.

In the following simulation, we use subscript 'w' to denote the results of the control scheme with saturated reference signal, while subscript 'w/o' is used to denote the results of the control scheme without saturating the reference signal. The reference altitude signal $h_{\rm r}(t)$, the UAV altitudes $h_{\rm w}(t)$ and $h_{\rm w/o}(t)$, and the tracking errors $e_{\rm w}(t)$ and $e_{\rm w/o}(t)$ are shown in Figure 4.3. The reference pitch angles $r_{\rm w}(t)$ and $r_{\rm w/o}(t)$, the UAV pitch angles $\theta_{\rm w}(t)$ and $\theta_{\rm w/o}(t)$, the angles of attack $\alpha_{\rm w}(t)$

and $\alpha_{\mathrm{w/o}}(t)$, and the deviations of elevator $\delta_{\mathrm{e,w}}(t)$ and $\delta_{\mathrm{e,w/o}}(t)$ are given in Figure 4.4. It can be observed that although the reference pitch angle is confined inside an envelope, the difference between the altitudes $h_{\mathrm{w}}(t)$ and $h_{\mathrm{w/o}}(t)$ is small. Meanwhile, the saturated reference pitch angle $r_{\mathrm{w}}(t)$ prevents the elevator input from saturation and keeps the pitch angle $\theta_{\mathrm{w}}(t)$ and the angle of attack $\alpha_{\mathrm{w}}(t)$ inside a relatively safer envelope, in which the UAV is less likely to crash or stall. It is clear that the multi-level SD control framework with the saturated reference signal ensures safety of the autonomous UAV in the presence of uncertainties.

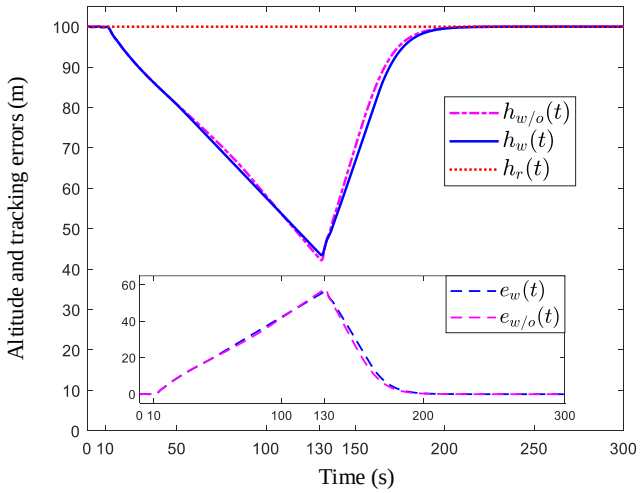

Figure 4.3: Altitudes and tracking errors under the motor failure scenario.

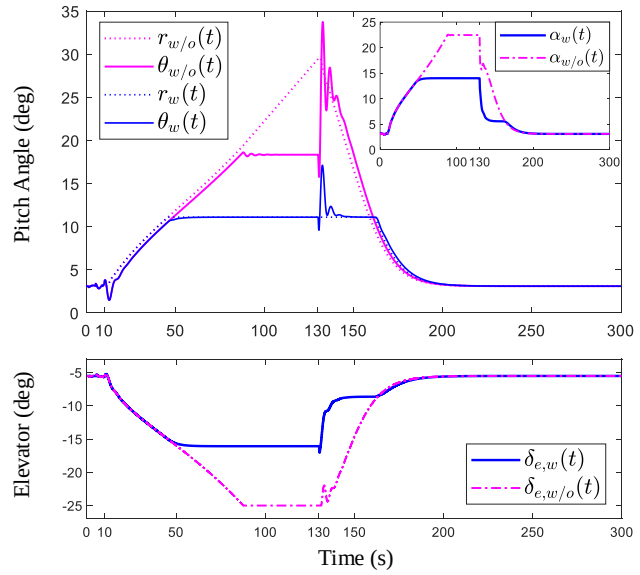

Figure 4.4: Pitch angles and elevator deviations under the motor failure scenario.

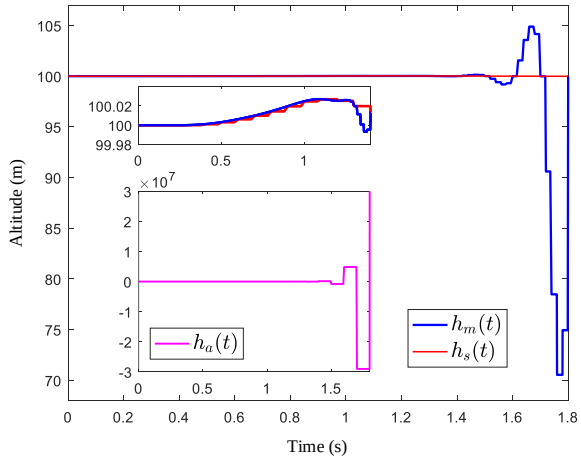

Figure 4.5: Pitch angle θ with the linearized UAV model under the zero-dynamics attack.

4.4.3. *Full-State UAV Model under Zero-Dynamics Attacks*

The multi-rate control scheme is also able to detect the stealthy zero-dynamics attacks. In this last scenario we show a zero-dynamics attack on a full-state UAV trim model via GPS or altimeter spoofing. With the same trim condition, when the sampling period of the digital control system is $T_{\rm s} = 5T = 0.1$ s, while the faster output sampling period is $T = 0.02$ s, discretizing the continuous transfer function from the elevator $\delta_{\rm e}$ to the UAV altitude $h(t)$ with the sampling period T generates a non-minimum-phase zero at $z = -6.0108$, which can be used for stealthy attack. The attack signal is generated by adding the following zero-dynamics attack signal

$$h_a(t) = \mathcal{Z}^{-1}\left[\frac{1}{z + 6.0108}\right] \tag{4.151}$$

into the normal altitude measurement signal $h(t)$. Under the zero-dynamics attack and in the p-resence of measurement noise, Figure 4.5 shows the zero-dynamics attack signal $h_{\rm a}(t)$, the altitude measurements from a single-rate controller $h_{\rm s}(t)$ and the altitude measurement from a multi-rate adaptive controller $h_{\rm m}(t)$. It is apparent that the single rate controller is not able to detect the drastic changes of UAV height caused by the zero-dynamics attack, while the multi-rate $\mathcal{L}_1$ con-troller can detect this anomaly at a relative earlier stage despite the contamination by measurement noise.

Remark 4.6. *After detection, zero-dynamics attack can be removed by considering a secure soft-ware/hardware architecture (Simplex design [15, 17]). In such structure, a backup controller will operate the system, when the normal mode controller is compromised due to a cyber attack. By switching from the normal mode to a secured backup controller, the unbounded stealthy attack can be removed (from the cyber space). Then the backup controller can recover the stability of the per-turbed system. For successful recovery the early detection is critical. Refer to [80, 114] for more details.*

CHAPTER 5

A Mutirate Sampled-Data Control Design for Under-Actuated Systems

The multirate $\mathcal{L}_1$ adaptive control design of Chapter 4 is limited to square MIMO systems with the same number of inputs and outputs. This chapter aims to extend the $\mathcal{L}_1$ adaptive control theory to under-actuated systems possibly with non-minimum-phase zeros. In [81,82], $\mathcal{L}_1$ controllers have been developed for under-actuated MIMO systems with stable transmission zeros. Compared to the continuous-time approach, the sampled-data framework provides a richer and more agile architecture for control of CPSs that use digital computers interacting with physical plants. The preliminary results in [78] on mutirate $\mathcal{L}_1$ control design are limited to square MIMO systems without unstable transmission zeros. This chapter extends the mutirate $\mathcal{L}_1$ control design to under-actuated systems possibly with non-minimum phase zeros, where the number of outputs is greater than or equal to the number of inputs. The controller design allows for detection and mitigation of actuator attacks.

In order to verify the effectiveness of the proposed approach, the multirate $\mathcal{L}_1$ adaptive controller is implemented for trajectory tracking control of a quadrotor in an indoor flight arena equipped with VICON cameras. By leveraging the multirate approach, the stealthy zero-dynamics attack becomes detectable. The controller recovers the stability of the quadrotor subject to such an attack. The estimation loop in the control structure, which has a faster rate than the control input, can timely detect the abnormality in the measured output data and trigger a switch to a safe mode control.

5.1. Problem Formulation

Consider the following MIMO system

$$\begin{aligned} \dot{x}(t) &= A_{\rm m}x(t) + B_{\rm m}\left(u(t) + d(t)\right), \quad x(0) = x_0, \\ y(t) &= C_{\rm m}x(t), \end{aligned} \tag{5.1}$$

where $x(t) \in \mathbb{R}^n$ is the state vector, $u(t) \in \mathbb{R}^p$ is the input signal, and $y(t) \in \mathbb{R}^q$ is the system output vector, where $p \leq q$. Also, $\{A_{\rm m} \in \mathbb{R}^{n\times n}, B_{\rm m} \in \mathbb{R}^{n\times p}, C_{\rm m} \in \mathbb{R}^{q\times n}\}$ is an observable-controllable triple, where $A_{\rm m}$ is Hurwitz, and $B_{\rm m}$, $C_{\rm m}$ are full rank matrices. The unknown initial condition x_0 is assumed to be inside an arbitrarily large known set, so that $\|x_0\|_\infty \leq \rho_0 < \infty$ for some known $\rho_0 > 0$. The transfer function

$$M(s) \triangleq C_{\rm m}(s\mathbb{I}_n - A_{\rm m})^{-1}B_{\rm m} \tag{5.2}$$

represents the desired dynamics.

The control input, which is implemented via a zero-order hold mechanism with time period of

$T_{\rm s} > 0$, is given by

$$u(t) = u_{\rm d}[k], \quad t \in [kT_{\rm s}, (k+1)T_{\rm s}), \quad k \in \mathbb{Z}_{\geq 0}, \tag{5.3}$$

where $u_{\rm d}[k]$ is the discrete-time control law. The output is sampled N times faster with the sampling period of $\frac{T_{\rm s}}{N}$. For each period $T_{\rm s}$, the N sampled outputs are grouped in a vector form given by

$$\bar{y}_{\rm d}[k] = \left[y^\top (kT_{\rm s}), \ldots, y^\top \left(\frac{(Nk+N-1)T_{\rm s}}{N} \right) \right]^\top. \tag{5.4}$$

Finally, the system uncertainties, disturbances, and the actuator attack are represented by

$$d(t) = f(kT_{\rm s}, x(kT_{\rm s})), \quad t \in [kT_{\rm s}, (k+1)T_{\rm s}), \quad k \in \mathbb{Z}_{\geq 0}, \tag{5.5}$$

where $f(\cdot,\cdot) : (\mathbb{R}, \mathbb{R}^n) \to \mathbb{R}^p$ is an unknown function.

Assumption 5.1. *The system $M(s)$ in (5.2) does not have a transmission zero at the origin.*

Assumption 5.2. *For arbitrary $\delta > 0$ there exist $K_\delta > 0$ and $L_0 > 0$, such that*

$$\|f(t_2, x_2) - f(t_1, x_1)\|_\infty \leq L_0 |t_2 - t_1| + K_\delta \|x_2 - x_1\|_\infty$$

holds for all $\|x_i\| \leq \delta$, and $t_i \geq 0$, $i \in \{1, 2\}$.

Assumption 5.3. *There exists constant $B_0 > 0$, such that*

$$\|f(t, 0)\|_\infty \leq B_0$$

holds uniformly in $t \geq 0$.

Remark 5.1. *In the case of zero-dynamics attack, the boundedness of the attack signal $d(t)$ can be realized by assuming a secure software/hardware structure for the CPS (Simplex architecture [14–17]). In such structure, a backup controller will operate the system, when the normal mode controller is compromised due to a cyber attack. By switching from the normal mode to a secured backup controller, the unbounded stealthy attack can be removed (from the cyber space), rendering $d(t)$ bounded. However, sensor/actuator attacks, such as zero-dynamics attack, can undermine the effectiveness of model-based detection and control algorithms needed to operate the Simplex architecture. For example, the control design in [17] does not consider the sampled-data structure of CPSs and hence is oblivious to stealthy zero-dynamics attacks. This motivates to address the detection and control problem for Simplex structures in the presence of zero-dynamics attacks.*

The control objective is to design an output feedback controller $u(t)$ such that the system output $y(t)$ tracks the desired response $y_{\rm m}(t)$ governed by $y_{\rm m}(s) = M(s)r(s)$, where $r(s)$ is the

Laplace transform of the piece-wise constant signal $r(t)$ given by

$$r(t) = r_{\mathrm{d}}[k], \quad t \in [kT_{\mathrm{s}}, (k+1)T_{\mathrm{s}}), \quad k \in \mathbb{Z}_{\geq 0}, \tag{5.6}$$

with $r_{\mathrm{d}}[k]$ being the discrete-time signal. Let $\|r\|_{\mathcal{L}_\infty} \leq M_{\mathrm{r}}$, where M_{r} is a positive constant.

5.2. Control Design

First, we define a few variables of interest and design constraints. For design of the controller, we consider a strictly proper stable transfer function $C(s)$ such that $C(0) = \mathbb{I}_p$. Let

$$\begin{aligned} H(s) &\triangleq (s\mathbb{I}_n - A_{\mathrm{m}})^{-1} B_{\mathrm{m}}, \\ G(s) &\triangleq H(s)\left(\mathbb{I}_p - C(s)\right). \end{aligned} \tag{5.7}$$

The selection of $C(s)$ must ensure that for a given ρ_0, there exists $\rho_{\mathrm{r}} > 0$ such that the following $\mathcal{L}_1$-norm condition holds:

$$\|G(s)\|_{\mathcal{L}_1} < \frac{\rho_{\mathrm{r}} - \|H(s)C(s)K_{\mathrm{g}}\|_{\mathcal{L}_1} M_{\mathrm{r}} - \rho_{\mathrm{in}}}{L_{\rho_{\mathrm{r}}}\rho_{\mathrm{r}} + B_0}, \tag{5.8}$$

where

$$\rho_{in} \triangleq \left\| s(s\mathbb{I}_n - A_{\mathrm{m}})^{-1} \right\|_{\mathcal{L}_1} \rho_0. \tag{5.9}$$

Further, for every $\delta > 0$ let

$$L_\delta \triangleq \frac{\bar{\gamma}_1 + \delta}{\delta} K_{(\bar{\gamma}_1 + \delta)}, \tag{5.10}$$

where K_δ is introduced in Assumption 5.2, and $\bar{\gamma}_1$ is an arbitrarily small positive constant.

To deal with the multirate structure of the controller, where the rate of sampling at the output is N times faster than the rate of hold at the input, we use the standard lifting technique to represent the system matrices. The desired plant $M(s)$ with dual-rate sampling and hold can be described by the discrete-time mapping, given by

$$\bar{M}_{\mathrm{d}} = \mathcal{S}_N M \mathcal{H}.$$

One can obtain a step-invariant LTI description of the discrete-time system $\bar{M}_{\mathrm{d}}$ by grouping the plant outputs as in (5.4). A state-space description of $\bar{M}_{\mathrm{d}}$ can be obtained as follows:

$$\bar{A}_{\mathrm{d}} = A^N, \quad \bar{B}_{\mathrm{d}} = \sum_{k=0}^{N-1} A^k B, \quad \bar{C}_{\mathrm{d}} = \begin{bmatrix} C \\ CA \\ \vdots \\ CA^{N-1} \end{bmatrix}, \quad \bar{D}_{\mathrm{d}} = \begin{bmatrix} 0_{q\times p} \\ CB \\ \vdots \\ C\sum_{k=0}^{N-2} A^k B \end{bmatrix}, \tag{5.11}$$

where

$$A = e^{A_{\mathrm{m}}\frac{T}{N}}, \quad B = \int_0^{\frac{T}{N}} e^{A_{\mathrm{m}}\tau} B_{\mathrm{m}} d\tau, \quad C = C_{\mathrm{m}}. \tag{5.12}$$

For brevity the dependence of $\bar{A}_{\mathrm{d}}$, $\bar{B}_{\mathrm{d}}$, $\bar{C}_{\mathrm{d}}$ and $\bar{D}_{\mathrm{d}}$ on the parameter T_{s} has been dropped. Assuming that the sampling is not pathological [41], the realization (A, B, C) is controllable/observable. For the multirate control design, $N \in \mathbb{N}$ is selected so that

$$Z \triangleq \begin{bmatrix} C \\ CA \\ \vdots \\ CA^{N-2} \end{bmatrix} \tag{5.13}$$

is full column rank, where matrices A, B and C are given in (5.12). This condition holds for large enough N, in particular $N = n + 1$, since the pair (A, C) is observable. It ensures that $\bar{C}_{\mathrm{d}}$ is also full rank.

Remark 5.2. *Using the results obtained in [42], if* $\mathrm{rank}(Z) = n$ *and Assumption 5.1 is true, it can be shown that the lifted system* $\bar{M}_{\mathrm{d}}$ *does not have a non-minimum-phase zero. Therefore, a stealthy zero-dynamics attack is impossible.*

Define

$$K(T_{\mathrm{s}}) \triangleq ((\bar{A}_{\mathrm{d}} - \mathbb{I})\bar{C}_{\mathrm{d}}^{\dagger}\bar{D}_{\mathrm{d}} - \bar{B}_{\mathrm{d}})^{\dagger}, \tag{5.14}$$

where † denotes the left pseudo inverse.

Let (A_{f}, B_{f}, C_{f}) be a minimal state-space realization such that

$$C_{\mathrm{f}}(s\mathbb{I}_{n_{\mathrm{c}}} - A_{\mathrm{f}})^{-1}B_{\mathrm{f}} \triangleq C(s), \tag{5.15}$$

where n_{c} is the order of $C(s)$. Define the function $\Gamma(\cdot)$ as

$$\Gamma(T_{\mathrm{s}}) \triangleq \alpha_1(T)\left\|(s\mathbb{I}_{n_{\mathrm{c}}} - A_{\mathrm{f}})^{-1}B_{\mathrm{f}}\right\|_{\mathcal{L}_1} + \alpha_2(T_{\mathrm{s}}), \tag{5.16}$$

where

$$\alpha_1(T_{\mathrm{s}}) \triangleq \max_{t\in[0,\,T_{\mathrm{s}}]} \left\|C_{\mathrm{f}}\left(e^{A_{\mathrm{f}}t} - \mathbb{I}_{n_{\mathrm{c}}}\right)\right\|_{\infty}, \quad \alpha_2(T_{\mathrm{s}}) \triangleq \max_{t\in[0,\,T_{\mathrm{s}}]} \int_0^t \left\|C_{\mathrm{f}}e^{A_{\mathrm{f}}(t-\tau)}B_{\mathrm{f}}\right\|_{\infty} d\tau.$$

Let

$$\begin{aligned}
\Omega(T_{\rm s}) =& \left(\left\|\bar{A}_{\rm d}\bar{C}_{\rm d}^{+}\bar{D}_{\rm d}-\bar{B}_{\rm d}\right\|_{\infty}+\left\|\bar{C}_{\rm d}^{+}\bar{D}_{\rm d}\right\|_{\infty}\right)\left(B_0+L_{\rho_{\rm r}}\rho_{\rm r}\right),\\
\rho_{\rm u}(T_{\rm s}) =& \|C(s)\|_{\mathcal{L}_1}\|K(T_{\rm s})\|_{\infty}\Omega(T_{\rm s}),\\
\gamma_{\rm dx}(T_{\rm s}) =& L_{\rho_{\rm r}}\left(\left\|\bar{A}_{\rm d}-\mathbb{I}_n\right\|_{\infty}\rho_{\rm r}+\left\|\bar{B}_{\rm d}\right\|_{\infty}\left(\rho_{\rm u}(T_{\rm s})+B_0+L_{\rho_{\rm r}}\rho_{\rm r}\right)\right)+L_0T_{\rm s},\\
\gamma_0(T_{\rm s}) =& \left\|\left(\mathbb{I}_p+K(T_{\rm s})\bar{C}_{\rm d}^{\dagger}\bar{D}_{\rm d}\right)\right\|_{\infty}\gamma_{\rm dx}(T_{\rm s}),\\
\gamma_{\rm C}(T_{\rm s}) =& \Gamma(T_{\rm s})\|C(s)\|_{\mathcal{L}_1}(B_0+L_{\rho_{\rm r}}\rho_{\rm r}+\gamma_0(T_{\rm s}))+\Gamma(T_{\rm s})\|K_{\rm g}\|_{\infty}M_{\rm r},\\
\rho_{\rm d_0} =& \|sH(s)C(s)\|_{\mathcal{L}_1}\left(B_0+L_{\rho_{\rm r}}\rho_{\rm r}\right),
\end{aligned}\tag{5.17}$$

where $K_{\rm g}\triangleq -C_{\rm m}A_{\rm m}^{-1}B_{\rm m}$, $H(s)$ is defined in (5.7), and $\Gamma(\cdot)$ is given in (5.16). Matrices $\bar{A}_{\rm d}$, $\bar{B}_{\rm d}$, $\bar{C}_{\rm d}$ and $\bar{D}_{\rm d}$ are introduced in (5.11). Also, $\bar{C}_{\rm d}^{\dagger}$ denotes the pseudo-inverse of $\bar{C}_{\rm d}$. Finally let

$$\gamma_{\rm x}(T_{\rm s})=\frac{\|G(s)\|_{\mathcal{L}_1}\gamma_{\rm dx}(T_{\rm s})+\|H(s)\|_{\mathcal{L}_1}\gamma_{\rm C}(T_{\rm s})+\|H(s)C(s)\|_{\mathcal{L}_1}\gamma_0(T_{\rm s})+T_{\rm s}\rho_{\rm d_0}}{1-L_{\rho_{\rm r}}\|G(s)\|_{\mathcal{L}_1}}.\tag{5.18}$$

The sampling time $T_{\rm s}$ of the digital controller is chosen such that

$$\gamma_{\rm x}(T_{\rm s})<\bar{\gamma}_1,\tag{5.19}$$

where $\bar{\gamma}_1>0$ is introduced in (5.10), and $\gamma_{\rm x}(\cdot)$ is given in (5.18). Also, the sampling time $T_{\rm s}$ should not be pathological.

Remark 5.3. *Existence of such $T_{\rm s}$ depends on the uncertainty bounds and the system parameters. For certain class of MIMO systems that additionally satisfy*

$$\operatorname{rank}\left(\begin{bmatrix} C_{\rm m}\\ \vdots\\ C_{\rm m}A_{\rm m}^{l-1}\end{bmatrix}\right)=n,\tag{5.20}$$

where l and n are the relative degree and order of $M(s)$ in (5.2) *respectively, we will show in Theorem 5.1 that the continuous-time function $\gamma_{\rm x}(T_{\rm s})$ tends to zero as $T_{\rm s}$ goes to zero. As a result, if the relation* (5.20) *is true, the condition in* (5.19) *can be met by choosing small enough sampling time $T_{\rm s}$.*

The elements of the proposed multirate adaptive controller are stated next. The predicted output $\hat{\bar{y}}_{\rm d}[k]$ is given by

$$\begin{aligned}
\hat{x}_{\rm d}[k+1] &= \bar{A}_{\rm d}\hat{x}_{\rm d}[k]+\bar{B}_{\rm d}u_{\rm d}[k]+\hat{d}_{\rm d}[k],\quad \hat{x}_{\rm d}[0]=\bar{C}_{\rm d}^{\dagger}\bar{y}_0,\\
\hat{\bar{y}}_{\rm d}[k] &= \bar{C}_{\rm d}\hat{x}_{\rm d}[k]+\bar{D}_{\rm d}u_{\rm d}[k],
\end{aligned}\tag{5.21}$$

where

$$\bar{y}_0=\underbrace{[y_0,\ ...,\ y_0]}_{N}^{\top},\quad y_0=C_{\rm m}x_0,\tag{5.22}$$

and $\hat{d}_{\rm d}[k] \in \mathbb{R}^n$, $u_{\rm d}[k] \in \mathbb{R}^p$ are provided by adaptation and control laws, respectively. Also, $\bar{A}_{\rm d}$, $\bar{B}_{\rm d}$, $\bar{C}_{\rm d}$, $\bar{D}_{\rm d}$ are defined in (5.11). The update law for $\hat{d}_{\rm d}[k]$ is given by

$$\hat{d}[k] = -\bar{A}_{\rm d}\bar{C}_{\rm d}^{\dagger}\tilde{y}_{\rm d}[k], \tag{5.23}$$

where $\tilde{y}_{\rm d}[k] = \hat{\bar{y}}_{\rm d} - \bar{y}_{\rm d}[k]$ and $C_{\rm d}^{\dagger}$ is the left inverse of $\bar{C}_{\rm d}$. Finally, the control signal is defined as

$$u_{\rm d}[z] = C_{\rm d}[z]\left(K_{\rm g} r_{\rm d}[z] + K(T_{\rm s})\bar{A}_{\rm d}^{-1}\hat{d}_{\rm d}[z]\right), \tag{5.24}$$

where

$$C_{\rm d}[z] = C_{\rm f}\left(z\mathbb{I}_{n_{\rm c}} - e^{A_{\rm f}T_{\rm s}}\right)^{-1} A_{\rm f}^{-1}\left(e^{A_{\rm f}T_{\rm s}} - \mathbb{I}_{n_{\rm c}}\right) B_{\rm f},$$

and ($A_{\rm f}$, $B_{\rm f}$, $C_{\rm f}$) is a minimal state-space realization of $C(s)$. Also, $\hat{d}_{\rm d}[z]$ is the z-transform of the discrete-time signal $\hat{d}_{\rm d}[k]$ given by (5.23).

5.3. Analysis of the Closed-Loop Multirate System

We proceed by defining a few variables of interest:

$$\begin{aligned}
\rho_{\rm x} =& \rho_{\rm r} + \bar{\gamma}_1, \\
\rho_{\rm ur} =& \|C(s)K_{\rm g}\|_{\mathcal{L}_1} M_{\rm r} + \|C(s)\|_{\mathcal{L}_1}\left(L_{\rho_{\rm r}}\rho_{\rm r} + B_0\right), \\
\rho_{\rm d_1} =& \|sC(s)\|_{\mathcal{L}_1}\left(B_0 + L_{\rho_{\rm r}}\rho_{\rm r}\right), \\
\gamma_{\rm u}(T_{\rm s}) =& \|C(s)\|_{\mathcal{L}_1}\left(\gamma_0(T_{\rm s}) + L_{\rho_{\rm r}}\gamma_{\rm x}(T_{\rm s}) + \gamma_{\rm dx}(T_{\rm s})\right) + \gamma_{\rm C}(T_{\rm s}) + T_{\rm s}\rho_{\rm d_1},
\end{aligned} \tag{5.25}$$

where $\bar{\gamma}_1$ is introduced in (5.10), and $\gamma_{\rm x}(\cdot)$ is defined in (5.18). Also, $\gamma_0(\cdot)$, $\gamma_{\rm dx}(\cdot)$ and $\gamma_{\rm C}(\cdot)$ are given in (5.17).

Lemma 5.1. *Consider the system $M(s)$ in (5.2), subject to Assumption 5.1, with the minimum realization ($A_{\rm m}$, $B_{\rm m}$, $C_{\rm m}$), where $A_{\rm m}$ is Hurwitz, and $B_{\rm m}$, $C_{\rm m}$ are full rank. Then $((\bar{A}_{\rm d} - \mathbb{I})\bar{C}_{\rm d}^{\dagger}\bar{D}_{\rm d} - \bar{B}_{\rm d})$ has full column rank, and its left inverse introduced in (5.14) is well-defined.*

Proof. We can write

$$((\bar{A}_{\rm d} - \mathbb{I}_n)\bar{C}_{\rm d}^{\dagger}\bar{D}_{\rm d} - \bar{B}_{\rm d}) = (\bar{A}_{\rm d} - \mathbb{I}_n)\left[(\mathbb{I}_n - A)^{-1}B + \bar{C}_{\rm d}^{\dagger}\bar{D}_{\rm d}\right]. \tag{5.26}$$

Since $(\bar{A}_{\rm d} - \mathbb{I})$ is invertible, it is sufficient to show that $(\mathbb{I} - A)^{-1}B + \bar{C}_{\rm d}^{\dagger}\bar{D}_{\rm d}$ is full column rank. Notice that we can rewrite $\bar{D}_{\rm d}$ as

$$\bar{D}_{\rm d} = \begin{bmatrix} C\left(\mathbb{I}_n - A\right) \\ \vdots \\ C\left(\mathbb{I}_n - A^{N-1}\right) \end{bmatrix} (\mathbb{I}_n - A)^{-1}B. \tag{5.27}$$

It follows from (5.27) that

$$\bar{C}_{\mathrm{d}}^{\top}\bar{D}_{\mathrm{d}} = \left[\left(\sum_{j=0}^{N-1} A^{j}\right)^{\top} C^{\top}C - \bar{C}_{\mathrm{d}}^{\top}\bar{C}_{\mathrm{d}}\right](\mathbb{I}_n - A)^{-1}B.$$

Given that $\bar{C}_{\mathrm{d}}^{\dagger} = (\bar{C}_{\mathrm{d}}^{\top}\bar{C}_{\mathrm{d}})^{-1}\bar{C}_{\mathrm{d}}^{\top}$, one can obtain

$$\bar{C}_{\mathrm{d}}^{\dagger}\bar{D}_{\mathrm{d}} = \left[(\bar{C}_{\mathrm{d}}^{\top}\bar{C}_{\mathrm{d}})^{-1}\left[C(\mathbb{I}_n - A)^{-1}(\mathbb{I}_n - A^{N})\right]^{\top}C - \mathbb{I}\right](\mathbb{I}_n - A)^{-1}B,$$

where matrices A, B and C are given in (5.12). It follows

$$(\mathbb{I}_n - A)^{-1}B + \bar{C}_{\mathrm{d}}^{\dagger}\bar{D}_{\mathrm{d}} = (\bar{C}_{\mathrm{d}}^{\top}\bar{C}_{\mathrm{d}})^{-1}\left[C(\mathbb{I}_n - A)^{-1}(\mathbb{I}_n - A^{N})\right]^{\top}C(\mathbb{I} - A)^{-1}B. \tag{5.28}$$

Since C is full row rank and $(\mathbb{I}_n - A)^{-1}(\mathbb{I}_n - A^{N})$ is invertible, $\left[C(\mathbb{I}_n - A)^{-1}(\mathbb{I}_n - A^{N})\right]^{\top}$ has full column rank. Also, notice that $C(\mathbb{I}_n - A)^{-1}B = -C_{\mathrm{m}}A_{\mathrm{m}}^{-1}B_{\mathrm{m}}$. Since $s = 0$ is neither eigenvalue of A_{m}, nor transmission zero of $M(s)$ (by Assumption 5.1), $C(\mathbb{I}_n - A)^{-1}B$ is full column rank. Then the Sylvester rank inequity implies that $\left[C(\mathbb{I}_n - A)^{-1}(\mathbb{I}_n - A^{N})\right]^{\top}C(\mathbb{I}_n - A)^{-1}B$, and hence $(\mathbb{I}_n - A)^{-1}B + \bar{C}_{\mathrm{d}}^{\dagger}\bar{D}_{\mathrm{d}}$ has full column rank. This concludes the proof. ■

Lemma 5.2. *The following relations are true*

$$\lim_{T_{\mathrm{s}}\to 0} T_{\mathrm{s}}K(T_{\mathrm{s}}) = -\left(C_{\mathrm{m}}^{\top}C_{\mathrm{m}}A_{\mathrm{m}}^{-1}B_{\mathrm{m}}\right)^{\dagger}C_{\mathrm{m}}^{\top}C_{\mathrm{m}}A_{\mathrm{m}}^{-1}, \tag{5.29}$$

$$\left\|\bar{C}_{\mathrm{d}}^{\dagger}\bar{D}_{\mathrm{d}}\right\|_2 \le \left\|A_{\mathrm{m}}^{-1}B_{\mathrm{m}}\right\|_2, \quad \forall T_{\mathrm{s}} > 0. \tag{5.30}$$

Additionally, if the condition in (5.20) *holds, we have*

$$\lim_{T_{\mathrm{s}}\to 0} \bar{C}_{\mathrm{d}}^{\dagger}\bar{D}_{\mathrm{d}} = 0_{n\times p}, \tag{5.31}$$

where $K(T_{\mathrm{s}})$ is defined in (5.14)*, and $C_{\mathrm{d}}^{\dagger}$, $\bar{D}_{\mathrm{d}}$ are given in* (5.11)*.*

Proof. Let

$$X \triangleq \underbrace{\begin{bmatrix} \mathbb{I}_q & 0_{q\times q} & 0_{q\times q} & \cdots & 0_{q\times q} \\ \mathbb{I}_q & -\mathbb{I}_q & 0_{q\times q} & \ddots & \vdots \\ 0_{q\times q} & \mathbb{I}_q & -\mathbb{I}_q & \ddots & 0_{q\times q} \\ \vdots & \ddots & \ddots & \ddots & 0_{q\times q} \\ 0_{q\times q} & \cdots & 0_{q\times q} & \mathbb{I}_q & -\mathbb{I}_q \end{bmatrix}}_{N}.$$

Then one can obtain

$$X\bar{C}_{\rm d} = \left[\begin{array}{c} C \\ Z\left(\mathbb{I}_n - A\right) \end{array} \right],\ X\bar{D}_{\rm d} = \left[\begin{array}{c} 0_{q\times n} \\ -ZB \end{array} \right], \tag{5.32}$$

where Z is defined in (5.13). The term $\bar{C}_{\rm d}^{\dagger}\bar{D}_{\rm d}$ can be written as follows

$$\bar{C}_{\rm d}^{\dagger}\bar{D}_{\rm d} = \left(X\bar{C}_{\rm d}\right)^{\dagger} X\bar{D}_{\rm d}. \tag{5.33}$$

Define

$$S(T_{\rm s}) \triangleq \left(\mathbb{I}_n - A^{\top}\right) Z^{\top} Z \left(\mathbb{I}_n - A\right), \tag{5.34}$$

and

$$W(T_{\rm s}) \triangleq \left(C^{\top}C + S(T_{\rm s})\right)^{-1} S(T_{\rm s}) \left(-A_{\rm m}^{-1}B_{\rm m}\right). \tag{5.35}$$

It follows from (5.26) and (5.28) that the matrix $K(T_{\rm s})$ in (5.14) can be rewritten as follows

$$K(T_{\rm s}) = \left(C_{\rm m}^{\top}C_{\rm m}A_{\rm m}^{-1}B_{\rm m}\right)^{\dagger} \left(\mathbb{I}_n + ... + A^{N-1}\right)^{-\top} \left(\bar{C}_{\rm d}^{\top}\bar{C}_{\rm d}\right) \left(\mathbb{I}_n - \bar{A}_{\rm d}\right)^{-1}. \tag{5.36}$$

We have

$$\left(\mathbb{I}_n - \bar{A}_{\rm d}\right)^{-1} = \left(-T_{\rm s}A_{\rm m} - \frac{T_{\rm s}^2}{2!}A_{\rm m}^2 + ...\right)^{-1}. \tag{5.37}$$

From (5.36) and (5.37) we can obtain the relationship in (5.29).

Next we prove (5.30) and (5.31). From (5.32)-(5.35) it follows

$$\bar{C}_{\rm d}^{+}\bar{D}_{\rm d} = W(T_{\rm s}). \tag{5.38}$$

Since Z is assumed to be full column rank, $S(T_{\rm s})$ in (5.34) is positive-definite matrix for all $T_{\rm s} \in \mathbb{R}_{>0}$. Then $W(T_{\rm s})$ is also non-singular, and it can be shown that

$$\left\|W(T_{\rm s})\right\|_2 \leq \left\|A_{\rm m}^{-1}B_{\rm m}\right\|_2, \quad \forall T_{\rm s} > 0, \tag{5.39}$$

which proves (5.30). By expanding the exponential terms due to $A = e^{A_{\rm m}\frac{T}{N}}$, $S(T_{\rm s})$ can be written as

$$S(T_{\rm s}) = \sum_{i=1}^{\infty}\sum_{j=1}^{\infty} \kappa_{ij} T_{\rm s}^{i+j} (A_{\rm m}^{\top})^{i} C^{\top} C A_{\rm m}^{j}, \tag{5.40}$$

where κ_{ij}'s are non-zero constant coefficients. From (5.35) it follows

$$S(T_{\rm s}) \left(-A_{\rm m}^{-1}B_{\rm m}\right) = \left(C^{\top}C + S(T_{\rm s})\right) W(T_{\rm s}). \tag{5.41}$$

By taking the limit of both sides of (5.41) as $T_{\rm s} \to 0$, we have

$$\lim_{T_{\rm s}\to 0} C^{\top}CW(T_{\rm s}) = 0. \tag{5.42}$$

For $M(s)$ with relative degree l, we have

$$C_{\mathrm{m}} A_{\mathrm{m}}^{j} B_{\mathrm{m}} = 0, \quad j \in \{0, ..., l-2\}.$$

If the relative degree of $M(s)$ is two or higher, by multiplying both sides of (5.41) with $\frac{1}{T_{\mathrm{s}}^2}$ and taking limit, we obtain

$$\lim_{T_{\mathrm{s}} \to 0} \left(\frac{1}{T_{\mathrm{s}}^2} C^\top C + \kappa_{11} A_{\mathrm{m}}^\top C^\top C A_{\mathrm{m}} \right) W(T_{\mathrm{s}}) = 0. \tag{5.43}$$

In similar procedures as above, by multiplying both sides of (5.41) with higher order powers of $\frac{1}{T_{\mathrm{s}}}$ and taking the limit, we have

$$\lim_{T_{\mathrm{s}} \to 0} \Theta(T_{\mathrm{s}}) W(T_{\mathrm{s}}) = 0, \tag{5.44}$$

where

$$\Theta(T_{\mathrm{s}}) = \begin{bmatrix} C^\top C \\ \frac{1}{T_{\mathrm{s}}^2} C^\top C + \kappa_{11} A_{\mathrm{m}}^\top C^\top C A_{\mathrm{m}} \\ \vdots \\ \frac{1}{T_{\mathrm{s}}^l} C^\top C + \sum_{j=2}^{l} \sum_{i=1}^{j-1} \kappa_{i(j-i)} \frac{1}{T_{\mathrm{s}}^{(l-j)}} (A_{\mathrm{m}}^\top)^i C^\top C A_{\mathrm{m}}^{(j-i)} \end{bmatrix}. \tag{5.45}$$

The condition in (5.20) implies that $\Theta(T_{\mathrm{s}})$ given in (5.45) is full column rank. Then from the limit in (5.44) it follows

$$\lim_{T_{\mathrm{s}} \to 0} W(T_{\mathrm{s}}) = 0. \tag{5.46}$$

Hence, the limiting relationship in (5.31) holds. This concludes the proof. ■

Lemma 5.3. *Let $C_{\mathrm{d}}[z]$ denote the z-transform of a step-invariant discrete-time approximation of $C(s)$, defined in* (5.15)*. Given a bounded discrete-time signal $r_{\mathrm{d}}[j]$, define $r(t) = r_{\mathrm{d}}[j]$ for $t \in [jT_{\mathrm{s}}, (j+1)T_{\mathrm{s}})$, $j \in \mathbb{Z}_{\geq 0}$, where $T_{\mathrm{s}} > 0$ is a sampling time. Then*

$$\left\| (\varepsilon - \varepsilon')_t \right\|_{\mathcal{L}_\infty} \leq \Gamma\left(T_{\mathrm{s}}\right) \left\| r_t \right\|_{\mathcal{L}_\infty}, \tag{5.47}$$

where $\Gamma(\cdot)$ is defined in (5.16)*, $\varepsilon(t)$ is the signal with Laplace transform $\varepsilon(s) = C(s)r(s)$, and $\varepsilon'(t) = \varepsilon_{\mathrm{d}}[j]$, $t \in [jT_{\mathrm{s}}, (j+1)T_{\mathrm{s}})$, $j \in \mathbb{Z}_{\geq 0}$, while $\varepsilon_{\mathrm{d}}[j]$ is the discrete signal with the z-transform $\varepsilon_{\mathrm{d}}[z] = C_{\mathrm{d}}[z] r_{\mathrm{d}}[z]$.*

Proof. The proof is straightforward and hence omitted. ■

Theorem 5.1. *If the condition in* (5.20) *holds, the following limiting relationship is true*

$$\lim_{T_{\mathrm{s}} \to 0} \gamma_{\mathrm{x}}(T_{\mathrm{s}}) = 0, \tag{5.48}$$

where $\gamma_{\mathrm{x}}(T_{\mathrm{s}})$ is defined in (5.18)*.*

Proof. Using the results of Lemmas 5.1-5.3, it is straightforward to verify that $\gamma_0(T_\mathrm{s})$, $\gamma_{\mathrm{dx}}(T_\mathrm{s})$ and $\gamma_\mathrm{C}(T_\mathrm{s})$, given in (5.17), tend to zero as the sampling time T_s goes to zero. Hence, the limiting relationship in (5.48) is true. ■

Consider the following closed-loop reference system

$$\begin{aligned} \dot{x}_{\mathrm{ref}}(t) &= A_\mathrm{m} x_{\mathrm{ref}}(t) + B_\mathrm{m}\left(u_{\mathrm{ref}}(t) + d_{\mathrm{ref}}(t)\right), \quad x_{\mathrm{ref}}(0) = x_0, \\ u_{\mathrm{ref}}(s) &= C(s)\left(K_\mathrm{g} r(s) - d_{\mathrm{ref}}(s)\right), \\ y_{\mathrm{ref}}(t) &= C_\mathrm{m} x_{\mathrm{ref}}(t), \end{aligned} \tag{5.49}$$

where $d_{\mathrm{ref}}(s)$ is the Laplace transform of $d_{\mathrm{ref}}(t) \triangleq f(t,\, x_{\mathrm{ref}}(t))$.

The reference system in (5.49) defines *the achievable response* by the closed-loop system given by (5.1), (5.21)-(5.24), where instead of the estimates the actual unknown signals are used in (5.49). Notice that $d_{\mathrm{ref}}(t)$ is unknown, and this reference system is used only for analysis. To prove the stability of the closed-loop sampled-data system with the multirate controller proposed in (5.21)-(5.24), we introduce a condition for stability of the reference system in (5.49). Then we establish uniform bounds between the reference system and the closed-loop system given by (5.1) and (5.21)-(5.24).

Lemma 5.4. *For the closed-loop reference system in* (5.49)*, subject to the* $\mathcal{L}_1$*-norm condition* (5.8)*, if* $\|x_0\|_\infty \le \rho_0$*, then*

$$\|x_{\mathrm{ref}}\|_{\mathcal{L}_\infty} < \rho_\mathrm{r}, \tag{5.50}$$

$$\|u_{\mathrm{ref}}\|_{\mathcal{L}_\infty} < \rho_{\mathrm{ur}}, \tag{5.51}$$

where ρ_r *is introduced in* (5.8)*, and* ρ_{ur} *is given in* (5.25)*.*

Proof. It follows from (5.49) and the definition of $H(s)$ and $G(s)$ in (5.7) that

$$x_{\mathrm{ref}}(s) = H(s)C(s)K_\mathrm{g} r(s) + H(s)\left(\mathbb{I}_p - C(s)\right) d_{\mathrm{ref}}(s) + \left(s\mathbb{I}_n - A_\mathrm{m}\right)^{-1} x_0. \tag{5.52}$$

Then for arbitrary $\tau > 0$, we have

$$\|x_{\mathrm{ref}\,\tau}\|_{\mathcal{L}_\infty} \le \|G(s)\|_{\mathcal{L}_1} \|d_{\mathrm{ref}\,\tau}\|_{\mathcal{L}_\infty} + \rho_{\mathrm{in}} + \|H(s)C(s)K_\mathrm{g}\|_{\mathcal{L}_1} M_\mathrm{r}. \tag{5.53}$$

Since $\left\| s(s\mathbb{I}_n - A_\mathrm{m})^{-1} \right\|_{\mathcal{L}_1} > 1$, we have $\rho_0 < \rho_{\mathrm{in}}$. The condition in (5.8) implies that $\|x_{\mathrm{ref}}(0)\|_\infty = \|x_0\|_\infty < \rho_\mathrm{r}$. In addition, $x_{\mathrm{ref}}(t)$ is continuous. Therefore, if the bound in (5.50) is not true, there exists a time $\tau_1 > 0$ such that

$$\begin{aligned} &\|x_{\mathrm{ref}}(t)\|_\infty < \rho_\mathrm{r}, \quad \forall t \in [0,\, \tau_1), \\ &\|x_{\mathrm{ref}}(\tau_1)\|_\infty = \rho_\mathrm{r}, \end{aligned}$$

which implies that

$$\left\|x_{\mathrm{ref}\tau_1}\right\|_{\mathcal{L}_\infty} = \rho_{\mathrm{r}}. \tag{5.54}$$

The redefinition in (5.10) implies $K_{\rho_{\mathrm{r}}} \leq L_{\rho_{\mathrm{r}}}$. It follows from the bound in (5.54), and Assumptions 5.2 and 5.3 that

$$\left\|d_{\mathrm{ref}\tau_1}\right\|_{\mathcal{L}_\infty} \leq L_{\rho_{\mathrm{r}}}\left\|x_{\mathrm{ref}\tau_1}\right\|_{\mathcal{L}_\infty} + B_0. \tag{5.55}$$

The bound in (5.55), together with the upper bound in (5.53), lead to

$$\|x_{\mathrm{ref}\tau_1}\|_{\mathcal{L}_\infty} \leq \frac{\|G(s)\|_{\mathcal{L}_1} B_0 + \|H(s)C(s)K_{\mathrm{g}}\|_{\mathcal{L}_1} M_{\mathrm{r}} + \rho_{\mathrm{in}}}{1 - \|G(s)\|_{\mathcal{L}_1} L_{\rho_{\mathrm{r}}}}.$$

The condition in (5.8) can be solved for ρ_{r} to obtain the bound

$$\frac{\|G(s)\|_{\mathcal{L}_1} B_0 + \|H(s)C(s)K_{\mathrm{g}}\|_{\mathcal{L}_1} M_{\mathrm{r}} + \rho_{\mathrm{in}}}{1 - \|G(s)\|_{\mathcal{L}_1} L_{\rho_{\mathrm{r}}}} < \rho_{\mathrm{r}},$$

which leads to

$$\left\|x_{\mathrm{ref}\tau_1}\right\|_{\mathcal{L}_\infty} < \rho_{\mathrm{r}}.$$

This contradicts the equality in (5.54), thus proving the bound in (5.50). This further implies that the upper bound in (5.55) holds for all $\tau > 0$ with strict inequality, which in turn implies that

$$\|d_{\mathrm{ref}}\|_{\mathcal{L}_\infty} < L_{\rho_{\mathrm{r}}}\rho_{\mathrm{r}} + B_0. \tag{5.56}$$

The bound on $u_{\mathrm{ref}}(t)$ follows from (5.49)

$$\|u_{\mathrm{ref}\tau}\|_{\mathcal{L}_\infty} < \|C(s)K_{\mathrm{g}}\|_{\mathcal{L}_1} M_{\mathrm{r}} + \|C(s)\|_{\mathcal{L}_1} \left(L_{\rho_{\mathrm{r}}}\rho_{\mathrm{r}} + B_0\right),$$

which proves (5.51). ■

Lemma 5.5. *Consider the system in* (5.1) *and the controller in* (5.21)-(5.24)*, subject to conditions in* (5.8)*. If* T_{s} *satisfies* (5.19)*, and*

$$\|x_\tau\|_{\mathcal{L}_\infty} < \rho_{\mathrm{x}} \tag{5.57}$$

holds, then

$$\left\|(K(T_{\mathrm{s}})\bar{C}_{\mathrm{d}}^{\dagger}\tilde{y}(s) - d'(s))_\tau\right\|_{\mathcal{L}_\infty} \leq \gamma_0(T_{\mathrm{s}}), \tag{5.58}$$

where $\tilde{y}(s)$ *is the Laplace transform of* $\tilde{y}(t)$ *given by*

$$\tilde{y}(t) = \tilde{y}_{\mathrm{d}}[k], \quad t \in [kT_{\mathrm{s}}, (k+1)T_{\mathrm{s}}), \quad k \in \mathbb{Z}_{\geq 0}, \tag{5.59}$$

and $\tilde{y}[k]$ *is the prediction error defined in* (5.23)*. Also,* $d'(s)$ *is the Laplace transform of* $d'(t)$ *defined by*

$$d'(t) = \begin{cases} d(t), & T_{\mathrm{s}} \leq t, \\ 0, & 0 \leq t < T_{\mathrm{s}}. \end{cases} \tag{5.60}$$

The bounds $\gamma_0(T_\mathrm{s})$ and ρ_x are given in (5.17) *and* (5.25)*, respectively.*

Proof. Since $\bar{C}_\mathrm{d}^\dagger \tilde{y}_\mathrm{d}[0] = 0$, the definition in (5.60) implies that the left side of (5.58) is zero for every $\tau \in [0,\, T_\mathrm{s})$, and the inequality in (5.58) holds. In the following, we show that (5.58) is true for $\tau \geq T_\mathrm{s}$.

The step-invariant discrete-time system equivalent to the continuous-time system in (5.1) is given by

$$\begin{aligned} x_\mathrm{d}[k+1] =& \bar{A}_d x_\mathrm{d}[k] + \bar{B}_\mathrm{d}\left(u_\mathrm{d}[k] + d_\mathrm{d}[k]\right), \quad x_\mathrm{d}[0] = x_0, \\ \bar{y}_\mathrm{d}[k] =& \bar{C}_\mathrm{d} x_\mathrm{d}[k] + \bar{D}_\mathrm{d}\left(u_\mathrm{d}[k] + d_\mathrm{d}[k]\right). \end{aligned} \tag{5.61}$$

Define

$$\tilde{x}_\mathrm{d}[k] \stackrel{\Delta}{=} \hat{x}_\mathrm{d}[k] - x_\mathrm{d}[k]. \tag{5.62}$$

Then from (5.61) and the predictor dynamics in (5.21) it follows

$$\begin{aligned} \tilde{x}_\mathrm{d}[k+1] &= \bar{A}_\mathrm{d}\tilde{x}_\mathrm{d}[k] + \hat{d}[k] - \bar{B}_\mathrm{d} d_\mathrm{d}[k], \quad \tilde{x}_\mathrm{d}[0] = \bar{C}_\mathrm{d}^\dagger \bar{y}_0 - x_0, \\ \tilde{y}_\mathrm{d}[k] &= \bar{C}_\mathrm{d}\tilde{x}_\mathrm{d}[k] - \bar{D}_\mathrm{d} d_\mathrm{d}[k], \end{aligned} \tag{5.63}$$

where $\tilde{y}_\mathrm{d}[k]$ is defined in (5.23). From (5.63) one can obtain

$$\bar{C}_\mathrm{d}^\dagger \tilde{y}_\mathrm{d}[k+1] = \left(\bar{A}_\mathrm{d}\bar{C}_\mathrm{d}^{+}\bar{D}_\mathrm{d} - \bar{B}_\mathrm{d}\right) d_\mathrm{d}[k] - \bar{C}_\mathrm{d}^\dagger \bar{D}_\mathrm{d} d_\mathrm{d}[k+1]. \tag{5.64}$$

By multiplying both sides of (5.64) by $K(T_\mathrm{s})$, which is defined in (5.14), and subtracting $d_\mathrm{d}[k+1]$, we have

$$K(T_\mathrm{s})\bar{C}_\mathrm{d}^\dagger \tilde{y}_\mathrm{d}[k+1] - d_\mathrm{d}[k+1] = -\left(\mathbb{I} + K(T_\mathrm{s})\bar{C}_\mathrm{d}^\dagger \bar{D}_\mathrm{d}\right)\left(d_\mathrm{d}[k+1] - d_\mathrm{d}[k]\right).$$

For all $k \in \mathbb{Z}_{\geq 0}$ such that $(k+1)T_\mathrm{s} \leq \tau$, since (5.57) holds, one can obtain

$$\left\| K(T_\mathrm{s})\bar{C}_\mathrm{d}^\dagger \tilde{y}_\mathrm{d}[k+1] - d_\mathrm{d}[k+1] \right\|_\infty \leq \left\| \left(\mathbb{I} + K(T_\mathrm{s})\bar{C}_\mathrm{d}^\dagger \bar{D}_\mathrm{d}\right) \right\|_\infty \left\| d_\mathrm{d}[k+1] - d_\mathrm{d}[k] \right\|_\infty. \tag{5.65}$$

Also, we have

$$\left\| d_\mathrm{d}[k+1] - d_\mathrm{d}[k] \right\|_\infty = \left\| f\left((k+1)T_\mathrm{s}, x_\mathrm{d}[k+1]\right) - f\left(kT_\mathrm{s},\, x_\mathrm{d}[k]\right) \right\|_\infty \leq \gamma_\mathrm{dx}(T_\mathrm{s}), \tag{5.66}$$

where $\gamma_\mathrm{dx}(T_\mathrm{s})$ is defined in (5.17). From (5.65) and (5.66), and given the fact that $\tilde{y}(t)$ and $d(t)$ are piece-wise constant, one can obtain the bound in (5.58). ■

Theorem 5.2. *Consider the system in* (5.1) *and the controller in* (5.21)-(5.24)*, subject to the*

condition in (5.8). *If* T_s *satisfies* (5.19), *then*

$$\|x\|_{\mathcal{L}_\infty} < \rho_\mathrm{x}, \tag{5.67}$$

and

$$\|x_\mathrm{ref} - x\|_{\mathcal{L}_\infty} \leq \gamma_\mathrm{x}(T_\mathrm{s}), \quad \|u_\mathrm{ref} - u\|_{\mathcal{L}_\infty} \leq \gamma_\mathrm{u}(T_\mathrm{s}), \tag{5.68}$$

where ρ_x *is given in* (5.25). *Also,* $\gamma_\mathrm{x}(\cdot)$ *and* $\gamma_\mathrm{u}(\cdot)$ *are defined in* (5.18) *and* (5.25) *respectively.*

Proof. Consider the reference system in (5.49) and define

$$\begin{aligned}
\tilde{x}_\mathrm{ref}(t) &= x_\mathrm{ref}(t) - x(t), \quad \tilde{y}_\mathrm{ref}(t) = y_\mathrm{ref}(t) - y(t),\\
\tilde{u}_\mathrm{ref}(t) &= u_\mathrm{ref}(t) - u(t), \quad \tilde{d}_\mathrm{ref}(t) = d_\mathrm{ref}(t) - d(t).
\end{aligned}$$

Then from (5.1) and (5.49) it follows

$$\begin{aligned}
\dot{\tilde{x}}_\mathrm{ref}(t) &= A_\mathrm{m}\tilde{x}_\mathrm{ref}(t) + B_\mathrm{m}\left(\tilde{u}_\mathrm{ref}(t) + \tilde{d}_\mathrm{ref}(t)\right), \quad \tilde{x}_\mathrm{ref}(0) = 0\\
\tilde{y}_\mathrm{ref}(t) &= C_\mathrm{m}\tilde{x}_\mathrm{ref}(t).
\end{aligned} \tag{5.69}$$

The continuous-time step-invariant equivalent of the control input in (5.24) is given by

$$u_\mathrm{C}(s) = C(s)\left(K_\mathrm{g}r(s) + K(T_\mathrm{s})\bar{A}_\mathrm{d}^{-1}\hat{d}(s)\right), \tag{5.70}$$

where $\hat{d}(s)$ is the Laplace transform of $\hat{d}(t)$ given by

$$\hat{d}(t) = \hat{d}_\mathrm{d}[k], \quad t \in [kT_\mathrm{s}, (k+1)T_\mathrm{s}), \quad k \in \mathbb{Z}_{\geq 0}.$$

It follows

$$\tilde{u}_\mathrm{ref}(s) = u_\mathrm{ref}(s) - u_\mathrm{C}(s) + u_\mathrm{C}(s) - u(s). \tag{5.71}$$

Notice that $\bar{C}_\mathrm{d}^\dagger\tilde{y}_\mathrm{d}[0] = 0$. We have

$$u_\mathrm{ref}(s) - u_\mathrm{C}(s) = -C(s)d(0)\tfrac{1-e^{-sT_\mathrm{s}}}{s} + C(s)\left(K(T_\mathrm{s})\bar{C}_\mathrm{d}^\dagger\tilde{y}(s) - d'(s) - \tilde{d}_\mathrm{ref}(s)\right), \tag{5.72}$$

where $d'(s)$ is the Laplace transform of $d'(t)$ defined in (5.60). Then from (5.69), (5.71) and (5.72) one can obtain

$$\tilde{x}_\mathrm{ref}(s) = G(s)\tilde{d}_\mathrm{ref}(s) - \frac{1-e^{-sT_\mathrm{s}}}{s}H(s)C(s)d(0) + H(s)C(s)\left(K(T_\mathrm{s})\bar{C}_\mathrm{d}^\dagger\tilde{y}(s) - d'(s)\right) + H(s)\left(u_\mathrm{C}(s) - u(s)\right). \tag{5.73}$$

The condition in (5.8) implies that $\|x(0)\|_\infty = \|x_0\|_\infty < \rho_\mathrm{r}$. Then we have $\|x(0)\|_\infty < \rho_\mathrm{x}$. In addition, $x(t)$ is continuous. Therefore, if the bound in (5.67) does not hold, there exists a time

$\tau_1 > 0$ such that

$$\|x(t)\|_\infty < \rho_{\rm x}, \quad \forall t \in [0,\, \tau_1),$$
$$\|x(\tau_1)\|_\infty = \rho_{\rm x},$$

which implies that

$$\|x_{\tau_1}\|_{\mathcal{L}_\infty} = \rho_{\rm x}. \tag{5.74}$$

Using Lemma 5.3 and the definition in (5.70), the following bound holds

$$\|(u_{\rm C} - u)_{\tau_1}\|_{\mathcal{L}_\infty} \leq \gamma_{\rm C}(T_{\rm s}), \tag{5.75}$$

where $\gamma_{\rm C}(\cdot)$ is defined in (5.17).

For all $k \in \mathbb{Z}_{\geq 0}$ and $t \in [kT_{\rm s},\, (k+1)T_{\rm s})$, we have

$$\tilde{d}_{\rm ref}(t) = f(t, x_{\rm ref}(t)) - f(t,\, x(t)) + f(t,\, x(t)) - f(kT_{\rm s}, x(kT_{\rm s})). \tag{5.76}$$

It follows

$$\left\|\tilde{d}_{{\rm ref}_{\tau_1}}\right\|_{\mathcal{L}_\infty} \leq L_{\rho_{\rm r}} \left\|\tilde{x}_{{\rm ref}_{\tau_1}}\right\|_{\mathcal{L}_\infty} + \gamma_{\rm dx}(T_{\rm s}), \tag{5.77}$$

where $\gamma_{\rm dx}(T_{\rm s})$ is given in (5.25). In addition, from Lemma 5.5 we have

$$\left\|(K(T_{\rm s})\bar{C}_{\rm d}^\dagger \tilde{y} - d')_{\tau_1}\right\|_{\mathcal{L}_\infty} \leq \gamma_0(T_{\rm s}). \tag{5.78}$$

Then from (5.73)-(5.78) we can obtain the following bound

$$\left\|\tilde{x}_{{\rm ref}_{\tau_1}}\right\|_{\mathcal{L}_\infty} \leq \frac{\|G(s)\|_{\mathcal{L}_1}\gamma_{\rm dx}(T_{\rm s}) + \|H(s)\|_{\mathcal{L}_1}\gamma_{\rm C}(T_{\rm s}) + \|H(s)C(s)\|_{\mathcal{L}_1}\gamma_0(T_{\rm s}) + T_{\rm s}\rho_{\rm d_0}}{1 - L_{\rho_{\rm r}}\|G(s)\|_{\mathcal{L}_1}}. \tag{5.79}$$

Since the condition in (5.19) holds, we have

$$\left\|\tilde{x}_{{\rm ref}_{\tau_1}}\right\|_{\mathcal{L}_\infty} < \bar{\gamma}_1. \tag{5.80}$$

Therefore

$$\|x_{\tau_1}\|_{\mathcal{L}_\infty} < \rho_{\rm r} + \bar{\gamma}_1 = \rho_{\rm x},$$

which contradicts (5.74), thus proving (5.67). From (5.79) the first inequality in (5.68) also holds. In the following, we show that the second inequality is true. By combining (5.71), (5.72), (5.75), (5.77), (5.78) and (5.80), we have

$$\|\tilde{u}_{\rm ref}(s)\|_{\mathcal{L}_\infty} \leq \|C(s)\|_{\mathcal{L}_1} (\gamma_0(T_{\rm s}) + L_{\rho_{\rm r}}\gamma_{\rm x}(T_{\rm s}) + \gamma_{\rm dx}(T_{\rm s})) + \gamma_{\rm C}(T_{\rm s}) + T_{\rm s}\rho_{\rm d_1},$$

where $\rho_{\rm d_1}$ is defined in (5.25). Therefore the second inequality in (5.68) is true. This concludes the proof. ■

Remark 5.4. *For MIMO systems that satisfy the condition in* (5.20)*, Theorem 5.1 and Lemmas 5.1-5.3 imply that the bounds in* (5.68) *can be made arbitrarily small as the sampling time* $T_{\rm s}$ *tends to zero. Therefore the closed-loop sampled-data system uniformly recovers the performance of the reference system defined in* (5.49)*.*

5.4. Experimental Study: A Quadrotor Flight Test under Zero-Dynamics Attack

To verify the main results of this chapter, we implemented the proposed controller for trajectory tracking of a Crazyflie quadrotor in x-y plane. Also, the effectiveness of the multirate controller is compared with a standard $\mathcal{L}_1$ adaptive control, which is implemented with uniform sampling time in [114]. In this experiment, we consider PID as the baseline control, augmented with $\mathcal{L}_1$ adaptive output-feedback to improve the tracking performance and robustness of the closed-loop system. Then a zero-dynamics actuator attack is injected into the control input channel. In the following, the flight test results are provided to demonstrate the capability of the proposed multirate adaptive controller in timely detection and mitigation of actuator attacks.

In the multirate trajectory tracking control setup the pitch and roll command signals are sent to the quadrotor from Simulink with the sampling period of $T_{\rm s} = 0.03sec$, and the position measurement signal from Vicon is received with $N = 3$ times faster rate at the sampling period of $\frac{T_{\rm s}}{N} = 0.01sec$. For comparison we also implemented the $\mathcal{L}_1$ controller with uniform rate of $T_{\rm s} = 0.03sec$. The rest of the closed-loop system parameters are chosen the same for the singlerate and multirate implementations. The desired dynamics and the low-pass filter are chosen as

$$M(s) = \begin{bmatrix} \frac{4}{s^2+1.5s+4} & 0 \\ 0 & \frac{4}{s^2+1.5s+4} \end{bmatrix}, \quad C(s) = \begin{bmatrix} \frac{2.5^3}{(s+2.5)^3} & 0 \\ 0 & \frac{2.5^3}{(s+2.5)^3} \end{bmatrix}. \tag{5.81}$$

In this experiment the pitch angle command navigates the quadrotor in x-axis direction, while the roll angle command controls the y-axis position. Therefore the dynamics governing the position of the quadrotor are decoupled in x and y directions. Using Matlab system identification toolbox and by collecting input/output data, the following transfer functions for the model of quadrotor dynamics with the baseline PID controller from the reference commands $R_{\rm x}$ and $R_{\rm y}$ to the actual x-axis and y-axis positions X and Y are obtained

$$\frac{X(s)}{R_{\rm x}(s)} = \frac{1.276s^2 + 12.33s + 7.058}{s^4 + 3.762s^3 + 8.984s^2 + 14.75s + 7.013}, \tag{5.82}$$

$$\frac{Y(s)}{R_{\rm y}(s)} = \frac{-2675s^3 + 4.167s^2 + 3.556s + 13.39}{s^4 + 1.449s^3 + 7.796s^2 + 5.325s + 11.92}. \tag{5.83}$$

We notice that if the transfer functions in (5.82) and (5.83) are sampled at a single rate with sampling time $T_{\rm s} = 0.03sec$, the discrete-time plants have unstable zeros at $z_{\rm x} = -1.06$ and

$z_{\rm y} = 1.66$ respectively. These unstable zeros can be used to devise an attack signal in the form of

$$d[k] = [\epsilon_{\rm x} z_{\rm x}^k,\, \epsilon_{\rm y} z_{\rm y}^k]^\top, \tag{5.84}$$

where $\epsilon_{\rm x} = 10^{-20}$ and $\epsilon_{\rm y} = 5 \times 10^{-177}$ are small constants. Also, $z_{\rm x} = -1.06$ and $z_{\rm y} = 1.66$ are the unstable sampling zeros for the discrete-time model of quadrotor dynamics in (5.82) and (5.83) respectively. Using the multirate control approach these unstable zeros can be removed.

Since a cyber attack, such as the zero-dynamics attack in (5.84), can involve unbounded signals (implemented in cyber space), the feedback control algorithm by itself cannot mitigate the attack. Therefore the controller should be integrated with a secure software/hardware architecture such as Simplex structure [14–17]. This structure includes normal control environment and a backup secure control environment. After a cyber attack is detected, the control is switched from normal mode to the safe mode. An ideal control algorithm for Simplex architecture should detect the attack fast enough and maintain the stability of the perturbed system. This Simplex structure can be achieved using modern multicore processors and virtualization technology [115], which is out of the scope of this research. A simple way to simulate the Simplex structure for this experiment is to remove the attack signal as soon as it is detected.

In the following we consider a residual for attack detection that triggers switching to a safe mode, which is calculated using the output prediction error. The one-time switch is triggered, once the criteria

$$\left\| \left[\; w\tilde{y}_{\rm d}^\top[k+1], \quad \tilde{y}_{\rm d}^\top[k+1] - \tilde{y}_{\rm d}^\top[k] \; \right]^\top \right\|_\infty > \Delta, \quad k \in \mathbb{N} \tag{5.85}$$

is met, where the output prediction error $\tilde{y}_{\rm d}[k]$ is defined in (5.23), Δ is the detection threshold, and $w \in \mathbb{R}$ is a weighting coefficient. The residual is a weighted norm of the output prediction error, and its rate of change is defined in 5.85. In the multirate approach $\Delta = 0.03$ is chosen, while the threshold is $\Delta = 0.02$ for the singlerate control. Also, the weighting coefficient is selected to be $w = 0$ in (5.85). Figure 5.1 shows the residuals over time calculated for multirate and singlerate controllers. As shown in Figure 5.1, the thresholds are chosen above the level of errors due to measurement noise or system uncertainties in order to reduce the number of false alarms. For the same attack signals the multirate detection happens $0.45sec$ sooner than the singlerate detection (Figure 5.1), which is sufficient enough to save the quadrotor from crash. Fast detection is esspecially important to recover the stability in the case of exponentially growing attack signals. In addition, Figure 5.2 shows the norm of the output prediction error $\|\tilde{y}_{\rm d}[k]\|_\infty$ for multirate and singlerate $\mathcal{L}_1$ controllers. In Figure 5.2 for multirate approach we can notice a change in the profile of prediction error norm, when the attack signals start to grow to significant levels (after $t = 21.5sec$). However, a change in the prediction error norm can be detected from $t = 23.5sec$ in Figure 5.2 for singlerate method. This indicates that the singlerate detection has a considerable latency compared to the multirate detection in the case of zero-dynamics attacks. In addition, the comparison of plots in Figure 5.2 reveals that the output prediction error norm is smaller under

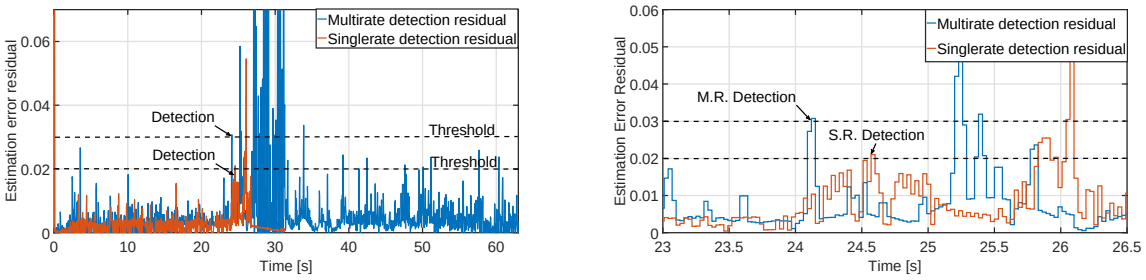

Figure 5.1: Calculated residual given by (5.85) for attack detection. (Left) Residual history over the flight test interval. (Right) Residual history over the active attack interval. For each flight test the attack signals are removed as soon as the residual exceeds the threshold ($\Delta_{\text{multirate}} = 0.03, \quad \Delta_{\text{singlerate}} = 0.02$). The multirate $\mathcal{L}_1$ controller provides a $0.45sec$ faster detection compared to the controller with uniform rate.

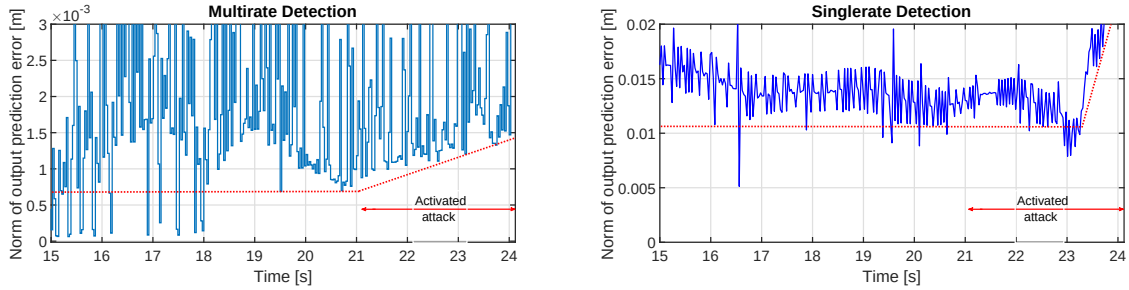

Figure 5.2: Norm of the output prediction error $\|\tilde{y}_{\text{d}}[k]\|_{\infty}$ for multirate $\mathcal{L}_1$ controller (Left), and for singlerate $\mathcal{L}_1$ controller (Right). The active attack interval is marked in the plots. A change in the profile of prediction error norm can be observed in the left figure during the active attack interval, while the profile change in the right figure becomes noticeable with about $2sec$ delay.

multirate controller, which indicates a better performance in tracking the $\mathcal{L}_1$ reference system. The rest of the flight test results are illustrated in Figures 5.3-5.5.

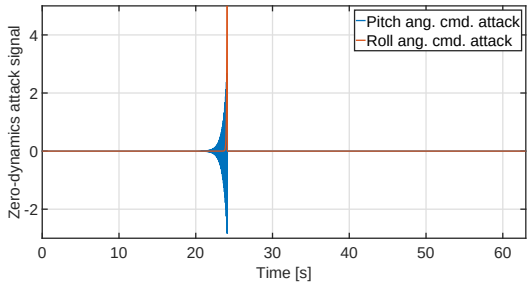

Figure 5.3: A zero-dynamics attack signal of the form $d[k] = [\epsilon_{\text{x}} z_{\text{x}}^k, \epsilon_{\text{y}} z_{\text{y}}^k]^{\top}$ is injected at control input.

Figure 5.3 shows the zero-dynamics attack signals on pitch and roll commands, which become noticeable at around $t = 21.5sec$ and grow exponentially till $t = 24.12sec$, when the attack is detected as the residual exceeds the threshold (Figure 5.1). After being detected, the attack signals can be removed by switching to a secure computing platform, which performs as a backup for the compromised controller software. The x and y trajectories of the quadrotor versus time are shown in Figures 5.4 under augmented single-rate and multirate $\mathcal{L}_1$ adaptive controllers in two separate

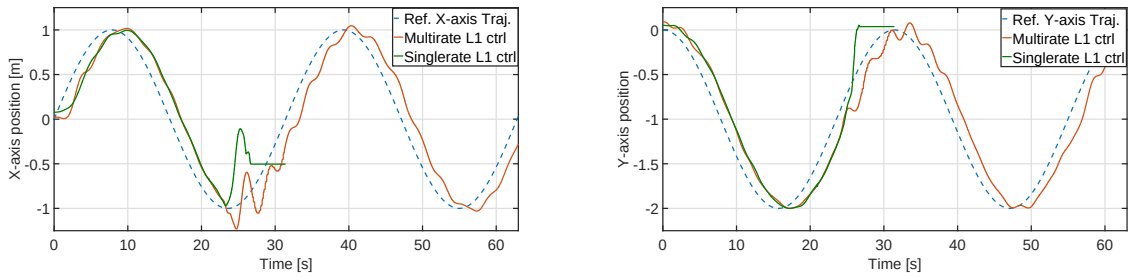

Figure 5.4: Response of the closed-loop quadtotor system to the sinosoidal reference command $r_{\mathrm{d}}[k] = [\sin(0.2kT_{\mathrm{s}}), \cos(0.2kT_{\mathrm{s}}) - 1]^{\top}$ subject to the attack signal. (Left) The x-axis position of Crazyflie vs. time measured by VICON system. (Right) The y-axis position of Crazyflie vs. time measured by VICON system.

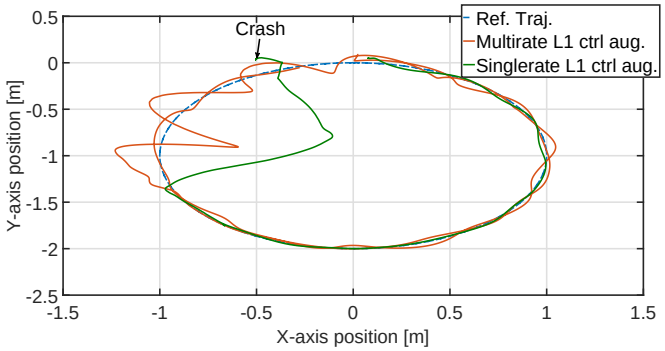

Figure 5.5: Quadrotor trajectory in x-y plane, under singlerate/multirate $\mathcal{L}_1$ controllers.

flight tests. Figure 5.5 shows the trajectory of the quadrotor in x-y plane. We can see that the closed-loop system with single-rate controller crashes due to zero-dynamics attack, however the system with multirate controller is robust to the attack.

Remark 5.5. *The results of this experiment and choice of the threshold in* (5.85) *depend on the quality of the measurement outputs and the level of noise in the motion capture system. In the flight tests similar to above, false alarm cases can occur due to the inaccuracy in the measurements.*

CHAPTER 6

An Optimization Method for Design of the Filter in the Control Structure

As mentioned in Remark 3.3, the lowpass filter in $\mathcal{L}_1$ adaptive control architectures plays the key role for performance and robustness tradeoff, [47]. The lowpass filter essentially decouples the estimation from control, enabling to use fast estimation rates without losing robustness. While partial guidelines are given in [47] for the full state-feedback architecture, the filter design problem is still mostly open and challenging in many cases. A filter design method to trade off the filter bandwidth and the time-delay margin is attempted in [104] using an LMI approach based on star-norm optimization. In [105], μ-analysis and synthesis is used for the filter design in $\mathcal{L}_1$ adaptive output-feedback architecture. Design schemes for an optimal trade-off between performance and robustness, based on a randomized search for design parameters and coefficients of the filter in $\mathcal{L}_1$ adaptive controller are presented in [106]. A filter design method with a new stability condition is proposed in [100], where a suitable parameterization of the lowpass filter makes the design problem solvable in a standard $\mathcal{H}_\infty$ optimization framework.

In this chapter an extended $\mathcal{L}_1$-norm stability condition is formulated, which includes a lower bound on the time-delay margin. A mixed $\mathcal{L}_1/\mathcal{H}_2$ performance measure is used as the cost function and the $\mathcal{L}_1$-norm stability condition is set as the constraint function. This mixed $\mathcal{L}_1/\mathcal{H}_2$ norm optimization ensures satisfactory transient and steady-state responses. Since the optimization problem involving $\mathcal{L}_1$-norm in continuous-time framework is non-convex, as explained in [47], and analytical solutions result in irrational transfer functions as shown in [116, 117], we will solve the equivalent problem in discrete-time framework. The equivalent multi-objective optimization problem can be formulated as a numerically efficient linear/quadratic programming (LP/QP). For discrete-time systems, general multi-objective optimal (GMO) control method is proposed in [118, 119] to address control problems involving $\mathcal{L}_1/\mathcal{H}_2/\mathcal{H}_\infty$ norm objectives, and a MATLAB package for synthesizing GMO problems is introduced in [120]. Earlier similar approaches can be tracked in the treatment of ℓ_1-optimal control problem in [121] for MIMO discrete-time systems. A novel synthesis method was developed in [122] using linear programming (LP) approach. In [123], a discrete-time formulation for state-feedback $\mathcal{L}_1$ adaptive system and a filter optimization method based on linear programming were proposed.

In this chapter, the Euler approximation is used to obtain the discrete-time generalized plant. The resulting filter from the optimization algorithm is then converted back to continuous-time to synthesize the $\mathcal{L}_1$ adaptive controller to meet robustness/performance trade-off criteria. Note that solving the equivalent optimization problem in discrete-time results in a sub-optimal solution. It is shown that the continuous-time compensator derived from the optimization setup for the discrete-time equivalent system satisfies the norm constraints on the closed-loop continuous-time system, and the performance metric tends arbitrarily close to the optimum using sufficiently small sampling

time in the Euler approximation method.

With the proposed filter optimization method a trajectory tracking controller for the Crazyflie quadrotor is discussed as an example. The Crazyflie 2.0 is an open-source micro quadrotor UAV [124]. Due to its small size and lightweight, it is less intimidating to fly in the proximity of people. Hence it can be used to deliver small household items like pills. Its small size however makes it prone to aerodynamic uncertainty, and the relatively short battery discharging time introduces more uncertainty into the system. These uncertainties make it an ideal testbed for the $\mathcal{L}_1$ adaptive controller. Some previous studies using Crazyflie can be found in [125–127]. There were several studies on the $\mathcal{L}_1$ adaptive controller design for quadrotors in [128–132], but no dedicated study has been focused on filter optimization. For the Crazyflie quadrotor a baseline PD controller was designed for each of the x and y direction, and a PID controller for z direction. With these baseline controllers, three single-input-single-output (SISO) transfer functions from the position command to position output were obtained via system identification (system ID). Based on these SISO transfer functions, an $\mathcal{L}_1$ adaptive controller was designed for each direction. The closed-loop system was then tested in a lab environment equipped with the Vicon Motion Capture System [133].

6.1. Analysis of the Reference System with Input Delay

In this chapter the analysis is limited to a single-input single-output (SISO) delayed system

$$y(s) = A(s)\left(e^{-sT_{\mathrm{d}}}u(s) + d(s)\right), \tag{6.1}$$

where $u(t) \in \mathbb{R}$ is the input signal, $y(t) \in \mathbb{R}$ is the system output, $A(s)$ is a strictly proper unknown transfer function, and $T_{\mathrm{d}} > 0$ is an unknown input delay. Finally, $d(s)$ is the Laplace transform of the time-varying uncertainties and disturbances

$$d(t) = f\left(t,\, y(t)\right), \tag{6.2}$$

where $f : \mathbb{R} \times \mathbb{R} \to \mathbb{R}$ is a nonlinear function representing uncertainties. To proceed, the following assumptions are introduced.

Assumption 6.1. *There exist constants $L > 0$ and $L_0 > 0$, such that*

$$\left|f\left(t,\, y_1\right) - f\left(t,\, y_2\right)\right| \leq L\left|y_1 - y_2\right|, \qquad \left|f\left(t,\, y\right)\right| \leq L\left|y\right| + L_0$$

hold uniformly in $t \geq 0$.

Assumption 6.2. *The unknown LTI plant $A(s)$ in (6.1) can be modeled as*

$$A(s) = P_{21}(s)\Delta_{\mathrm{p}}(\mathbb{I}_{n_{\mathrm{A}}\times n_{\mathrm{A}}} - P_{11}(s)\Delta_{\mathrm{p}})^{-1}P_{12}(s) + P_{22}(s) = f_{\mathrm{u}}\left(\left[\begin{array}{cc} P_{11}(s) & P_{12}(s) \\ P_{21}(s) & P_{22}(s) \end{array}\right]_{n_{\mathrm{A}}+1,n_{\mathrm{A}}+1}, \Delta_{\mathrm{p}}\right), \tag{6.3}$$

where Δ_{p} *is the unknown* $n_{\mathrm{A}} \times n_{\mathrm{A}}$ *matrix with* $\|\Delta_{\mathrm{p}}\|_{\mathcal{L}_1} \leq 1$ *representing system parametric uncertainties,* $P_{11}(s)$*,* $P_{12}(s)$*,* $P_{21}(s)$ *and* $P_{22}(s)$ *are known LTI transfer functions with dimensions* $n_{\mathrm{A}} \times n_{\mathrm{A}}$*,* $n_{\mathrm{A}} \times 1$*,* $1 \times n_{\mathrm{A}}$ *and* 1×1 *respectively. The notation* $f_{\mathrm{u}}(\cdot)$ *represents the linear upper fractional transformation from [134].*

The control objective is to design an adaptive output feedback controller $u(t)$ such that the system output $y(t)$ tracks the desired response $y_{\mathrm{m}}(t)$ given by $y_{\mathrm{m}}(s) = M(s)r(s)$, where $r(s)$ is the Laplace transform of a given bounded continuous reference command $r(t)$, and $M(s)$ is a minimum-phase stable transfer function.

Similar to previous chapters, the closed loop of the system in (6.1) with an $\mathcal{L}_1$ adaptive output-feedback controller recovers the response of a continuous-time reference system as the sampling time tends to zero. Here the closed-loop reference system, in which the uncertainties are compensated for within the bandwidth of a low-pass filter $C(s)$, is given by

$$y_{\mathrm{ref}}(s) = M(s)\left(u_{\mathrm{ref}}(s) + \sigma_{\mathrm{ref}}(s)\right), \tag{6.4}$$

$$u_{\mathrm{ref}}(s) = C(s)\left(r(s) - \sigma_{\mathrm{ref}}(s)\right), \tag{6.5}$$

where

$$\sigma_{\mathrm{ref}}(s) = \frac{\left(e^{-sT_{\mathrm{d}}}A(s) - M(s)\right)u_{\mathrm{ref}}(s) + A(s)d_{\mathrm{ref}}(s)}{M(s)}, \tag{6.6}$$

and $d_{\mathrm{ref}}(s)$ is the Laplace transform of $d_{\mathrm{ref}}(t) = f\left(t,\, y_{\mathrm{ref}}(t)\right)$. We refer to the closed-loop system in (6.4) - (6.6) as $\mathcal{L}_1$ reference system.

The controller design proceeds by considering a strictly proper transfer function $C(s)$ such that $C(0) = 1$. Further, the selection of $C(s)$ and $M(s)$ must ensure that

$$H_{T_{\mathrm{d}}}(s) \triangleq \frac{A(s)M(s)}{C(s)e^{-sT_{\mathrm{d}}}A(s) + \left(1 - C(s)\right)M(s)} \qquad \text{is stable,} \tag{6.7}$$

and that the following $\mathcal{L}_1$-norm condition holds

$$\left\|G_{T_{\mathrm{d}}}(s)\right\|_{\mathcal{L}_1} L < 1, \tag{6.8}$$

where

$$G_{T_{\mathrm{d}}}(s) \triangleq H_{T_{\mathrm{d}}}(s)\left(1 - C(s)\right). \tag{6.9}$$

Lemma 6.1. *The closed loop reference system in* (6.4) - (6.6)*, together with Assumptions 6.1 and 6.2, is bounded-input bounded-output (BIBO) stable, if* $C(s)$ *and* $M(s)$ *verify the* $\mathcal{L}_1$*-norm condition in* (6.8)*.*

Proof. It follows from (6.5) and (6.6) that

$$u_{\text{ref}}(s) = \frac{C(s)M(s)r(s) - C(s)A(s)d_{\text{ref}}(s)}{C(s)e^{-sT_{\text{d}}}A(s) + (1 - C(s))\,M(s)}, \tag{6.10}$$

which, along with (6.4), yields

$$y_{\text{ref}}(s) = H_{T_{\text{d}}}(s)\left(C(s)r(s) + (1 - C(s))\,d_{\text{ref}}(s)\right). \tag{6.11}$$

Moreover, Assumption 6.1 implies

$$\|y_{\text{ref}}\|_{\mathcal{L}_\infty} \leq \|H_{T_{\text{d}}}(s)C(s)\|_{\mathcal{L}_1}\|r\|_{\mathcal{L}_\infty} + \|G_{T_{\text{d}}}(s)\|_{\mathcal{L}_1}\left(L\|y_{\text{ref}}\|_{\mathcal{L}_\infty} + L_0\right). \tag{6.12}$$

It follows from (6.12) that

$$\|y_{\text{ref}}\|_{\mathcal{L}_\infty} \leq \frac{\|H_{T_{\text{d}}}(s)C(s)\|_{\mathcal{L}_1}\|r\|_{\mathcal{L}_\infty} + \|G_{T_{\text{d}}}(s)\|_{\mathcal{L}_1}L_0}{1 - \|G_{T_{\text{d}}}(s)\|_{\mathcal{L}_1}L}. \tag{6.13}$$

Since $H_{T_{\text{d}}}(s)$, $G_{T_{\text{d}}}(s)$ are strictly proper and stable, $\|y_{\text{ref}}\|_{\mathcal{L}_\infty}$ is bounded, which completes the proof. ■

The stability condition in (6.8) is not easy to verify, since it depends on the unknown time delay and the system's parametric uncertainties. For the purposes of filter design, we derive the modified $\mathcal{L}_1$-norm condition, which guarantees a lower bound for the time-delay margin.

Define

$$f_1(t, y) \triangleq f(t, y) - f(t, 0), \quad f_0(t) \triangleq f(t, 0). \tag{6.14}$$

Let $d_1(t) = f_1(t, y(t))$ and $d_0(t) = f_0(t)$ be time varying uncertainties and disturbances. From (6.2) one can write

$$d(t) = d_1(t) + d_0(t). \tag{6.15}$$

Let

$$\Delta_{\text{d}}(s) = \frac{d_1(s)}{y(s)}, \tag{6.16}$$

where $d_1(s)$ and $d_0(s)$ are the Laplace transforms of $d_1(t)$ and $d_0(t)$, respectively. Then, the following holds

$$d(s) = d_1(s) + d_0(s) = \Delta_{\text{d}}(s)y(s) + d_0(s). \tag{6.17}$$

Using Assumption 6.1 one can find the following upper bounds

$$\|\Delta_{\text{d}}(s)\|_{\mathcal{L}_1} = \sup_{\|y\|_{\mathcal{L}_\infty} \leq 1} \frac{\|d_1\|_{\mathcal{L}_\infty}}{\|y\|_{\mathcal{L}_\infty}} \leq L, \quad \|d_0\|_{\mathcal{L}_\infty} \leq L_0. \tag{6.18}$$

The input delay in the system (6.1) is typically unknown. We define the following uncertainty

related to this time delay

$$\Delta_{T_{\rm d}}(s) \triangleq \frac{1}{s}\left(e^{-sT_{\rm d}}-1\right), \tag{6.19}$$

where $T_{\rm d}$ is the input time delay, and $\|\Delta_{T_{\rm d}}\|_{\mathcal{L}_1} = T_{\rm d}$. For the purpose of filter design the optimization variable is defined as

$$K(s) \triangleq \frac{sC(s)}{(1-C(s))\,M(s)}. \tag{6.20}$$

Theorem 6.1. *Let T_d^* be a positive constant. Given the system* (6.1) *with Assumptions 6.1 and 6.2, the reference system given by* (6.4)-(6.4) *is BIBO stable for all $T_{\rm d} < T_{\rm d}^*$ (i.e. $T_{\rm d}^*$ is a lower bound on the time delay margin), if*

$$\|\Psi(s)\|_{\mathcal{L}_1} < 1, \tag{6.21}$$

where

$$\Psi(s) \triangleq \begin{bmatrix} -T_{\rm d}^*K(s)\Omega(s)P_{22}(s) & -LK(s)\Omega(s)P_{22}(s) & -K(s)\Omega(s)P_{21}(s) \\ T_{\rm d}^*\Omega(s)P_{22}(s) & L\Omega(s)P_{22}(s) & \Omega(s)P_{21}(s) \\ T_{\rm d}^*P_{12}(s)\Omega(s) & LP_{12}(s)\Omega(s) & P_{11}(s)-\frac{1}{s}P_{12}(s)K(s)\Omega(s)P_{21}(s) \end{bmatrix}, \tag{6.22}$$

and $K(s)$ is defined in (6.20)*, $P_{ij}(s)$ $(i,j=1,2)$ is given in Assumption 6.2, and $\Omega(s) \triangleq \left(1+\frac{1}{s}P_{22}(s)K(s)\right)^{-1}$.*

Proof. Substituting (6.3) and (6.17) into (6.4), we get

$$y_{\rm ref}(s) = P_{21}(s)\Delta_{\rm p}y_{\rm p}(s) + P_{22}(s)\left(e^{-sT_{\rm d}}u_{\rm ref}(s) + \Delta_{\rm d}(s)y_{\rm ref}(s) + d_0(s)\right), \tag{6.23}$$

where

$$y_{\rm p}(s) \triangleq (\mathbb{I} - P_{11}(s)\Delta_{\rm p})^{-1}P_{12}(s)\left(e^{-sT_{\rm d}}u_{\rm ref}(s) + \Delta_{\rm d}(s)y_{\rm ref}(s) + d_0(s)\right).$$

Let

$$y_s(s) \triangleq su_{\rm ref}(s). \tag{6.24}$$

Then using (6.19) and (6.24), one can rewrite (6.23) as

$$y_{\rm ref}(s) = P_{21}(s)\Delta_{\rm p}y_{\rm p}(s) + P_{22}(s)\left(\Delta_{T_{\rm d}}(s)+\frac{1}{s}\right)y_{\rm s}(s) + P_{22}(s)\Delta_{\rm d}(s)y_{\rm ref}(s) + P_{22}(s)d_0(s). \tag{6.25}$$

Notice that $y_{\rm p}(s)$ is given by

$$y_{\rm p}(s) = P_{11}(s)\Delta_{\rm p}y_{\rm p}(s) + P_{12}(s)\left(\Delta_{T_{\rm d}}(s)+\frac{1}{s}\right)y_{\rm s}(s) + P_{12}(s)\Delta_{\rm d}(s)y_{\rm ref}(s) + P_{12}(s)d_0(s). \tag{6.26}$$

Moreover, combining (6.4), (6.5), (6.20) and (6.24) yields

$$y_{\rm s}(s) = K(s)M(s)r(s) - K(s)y_{\rm ref}(s).$$

Defining $\Omega(s) \triangleq \left(1 + \frac{1}{s}P_{22}(s)K(s)\right)^{-1}$ and using (6.23) and (6.25), one obtains

$$\begin{aligned} y_{\rm s}(s) =& K(s)\Omega(s)M(s)r(s) - K(s)\Omega(s)P_{21}(s)\Delta_{\rm p}y_{\rm p}(s) - K(s)\Omega(s)P_{22}(s)\Delta_{T_{\rm d}}(s)y_{\rm s}(s) \\ & - K(s)\Omega(s)\Delta_{\rm d}(s)y_{\rm ref}(s) - K(s)\Omega(s)P_{22}(s)d_0(s). \end{aligned} \tag{6.27}$$

From (6.25) and (6.26), together with (6.27), it follows that

$$\begin{aligned} y_{\rm ref}(s) =& \frac{1}{s}P_{22}(s)K(s)\Omega(s)M(s)r(s) + \Omega(s)P_{21}(s)\Delta_{\rm p}y_{\rm p}(s) + \Omega(s)P_{22}(s)\Delta_r(s)y_{\rm s}(s) \\ & + \Omega(s)\Delta_{\rm d}(s)y_{\rm ref}(s) + \Omega(s)P_{22}(s)d_0(s), \\ y_{\rm p}(s) =& \frac{1}{s}P_{12}(s)K(s)\Omega(s)M(s)r(s) + \left(P_{11}(s) - \frac{1}{s}P_{12}(s)K(s)\Omega(s)P_{21}(s)\right)\Delta_{\rm p}y_{\rm p}(s) \\ & + \left(P_{12}(s) - \frac{1}{s}P_{12}(s)K(s)\Omega(s)P_{22}(s)\right)\left(\Delta_{T_{\rm d}}(s)y_{\rm s}(s) + \Delta_{\rm d}(s)y_{\rm ref}(s) + d_0(s)\right). \end{aligned} \tag{6.28}$$

Now let

$$\Delta(s) \triangleq \begin{bmatrix} \frac{1}{T_{\rm d}^*}\Delta_{T_{\rm d}}(s) & 0 & 0 \\ 0 & \frac{1}{L}\Delta_{\rm d}(s) & 0 \\ 0 & 0 & \Delta_{\rm p} \end{bmatrix},\ Y(s) \triangleq \begin{bmatrix} y_{\rm s}(s) \\ y_{\rm ref}(s) \\ y_{\rm p}(s) \end{bmatrix},\ U(s) \triangleq \begin{bmatrix} d_0(s) \\ r(s) \end{bmatrix},$$

$$B(s) \triangleq \begin{bmatrix} -K(s)\Omega(s)P_{22}(s) & K(s)\Omega(s)M(s) \\ \Omega(s)P_{22}(s) & \frac{1}{s}P_{22}(s)K(s)\Omega(s) \\ P_{12}(s) - \frac{1}{s}P_{12}(s)K(s)\Omega(s)P_{22}(s) & \frac{1}{s}P_{22}(s)K(s)\Omega(s)M(s) \end{bmatrix}.$$

Notice that $\|\Delta(s)\|_{\mathcal{L}_1} \leq 1$. One can rewrite (6.27) and (6.28) in a matrix form as follows

$$Y(s) = \Psi(s)\Delta(s)Y(s) + B(s)U(s). \tag{6.29}$$

Since $r(t)$ and $d_0(t)$ are bounded signals, the system in (6.29) is stable if $(\mathbb{I} - \Psi(s)\Delta)^{-1}$ is analytic in right-half s-plane. Using small gain theorem, a sufficient condition for stability is given by

$$\|\Psi(s)\Delta(s)\|_{\mathcal{L}_1} < 1.$$

Since $\|\Delta(s)\|_{\mathcal{L}_1} \leq 1$, the stability of the system in (6.29) follows from the condition in (6.21).

Next we show that the condition in (6.21) verifies $\|G_{T_{\rm d}}\|_{\mathcal{L}_1}L < 1$ for all $T_{\rm d} \leq T_{\rm d}^*$ by using a contradiction argument (for simplicity, we assume $r(t)$, $d_0(t) \equiv 0$). Suppose it does not hold. Then there exists $T_{\rm d} \leq T_{\rm d}^*$ such that

$$\|G_{T_{\rm d}}(s)\|_{\mathcal{L}_1}L \geq 1\,, \tag{6.30}$$

so that for some $d(s)$, $\|d_1(s)\| \leq 1$ the following holds

$$\|G_{T_{\rm d}}(s)d_1(s)\|_{\mathcal{L}_\infty} \geq \frac{\|d_1(s)\|_{\mathcal{L}_\infty}}{L}. \tag{6.31}$$

Combining (6.11) and (6.17) yields

$$y_{\text{ref}} = G_{T_\text{d}}(s)d_1(s). \tag{6.32}$$

Moreover, it follows from (6.17), (6.32) and (6.29) that

$$\begin{bmatrix} y_\text{s}(s) \\ y_{\text{ref}}(s) \\ y_\text{p}(s) \end{bmatrix} = \Psi(s) \begin{bmatrix} \frac{1}{T_\text{d}^*}\Delta_{T_\text{d}}(s)y_\text{s}(s) \\ \frac{1}{L}d_1(s) \\ \Delta_\text{p}y_\text{p}(s) \end{bmatrix}. \tag{6.33}$$

Notice that

$$\left\| \frac{1}{T_\text{d}^*}\Delta_{T_\text{d}}(s)y_\text{s}(s) \right\|_{\mathcal{L}_\infty} \leq \left\| \frac{1}{T_\text{d}^*}\Delta_{T_\text{d}}(s) \right\|_{\mathcal{L}_1} \|y_\text{s}(s)\|_{\mathcal{L}_\infty} \leq \|y_\text{s}(s)\|_{\mathcal{L}_\infty}, \tag{6.34}$$

and

$$\|\Delta_\text{p}y_\text{p}(s)\|_{\mathcal{L}_\infty} \leq \|\Delta_\text{p}\|_{\mathcal{L}_1}\|y_\text{p}(s)\|_{\mathcal{L}_\infty} \leq \|y_\text{p}(s)\|_{\mathcal{L}_\infty}. \tag{6.35}$$

Finally, combining (6.34), (6.35) and (6.31) we get

$$\left\| \begin{bmatrix} y_\text{s}(s) \\ y_{\text{ref}}(s) \\ y_\text{p}(s) \end{bmatrix} \right\|_{\mathcal{L}_\infty} \geq \left\| \begin{bmatrix} \frac{1}{T_\text{d}^*}\Delta_{T_\text{d}}(s)y_\text{s}(s) \\ \frac{1}{L}d_1(s) \\ \Delta_\text{p}y_\text{p}(s) \end{bmatrix} \right\|_{\mathcal{L}_\infty}, \tag{6.36}$$

which contradicts $\|\Psi(s)\|_{\mathcal{L}_1} < 1$. Therefore, $\|G_{T_\text{d}}(s)\|_{\mathcal{L}_1}L < 1$ holds for all $T_\text{d} \leq T_\text{d}^*$, which, along with Lemma 6.1, implies that the reference system system is BIBO stable for each $T_\text{d} \leq T_\text{d}^*$. This completes the proof. ■

6.2. Optimization Problem and the Synthesis Method

In this section, the optimal filter design is formulated as a constrained optimization problem, and then a synthesis procedure is presented to solve the optimization problem. In addition to robust stability condition, which was introduced in the previous section, the performance criteria for the trade-off of robust stability and robust performance are defined.

Consider the following definitions

$$
\begin{aligned}
K(s) &= \frac{sC(s)}{(1-C(s))\,M(s)}\,,\\
e_{\mathrm{ref}}(s) &= M(s)r(s) - y_{\mathrm{ref}}(s)\,,\\
u_{\mathrm{K}}(s) &= K(s)e_{\mathrm{ref}}(s), \quad y(s) = u_{\mathrm{K}}(s),\\
u_{\mathrm{s}}(s) &= \Delta_{T_{\mathrm{d}}}(s)y_{\mathrm{s}}(s)\,,\\
d_{\mathrm{ref}}(s) &= \Delta_{\mathrm{d}}(s)y_{\mathrm{ref}}(s)\,,\\
y_{\mathrm{p}}(s) &= P_{12}(s)(u_{\mathrm{s}}(s) + d_{\mathrm{ref}}(s)) + P_{11}(s)u_{\mathrm{p}}(s) + \frac{1}{s}P_{12}(s)u_{\mathrm{K}}(s),\\
u_{\mathrm{p}}(s) &= \Delta_{\mathrm{p}}y_{\mathrm{p}}(s),\\
\Delta(s) &= \mathrm{diag}\left(\frac{1}{T_{\mathrm{d}}^*}\Delta_{T_{\mathrm{d}}}, \frac{1}{L}\Delta_d, \Delta_{\mathrm{p}}\right),
\end{aligned}
$$

where $y_{\mathrm{ref}}(s)$ is the reference output, defined in (6.4), and $r(s)$ is Laplace transform of reference command $r(t)$. The matrices Δ_{p} and $P_{ij}(s)$ of parametric uncertainties are defined in Assumption 6.2. Moreover, $\Delta_{T_{\mathrm{d}}}(s)$ is given in (6.19). Let $Z_{\mathrm{e}}(t)$ and $Z_{\mathrm{u}}(t)$ represent performance outputs defined as

$$
Z_{\mathrm{e}}(s) = W_{\mathrm{e}}(s)e_{\mathrm{ref}}(s), \quad Z_{\mathrm{u}}(s) = W_{\mathrm{u}}(s)\frac{1}{s}u_{\mathrm{K}}(s),
$$

where $W_{\mathrm{e}}(s)$ and $W_{\mathrm{u}}(s)$ are the weight functions on the error signal and control input, respectively.

By minimizing the norm defined for weighted control input in the cost function, one can reduce the undesirable control actuation. The corresponding generalized plant $G(s)$ is given by

$$
\begin{bmatrix} T_{\mathrm{d}}^*y_{\mathrm{s}} \\ Ly_{\mathrm{ref}} \\ y_{\mathrm{p}} \\ Z_{\mathrm{e}} \\ Z_{\mathrm{u}} \\ e_{\mathrm{ref}} \end{bmatrix} = \underbrace{\begin{bmatrix} 0 & 0 & 0 & 0 & T_d^* \\ LP_{22}(s) & LP_{22}(s) & LP_{21}(s) & 0 & \frac{1}{s}LP_{22}(s) \\ P_{12}(s) & P_{12}(s) & P_{11}(s) & 0 & \frac{1}{s}P_{12}(s) \\ -W_{\mathrm{e}}(s)P_{22}(s) & -W_e(s)P_{22}(s) & -W_e(s)P_{21}(s) & W_e(s)M(s) & -\frac{1}{s}W_e(s)P_{22}(s) \\ 0 & 0 & 0 & 0 & \frac{1}{s}W_u(s) \\ -P_{22}(s) & -P_{22}(s) & -P_{21}(s) & M(s) & -\frac{1}{s}P_{22}(s) \end{bmatrix}}_{\triangleq G(s)} \begin{bmatrix} u_{\mathrm{s}} \\ d_{\mathrm{ref}} \\ u_{\mathrm{p}} \\ r \\ u_{\mathrm{K}} \end{bmatrix}.
$$

The LFT formulation of the closed-loop system can be written as

$$
T(s) = f_{\mathrm{l}}\left(f_{\mathrm{u}}\left(G(s),\, \Delta(s)\right),\, K(s)\right), \tag{6.37}
$$

where $f_{\mathrm{u}}(\cdot)$ and $f_{\mathrm{l}}(\cdot)$ denote linear upper and linear lower fractional transformations, respectively. The LFT problem setup is shown in Figure 6.1.

To formulate the optimization problem, one needs to specify the performance criteria. Consider minimization of the $\mathcal{H}_2$-norm of the transfer functions from the reference input r to the performance output signals Z_{e} and Z_{u}, which ensures a zero steady-state tracking error (it corresponds to *dc*-

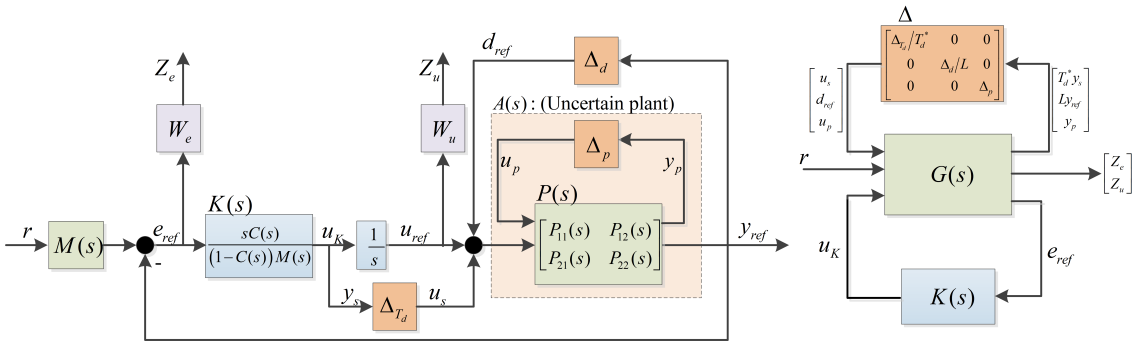

Figure 6.1: The Reference output-feedback system with input delay and its LFT model.

gain condition for the filter design (*i.e.* $C(0) = 1$)). In addition, we add a weighted $\mathcal{L}_1$-norm of the transfer function from the input u_s to the output y_s (shown in Figure 6.1) to the cost function in order to optimize the time-delay margin at the input.

As shown in Theorem 6.1, the closed-loop system is robustly stable in the presence of input time delay $T_\mathrm{d} \leq T_\mathrm{d}^*$, input nonlinearities, subject to Assumption 6.1, and parametric uncertainties of the plant $A(s)$, if the $\mathcal{L}_1$-norm condition in (6.21) is satisfied. A combination of a mixed $\mathcal{L}_1/\mathcal{H}_2$ cost-function and $\mathcal{L}_1$ robust stability constraint ensures uniform bound on transient response and zero steady-state error. Therefore the constrained optimization problem for filter design is proposed as follows

$$\inf_{K(s)\,\text{stabilizing}} \left\|T_{44}\left(K(s)\right)\right\|_{\mathcal{H}_2}^2 + \left\|T_{45}\left(K(s)\right)\right\|_{\mathcal{H}_2}^2 + c\left\|T_{11}\left(K(s)\right)\right\|_{\mathcal{L}_1}, \quad \text{s.t.} \quad \left\|\Psi(K(s))\right\|_{\mathcal{L}_1} < 1, \tag{6.38}$$

where $T_{ji} : w_i \to v_j$ is a mapping from the input w_i (i^{th} element of input vector $w^\top = [u_\mathrm{s},\, d_\mathrm{ref},\, u_\mathrm{p},\, r]$) to the output v_j (j^{th} element of output vector $v^\top = [y_\mathrm{s},\, y_\mathrm{ref},\, y_\mathrm{p},\, Z_\mathrm{e},\, Z_\mathrm{u}]$). Note that in this formulation the $\mathcal{L}_1$-norm constraint ensures stability of the closed-loop system in the presence of three sources of uncertainties (*i.e.* input delay, input nonlinearities and disturbances, and system parametric uncertainties). Dependent on the specific problem, if some of the uncertainties are not present, the mapping Ψ can be reduced to a lower dimensional system.

Next we address the optimization problem in (6.38), in which we optimize over $\mathcal{H}_2$ performance measure, while satisfying the robust stability constraint based on the $\mathcal{L}_1$-norm. Due to the challenges in the optimization problem, involving $\mathcal{L}_1$-norm in continuous-time framework [116, 117], a problem equivalent to the one in (6.38) is solved in discrete-time framework. This equivalent multi-objective optimization problem can be solved numerically through efficient linear/quadratic programming (LP/QP,) [120]. First, the discrete-time MIMO open-loop transfer function $G(z)$, which approximates the generalized plant $G(s)$, is obtained. Let $K(z)$ be the z-transform of the controller $K(s)$ (as shown in Figure 6.1). We treat $K(z)$ as the optimization variable. The optimization algorithm results in optimal controller, $K^*(z)$, and is converted to continuous time to

obtain $K^*(s)$. Then the optimal filter is given by $C^*(s) = \frac{K^*(s)M(s)/s}{1+K^*(s)M(s)/s}$.

In this chapter Euler approximation method is used to convert a continuous-time LTI system to discrete-time and vise-versa. Note that solving the equivalent optimization problem in discrete-time results in a sub-optimal solution. In the sequel we show that the $\mathcal{L}_1$ and $\mathcal{H}_2$ norms of continuous-time systems are bounded above by the ℓ_1 and $\mathcal{H}_2$ norms of discrete-time counterparts respectively. The norms of continuous-time system and discrete-time counterpart become arbitrarily close using sufficiently small sampling time for the Euler approximation. This approach also ensures that the continuous-time compensator derived from the optimization setup for the discrete-time equivalent system satisfies the norm constraints on the closed-loop continuous-time system, and the performance measure tends arbitrarily close to the optimum using sufficiently small sampling time.

Theorem 6.2. *Consider the stable strictly proper system $G(s)$ with the system matrices $(A,\, B,\, C)$ and the Euler approximation system (EAS) $G(z,\, \tau)$ with the system matrices $(\mathbb{I} + \tau A, \tau B, C)$. Let $\tau \in (0, \tau_{\max})$, where $\tau_{\max} \triangleq \min\limits_{\lambda\in\Lambda} \left\{ \frac{-2\mathrm{Re}(\lambda)}{|\lambda|^2} \right\}$, and Λ be the set of all eigenvalues of A. Then*

(i) $G(z,\, \tau)$ is stable if and only if $G(s)$ is stable for $\tau \in (0, \tau_{\max})$;

(ii) $\frac{1}{\tau}\, \|G(z,\tau)\|_{\mathcal{H}_2}^2 \geq \|G(s)\|_{\mathcal{H}_2}^2$ for $\tau \in (0, \tau_{\max})$;

(iii) $\lim\limits_{\tau\to 0} \frac{1}{\tau}\, \|G(z,\tau)\|_{\mathcal{H}_2}^2 = \|G(s)\|_{\mathcal{H}_2}^2$.

Proof. Consider the transformation $z = 1 + \tau s$ corresponding to the Euler approximation method. Let s_i be the pole of $G(s)$ in the s-plane and $z_i = 1 + \tau s_i$ be the corresponding pole of $G(z, \tau)$. The stability of discrete-time system implies that all poles are in the open unit disk, *i.e.*, $|z_i| < 1$. For $\tau \in (0, \tau_{\max})$, the transformation $z = 1 + \tau s$ maps all the left-half s-plane stable poles of $G(s)$ to the open unit disk in the z-plane, where $\tau_{\max} = \min\limits_{\lambda\in\Lambda} \left\{ \frac{-2\mathrm{Re}(\lambda)}{|\lambda|^2} \right\}$, and Λ is the set of all eigenvalues of A. Therefore $G(z, \tau)$ is stable. On the other hand, since this transformation is a bijective mapping, the converse argument also holds, *i.e.* stability of $G(z, \tau)$ implies the stability of $G(s)$ for $\tau \in (0, \tau_{\max})$. This proves (i).

Next we prove the claim in (ii). Using Euler approximation, the matrices of the discrete-time system are written as

$$A_{\mathrm{D}} = \mathbb{I} + \tau A,\ B_{\mathrm{D}} = \tau B,\ C_{\mathrm{D}} = C.$$

The $\mathcal{H}_2$-norms of $G(z, \tau)$ and $G(s)$ are given by

$$\|G(z,\tau)\|_{\mathcal{H}_2}^2 = \mathrm{trace}\left(C_{\mathrm{D}} P_{\mathrm{D}} C_{\mathrm{D}}{}^{\top}\right), \quad \|G(s)\|_{\mathcal{H}_2}^2 = \mathrm{trace}\left(CPC^{\top}\right), \tag{6.39}$$

where the positive definite matrices P_{D} and P solve Lyapunov equations

$$A_{\mathrm{D}} P_{\mathrm{D}} A_{\mathrm{D}}^{\top} - P_{\mathrm{D}} + B_{\mathrm{D}} B_{\mathrm{D}}^{\top} = 0\,, \tag{6.40}$$

$$PA + A^\top P + BB^\top = 0\,, \tag{6.41}$$

respectively. P is the unique solution for (6.41), since the pair $(A,\, B)$ is controllable. In addition, controllability of the pair $(A,\, B)$ is equivalent to controllability of the pair $(A_{\rm D}, B_{\rm D})$ for all $\tau \leq \tau_{\max}$. Therefore, $P_{\rm D}$ is also the unique solution for (6.40). From (6.39) it follows that

$$\frac{1}{\tau}\left\|G(z,\tau)\right\|_{\mathcal{H}_2}^2 - \left\|G(s)\right\|_{\mathcal{H}_2}^2 = \frac{1}{\tau}\mathrm{trace}\left(C_{\rm D}P_{\rm D}{C_{\rm D}}^\top\right) - \mathrm{trace}\left(CPC^\top\right) = \mathrm{trace}\left(C\Delta PC^\top\right)\,, \tag{6.42}$$

where $\Delta P = \frac{1}{\tau}P_{\rm D} - P$. In order to ensure that the argument in (ii) holds, it suffices to show that ΔP in (6.42) is positive definite for all $\tau \leq \tau_{\max}$. By using Euler approximation, Equation (6.40) can be rewritten as

$$P_{\rm D}A^\top + AP_{\rm D} + \tau\left(AP_{\rm D}A^\top + BB^\top\right) = 0. \tag{6.43}$$

Since $\frac{1}{\tau}P_{\rm D} = P + \Delta P$, it follows from (6.40) and (6.43) that

$$\Delta PA + A^\top\Delta P = -A_{\rm D}P_{\rm D}A_{\rm D}^\top. \tag{6.44}$$

Notice that A is Hurwitz, and $A_{\rm D}P_{\rm D}A_{\rm D}^\top$ is a positive definite matrix for each $\tau \leq \tau_{\max}$. Therefore ΔP is a positive definite matrix. This proves the claim in (ii).

Finally, we will show that the argument in (iii) holds, by proving $\left\|\Delta P\right\|_2 \to 0$ as $\tau \to 0$. Let

$$S_n\left(\tau\right) \triangleq \sum_{k=0}^{n} p_k\left(\tau\right), \quad \tau \in (0,\, \tau_{\max})\,,$$

where

$$p_k\left(\tau\right) \triangleq A_{\rm D}^k B_{\rm D}B_{\rm D}^\top\left(A_{\rm D}^\top\right)^k = \tau^2(\mathbb{I} + \tau A)^k BB^\top\left(\mathbb{I} + \tau A^\top\right)^k. \tag{6.45}$$

Since the closed-form solution of $P_{\rm D}$ for each $\tau \leq \tau_{\max}$ is given by

$$P_{\rm D}(\tau) = \sum_{k=0}^{\infty} A_{\rm D}^k B_{\rm D}B_{\rm D}^\top\left(A_{\rm D}^\top\right)^k,$$

$\lim\limits_{n\to\infty} S_n\left(\tau\right) = P_{\rm D}\left(\tau\right)$ for $\tau \in (0,\, \tau_{\max})$ holds. Notice that

$$\left\|S_m\left(\tau\right) - S_n\left(\tau\right)\right\|_2 \leq \sum_{k=n}^{m}\left\|p_k\left(\tau\right)\right\|_2\,,$$

which, together with (6.45), leads to

$$\left\|S_m\left(\tau\right) - S_n\left(\tau\right)\right\|_2 \leq \sum_{k=n}^{m}\left\|\tau^2(\mathbb{I} + \tau A)^k BB^\top\left(\mathbb{I} + \tau A^\top\right)^k\right\|_2 \leq \tau^2\sigma_{\max}^2\left(B\right)\sum_{k=n}^{m}\lambda_{\max}^k\left(A_{\rm D}A_{\rm D}^\top\right). \tag{6.46}$$

Since $A_{\rm D}$ is stable, $\left|\lambda_{\max}\left(A_{\rm D}A_{\rm D}^\top\right)\right| < 1$ holds, which yields $\lambda_{\max}^n\left(A_{\rm D}A_{\rm D}^\top\right) \to 0$ as $n \to \infty$. Therefore,

by taking limits of both sides in (6.46), it follows that for each $\tau \leq \tau_{\max}$

$$\|S_m(\tau) - S_n(\tau)\|_2 \to 0 \text{ as } n, m \to \infty,$$

which implies that the sequence $\{S_n(\tau)\}$ converges uniformly. Since $S_n(\tau)$ is continuous on the interval $(0,\ \tau_{\max})$, by applying Uniform limit theorem [135], it follows that $P_{\mathrm{D}}(\tau)$ is continuous on $(0,\ \tau_{\max})$. Hence

$$\lim_{\tau\to 0} P_{\mathrm{D}}(\tau) = \lim_{\tau\to 0}\lim_{n\to\infty} S_n(\tau) = \lim_{n\to\infty}\lim_{\tau\to 0} S_n(\tau) = 0.$$

Since A is stable, $\int_0^\infty \left\|e^{At}A\right\|_2 dt < \infty$, and

$$\|\Delta P\|_2 = \left\| \int_0^\infty e^{At} A P_{\mathrm{D}} A^\top e^{A^\top t} dt \right\|_2 \leq \left\|P_{\mathrm{D}}^{1/2}\right\|_2 \int_0^\infty \left\|e^{At}A\right\|_2 dt\,,$$

$\lim_{\tau\to 0} P_{\mathrm{D}}(\tau) = 0$ implies $\|\Delta P\|_2 \to 0$ as $\tau \to 0$. This concludes the proof. Notice that Theorem 6.2 appears in [117] without the proof. In order to make this chapter self-contained, we proved Theorem 6.2. ■

Theorem 6.3. *Consider the system*

$$\begin{aligned} \dot{x} &= Ax + B_1 w, \quad x(0) = 0, \\ \hat{v} &= C_1 x + D_{11} w. \end{aligned} \tag{6.47}$$

Assume that the corresponding Euler approximation system (EAS)

$$\begin{aligned} x_{k+1} &= (\mathbb{I} + \tau A)\, x_k + \tau B_1 w_k, \quad x_0 = 0, \\ \hat{v}_k &= C_1 x_k + D_{11} w_k \end{aligned} \tag{6.48}$$

is asymptotically stable, and

$$\left\|T_{\hat{\mathrm{v}}\mathrm{w}}^{(\mathrm{EAS})}\right\|_1 = \sup_{\substack{w\in\ell_\infty,\ \|w\|\leq 1 \\ x_0=0}} \|\hat{v}_k\|_\infty \stackrel{\Delta}{=} \mu_{\mathrm{E}}(\tau)\,. \tag{6.49}$$

Then the system (6.47) *is asymptotically stable and*

$$\|T_{\hat{\mathrm{v}}\mathrm{w}}\|_{\mathcal{L}_1} = \sup_{\substack{w\in\mathcal{L}_\infty,\ \|w\|\leq 1 \\ x_0=0}} \|\hat{v}(t)\|_\infty \stackrel{\Delta}{=} \mu_{\mathrm{c}} \leq \mu_{\mathrm{E}}(\tau)\,. \tag{6.50}$$

Conversely, if (6.47) *is asymptotically stable, and* $\|T_{\hat{\mathrm{v}}\mathrm{w}}\|_{\mathcal{L}_1} \stackrel{\Delta}{=} \mu_{\mathrm{c}}$, *then for all* $\mu > \mu_{\mathrm{c}}$ *there exists* $\tau^* > 0$, *such that for all* $0 < \tau \leq \tau^*$ *the EAS* (6.48) *is asymptotically stable, and* $\left\|T_{\hat{\mathrm{v}}\mathrm{w}}^{(\mathrm{EAS})}\right\|_1 \leq \mu$.

Proof. The proof of this theorem is given in [116]. ■

Theorem 6.4. *Consider the system in* (6.47) *and the corresponding Euler approximation system*

(EAS) in (6.48). *Let* $\{\tau_i\}$ *be a strictly decreasing sequence, such that* $\lim_{i\to\infty} \tau_i = 0$, *and let* $\mu_i = \mu_{\mathrm{E}}(\tau_i)$ *denote the* ℓ_1*-norm defined in* (6.49). *Then the sequence* $\{\mu_i\}$ *is non-increasing, and* $\lim_{i\to\infty} \mu_i = \mu_{\mathrm{c}}$, *where* $\mu_{\mathrm{c}} = \|T_{\hat{\mathrm{vw}}}\|_{\mathcal{L}_1}$ *denotes the* $\mathcal{L}_1$*-norm defined in* (6.50).

Proof. The proof of this theorem can be found in [116]. ■

In the multi-objective approach of GMO control synthesis method multiple signal measures are used to evaluate the performance of the controller, which allows for consideration of different sources of uncertainties in control systems [120]. The problem formulation of this control synthesis method [120] is presented in the sequel.

Consider the system shown in Figure 6.2, where $G(z) = [G_{\mathrm{vw}}(z)\ G_{\mathrm{vu}}(z);\ G_{\mathrm{yw}}(z)\ G_{\mathrm{yu}}(z)]$ is the generalized discrete-time linear time-invariant open-loop transfer matrix from $[w;\ u]$ to $[v;\ y]$, and $K(z)$ is the controller. The signals w, v, u, and y are the exogenous input, regulated output, control input and measured output respectively, and r is a given scalar reference input, while $\mathcal{S}$ is the time-response output.

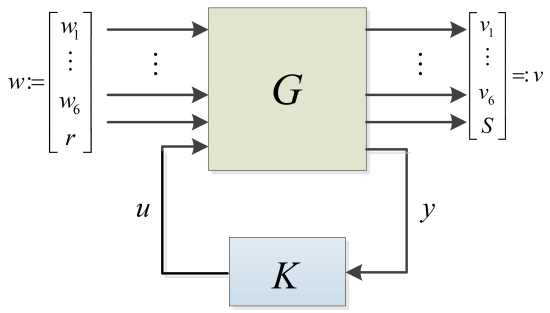

Figure 6.2: Closed-loop System

Let $\hat{R}(z)$ denote the closed-loop transfer matrix from w to v. From [136] the set of all the achievable closed-loop maps is given by

$$\left\{\hat{R}(z) = G_{\mathrm{vw}}(z) + G_{\mathrm{vu}}(z)K(z)(\mathbb{I} - G_{\mathrm{yu}}(z)K(z))^{-1}G_{\mathrm{yw}}(z)\,|K(z)\,\text{stabilizing and structured}\right\}.$$

In the sequel, $\hat{R}^i(z)\,(i = 1,\ ...,6)$ denotes the closed-loop transfer matrix from w_i to v_i, and $R^i(k)$ is the corresponding time-domain response, such that $\hat{R}^i(z) = \sum_{k=0}^{\infty} R^i(k)z^{-k}$. $\hat{R}^7(z)$ is the transfer function from r to $\mathcal{S}$. The general multi-objective optimization (GMO) problem, as formulated in [120], can be stated as follows:

Given the plant $G(z)$, *constants* $c_i > 0, i = 1, ..., 6$, *and two sequences* $\{a_{\mathrm{temp}}\,(k)\}_{k=0}^{\infty}$ *and*

$\{b_{\text{temp}}(k)\}_{k=0}^{\infty}$, *solve the following problem*:

$$\inf_{K \text{ stabilizing and structured}} \left\{ c_1 \left\| R^1(K) \right\|_1 + c_2 \left\| R^2(K) \right\|_2^2 + c_3 \left\| \hat{R}^3(K) \right\|_{\mathcal{H}_\infty} \right\}$$

$$\begin{aligned} \text{subject to} \\ & \left\| R^4(K) \right\|_1 \leq c_4, \\ & \left\| R^5(K) \right\|_2^2 \leq c_5, \\ & \left\| \hat{R}^6(K) \right\|_{\mathcal{H}_\infty} \leq c_6, \\ & a_{\text{temp}}(k) \leq \mathcal{S}(k) \leq b_{\text{temp}}(k),\ k = 0,\ 1,\ 2,\ ..., \end{aligned}$$

where $\{\mathcal{S}(k)\}_{k=0}^{\infty}$ denotes the time response of the closed-loop system due to the exogenous reference input r with $w_i = 0, i = 1, ..., 6$.

6.3. Experimental Study: Optimizing the Position Controller for A Quadrotor

In this section the trajectory tracking control of Crazyflie is presented. In this scheme we consider PD/PID controllers as baseline controllers and augment those with $\mathcal{L}_1$ adaptive output-feedback to enhance the performance and robustness of the quadrotor's trajectory tracking. For the design of the filter, we apply the filter optimization method presented in Section 6.2. Moreover, flight test results are presented to compare the trajectory tracking performance of the quadrotor system with and without augmented $\mathcal{L}_1$ controller.

6.3.1. *Introduction to the Quadrotor and the Test Environment*

The Crazyflie used in this study is shown in Figure 6.3 with additional frame and markers. It is equipped with an onboard auto-pilot, which receives attitude and thrust command and generates corresponding output. This auto-pilot will be used in the controller design. It is valid to assume that these channels work independently, and that command in one attitude will be followed without affecting other attitudes. Table 6.1 lists a few specifications of this platform. For more information about the Crazyflie refer to [124] and previous studies [125, 126].

Figure 6.3: Crazyflie 2.0 with frame and markers

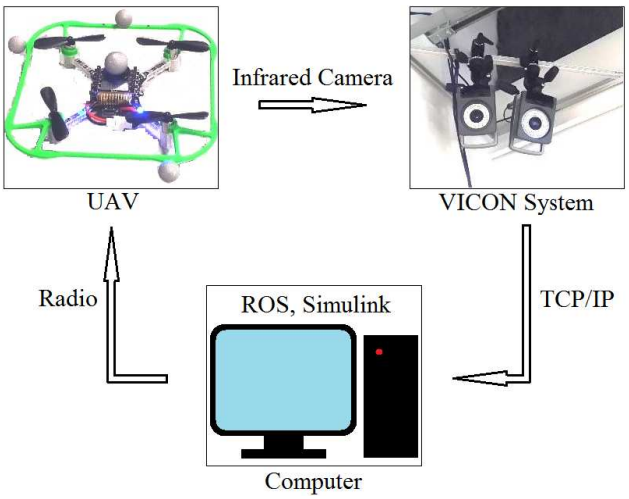

Figure 6.4: Test environment setup

Mass	27g
Size (W×H×D)	92 × 92 × 92mm
Max Recommended Payload	15g

Table 6.1: Basic Specifications of Crazylie 2.0 [137]

The flight test was conducted at the Intelligent Robotics Laboratory under the Coordinated Science Laboratory of University of Illinois, Urbana-Champaign. The setup of the lab is shown in Figure 6.4. The controller is implemented in Simulink. Simulink models communicate with the Robot Operating System (ROS) to send the control signals to the UAV. The Vicon Motion Capture System, which has been widely used in quadrotor flight test [138, 139], is used to measure the position and attitude of the UAV and then send the measurements to Simulink model via ROS. To enable the Vicon measurement, a frame was designed and 3D-printed with four markers installed on it, as shown in Figure 6.3.

6.3.2. *Quadrotor Modeling and Baseline Controller design*

Let $\mathcal{F}$ denote an inertial coordinate system defined by axes x, y, and z. Let $\mathbf{r}^{\mathcal{F}}$ denote the position vector of center of mass of the quadrator in $\mathcal{F}$, and ψ, ϕ and θ be Z-X-Y Euler angles. At hovering state the speed of the UAV is zero, so are the pitch and roll angles θ and ϕ. At an equilibrium corresponding to hovering state, under the assumption of small perturbations, the linearized equations of motion take the following form [138]:

$$\ddot{\mathbf{r}}^{\mathcal{F}} = \begin{bmatrix} g(\Delta\theta\cos\psi + \Delta\phi\sin\psi) \\ g(\Delta\theta\sin\psi - \Delta\phi\cos\psi) \\ \frac{\Delta u}{m} \end{bmatrix}, \tag{6.51}$$

where m is the mass of the UAV, g is the gravitational acceleration, and ψ is the yaw angle. Also, $\Delta\phi$ and $\Delta\theta$ indicate perturbations from the equilibrium angles. We define another coordinate system denoted by $\mathcal{F}_t$ with axes x_t, y_t and z_t, as shown in Figure 6.5. The transformation matrix R from $\mathcal{F}$ to $\mathcal{F}_t$ is given by

$$R = \begin{bmatrix} \cos\psi & \sin\psi & 0 \\ -\sin\psi & \cos\psi & 0 \\ 0 & 0 & 1 \end{bmatrix}$$

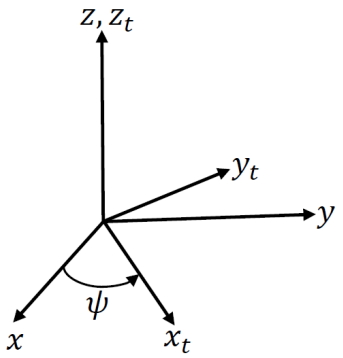

Figure 6.5: Coordinate Systems

Assuming a constant yaw angle $\psi = \psi_0$, the linearized equation of motion in (6.51) can be rewritten as

$$\ddot{\mathbf{r}}^{\mathcal{F}_t} = R\ddot{\mathbf{r}}^{\mathcal{F}} = \begin{bmatrix} g\Delta\theta \\ g\Delta\phi \\ \frac{\Delta u}{m} \end{bmatrix}. \tag{6.52}$$

From (6.52) it can be seen that the motions in x_t, y_t and z_t directions are decoupled. The yaw angle can be regulated at a desired angle $\psi_{\text{des}}(t) = \psi_0$ by implementing a PD controller. With the motion in x_t, y_t and z_t axes decoupled, well-tuned PD/PID controllers with negative feedback are designed for each axis. The objective of the baseline control law is twofold. First, it yields a satisfactory position control of quadrotor for tracking a desired position command $\mathbf{r}_{\text{des}}(t) = [x_{\text{des}}(t), y_{\text{des}}(t), z_{\text{des}}(t)]^\top$ in $\mathcal{F}$. At the same time it renders a stable closed-loop system, on which system ID will be done to obtain approximate transfer functions for filter optimization. The gains of the baseline controller have been well tuned in order to achieve a reasonable position tracking performance. However, due to nonlinearities and uncertain parameters, the tracking performance of baseline PD/PID controllers is limited.

With these PD/PID controllers and using the linearized equation of motion in (6.52) the

required attitude angles and thrust can be obtained by

$$\theta_{\text{cmd}} = \Delta\theta_{\text{cmd}} = \frac{k_{\text{d,x}}\dot{e}_{\text{x}_\text{t}} + k_{\text{p,x}}e_{\text{x}_\text{t}}}{g}$$
$$\phi_{\text{cmd}} = \Delta\phi_{\text{cmd}} = -\frac{k_{\text{d,y}}\dot{e}_{\text{y}_\text{t}} + k_{\text{p,y}}e_{\text{y}_\text{t}}}{g}$$
$$u = u_0 + \Delta u_{\text{cmd}} = mg + m\left(k_{\text{d,z}}\dot{e}_{\text{z}_\text{t}} + k_{\text{p,z}}e_{\text{z}_\text{t}} + k_{\text{i,z}}\int e_{\text{z}_\text{t}}dt\right),$$

where $[e_{\text{x}_\text{t}}, e_{\text{y}_\text{t}}, e_{\text{z}_\text{t}}]^\top = R(\mathbf{r}_{\text{des}} - \mathbf{r}^{\mathcal{F}})$ are tracking errors represented in $\mathcal{F}_t$, and $k_{\text{p,x}}$, $k_{\text{p,y}}$, $k_{\text{p,z}}$, $k_{\text{d,x}}$, $k_{\text{d,y}}$, $k_{\text{d,z}}$ and $k_{\text{i,z}}$ are PID control gains. The onboard auto-pilot can follow the angle command generated by the outer loop trajectory tracking controller relatively fast. Therefore, we can assume a time scale decoupling between the outer loop off-board controller and the onboard auto-pilot.

Augmented with the baseline control law derived above, the closed-loop system receives position command in terms of $\mathbf{r}_{\text{des}}(t)$. Then the command is transformed into body frame commands, and position outputs are generated independently. Under the assumption of small attitude angles the motions in three axes are decoupled; each of these motions is governed by a separate dynamic equation, indicating that three SISO subsystems are generated. For these SISO subsystems a SISO transfer function for each direction describes the relationship between the input and the output. Next system identification is carried out for each direction to obtain an approximate transfer function from position command input to position output.

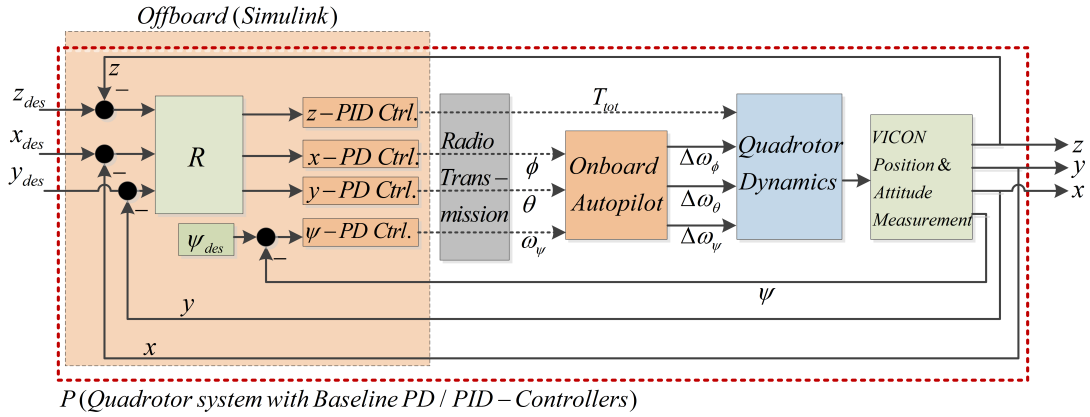

Figure 6.6: Diagram of quadrotor system stabilized with baseline PD/PID controllers, which are implemented in an offboard computer.

6.3.3. *Transfer Functions of SISO Subsystems*

For $\mathcal{L}_1$ adaptive controller design and filter optimization, the closed loop of the quadrotor with the baseline PD/PID controllers (P in Figure 6.6) is approximated by a transfer function P_0. In the system ID procedure, sinusoidal position command inputs with different frequencies were applied to the system in x, y, and z directions, and the corresponding position outputs were measured. A

From x_{des} to x (From y_{des} to y)	$\frac{-0.3611s + 6.435}{s^2 + 3.174s + 6.41}$
From z_{des} to z	$\frac{1.009s + 6.168}{s^2 + 2.017s + 6.275}$

Table 6.2: Transfer functions from position input to position output in x, y and z directions.

transfer function for each direction was then obtained based on the input and the output signals. Here we assume that the system is symmetric with respect to x and y axes. Therefore the transfer functions in x and y directions are assumed to be the same. Table 6.2 shows the transfer functions obtained from system ID. They will be used in the subsequent design.

6.3.4. *Reference System Optimization*

Next an $\mathcal{L}_1$ adaptive output feedback controller is designed for trajectory tracking control of Crazyflie and implemented in an off-board computer. The closed loop of the quadrotor system with the baseline controller is augmented with an outer-loop $\mathcal{L}_1$ controller, as shown in Figure 6.7. Using the transfer functions, obtained by system ID (Table 6.2), the $\mathcal{L}_1$ controller is optimized and augmented to improve the trajectory tracking performance and robustness of the closed-loop system.In order to account for uncertain parameters and weak coupling effects in the plant P, we assume bounded perturbation for plant dynamics in each direction. The uncertain model of the plant with additive perturbation is given by

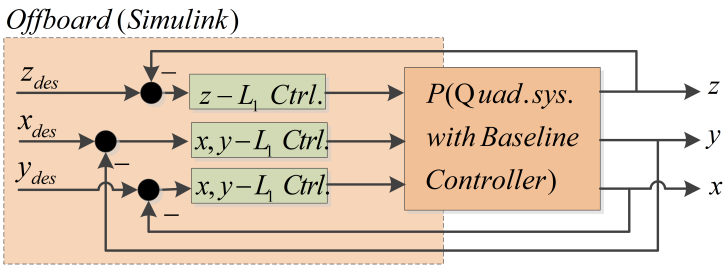

Figure 6.7: Closed-loop diagram of PD/PID-controlled quadrotor system augmented with $\mathcal{L}_1$ adaptive controller implemented in an offboard computer.

$$P(s) = P_0(s) + \Delta P(s) = f_{\text{u}}\left(\begin{bmatrix} 0_{3\times3} & \mathbf{L} \\ \mathbb{I}_{3\times3} & P_0(s) \end{bmatrix}, \Delta_{\text{p}}(s)\right), \quad \|\Delta_{\text{p}}(s)\| \leq 1, \tag{6.53}$$

where

$$\mathbf{L} = \text{diag}\left(L_{\text{x}}, L_{\text{y}}, L_{\text{z}}\right), \quad \Delta_{\text{p}}(s) = \text{diag}\left(\frac{1}{L_{\text{x}}}\Delta_{\text{px}}(s), \frac{1}{L_{\text{y}}}\Delta_{\text{py}}(s), \frac{1}{L_{\text{z}}}\Delta_{\text{pz}}(s)\right),$$

and $P_0(s)$ approximates the dynamics of the closed loop of the quadrotor system with the baseline controller, $\Delta_{\text{p}}(s)$ is the additive uncertainty whose upper bound is specified by $\mathbf{L}$, T^* is the lower

bound on the time-delay margin at the control input. The structure of the $\mathcal{L}_1$ reference system for the trajectory tracking control of Crazyflie is shown in Figure 6.8. The formulation in (6.53)

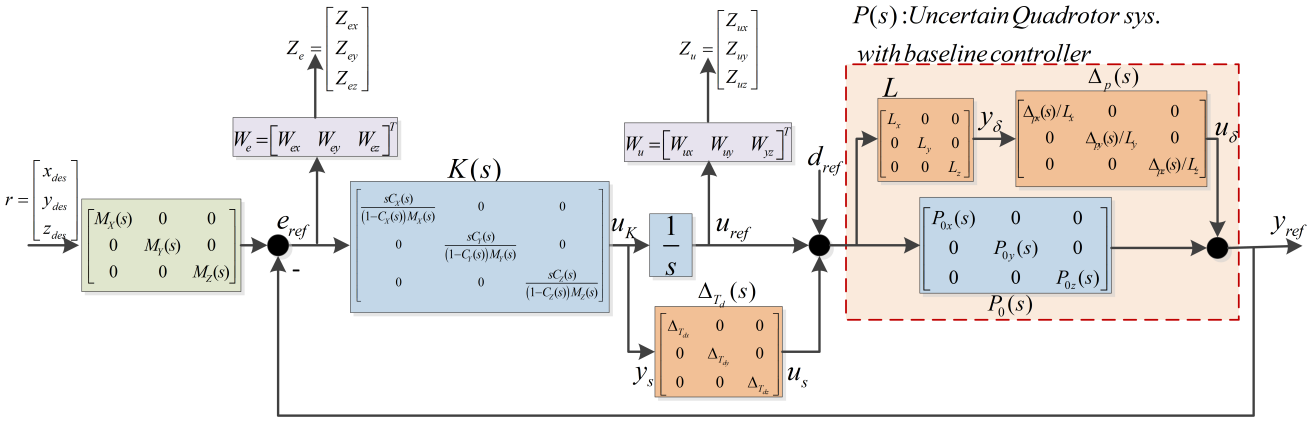

Figure 6.8: Reference system design for trajectory tracking control of Crazyflie.

for modeling of the system allows to approximate the closed-loop system with three decoupled subsystems, shown in Figure 6.8. Then for each of these decoupled subsystems we design a SISO $\mathcal{L}_1$ adaptive controller. In the following, the procedure for filter design for the $\mathcal{L}_1$ controller in x direction is illustrated. The LFT model of $\mathcal{L}_1$ reference system for x direction is shown in Figure 6.9, where the generalized plant $G_{\mathrm{x}}(s)$ is defined as follows

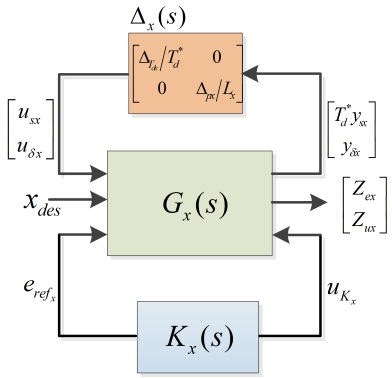

Figure 6.9: LFT model of the closed-loop $\mathcal{L}_1$ reference system for x direction.

$$\begin{bmatrix} T_{\mathrm{d}}^{*} y_{sx} \\ y_{\delta \mathrm{x}} \\ Z_{\mathrm{ex}} \\ Z_{\mathrm{ux}} \\ e_{\mathrm{ref_x}} \end{bmatrix} = \underbrace{\begin{bmatrix} 0 & 0 & 0 & T_{\mathrm{d}}^{*} \\ L_{\mathrm{x}} & 0 & 0 & \frac{L_{\mathrm{x}}}{s} \\ -W_{\mathrm{ex}}(s)P_{0\mathrm{x}}(s) & -W_{\mathrm{e}} & W_{\mathrm{ex}}(s)M_{\mathrm{x}}(s) & -\frac{1}{s}W_{\mathrm{ex}}(s)P_{0\mathrm{x}}(s) \\ 0 & 0 & 0 & \frac{1}{s}W_{\mathrm{ux}}(s) \\ -P_{0\mathrm{x}}(s) & -1 & M_{\mathrm{x}}(s) & -\frac{1}{s}P_{0\mathrm{x}}(s) \end{bmatrix}}_{\triangleq G_{\mathrm{x}}(s)} \begin{bmatrix} u_{\mathrm{sx}} \\ u_{\delta \mathrm{x}} \\ x_{\mathrm{des}} \\ u_{\mathrm{K_x}} \end{bmatrix}. \tag{6.54}$$

The reference system $M_{\mathrm{x}}(s)$ is given by

$$M_{\mathrm{x}}(s) = \frac{10}{s+10}.$$

In the LFT setup, as shown in Figure 6.9, the uncertainty $\Delta_{\mathrm{x}}(s)$ and the optimization variable $K_{\mathrm{x}}(s)$ are defined as follows

$$\Delta_{\mathrm{x}}(s) \triangleq \begin{bmatrix} \frac{1}{T_{\mathrm{d}}^{*}}\Delta_{T_{\mathrm{dx}}}(s) & 0 \\ 0 & \frac{1}{L_{\mathrm{x}}}\Delta_{\mathrm{px}}(s) \end{bmatrix}, \quad K_{\mathrm{x}}(s) \triangleq \frac{sC_{\mathrm{x}}(s)}{(1-C_{\mathrm{x}}(s))\,M_{\mathrm{x}}(s)},$$

where $\Delta_{T_{\mathrm{dx}}}(s) \triangleq \frac{1}{s}(e^{-sT_{\mathrm{dx}}} - 1)$.

Next we obtain the discrete-time MIMO generalized plant $G_{\mathrm{x}}(z)$, equivalent to $G_{\mathrm{x}}(s)$ defined in (6.54), using the Euler approximation method. The sampling time of $\tau = 0.005s$ is chosen for this system. We define

$$R^{\mathrm{x}}(z) = f_{\mathrm{l}}\left(G_{\mathrm{x}}(z), K_{\mathrm{x}}(z)\right),$$

where $K_{\mathrm{x}}(z)$, the z-transform of $K_{\mathrm{x}}(s)$, is the optimization variable. Then the optimization problem is given by

$$\inf_{K_{\mathrm{x}}(z)} \left\{ \|R_{33}^{\mathrm{x}}(z)\|_{\mathcal{H}_2}^2 + \|R_{43}^{\mathrm{x}}(z)\|_{\mathcal{H}_2}^2 + c_{\mathrm{x}}\|R_{11}^{\mathrm{x}}(z)\|_{\ell_1} \right\}, \quad \text{s.t.} \quad \left\| \begin{bmatrix} R_{11}^{\mathrm{x}} & R_{12}^{\mathrm{x}} \\ R_{21}^{\mathrm{x}} & R_{22}^{\mathrm{x}} \end{bmatrix} \right\|_{\ell_1} < 1, \tag{6.55}$$

where $R_{ij}^{\mathrm{x}}(z)$ is the transfer function between the i^{th} output and the j^{th} input. By choosing the weighting functions $W_{\mathrm{ux}}(s)$ and $W_{\mathrm{ex}}(s)$ (in the generalized plant (6.54)) and the coefficient c_{x} in (6.55), one can define the cost-function such that a specific control design requirement is achieved for x direction. In a similar procedure we formulate the filter optimization problem for SISO $\mathcal{L}_1$ adaptive controllers in y and z directions. Since we assumed that the system is symmetric with respect to x and y directions, the $\mathcal{L}_1$ controller design for y direction is the same as for the x direction. The weighting functions $W_{\mathrm{uz}}(s)$ and $W_{\mathrm{ez}}(s)$ and also the coefficient c_{z} can be specified to define the optimization problem (similar to (6.55)) for filter design corresponding to z direction.

The reference model for z direction is given by

$$M_{\rm z}(s) = \frac{10}{s+10}.$$

In the sequel, the scenario for filter optimization problem is illustrated. Here we aim to improve the tracking performance, while maintaining the closed loop robustness to input time-delay and uncertainties. Therefore we minimize the tracking error within the feasibility set of solutions, defined by the ℓ_1-norm constraints of the optimization problem. A natural strategy is to select a relatively large weight on the tracking error signal. Therefore we choose $W_{\rm ex} = W_{\rm ey} = W_{\rm ez} = 100$, $W_{\rm ux} = W_{\rm uy} = W_{\rm uz} = 0.1$ and $c_{\rm x} = c_{\rm y} = c_{\rm z} = 0$. The lower bound on the time-delay margin is selected to be $T_{\rm d}^* = 0.1sec$. The uncertainty bounds are considered to be $L_{\rm x} = L_{\rm y} = L_{\rm z} = 0.3$.

Note that the optimization procedure results in high-order transfer functions. We use Hankel SVD model reduction method to obtain lower order filters. The reduced-order optimized filters are given by

$$C_{\rm x}^*(s) = C_{\rm y}^*(s) = \frac{0.0609s^3 \ + \ 4.463s^2 \ + \ 24.69s \ + \ 25.36}{s^4 \ + \ 4.493s^3 \ + \ 52.24s^2 \ + \ 61.77s \ + \ 25.36}, \tag{6.56}$$

$$C_{\rm z}^*(s) = \frac{-0.169s^3 \ + \ 73.5s^2 \ + \ 64.8s \ + \ 368.4}{s^4 \ + \ 35.35s^3 \ + \ 315s^2 \ + \ 479.1s \ + \ 368.4}. \tag{6.57}$$

Figure 6.10 illustrates the flight test results. The reference tracking response of the closed-loop system to step command in x, y and z directions is shown. As shown in Figure 6.10, the $\mathcal{L}_1$ adaptive controller with optimized filter is significantly improving the tracking performance in z direction. The closed loop with augmented $\mathcal{L}_1$ controller has smaller overshoot after takeoff and smaller settling time, yielding a faster convergence to the desired trajectory. In the subplot of the z direction (vertical position) the last 10 seconds of the flight test show that the quadrotor with augmented $\mathcal{L}_1$ controller could safely land without the need to switch off the motors. For the PID controller, as we can observe, this task could not be achieved easily due to the ground effects, and the quadrotor remains at a small altitude above the ground. In addition, augmentation of the optimized $\mathcal{L}_1$ adaptive controller provides moderate improvements in x and y directions. Figure 6.10 shows that the well-tuned baseline controller has some bias with the reference command, which might be caused by the uncertain battery position after each battery change, among some other uncertainties, while augmentation of the optimized $\mathcal{L}_1$ controller eliminates the bias, and the trajectory has less fluctuations. Plots on the right show the outputs of the $\mathcal{L}_1$ adaptive controllers. The reader can see how the reference inputs were modified by the $\mathcal{L}_1$ adaptive controllers to guarantee a better tracking performance in each direction.

It is worth mentioning that the design of $\mathcal{L}_1$ adaptive controller only requires an approximate model of the system. The robustness and performance requirements can be met by proper selection of the cost function and parameters for optimization of the filter in $\mathcal{L}_1$ adaptive controller using the systematic method described in this chapter.

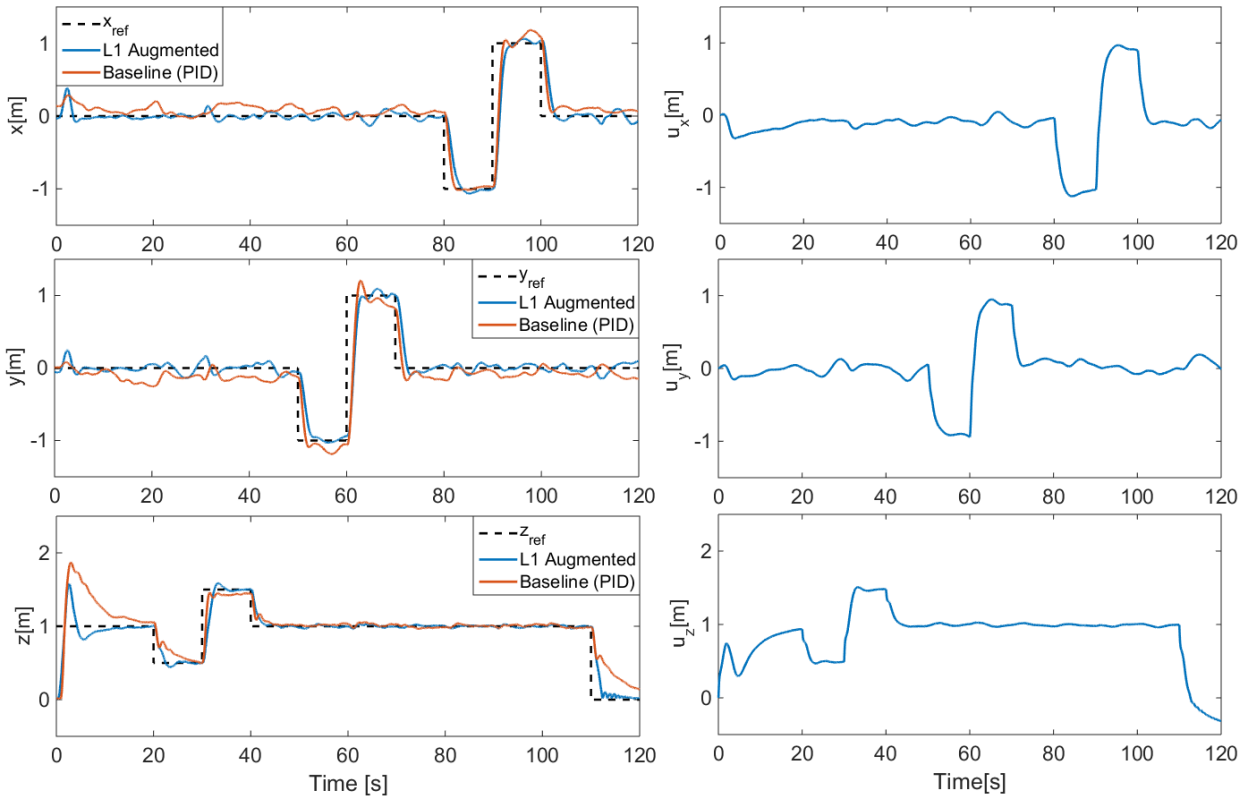

Figure 6.10: Flight test results: (Left) response of the closed-loop system to step reference inputs for x, y and z directions. (Right) $\mathcal{L}_1$ adaptive control input. The positions are measured via Vicon system.

CHAPTER 7

Conclusion and Future Research

In this dissertation a sampled-data (SD) approach is developed for resilient and secure control of autonomous CPSs using the $\mathcal{L}_1$ adaptive output-feedback control structure. The SD design facilitates the implementation of control laws on digital computers in CPSs, where the input/output signals are available at discrete time instances with different sampling rates.

The SD output-feedback controller design with uniform rate is considered in Chapter 3, while Chapter 4 extends the results to a multi-rate scheme for a class of nested, uncertain, MIMO systems, with possibly non-minimum phase zeros, subject to reference command saturation. Also, the multirate design allows the zero-dynamics attacks to be detected. A navigation and control problem is formulated for autonomous systems using a multi-level control structure, in which the high-level reference commands are limited by a saturation function, while the low-level controller tracks the reference by compensating for disturbances and uncertainties. In Chapter 4, we have assumed that a feasible mission is computed (*i.e.* the desired trajectory in (4.9) is given). Mission re-planning and trajectory generation are critical functionalities for autonomous CPSs that can be integrated into the proposed multi-level control framework in the future work. By extending the multi-level structure to include global missions, local goals and low-level tasks, the safety of an autonomous CPS can be addressed in the presence of large uncertainties. We have dealt with the problem of robust design for the low-level controller (low-level task), as well as the reference command generation within an operational safety envelop (local goals). However, the mission control (global mission) has not been discussed in this dissertation. Large uncertainty mitigation requires mission adaptation and selection of a new trajectory that is still possible, given the remaining capabilities of the system. As shown in Figure 1.2, such multi-level approach can be integrated with the Simplex architecture for safe and secure navigation and control of an autonomous air vehicle in the presence of possible failures/attacks.

Chapter 5 extends the $\mathcal{L}_1$ adaptive SD control to the under-actuated systems with non-minimum-phase zeros. For only a certain class of MIMO systems that satisfy the condition in (5.20), the limiting properties of the proposed controller have been proven as the sampling time tends to zero (it guarantees the control performance). In the future work the results can be extended to a more general class of systems, and the condition in (5.20) can be relaxed. This can be achieved by modifying the output predictor (observer) in the control structure. Given the decoupling property of $\mathcal{L}_1$ adaptive controller, which allows for modification of the observer, the proposed solution is promising to address the problem.

In this dissertation, the experimental results for trajectory tracking control of a Crazyflie quadrotor, subject to stealthy zero-dynamics attacks, were provided in Chapter 5. The estimation loop in the multirate $\mathcal{L}_1$ controller can quickly detect any abnormal behavior, while the control

loop recovers the stability of the perturbed quadrotor. A simple way to simulate the Simplex structure for this experiment is to remove the malicious code as soon as the attack is detected. The Simplex structure can be implemented using modern multicore processors and virtualization technology [115], which is beyond the scope of this research. In the future experiments, the proposed autopilot algorithm can be programmed on a quadrotor equipped with an embedded multicore processor with hardware-assisted virtualization technology. Also, security of the quadrotor flight can also be examined against other types of adversarial activities, such as sensor/actuator spoofing, corruption of safety programs (*e.g.*, virtual geo-fence [115]) and hacking of quadrotor's position data.

In Chapter 6, the filter optimization problem for $\mathcal{L}_1$-adaptive output-feedback controllers is addressed. We showed that the filter design could be cast as a convex optimization problem allowing for efficient solutions using linear/quadratic programming (LP/QP). A trade-off scheme is established between performance and robustness in $\mathcal{L}_1$-adaptive control architecture by optimizing a mixed $\mathcal{L}_1/\mathcal{H}_2$-norm problem. The GMO optimization algorithm, which is used in this chapter, relies on the finite impulse response (FIR) approximation of the discretized system. If the length of the FIR approximation is large, the GMO algorithm suffers from computational complexities due to the large dimension of the corresponding optimization problem. Also, the order of the optimized filter can become very large, which is not desirable. For example, in systems with fast and slow modes the length of FIR for a reasonable approximation may be large. Therefore application of this method may be limited for such systems. Model reduction techniques can be utilized to address this problem.

REFERENCES

[1] "Sullenberger made the right move, landing on the Hudson." https://www.wired.com/2010/05/ntsb-makes-recommendations-after-miracle-on-the-hudson-investigation/.

[2] H. Sandberg, S. Amin, and K. H. Johansson, "Cyberphysical security in networked control systems: An introduction to the issue," *IEEE Control Systems*, vol. 35, no. 1, pp. 20–23, 2015.

[3] M. Abrams and J. Weiss, "Malicious control system cyber security attack case study–maroochy water services, australia," *McLean, VA: The MITRE Corporation*, 2008.

[4] J. Slay and M. Miller, "Lessons learned from the maroochy water breach," in *International Conference on Critical Infrastructure Protection*, pp. 73–82, Springer, 2007.

[5] R. McMillan, "Insider charged with hacking california canal system," *Computer World*, 2007.

[6] J. Weiss, *Protecting Industrial Control Systems from Electronic Threats*. Momentum Press, 2010.

[7] K. Koscher, A. Czeskis, F. Roesner, S. Patel, T. Kohno, S. Checkoway, D. McCoy, B. Kantor, D. Anderson, H. Shacham, and S. Savage, "Experimental security analysis of a modern automobile," in *Proceedings of the IEEE Symposium on Security and Privacy*, pp. 447–462, 2010.

[8] A. Y. Javaid, W. Sun, V. K. Devabhaktuni, and M. Alam, "Cyber security threat analysis and modeling of an unmanned aerial vehicle system," in *Proceedings of the IEEE Conference on Technologies for Homeland Security*, 2012.

[9] J.-S. Pleban, R. Band, and R. Creutzburg, "Hacking and securing the ar.drone 2.0 quadcopter: investigations for improving the security of a toy," in *Proc. of the SPIE Mobile Devices and Multimedia: Enabling Technologies, Algorithms, and Applications*, 2014.

[10] D. P. Shepard, J. A. Bhatti, T. E. Humphreys, and A. A. Fansler, "Evaluation of smart grid and civilian uav vulnerability to gps spoofing attacks," in *Proceedings of the ION GNSS Meeting*, 2012.

[11] "Exclusive: Computer virus hits u.s. drone fleet," [posted 07-October-2011]. https://www.wired.com/2011/10/virus-hits-drone-fleet/.

[12] D. Kushner, "The real story of stuxnet," *IEEE Spectrum*, vol. 50, no. 3, pp. 48 – 53, 2013.

[13] "Cyber-attack concerns raised over Boeing 787 chip's 'back door'," *The Guardian*, May 2012.

[14] L. Sha, "Dependable system upgrade," in *The 19th IEEE Real-Time Systems Symposium*, pp. 440–448, December 1998.

[15] L. Sha, "Using simplicity to control complexity," *IEEE Software*, vol. 18, pp. 20–28, Jul 2001.

[16] T. L. Crenshaw, E. Gunter, C. L. Robinson, L. Sha, and P. Kumar, "The simplex reference model: Limiting fault-propagation due to unreliable components in cyber-physical system architectures," in *28th IEEE International Real-Time Systems Symposium*, pp. 400–412, IEEE, 2007.

[17] X. Wang, N. Hovakimyan, and L. Sha, "L1simplex: fault-tolerant control of cyber-physical systems," in *Proceedings of the ACM/IEEE 4th International Conference on Cyber-Physical Systems*, pp. 41–50, 2013.

[18] M.-K. Yoon, B. Liu, N. Hovakimyan, and L. Sha, "VirtualDrone: Virtual sensing, actuation, and communication for attack-resilient unmanned aerial systems," in *Proceedings of the ACM/IEEE International Conference on Cyber-Physical Systems*, 2017.

[19] `http://www.nationaldefensemagazine.org/archive/2012/september/Pages/FedsFearCoordinatedPhysical,Cyber-AttacksonElectricalGrids.aspx`.

[20] B. Chaudhuri, B. C. Pal, A. Zolotas, I. M. Jaimoukha, and T. C. Green, "Mixed-sensitivity approach to H_∞ control of power system oscillations employing multiple facts devices," in *Proceedings of IEEE Power Engineering Society General Meeting*, vol. 4, pp. 1149–1156, July 2003.

[21] G. Boukarim, S. Wang, J. Chow, G. Taranto, and N. Martins, "A comparison of classical, robust, and decentralized control designs for multiple power system stabilizers," *IEEE Transactions on Power Systems*, vol. 15, pp. 1287–1292, Nov 2000.

[22] K. A. Wise, "Flight testing of the X-45A J-UCAS computational alpha-beta system," in *Proceedings of AIAA Guidance, Navigation and Control Conference and Exhibit*, vol. 332, 2006.

[23] F. L. Lewis, A. Yesildirek, and K. Liu, "Multilayer neural-net robot controller with guaranteed tracking performance," *IEEE Transactions on Neural Networks*, vol. 7, no. 2, pp. 388–399, 1996.

[24] V. V. Patel, C. Cao, N. Hovakimyan, K. A. Wise, and E. Lavretsky, "$\mathcal{L}_1$ adaptive controller for tailless unstable aircraft in the presence of unknown actuator failures," *International Journal of Control*, vol. 82, no. 4, pp. 705–720, 2009.

[25] N. Hovakimyan, C. Cao, E. Kharisov, E. Xargay, and I. M. Gregory, "$\mathcal{L}_1$ adaptive control for safety-critical systems," *IEEE Control Systems Magazine*, vol. 31, no. 5, pp. 54–104, 2011.

[26] C. Favre, "Fly-by-wire for commercial aircraft: the Airbus experience," *International Journal of Control*, vol. 59, no. 1, pp. 139–157, 1994.

[27] D. Brière and P. Traverse, "AIRBUS A320/A330/A340 electrical flight controls-a family of fault-tolerant systems," in *The 23rd International Symposium on Fault-Tolerant Computing*, pp. 616–623, IEEE, 1993.

[28] D. M. Wilbers and J. L. Speyer, "Detection filters for aircraft sensor and actuator faults," in *IEEE International Conference on Control and Applications*, pp. 81–86, 1989.

[29] T. E. Menke and P. S. Maybeck, "Multiple model adaptive estimation applied to the VISTA F-16 flight control system with actuator and sensor failures," in *Proceedings of the IEEE National Aerospace and Electronics Conference*, pp. 441–448, 1992.

[30] T. E. Menke and P. S. Maybeck, "Sensor/actuator failure detection in the vista F-16 by multiple model adaptive estimation," *IEEE Transactions on aerospace and electronic systems*, vol. 31, no. 4, pp. 1218–1229, 1995.

[31] N. A. White, P. S. Maybeck, and S. L. DeVilbiss, "Detection of interference/jamming and spoofing in a DGPS-aided inertial system," *IEEE Transactions on Aerospace and Electronic Systems*, vol. 34, no. 4, pp. 1208–1217, 1998.

[32] S. Kim, J. Choi, and Y. Kim, "Fault detection and diagnosis of aircraft actuators using fuzzy-tuning IMM filter," *IEEE Transactions on Aerospace and Electronic Systems*, vol. 44, no. 3, 2008.

[33] G. Lorden, "Procedures for reacting to a change in distribution," *The Annals of Mathematical Statistics*, pp. 1897–1908, 1971.

[34] D. P. Malladi and J. L. Speyer, "A generalized Shiryayev sequential probability ratio test for change detection and isolation," *IEEE Transactions on Automatic Control*, vol. 44, no. 8, pp. 1522–1534, 1999.

[35] J.-Y. Keller, L. Summerer, M. Boutayeb, and M. Darouach, "Generalized likelihood ratio approach for fault detection in linear dynamic stochastic systems with unknown inputs," *International journal of systems science*, vol. 27, no. 12, pp. 1231–1241, 1996.

[36] A. Benveniste, M. Basseville, and G. Moustakides, "The asymptotic local approach to change detection and model validation," *IEEE Transactions on Automatic Control*, vol. 32, no. 7, pp. 583–592, 1987.

[37] P. S. Maybeck and D. L. Pogoda, "Multiple model adaptive controller for the STOL F-15 with sensor/actuator failures," in *Proceedings of the 28th IEEE Conference on Decision and Control*, pp. 1566–1572, 1989.

[38] P. S. Maybeck and R. D. Stevens, "Reconfigurable flight control via multiple model adaptive control methods," *IEEE Transactions on Aerospace and Electronic systems*, vol. 27, no. 3, pp. 470–480, 1991.

[39] M. Bodson and J. E. Groszkiewicz, "Multivariable adaptive algorithms for reconfigurable flight control," *IEEE transactions on control systems technology*, vol. 5, no. 2, pp. 217–229, 1997.

[40] H. Lee, S. Snyder, and N. Hovakimyan, "An adaptive unknown input observer for fault detection and isolation of aircraft actuator faults," in *AIAA Guidance, Navigation, and Control Conference*, p. 0266, 2014.

[41] T. Chen and B. A. Francis, *Optimal sampled-data control systems*. Springer Science & Business Media, 2012.

[42] M. Naghnaeian, N. Hirzallah, and P. G. Voulgaris, "Dual rate control for security in cyber-physical systems," in *2015 54th IEEE Conference on Decision and Control*, pp. 1415–1420, December 2015.

[43] X. Wang, N. Hovakimyan, and L. Sha, "L1simplex: Fault-tolerant control of cyber-physical systems," in *International Conference on Cyber-Physical Systems (ICCPS13)*, pp. 41–50, April 2013.

[44] L. Sha, "Dependable system upgrade," in *The 19th IEEE Real-Time Systems Symposium*, pp. 440–448, December 1998.

[45] D. Hadziosmanovic, D. Bolzoni, S. Etalle, and P. Hartel, "Challenges and opportunities in securing industrial control systems," in *Complexity in Engineering*, pp. 1–6, 2012.

[46] C. Cao and N. Hovakimyan, "Design and analysis of a novel $\mathcal{L}_1$ adaptive control architecture with guaranteed transient performance," *IEEE Transactions on Automatic Control*, vol. 53, pp. 586–591, March 2008.

[47] N. Hovakimyan and C. Cao, $\mathcal{L}_1$ *Adaptive Control Theory: Guaranteed Robustness with Fast Adaptation*. Philadelphia, PA: Society for Industrial and Applied Mathematics, 2010.

[48] C. Cao and N. Hovakimyan, "$\mathcal{L}_1$ adaptive output-feedback controller for non-strictly-positive-real reference systems: Missile longitudinal autopilot design," *Journal of guidance, control, and dynamics*, vol. 32, no. 3, pp. 717–726, 2009.

[49] I. Gregory, E. Xargay, C. Cao, and N. Hovakimyan, "Flight test of an $\mathcal{L}_1$ adaptive controller on the NASA AirSTAR flight test vehicle," in *AIAA Guidance, Navigation, and Control Conference*, p. 8015, 2010.

[50] I. M. Gregory, C. Cao, E. Xargay, N. Hovakimyan, and X. Zou, "$\mathcal{L}_1$ adaptive control design for nasa airstar flight test vehicle," in *AIAA Guidance, Navigation and Control Conference*, (Chicago, IL), August 2009.

[51] K. Ackerman, E. Xargay, R. Choe, N. Hovakimyan, M. C. Cotting, R. B. Jeffrey, M. P. Blackstun, T. P. Fulkerson, T. R. Lau, and S. S. Stephens, "L1 stability augmentation system for calspan's variable-stability Learjet," in *AIAA Guidance, Navigation, and Control Conference*, p. 0631, 2016.

[52] M. C. Cotting, R. B. Jeffrey, M. P. Blackstun, T. P. Fulkerson, T. R. Lau, S. S. Stephens, K. Ackerman, E. Xargay, R. Choe, and N. Hovakimyan, "'can i get L1 on?!'providing consistent handling qualities on Calspan's variable-stability Learjet," in *AIAA Guidance, Navigation, and Control Conference*, p. 0632, 2016.

[53] K. A. Ackerman, E. Xargay, R. Choe, N. Hovakimyan, M. C. Cotting, R. B. Jeffrey, M. P. Blackstun, T. P. Fulkerson, T. R. Lau, and S. S. Stephens, "Evaluation of an $\mathcal{L}_1$ adaptive flight control law on calspans variable-stability learjet," *Journal of Guidance, Control, and Dynamics*, vol. 40, no. 4, pp. 1051–1060, 2017.

[54] E. Xargay, N. Hovakimyan, V. Dobrokhodov, I. Kaminer, C. Cao, and I. Gregory, "$\mathcal{L}_1$ adaptive control in flight," *Intelligent Systems: AIAA Progress in Aeronautics and Astronautics*, 2012.

[55] N. Hovakimyan, C. Cao, E. Kharisov, E. Xargay, and I. M. Gregory, "L1adaptive control for safety-critical systems," *IEEE Control Systems Magazine*, vol. 31, pp. 54–104, Oct 2011.

[56] T. Leman, E. Xargay, G. Dullerud, N. Hovakimyan, and T. Wendel, "$\mathcal{L}_1$ adaptive control augmentation system for the x-48b aircraft," in *AIAA guidance, navigation, and control conference*, p. 5619, 2009.

[57] I. Kaminer, A. Pascoal, E. Xargay, N. Hovakimyan, C. Cao, and V. Dobrokhodov, "Path following for small unmanned aerial vehicles using l1 adaptive augmentation of commercial autopilots," *Journal of guidance, control, and dynamics*, vol. 33, no. 2, pp. 550–564, 2010.

[58] J. Wang, C. Cao, N. Hovakimyan, R. Hindman, and D. B. Ridgely, "L1 adaptive controller for a missile longitudinal autopilot design," in *AIAA Guidance, Navigation and Control Conference and Exhibit*, p. 6282, 2008.

[59] T. Chen and B. A. Francis, *Optimal sampled-data control systems*. Springer Science & Business Media, 2012.

[60] E. Fridman, A. Seuret, and J.-P. Richard, "Robust sampled-data stabilization of linear systems: an input delay approach," *Automatica*, vol. 40, no. 8, pp. 1441–1446, 2004.

[61] E. Fridman, "A refined input delay approach to sampled-data control," *Automatica*, vol. 46, no. 2, pp. 421–427, 2010.

[62] N. Sivashankar and P. P. Khargonekar, "Characterization of the l_2-induced norm for linear systems with jumps with applications to sampled-data systems," *SIAM Journal on Control and Optimization*, vol. 32, no. 4, pp. 1128–1150, 1994.

[63] G. Dullerud and K. Glover, "Robust stabilization of sampled-data systems to structured lti perturbations," *IEEE transactions on automatic control*, vol. 38, no. 10, pp. 1497–1508, 1993.

[64] R. Yu, O. Ocali, and M. E. Sezer, "Adaptive robust sampled-data control of a class of systems under structured perturbations," *IEEE transactions on automatic control*, vol. 38, no. 11, pp. 1707–1713, 1993.

[65] D. Nesic, A. R. Teel, and D. Carnevale, "Explicit computation of the sampling period in emulation of controllers for nonlinear sampled-data systems," *IEEE Transactions on Automatic Control*, vol. 54, pp. 619–624, March 2009.

[66] W. Lin and W. Wei, "Robust stabilization of nonminimum-phase systems with uncertainty by sampled-data output feedback," in *55th IEEE Conference on Decision and Control*, pp. 4078–4083, Dec 2016.

[67] H. Chu, C. Qian, J. Yang, S. Xu, and Y. Liu, "Almost disturbance decoupling for a class of nonlinear systems via sampled-data output feedback control," *International Journal of Robust and Nonlinear Control*, 2015.

[68] A. R. Teel, D. Nesic, and P. V. Kokotovic, "A note on input-to-state stability of sampled-data nonlinear systems," in *Proceedings of the 37th IEEE Conference on Decision and Control*, vol. 3, pp. 2473–2478 vol.3, 1998.

[69] H. K. Khalil, "Performance recovery under output feedback sampled-data stabilization of a class of nonlinear systems," *IEEE Transactions on Automatic Control*, vol. 49, no. 12, pp. 2173–2184, 2004.

[70] J. H. Ahrens, X. Tan, and H. K. Khalil, "Multirate sampled-data output feedback control with application to smart material actuated systems," *IEEE Transactions on Automatic Control*, vol. 54, no. 11, pp. 2518–2529, 2009.

[71] S. Ahmed Ali, N. Langlois, and M. Guermouche, "Sampled-data disturbance observer for a class of nonlinear systems," in *19th World Congress*, vol. 19, pp. 3346–3351, 2014.

[72] C. Zhang and J. Yang, "Semi-global sampled-data output feedback disturbance rejection control for a class of uncertain nonlinear systems," *International Journal of Systems Science*, pp. 1–12, 2016.

[73] W. Liu, Q. Ma, and X. Jia, "Sampled-data output feedback control for a class of nonlinear systems with mismatched disturbances," in *35th Chinese Control Conference (CCC)*, pp. 380–385, July 2016.

[74] P. G. Voulgaris, M. A. Dahleh, and L. S. Valavani, "H_∞ and H_2 optimal controllers for periodic and multi-rate systems," in *Proceedings of the 30th IEEE Conference on Decision and Control*, pp. 214–216, December 1991.

[75] P. G. Voulgaris and B. Bamieh, "Optimal H_∞ control of hybrid multirate systems," in *Proceedings of the 31st IEEE Conference on Decision and Control*, pp. 457–462, December 1992.

[76] L. Qiu and T. Chen, "H_2 optimal design of multirate sampled-data systems," *IEEE Transactions on Automatic Control*, vol. 39, pp. 2506–2511, December 1994.

[77] C. Cao and N. Hovakimyan, "Stability margins of $\mathcal{L}_1$ adaptive control architecture," *IEEE Transactions on Automatic Control*, vol. 55, pp. 480–487, 2010.

[78] H. Jafarnejadsani, H. Lee, N. Hovakimyan, and P. G. Voulgaris, "Dual-rate $\mathcal{L}_1$ adaptive controller for cyber-physical sampled-data systems," in *IEEE Conference on Decision and Control*, (Melbourne, Australia), December 2017.

[79] H. Jafarnejadsani, H. Lee, N. Hovakimyan, and P. G. Voulgaris, "Dual-rate L1 adaptive controller for cyber-physical sampled-data systems," in *IEEE 56th Annual Conference on Decision and Control (CDC)*, pp. 6259–6264, Dec 2017.

[80] H. Jafarnejadsani, H. Lee, N. Hovakimyan, and P. G. Voulgaris, "A multirate adaptive control for MIMO systems with application to cyber-physical security," in *IEEE 57th Annual Conference on Decision and Control (CDC)*, 2018.

[81] H. Lee, V. Cichella, and N. Hovakimyan, "$\mathcal{L}_1$ adaptive output feedback control for underactuated mimo systems," in *20th IFAC World Congress*, July 2017.

[82] H. Lee, S. Sndyer, and N. Hovakimyan, "$\mathcal{L}_1$ adaptive output feedback augmentation for missile systems," in *IEEE Transactions on Aerospace and Electronic Systems*, 2017 (accepted).

[83] G. Goodwin and K. Sin, "Adaptive control of nonminimum phase systems," *IEEE Transactions on Automatic Control*, vol. 26, no. 2, pp. 478–483, 1981.

[84] J. B. Hoagg, "Model reference adaptive control for nonminimum-phase systems using a surrogate tracking error," in *Decision and Control and European Control Conference (CDC-ECC), 2011 50th IEEE Conference on*, pp. 360–365, IEEE, 2011.

[85] S. Dai, Z. Ren, and D. S. Bernstein, "Adaptive control of nonminimum-phase systems using shifted laurent series," *International Journal of Control*, vol. 90, no. 3, pp. 407–427, 2017.

[86] M. Makoudi and L. Radouane, "A robust model reference adaptive control for non-minimum phase systems with unknown or time-varying delay," *Automatica*, vol. 36, no. 7, pp. 1057–1065, 2000.

[87] N. Mohan and T. M. Undeland, *Power electronics: converters, applications, and design*. John Wiley & Sons, 2007.

[88] P. Zarchan, *Tactical and strategic missile guidance*. American Institute of Aeronautics and Astronautics, Inc., 2012.

[89] Y. Shtessel, J. Buffington, and S. Banda, "Tailless aircraft flight control using multiple time scale reconfigurable sliding modes," *IEEE Transactions on Control Systems Technology*, vol. 10, no. 2, pp. 288–296, 2002.

[90] H. Voos, "Nonlinear control of a quadrotor micro-uav using feedback-linearization," in *Mechatronics, 2009. ICM 2009. IEEE International Conference on*, pp. 1–6, IEEE, 2009.

[91] N. Cao and A. F. Lynch, "Inner-outer loop control for quadrotor uavs with input and state constraints.," *IEEE Trans. Contr. Sys. Techn.*, vol. 24, no. 5, pp. 1797–1804, 2016.

[92] F. Kendoul, I. Fantoni, R. Lozano, *et al.*, "Asymptotic stability of hierarchical inner-outer loop-based flight controllers," in *Proceedings of the 17th IFAC world congress*, pp. 1741–1746, 2008.

[93] M. M. Nicotra, E. Garone, R. Naldi, and L. Marconi, "Nested saturation control of an uav carrying a suspended load," in *American Control Conference (ACC), 2014*, pp. 3585–3590, IEEE, 2014.

[94] P. Castillo, R. Lozano, and A. Dzul, "Stabilization of a mini rotorcraft with four rotors," *IEEE control systems magazine*, vol. 25, no. 6, pp. 45–55, 2005.

[95] N. Metni and T. Hamel, "A uav for bridge inspection: Visual servoing control law with orientation limits," *Automation in construction*, vol. 17, no. 1, pp. 3–10, 2007.

[96] A. R. Teel, "Global stabilization and restricted tracking for multiple integrators with bounded controls," *Systems & control letters*, vol. 18, no. 3, pp. 165–171, 1992.

[97] J. B. Conway, *A Course in Functional Analysis*. Springer New York, 1985.

[98] W. M. Haddad and V. Chellaboina, *Nonlinear Dynamical Systems and Control: A Lyapunov-Based Approach*. Princeton University Press, 2011.

[99] H. Khalil, *Nonlinear systems*. Prentice Hall Upper Saddle River, NJ, 2002.

[100] H. Lee, $\mathcal{L}_1$ *adaptive control for nonlinear and non-square multivariable systems*. PhD thesis, University of Illinois at Urbana-Champaign, 2017.

[101] X. Wang, N. Hovakimyan, and L. Sha, "Rsimplex: A robust control architecture for cyber and physical failures," *ACM Transactions on Cyber-Physical Systems*, vol. 2, no. 4, p. 27, 2018.

[102] E. Kharisov and N. Hovakimyan, "$\mathcal{L}_1$ adaptive output feedback controller for minimum phase systems," in *American Control Conference (ACC)*, pp. 1182–1187, IEEE, 2011.

[103] H. Jafarnejadsani, D. Sun, H. Lee, and N. Hovakimyan, "Optimized $\mathcal{L}_1$ adaptive controller for trajectory tracking of an indoor quadrotor," *Journal of Guidance, Control, and Dynamics*, 2017.

[104] D. Li, N. Hovakimyan, C. Cao, and K. A. Wise, "Filter design for feedback-loop trade-off of $\mathcal{L}_1$ adaptive controller: A linear matrix inequality approach," in *AIAA Guidance, Navigation and Control Conference*, Honolulu, Hawaii, August 2008.

[105] K. K. K. Kim, E. Kharisov, and N. Hovakimyan, "Filter design for $\mathcal{L}_1$ adaptive output-feedback controller," *50th IEEE Conference on Decision and Control*, pp. 5653–5658, Dec 2011.

[106] K. K. K. Kim and N. Hovakimyan, "Development of verification and validation approaches for $\mathcal{L}_1$-adaptive control: Multi-criteria optimization for filter design," in *Proceedings of the AIAA Guidance, Navigation and Control Conference, Toronto (Canada)*, 2010.

[107] M. Naghnaeian, P. G. Voulgaris, and N. Hovakimyan, "On robustness of $\mathcal{L}_1$ adaptive control with time varying perturbations & filter design," in *American Control Conference*, pp. 1937–1942, 2012.

[108] D. Nesic and D. S. Laila, "A note on input-to-state stabilization for nonlinear sampled-data systems," *IEEE Transactions on Automatic Control*, vol. 47, no. 7, pp. 1153–1158, 2002.

[109] A. Young, C. Cao, N. Hovakimyan, and E. Lavretsky, "An adaptive approach to nonaffine control design for aircraft applications," in *AIAA Guidance, Navigation, and Control Conference and Exhibit*, p. 6343, 2006.

[110] I. A. Shkolnikov and Y. B. Shtessel, "Aircraft nonminimum phase control in dynamic sliding manifolds," *Journal of Guidance, Control, and Dynamics*, vol. 24, no. 3, pp. 566–572, 2001.

[111] H. Fang, Z. Lin, and T. Hu, "Analysis of linear systems in the presence of actuator saturation and l2-disturbances," *Automatica*, vol. 40, no. 7, pp. 1229–1238, 2004.

[112] T. Hu and Z. Lin, *Control systems with actuator saturation: analysis and design*. Springer Science & Business Media, 2001.

[113] Y. C. Paw, *Synthesis and validation of flight control for UAV*. PhD thesis, University of Minnesota, 2009.

[114] H. Jafarnejadsani, H. Lee, and N. Hovakimyan, "An $\mathcal{L}_1$ adaptive control design for output-feedback sampled-data systems," in *American Control Conference*, (Seattle, WA), May 2017.

[115] M.-K. Yoon, B. Liu, N. Hovakimyan, and L. Sha, "Virtualdrone: virtual sensing, actuation, and communication for attack-resilient unmanned aerial systems," in *Proceedings of the 8th International Conference on Cyber-Physical Systems*, pp. 143–154, ACM, 2017.

[116] F. Blanchini and M. Sznaier, "Rational $\mathcal{L}_1$ suboptimal compensators for continuous-time systems," in *American Control Conference*, pp. 635–639, June 1993.

[117] T. Amishima and M. Sznaier, "Mixed $\mathcal{H}_2/\ \mathcal{L}_1$ controllers for continuous-time mimo systems," in *American Control Conference*, vol. 5, pp. 3362–3366 vol.5, 1999.

[118] M. V. Salapaka and M. Khammash, "Multi-objective MIMO optimal control design without zero interpolation," in *American Control Conference*, vol. 1, pp. 660–664, June 1998.

[119] M. V. Salapaka, M. Dahleh, and P. G. Voulgaris, "MIMO optimal control design: the interplay between the $\mathcal{H}_2$ and the ℓ_1 norms," *IEEE Transactions on Automatic Control*, vol. 43, pp. 1374–1388, October 1998.

[120] X. Qi, M. Khammash, and M. V. Salapaka, "A matlab package for multiobjective control synthesis," in *Proceedings of the* 40^{th} *IEEE Conference on Decision and Control*, vol. 4, pp. 3991–3996 vol.4, 2001.

[121] M. A. Dahleh and J. B. Pearson, "ℓ_1 -optimal feedback controllers for mimo discrete-time systems," *IEEE Transactions on Automatic Control*, vol. 32, pp. 314–322, Apr 1987.

[122] M. Khammash, "A new approach to the solution of the ℓ_1 control problem: the scaled-q method," *IEEE Transactions on Automatic Control*, vol. 32, no. 2, pp. 180–187, 2000.

[123] H. Jafarnejadsani and N. Hovakimyan, "Optimal filter design for a discrete-time formulation of $\mathcal{L}_1$ adaptive control," in *AIAA InfoTech at Aerospace*, (Kissimmee, FL), January 2015.

[124] "Home | bitcraze," https://www.bitcraze.io, accessed February 18, 2016.

[125] M. Furci, G. Casadei, R. Naldi, R. Sanfelice, and L. Marconi, "An open-source architecture for control and coordination of a swarm of micro-quadrotors," in *2015 International Conference on Unmanned Aircraft Systems (ICUAS)*, Denver, Colorado, June, 2015.

[126] W. Hönig, C. Milanes, L. Scaria, T. Phan, M. Bolas, and N. Ayanian, "Mixed reality for robotics," in *2015 IEEE/RSJ International Conference on Intelligent Robots and Systems (IROS)*, Hamburg, Germany, Sept 28 - Oct 2, 2015.

[127] D. Morgan, G. P. Subramanian, S.-J. Chung, and F. Y. Hadaegh, "Swarm assignment and trajectory optimization using variable-swarm, distributed auction assignment and sequential convex programming," *The International Journal of Robotics Research*, 2016.

[128] Z. Zuo and P. Ru, "Augmented $\mathcal{L}_1$ adaptive tracking control of quad-rotor unmanned aircrafts," *IEEE Transactions on Aerospace and Electronic Systems*, vol. 50, no. 4, pp. 3090–3101, 2014.

[129] M. Huynh, W. Zhao, and L. Xie, "$\mathcal{L}_1$ adaptive control for quadcopter: Design and implementation," in *13th International Conference on Control Automation Robotics & Vision (ICARCV)*, IEEE, December 2014.

[130] P. Monte and B. Lohmann, "Position Trajectory Tracking of a Quadrotor Helicoptor based on $\mathcal{L}_1$ adaptive control," in *2013 European Control Conference*, (Zurich, Switzerland), July 2013.

[131] S. Mallikarjunan, Z. Zuo, B. Nesbitt, and N. Hovakimyan, "$\mathcal{L}_1$ backstepping for robust trajectory tracking," in *2nd IFAC Workshop on Research, Education and Development of Unmanned Aerial Systems*, (Compiegne, France), November 2013.

[132] B. Michini and J. How, "$\mathcal{L}_1$ adaptive control for indoor autonomous vehicles: Design process and flight testing," in *AIAA Guidance, Navigation and Control Conference*, (Chicago, IL), August 2009.

[133] "Motion capture systems | vicon," http://www.vicon.com/, accessed February 25, 2016.

[134] K. Zhou, J. C. Doyle, K. Glover, *et al.*, *Robust and optimal control*, vol. 40. Englewood Cliffs, NJ, USA: Prentice-Hall, 1996.

[135] J. Munkres, *Topology (2nd Edition)*. ISBN 0-13-181629-2: Prentice Hall, 1999.

[136] M. A. Dahleh and I. J. Diaz-Bobillo, *Control of Uncertain Systems: A Linear Programming Approach*. Englewood Cliffs, NJ, USA: Prentice-Hall, 1995.

[137] "Crazyflie 2.0 | bitcraze," https://www.bitcraze.io/crazyflie-2, accessed February 18, 2016.

[138] N. Michael, D. Mellinger, Q. Lindsey, and V. Kumar, "The grasp multiple micro-uav testbed," *IEEE Robotics and Automation Magazine*, vol. 17, no. 3, pp. 56–65, 2010.

[139] G. Ducard and R. D'Andrea, "Autonomous quadrotor flight using a vision system and accommodating frames misalignment," in *IEEE International Symposium on Industrial Embedded Systems, SIES '09*, 2009.